AN ABSTRACT OF THE THESIS OF

Daniel A. Tingley for the degree of Doctor of Philosophy in Forest Products presented on May 10, 1996. Title: The Stress-Strain Relationships in Wood and Fiber-Reinforced Plastic Laminae of Reinforced Glued-Laminated Wood Beams.

Signature redacted for privacy.

Abstract Approved: _____
Robert J. Leichti

The reinforcement of wood and wood composite structural products to improve their mechanical properties has been in practice for many years. Recently, the use of high-strength fiber-reinforced plastic (FRP) as a reinforcement in such applications has been commercialized.

The reinforcement is manufactured using a standard pultrusion process or alternatively a sheet-forming process commonly referred to as "pulforming". The high-modulus fibers are predominately unidirectional, although off-axis fibers are often used to enhance off-axis properties. The fibers used are either of a single type or multiple types, which are called "hybrids".

Unidirectional, single, and hybrid fiber FRP physical properties and characteristics were compared to wood. Full-scale reinforced glulams were tested. Aramid-reinforced plastics (ARP) used as tensile reinforcements were found to be superior in strength applications to other types of FRP made with fiber, such as carbon and fiberglass. Carbon/aramid-reinforced plastic (CARP) was shown to be superior in both modulus and strength design situations. Fiberglass was shown to be suitable only in hybrid situations

with another fiber such as aramid or carbon and only in limited use situations where modulus was a design criteria.

The testing and analysis showed that the global response of reinforced glulam beams is controlled by localized strength variations in the wood such as slope of grain, knots, finger joints, etc. in the tensile zone. The elemental tensile strains in the extreme wood tensile laminae, due to global applied loads, were found to be well below the strain at failure in clear wood samples recovered from the failure area.

Two areas affecting the relationship between the wood and the FRP were investigated: compatibility of the wood and FRP materials and interface characteristics between the wood and FRP. The optimum strain value at yield point for an FRP was assessed to be slightly higher than the clear wood value in tension for a species/grade to be reinforced. The effects of localized strength variations in the tensile wood laminae adjacent to the FRP were found to be the predominate cause of failure in full-scale reinforced glulams with less than 1.5% by cross section reinforcement.

The Stress-Strain Relationships in Wood and Fiber-Reinforced Plastic Laminae of Reinforced Glued-Laminated Wood Beams

by

Daniel A. Tingley

A THESIS

submitted to

Oregon State University

in partial fulfillment of
the requirements for the
degree of

Doctor of Philosophy

Presented May 10, 1996
Commencement June 1997

Doctor of Philosophy thesis of Daniel A. Tingley presented on May 10, 1996

APPROVED

Signature redacted for privacy.

Major Professor, representing Forest Products

Signature redacted for privacy.

Head of Department of Forest Products

Signature redacted for privacy.

Dean of Graduate School

I understand my thesis will become part of the permanent collection of Oregon State University libraries. My signature below authorizes release of my thesis to any reader upon request.

Signature redacted for privacy.

Daniel A. Tingley, Author

ACKNOWLEDGMENTS

The author would like to express his sincere thanks to Elk River Enterprises, Ltd. and its subsidiaries, American Laminators, Inc. and Duco-Lam of Drain, OR, for partial funding of the research conducted in this project. Without their substantial support, the research would not have been possible.

In addition, the following companies contributed a substantial amount in financial support, technical assistance or materials in kind:

AKZO Nobel NV
PO Box 9300
6800 SB Arnhem
The Netherlands

DuPont
Laurel Run 2 South
Chestnut Run Plaza
Wilmington, DE 19880-0705

Reichhold Chemicals, Inc.
PO Box 13582
Research Triangle Park, NC 27709-3582

Western Wood Structures, Inc.
PO Box 130
Tualatin, OR 97062

I appreciate the financial and facilities support of the Center for Wood Utilization Research, Forest Research Laboratory of Oregon State University.

The continued direction and consultation of Dr. Robert Leichti and Dr. John Peterson were an important part of the success of this work as well. Finally, the staff of Wood Science & Technology Institute (N.S.), Ltd. were exceptional in their diligence to correctly record and organize data.

CONTRIBUTION OF AUTHORS

Dr. Robert Leichti and Dr. John Peterson were involved in experimental design, analysis and revision of each manuscript.

TABLE OF CONTENTS

TABLE OF CONTENTS (CONTINUED)

TABLE OF CONTENTS (CONTINUED)

TABLE OF CONTENTS (CONTINUED)

LIST OF FIGURES

LIST OF FIGURES (CONTINUED)

LIST OF FIGURES (CONTINUED)

Figure Page

LIST OF FIGURES (CONTINUED)

LIST OF TABLES

LIST OF TABLES (CONTINUED)

LIST OF APPENDIX FIGURES

LIST OF APPENDIX FIGURES (CONTINUED)

LIST OF APPENDIX TABLES

DEDICATION

I dedicate this thesis to my wife, Lori Ann.

THE STRESS-STRAIN RELATIONSHIPS IN WOOD AND FIBER-REINFORCED PLASTIC LAMINAE OF REINFORCED GLUED-LAMINATED WOOD BEAMS

CHAPTER 1

CURRENT STATE-OF-THE-ART OF REINFORCEMENT METHODOLOGIES FOR GLUED-LAMINATED TIMBER

Introduction

Wood and wood composites have been reinforced in many ways over the years in an effort to improve their performance in a variety of load situations. Research work on glulam reinforcement has been conducted in the commercial sector, for example, with steel flitch plates applied to wood lintels. Universities and government agencies have conducted tests on connector reinforcement in glued-laminated timber (glulams) and solid sawn lumber using glass-fiber reinforced plastics (GFRP) [Chen et al., 1994]. Still other industry-research cooperating research groups (TNO Building & Construction Research, The Netherlands) have investigated glass-fiber reinforced plastic reinforced glulams.

Reinforcement research involving the combination of wood and fiber-reinforced plastics (FRP) has been conducted by a variety of commercial, government and university researchers [Biblis, 1965; Permanez, 1974; Rowlands et al., 1986; Sonti et al., 1995a; Sonti et al., 1995b; Tingley, 1990; Tingley and Leichti, 1993; Tingley and Leichti, 1994c]. Recently, significant innovations have occurred involving the use of FRP with engineered wood composites (EWC). The use of FRP in the manufacture of reinforced wood and

wood composites, particularly glulams, has been recognized as a significant innovation by the Civil Engineering Research Foundation [Leichti and Tingley, 1996].

In the past three years, significant progress was made toward reinforcement for engineered wood products. Nearly 700 full-scale glulams reinforced with FRP were manufactured and tested. The research program included a wide range of component and adhesion testing, development of reinforcement panels, as well as full-scale testing. The evaluation programs included open-web joist and I-beams having various wood materials for flanges and webs. The program was extended to other EWCs that were reinforced with FRP's including laminated veneer lumber and plywood.

Reinforced glulams are now being used commercially. Major model building code approval was completed in 1995 [ICBO, 1995]. Commercial reinforced glulam was made feasible by discoveries that facilitated compatibility between wood and FRP. The compatibility issues were of critical importance since effectiveness of a reinforcement material relies on its adaptability to processes and adhesives used by the wood and wood composites industries. Compatibility issues between reinforcement and wood have been resolved to a great extent by the use of FRP types and methodology recently developed [Tingley, 1994a; Tingley, 1994b]. Many of the new methods of construction, production of the reinforcement and placement in the wood and wood composite are protected by patents [Tingley, 1994a; Tingley, 1995; Tingley, 1996a; Tingley, 1996c; Tingley, 1996d]. Relevant design formulation has been developed and methods for predicting the structural member size and configuration as well as reinforcement location and concentration are also patent pending. Testing to date has included a variety of wood species and FRP types as well as placement positions and concentrations of reinforcement within the beam

[Tingley, 1990; Tingley and Leichti, 1993; Tingley and Leichti, 1994a; Tingley and Leichti, 1994b; Plevris and Triantafillou, 1992; van de Kuilen, 1991].

Objectives and Overview

The overall objective of this thesis is to investigate the stress-strain relationships in the FRP and wood in a reinforced glulam.

Chapter 1 explores the historical background of reinforcement of EWCs, particularly glulams with FRP. An overview of the current state-of-the-art in reinforcement is also presented. Interface issues are discussed and material design parameters reviewed. Special emphasis is given to reinforcement strategies involving FRP and glulam beams. Finally, full-scale reinforced glulam test results are shown to demonstrate the FRP technology.

Chapter 2 reviews characteristic stress distributions in a reinforced glulam. Finite-element analysis and strain gauged full-scale test specimens served as the investigation tools to facilitate a better understanding of the stresses and strains that affect the FRP-wood interface.

Chapter 3 presents the stress-strain relationship between the wood and FRP as assessed by analysis and testing.

Finally, Chapter 4 presents conclusions of the analyses from prior chapters.

Reasons for Current Success of Reinforcement Concept

Although FRP has been used in the past with wood, its applications have not been widespread until recently. There are several reasons for this recent success.

- Increased cost and price volatility of wood fiber, particularly high grade wood fiber, caused by reduced supplies of old growth forests.
- Reduced costs for high strength advanced fibers, e.g., aramids, due to increased supply and expiring patents.
- Worldwide acceptance of composites in the structural market place.
- Recent developments in adhesion methodology allowing the use of conventional adhesives process and use limitations for adhering the FRP's to EWCs.
- The use of reinforcement for wood and wood composite structural products means stronger, safer, more environmentally friendly, lower-cost structural materials.
- Reinforcement technology is applicable to various types of structural wood composites (Figures 1.1 and 1.2).

The economic considerations reflected in the first two points are significant. In the last ten years, the costs of high strength fibers such as aramid and carbon have dropped 50%, while the cost of high grade wood has risen nearly 150%. In some countries, such as Australia, the increase in wood costs is even greater, making that the economic advantage of using reinforcement more substantial.

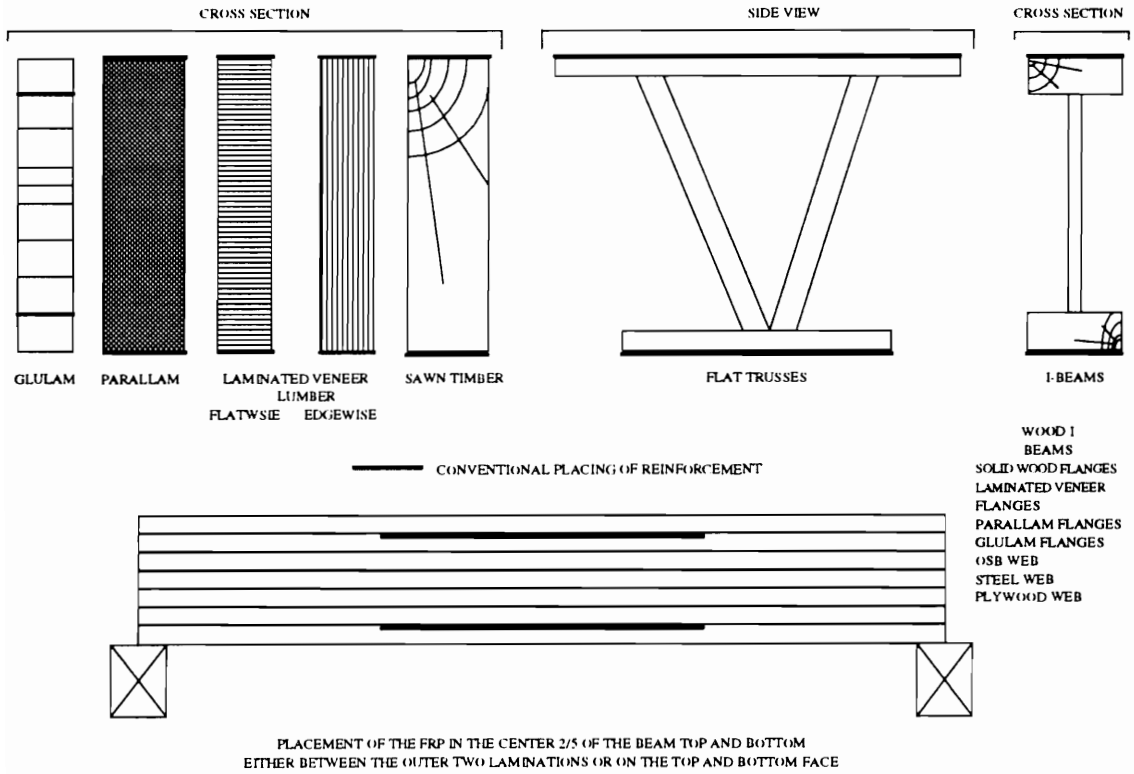

Figure 1.1 Sketches of wood-based composite structural products in which reinforcement with high-strength FRP is advantages.

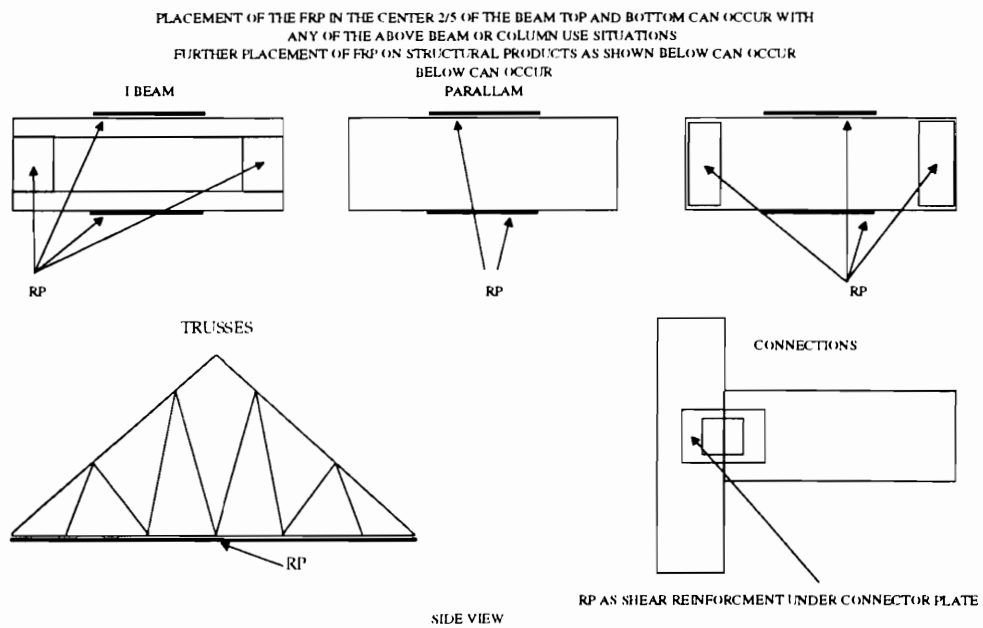

Figure 1.2. Likely placement locations for the FRP in wood-based structural products and systems.

The point relevant to the use of conventional adhesives is a very important issue in the widespread implementation of the FRP reinforcement concept to the industry. Epoxy-type adhesives are not considered friendly by manufacturers of engineered wood composites, which primarily use resorcinol, melamine, PVA and urea type adhesives. These adhesives are mechanical-type glues and are not conventionally satisfactory for FRP adhesion to wood. However, new technology now enables conventional wood-laminating adhesion technology to be used to adhere the FRP to the EWC with acceptable durability characteristics [Tingley, 1994a].

Fiber-Reinforced Plastic as Reinforcement for Wood Composites

Reinforcement Description

Lantos [1970] describes using steel bars, some greater than 0.5in (12.7 mm) in diameter, some were deformed rebar and some were smooth steel bars, placed in the high stress zones of glulams. Steel rebar, like that used in concrete, has been used in glulams [Bulleit et al., 1989]. Tapered splines manufactured from reinforced plastic have been used in glulams to increase shear capacity [Fox, 1975]. Flitch plates, external steel rod systems and vertical shear dowels have all been used to increase the capacity of glulams as well as sawn lumber and other combinations of structural wood composites for commercial structures that are still in service.

These traditional approaches have usually been solutions to problems with regard to load capacity where wood was the only material suitable for use. They were not generally economically advantageous, and, as such, were not used extensively [Bulleit,

1983; van de Kuilen, 1991; Zahn, 1983]. One major reason for this was the requirement that epoxy glues be used for bonding of the reinforcement to wood and to itself in multiple lamination reinforcement situations. Epoxy glues are generally not acceptable to the wood industry [Hoyle, 1985; Rowlands et al., 1986; Samuel et al., 1984].

Some FRP reinforcement types can be used with conventional laminating adhesives (phenol-resorcinols, melamines, urea-based and other mechanical-type adhesives). The reinforcement can be bonded to wood and to itself.

The reinforcement is manufactured to allow various percentages of fiber orientation depending upon end use. For example, when used as a tensile reinforcement, the fibers are 100% aligned. For connector reinforcement, they are 90% aligned, and 10% are off-axis. However, in most situations, the fiber is 100% unidirectional and pretensioned [Sonti et al., 1995b].

One type of FRP now used as a reinforcement for EWC's is produced in such a way as to allow direct bonding to the glue during adhesion through the hairing up process (Figure 1.3) [Tingley, 1994b; Tingley and Leichti, 1994a; Tingley and Leichti, 1994b]. This is similar to the use of randomly-orientated chopped fiber used by previous researchers for reinforcement of panel products [Smulski and Ifju, 1987a; Smulski and Ifju, 1987b] but provides much higher strength properties in the longitudinal direction. This is an improvement because the fibers are fully aligned while being connected to the glueline adhesive. Stresses can then transfer directly from the wood to fiber bundles.

A wide range of matrices can be used to manufacture FRP including thermoset types from polyester to epoxy as well as thermoplastics such as Nylon 66 or PET. These can be tailored to provide various shear translation strengths,

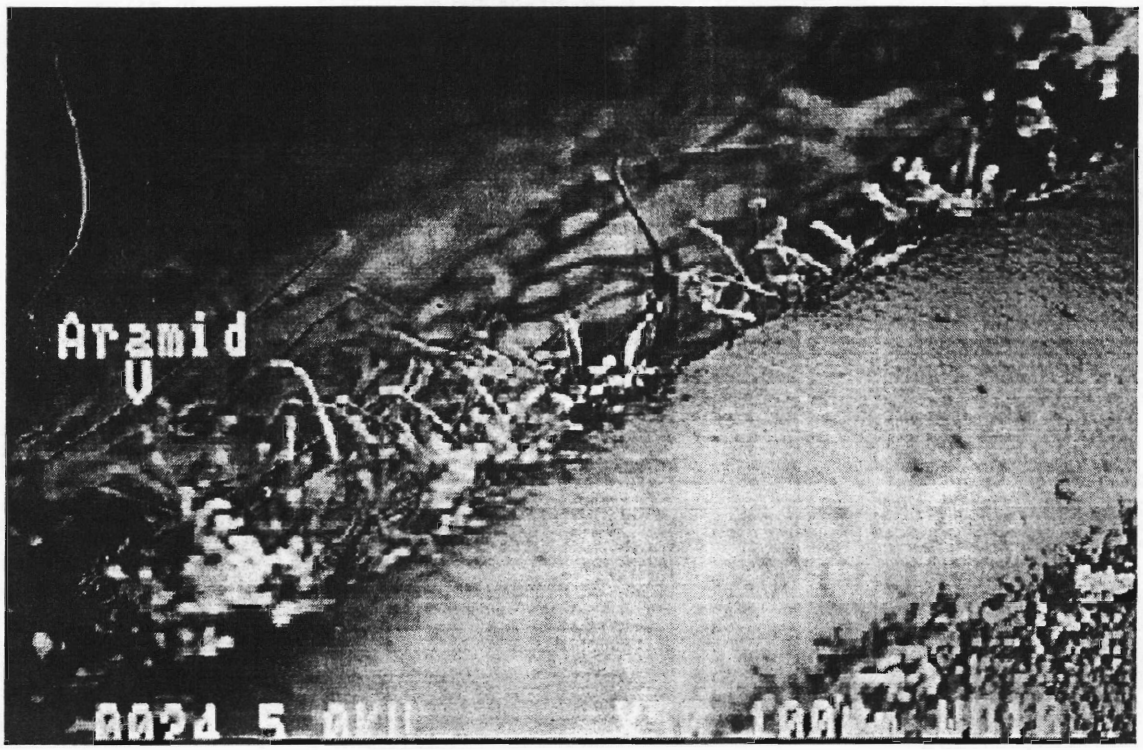

Figure 1.3. An electron photomicrograph showing the "haired-up" surface of an ARP.

fire/temperature protection and toughness properties to the reinforcement [Dailey et al., 1995; Tingley and Leichti, 1994a].

Various fibers such as fiberglass, aramid, carbon and high performance polyethylene can be used in their pure or hybrid form [Tingley and Leichti, 1994a] to manufacture FRP's. The degree of hybridization is generally determined by end use requirements. Fiberglass, for example, generally has very low tension-tension fatigue properties, much below the other fiber types. In addition, its creep to failure in tension, as a percentage of ultimate tensile strength (UTS), is 26% as opposed to 92% for aramid in a saturated condition (>9% moisture content) [ICBO, 1995]. Fiberglass is not ideally suited for use with wood in its pure form because glulam is conventionally manufactured at 12 to

14% moisture content, thus, the fiberglass becomes saturated when it is glued to wood. Finally, fiberglass is very susceptible to strength degradation in alkaline environments and because of this, situations where alkaline exposure is possible (i.e., bridges) need to be avoided when using fiberglass.

The FRP reinforcement can be manufactured in any width and length. Thickness is limited by bending radius attendant to reel requirements for shipping. Generally, FRP can be reeled in thickness up to 0.150 inch (3.81 mm) [Tingley, 1994b]. Storage on reels also lowers inventory costs. Cost reductions in this range have typically not been achieved by previous reinforcement types [Dailey et al., 1995; Triantafillou and Deskovic, 1992; van de Kuilen, 1991].

The FRP reinforcement can be used just as a wood laminate in a wood composite lay-up with the same glue-spread rate and open and close times. Since FRP is inert and lacks porosity, typical wood glues require longer to fully cure on its surface than on a wood. Seven days are generally required before the reinforced wood product can enter service [Dailey et al., 1995; Tingley and Leichti, 1994a].

Design Methodology for FRP Components

Design methodology for conventional glulam is readily available from AITC [AITC, 1988]. Reinforcement allowable design values have been developed by groups such as DuPont [DuPont, 1973], Hercules [Default, 1972], and Permanez [1974]. However, these values have been predominately used in the aerospace industry and are proprietary. These groups have published ultimate values for aramid-reinforced plastic

(ARP), carbon-reinforced plastic (CFRP) and fiberglass-reinforced plastics (GFRP) respectively.

Due to FRP tensile strength and the excellent shear and cleavage bond developed between FRP and wood in the current manufacturing methodology, the tensile-based design philosophy used with conventional glulam was modified for use with reinforced beams. A new compression-based design methodology is now being used [Tingley, 1994b]. There have been many investigations of reinforced wood members but none have developed a design methodology based on compressive strength of the wood and tensile capacity of the FRP [Biblis, 1965; Bulleit, 1983; Fox, 1975; Hoyle, 1985; Kobetz and Krueger, 1972; Lantos, 1970; Plevris and Triantafillou, 1992; Rowlands et al., 1986; Samuel et al., 1984; van de Kuilen, 1991; Zahn, 1983]. The compression-based formulas developed have been proven by extensive testing of full-scale beams [Tingley and Leichti, 1994b] and modeling to more effectively explain the distribution of stresses in a reinforced and unreinforced glulam beam. Others have also completed modeling, an accepted practice for predicting strength and stress distribution as well as localized failure initiations [Balinski et al., 1972; Samuel et al., 1984] on unreinforced and reinforced beams [Davalos and Barbero, 1991; Tingley, 1990].

The compression-based design assumes a compressive plasticity in bending members. This assumption is supported by other researchers [Anderson, 1981; Gurfinkel, 1981; Buchanan, 1986; Malhotra and Bazan, 1980]. For design purposes, the compressive force distribution is assumed to be square instead of the conventional triangular distribution, i.e. maximum at the outer fiber and zero at the neutral axis. The allowable compressive values provided by NDS-91 [NFPA, 1991] for each species and the

allowable design strength of the reinforcement in tension are used to calculate a resisting moment couple.

The allowable tensile strength of the FRP was developed by reducing the actual 5% lower exclusion limit value (75% confidence limits) for in-service characteristics such as tension-tension fatigue and further dividing by 1.3 to 1.6 depending upon FRP type and property variability. Various other design criteria have been developed as well for design allowable shear strength and modulus of elasticity [Tingley, 1994b; ICBO, 1995].

Material Considerations

It is important to understand the material characteristics of all of the individual components in a reinforced structural wood composite: the fibers used in the reinforcement, the polymer used to encase the fibers in the reinforcement, wood strength characteristics in tension, wood strength characteristics in compression, as well as localized features such as slope of grain, knots, juvenile wood, compression wood and finger joints.

Elastic Characteristics

Wood is an orthotropic material exhibiting planes of symmetry. Reinforcement is also orthotropic with planes of symmetry. The Poisson's ratio for wood in the longitudinal-transverse plane for the average domestic softwood is in a range of 0.33-0.47 while reinforcement with 100% unidirectional fiber in the same plane is in a range of 0.12-0.36 with a value of 0.33 being very common [DuPont, 1973; Default, 1972]. A new type of FRP, FiRP™ Reinforcement panel, now sold commercially, has a Poisson's ratio of

0.36. These characteristics serve to make FRP very compatible with wood. This compatibility between Poisson's ratio is only possible if the fiber and the matrix is connected to the glueline adhesive such that translation of all stresses/strains occurs between the wood and FRP and FRP to FRP [Tingley, 1994a].

The stiffness of wood is much lower than that of the FRP, the difference being directly related to the fiber used and the orientation of fiber (e.g., 100% unidirectional). The wood has a higher modulus of elasticity in tension (E_{wt}) than in compression (E_{wc}). The modular ratio (η) of wood between tension and compression is reported to be in the range of 1.0 to 1.05 [Gurfinkel, 1981]. The η value for FRP to wood in compression, for example, carbon-reinforced plastic (CFRP) and Douglas-fir, L-3 (12% moisture content at 72°F) [NFPA, 1991] can be approximately 14. Tables 1.1 and 1.2 show compressive and tensile values for L-3 Douglas-fir as determined by testing small clear specimens recovered from full-scale reinforced glulam beams. The average ultimate stress in tension and compression was found to be 11474 psi (79.11 MPa) and 5188 psi (35.76 MPa) respectively. The 5% lower exclusion level (LEL) at the 75% confidence interval for ultimate stress in tension and compression was 3574 psi (24.64 MPa) and 3159 psi (21.78 MPa) respectively. The values shown in Tables 1.1 and 1.2 have been normalized by a log factor. The formulas used for LEL are shown in Appendix A. The k factor was determined by using standard k values for the relevant population size [Lieberman, 1958]. Figures 1.4a and 1.4b show typical stress-strain curves from small-clear wood tests. It is important to note the nonlinearity and ductility in the compressive specimen compared to the tensile specimen.

Table 1.1. Compression test results of wood laminates for Douglas-fir L3 laminations using ASTM D-143 (ASTM 1994a). a) Test data, b) Statistical summary.

a) Test data.

Beam/Lam #	Ultimate Stress Adjusted 12% MC (psi)	E Adjusted 12% MC (psi)	YP Stress (psi)	YP Strain (%)	SG
M1802/L#1	6826	1620669	5689	0.4297	0.52
M1802/L#2	4443	1139042	3865	0.4019	0.40
M1802/L#3	4001	660628	3542	0.5880	0.38
M1802/L#4	3785	2165383	2804	0.1881	0.41
M1802/L#5	4226	1397708	4062	0.3421	0.36
M1803/L#1	7153	2250768	6349	0.3485	0.49
M1803/L#2	4342	1148386	4240	0.4233	0.42
M1803/L#3	6679	1787171	6272	0.4105	0.53
M1803/L#4	4145	859767	3061	0.4255	0.44
M1803/L#5	5941	1545174	5768	0.4255	0.40
M1805/L#1	4923	1815143	4447	0.3036	0.49
M1805/L#2	4673	2155332	3781	0.2416	0.41
M1805/L#3	7404	2542219	7143	0.3357	0.47
M1805/L#4	5683	1540688	5419	0.4084	0.36
M1805/L#5	5634	1400119	5204	0.4255	0.43
M1901/L#1	5034	1970208	4349	0.2202	0.46
M1901/L#2	4695	1689662	3787	0.2950	0.44
M1901/L#3	5760	1466998	5261	0.4233	0.42
M1901/L#4	5005	1581924	4574	0.3442	0.41
M1901/L#5	6595	1487920	6261	0.4704	0.48
M1902/L#1	6898	2080050	6298	0.3271	0.45
M1902/L#2	4894	1666054	4390	0.3250	0.40
M1902/L#3	4989	1093343	4461	0.4768	0.43
M1902/L#4	3680	1182953	3101	0.3314	0.36
M1902/L#5	4607	1690992	4243	0.3122	0.43

b) Statistical summary.

AITC[a] Comb.	Beam	Species	Sample Size	YP Stress			Ultimate Stress		
				Average (psi)	5% LEL[b] (psi)	5% LEL/1.9 (psi)	Average (psi)	5% LEL (psi)	5% LEL/1.9 (psi)
1	M1802	D-fir	5	3887	2068	1089	4546	2548	1341
1	M1803	D-fir	5	4953	2281	1201	5516	2985	1571
1	M1805	D-fir	5	5081	2830	1490	5590	3600	1895
1	M1901	D-fir	5	4775	2977	1567	5377	3844	2023
1	M1902	D-fir	5	4386	2362	1243	4911	2820	1484

[a] AITC-200 [AITC-200, 1988] combination number.

[b] Data normalized by log factor.

Table 1.2. Tensile test results of wood laminates for Douglas-fir L3 laminations using ASTM D-143 (ASTM 1994a), a) Test data, b) Statistical summary.

a) Test data.

ATIC Lam Grade	Lam Number	Ultimate Stress Adjusted to 12% MC	E Adjusted to 12% MC	YP Stress (psi)	YP Strain (% strain)	SG
L-3	6	6686	1274268	10705	0.6880	0.38
L-3	7	14175	1613454	9741	0.6686	0.23
L-3	9	7895	1435878	12639	0.6977	0.24
L-3	10	9316	1819817	14915	0.6783	0.23
L-3	11	15088	1476163	8763	0.7364	0.23
L-3	12	12502	2019577	7875	0.4419	0.39
L-3	5	10168	1745622	10646	0.6667	0.57
L-3	6	17965	1817549	9722	0.6027	0.53
L-3	7	10179	1527670	10652	0.7209	0.58
L-3	8	12742	1878669	14156	0.7171	0.57
L-3	9	12575	1014526	7592	0.8391	0.47
L-3	10	5033	1230189	8027	0.4031	0.54
L-3	11	4395	1302565	4418	0.6146	0.53
L-3	12	9285	2091375	7747	0.3527	0.43
L-3	5	8912	1455065	10100	0.6540	0.50
L-3	6	8358	926672	8890	0.9600	0.41
L-3	7	9687	1900181	10300	0.5200	0.54

b) Statistical summary.

			YP Stress (psi)			Ultimate Stress (psi)		
Grade	Species	Sample Size	Avg.	5% LEL[a]	5% LEL/1.9	Avg.	5% LEL	5% LEL/1.9
L-3	D-fir	3	9478	5481	2885	9685	4675	2461
L-3	D-fir	6	11208	6632	3491	15333	2723	1433
L-3	D-fir	8	8691	4091	2153	9405	3325	1750

[a]Data normalized by log factor.

a)

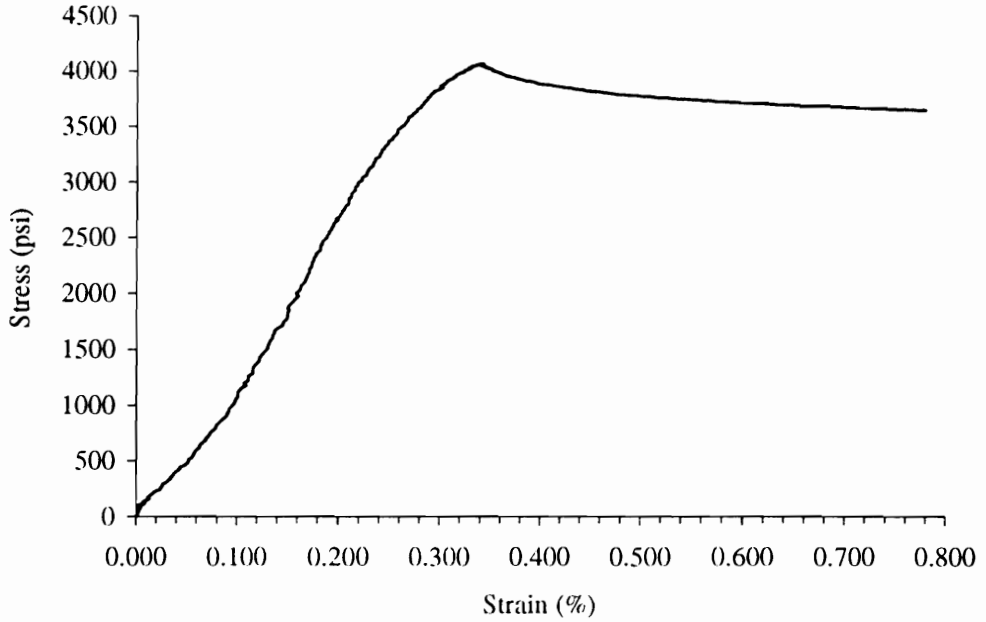

b)

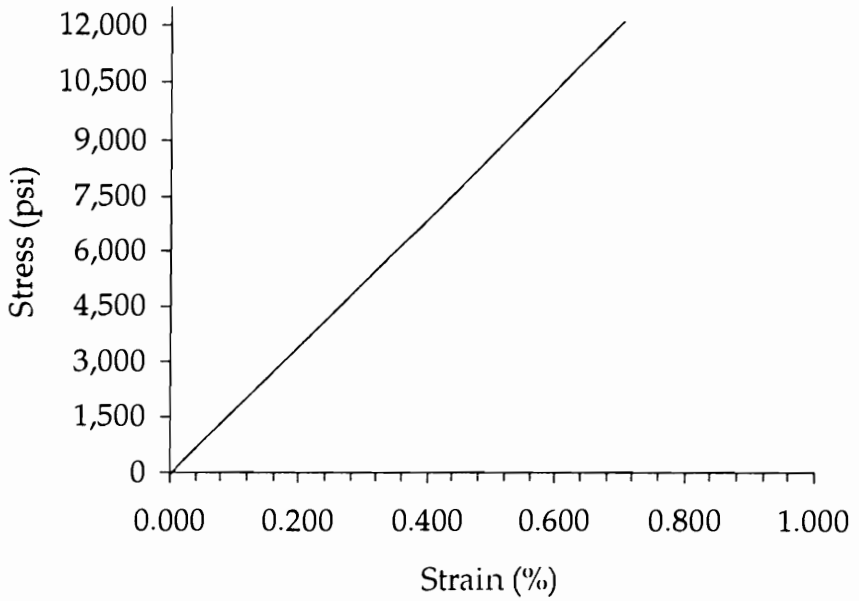

Figure 1.4. Stress-strain diagrams for small clear specimens cut from L-3 Douglas-fir, a) compression, b) tension.

The tensile modulus of elasticity of an FRP (E_n), such as (ARP), can reach values in the 12 x 10^6 psi (82,750 MPa) range (65/35 fiber/plastic ratio volume basis). Tables 1.3 and 1.4 show the results of ASTM D-3039 [ASTM, 1995b] testing on the ARP taken from a beam after destructive testing [Tingley, 1994b]. Figure 1.5 shows the stress/strain curves from which these values were derived.

The tensile strength of wood exceeds the compressive strength by a factor of more than two. Table 1.2 shows the results of ASTM D-143 [ASTM, 1995d] tests on Douglas-fir, L-3 coupons, recovered from laminations from full-scale beam tests. These values are in a range of 4,428 to 15,214 psi (30.53 to 104.92 MPa). The tensile strength of FRP, such as ARP, can reach values of 235,000 psi (1620 MPa) (65/35 fiber/plastic ratio on a volume basis). Table 1.3 and 1.4 show these values for reinforced test beams discussed in this report.

The compressive strength for Douglas-fir, L-3 (12% MC, 72°F), as shown in Table 1.1 has a mean value of 5188 psi (35.76 MPa), whereas the compressive strength of CFRP can reach 65,000 psi (44.82 MPa) (66/35 fiber/plastic ratio on a volume basis) as shown in Figure B-7 of Appendix B.

Strain at Yield Point

Strain at yield point is one of the most important compatibility issues affecting the strength of a reinforced wood or wood composite. Bending stiffness of the composite beam is not as greatly affected by strain at yield point of the FRP since stiffness is only a rate of deflection with the application of load. Bending modulus is a specific criteria as opposed to a strength criteria, such as bending moment capacity.

Table 1.3. Reinforcement tensile test results for ARP.
a) Dimensions, b) Test data, c) Statistical summary.

Test Type: ASTM D3039.
Sample Type: ASTM
Machine Parameters of Test:
Sample Rate (pts/sec): 10.00.
Crosshead Speed (in/min.): 0.120.
Humidity (%): 50.
Temperature (deg. F): 73.

a) Dimensions (in.):

	Specimen 1	Specimen 2	Specimen 3
Width	0.7540	0.7530	0.7440
Thickness	0.0750	0.0780	0.8000
Ext. Gauge length	0.9843	0.9843	0.9843
Spec. Gauge length	6.0000	6.0000	6.0000

b) Test data.

Specimen Number	Sample Number	Stress at Max. Load (ksi)	Modulus (segment) (ksi)	Load at Max. Load (lbs)	Est. Peak Strain % Strain
1	T1	210.4	10190	11900	2.065
2	T2	196.6	10210	11550	1.927
3	T3	199.8	9877	11890	2.023

c) Statistical summary.

	Stress at Max. Load (ksi)	Modulus (segment) (ksi)	Load at Max. Load (lbs)	Est. Peak Strain % Strain
Mean	202.3	10090	11780	2.005
Std. Dev.	7.2	186	199	0.071
Mean-1.00*Dev.	195.1	9905	11580	1.934
Mean + 1.00*Dev.	209.5	10280	11980	2.076

Table 1.4. Summary of tensile test results for ARP reinforcement.

	Ultimate Stress (ksi)	$^{s}E_{rt}$ (ksi)	Ultimate Strain (%)
Sample Size	15	15	15
Average	214	11123	1.92
Median	214	10920	1.92
Mode	212	10860	1.91
Geometric Mean	213	11093	1.92
Variance	147	736386	0.01
Standard Deviation	12	858	0.1
Standard Error	3	222	0.03
Minimum	196	9877	1.78
Maximum	239	12860	2.09
Coeff. of Variation	6	8	5.07

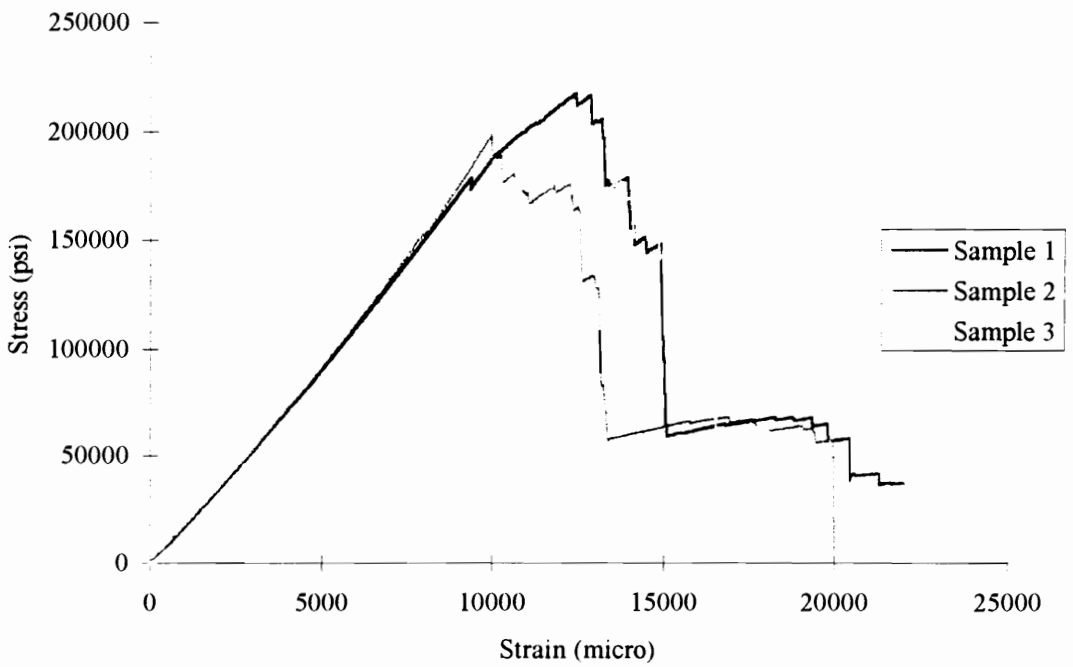

Figure 1.5. Tensile samples of ARP stress-strain curves for three replicates.

However, strain at yield point of the FRP directly affects the ultimate strength of the reinforced wood composite.

Yield strain is particularly critical in situations involving tensile reinforcement. Figure 1.4a shows a strain at yield point of 0.32% for wood in compression. The ultimate strain value of ARP is approximately 2.0% (shown in Figure 1.5). Figure 1.4b shows a stress-strain curve for wood in tension with a yield point of 0.7% strain. This means that the wood will reach its strain limit before the FRP. Failure deflection values of L/30 (L is length of span) in reinforced glulams display this relationship [Tingley, 1994b]. Steel has often been used as a reinforcement for wood since it is relatively low in cost compared to FRP and has high E values. The yield point strain of steel is 0.2%, which is well below that of wood. In steel reinforcement applications, the wood cannot reach its full capacity prior to the yielding of the reinforcement. The FRP reinforcement allows the wood strength to be fully utilized due to its yield strain limit.

Shear Strength

As shown in Table 1.5, the shear capacity of wood in small coupons is 1565 psi (10.79 MPa) for Douglas-fir, L-3 (12% MC, 72°F). These results were obtained using ASTM-D143 [ASTM, 1994b]. Table 1.6 shows reinforcement shear test results for ARP. The Iosipescu shear test method (modified for unidirectional FRP) [Adams and Walrath, 1987; Scale, 1973] was used to generate test results shown. The average ultimate shear strength of ARP was 1530 psi (MPa), which is close to the value obtained for Douglas-fir, grade L-3 (12% MC, 72°F) for small clear samples. Shear values can be tailored by making adjustments in the plastic matrix and the amount of off-axis fiber used.

Table 1.5. Overall summary of shear strength values for AITC combination #1, L-3 D-fir (AITC 500-92)

Wood Grade	L-3 D-fir
Sample Size	220
Average (psi)	1565
Median (psi)	1516
Mode (psi)	1982
Geometric Mean (psi)	1509
Variance	489196
Standard Deviation (psi)	699
Standard Error (psi)	47
Minimum (psi)	935
Maximum (psi)	1965
Coeff. of Variation (%)	45

Table 1.6. Shear strength test results of ARP reinforcement.

	Stress
Sample Size	7
Average (psi)	1530
Median (psi)	1494
Mode (psi)	1457
Geometric Mean (psi)	1468
Variance	220329
Standard Deviation (psi)	469
Standard Error (psi)	177
Minimum (psi)	905
Maximum (psi)	2230
Coeff. of Variation (%)	31

Reinforced Glulam Testing

Prior to beginning extensive testing of FRP-reinforced glulams a series of tests on full-scale FRP-reinforced glulams was performed.

Objective

The objective of the test series was to investigate the effect of the FRP reinforcement on the strength characteristics on Douglas-fir and Ponderosa Pine glulam beams.

Hypothesis

Prior to beginning the investigation of the effect of FRP on glulam performance it was hypothesized that;

- ARP tensile reinforcement would improve beam strength, stiffness, and variability.
- ARP tensile reinforcement would reduce the effect of finger joint strength on beam strength.
- ARP tensile reinforcement would improve lower grade glulam strength characteristics more than higher grades.
- Arranging the laminations of the glulam in order of highest E at the top (compression) and lowest E at the location adjacent to the FRP in the tensile zone would improve the effectiveness of the FRP.

Experimental Design

In order to prove the hypothesis true or false, a series of full-scale glulam beam tests were conducted. Douglas-fir high grade, V4-2400 [AITC-200, 1992], control beams were tested and compared to ARP, FRP reinforced V3-1600 [AITC-200, 1992] Douglas-fir glulams and Ponderosa pine E-stacked glulams. To test the improvement of the low grade Douglas-fir glulams, unreinforced V3-1600 glulams were also tested. To establish any size affects, various sizes of beams in each lay up type were also tested. The degree of reinforcement (the percentage by the cross section) was varied within the Douglas-fir beams to establish it's effects on beam strength enhancements and finger joints. In addition, knot size and location as well as finger joint location were recorded in each beam.

Test Apparatus and Procedure

The full-scale FRP-reinforced glulams were manufactured according to AITC 200-92 [AITC, 1992] except for specifications relating to FRP and tested according to ASTM D-198 [ASTM, 1995a]. Appendix B contains the specifications of the test apparatus. The FRP reinforcement panels used in all reinforced glulams was ARP placed in the glulam beam during manufacturing of the beam. The E-stacking consisted of using portable E monitoring equipment to organize the highest E-value lamina at the top of the glulam in the compressive zone and the lamina with the lowest E-value in the tensile zone adjacent to the reinforcement.

Results and Discussion

Figures 1.6 and 1.7 show a typical load-deflection curve for an FRP-reinforced glulam beam in bending and a photograph of a test on a reinforced Douglas-fir, all L-3 AITC combination 1 [AITC, 1991] beam. This beam had two layers of ARP, 0.07 in. (1.8 mm) thick, placed full length between the bottom two wood laminations in the tensile zone. The resulting composite beam E and modulus of rupture (MOR) were 2.53 x 10^6 psi (17,444 MPa) and 8,170 psi (56.33 MPa) respectively. The predicted values for stiffness and strength by using D-198 [ASTM, 1995d] and AITC-200 [1992] were greater than the predicted values for the unreinforced beam of 1.5 x 10^6 psi (10,300 MPa) and 3,150 psi (21.7 MPa) respectively.

Table 1.7 shows the results of 65 full-scale glulam beams tested to failure. The table shows both the design moment obtained by using NDS 1991 [NFPA, 1991] and the actual ultimate moment. The average increase in strength for V3-1600 Douglas-fir reinforced was 61% over the unreinforced control V3-1600 Douglas-fir beams. The average increase in E for Douglas-fir, V3-1600, was found to be 26% over the NDS published value [NFPA, 1991]. The percentage increase in E was higher in the Ponderosa pine than the Douglas-fir V3-1600. The use of E ranking with the highest E in the outermost compressive zone and the lowest adjacent to the FRP in the tensile zone produced the highest strength and stiffness increases as shown in Table 1.7. The increase was 185% and 35% respectively over the NDS published value [NFPA, 1991]. This demonstrated the value of resisting the tensile capacity of the FRP with high E-value compressive material. The data revealed that the reinforcement leads to greater

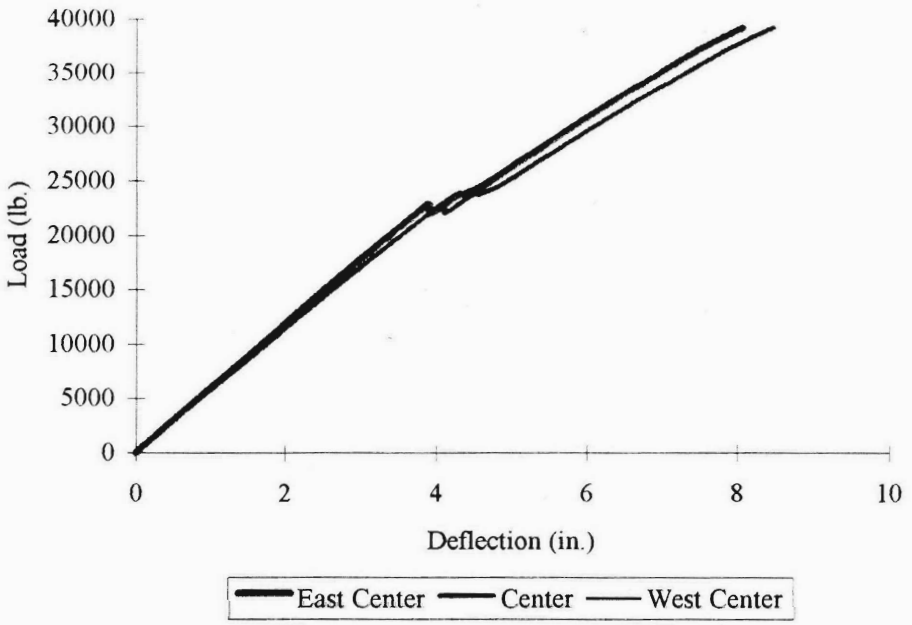

Figure 1.6. Load-deflection curve of reinforced glulam.

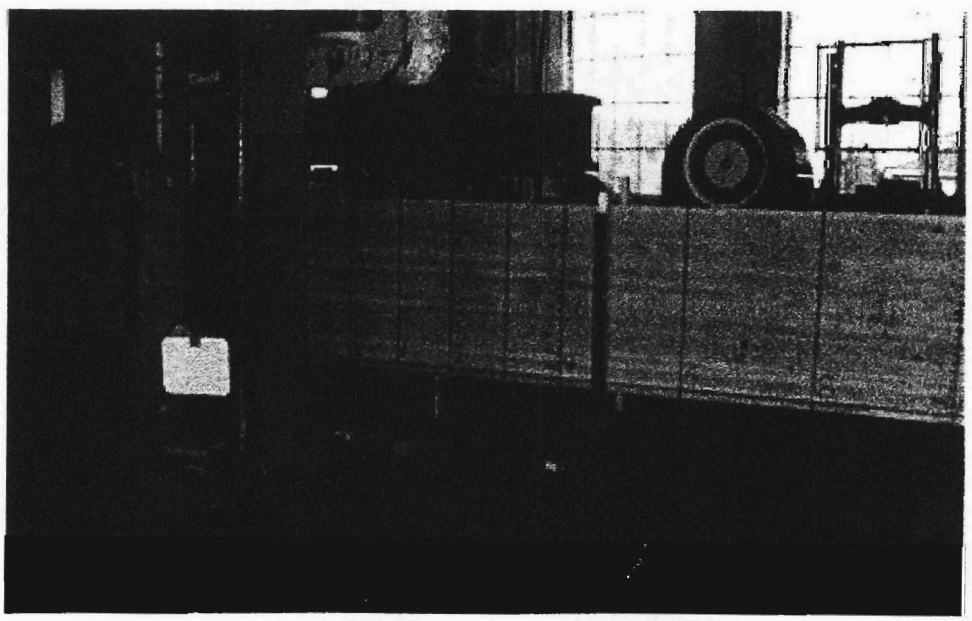

Figure 1.7. A reinforced glulam beam in bending.

Table 1.7. Statistical analysis results of full scale reinforced and unreinforced glulam beam ASTM D-198 test results.

Grade	Species	Span	L H [a] Span	Width	Depth	Rein-force-ment	Bumper Layer	Rein-froce-ment	Actual Ultimate Moment	Design Moment	Safety Factor	Design MOEbdng	Measured MOEbdng	Safety Factor
												x10e6 psi	x10e6 psi	
		(ft)	(ft)	(in)	(in)	type		%	(lb-ft)	(lb-ft)				
V4-2400	D-fir	16.5	5.5	5.125	15.5	N/A	N/A	0.00	89650	39343	2.28	1.8	1.65	0.92
V4-2400	D-fir	18	6	2.5	24	N/A	N/A	0.00	122100	46912	2.60	1.8	1.99	1.11
V4-2400	D-fir	18	6	2.5	24	N/A	N/A	0.00	137400	46912	2.93	1.8	2.00	1.11
V4-2400	D-fir	23	7.67	2.5	24	N/A	N/A	0.00	87392	45776	1.91	1.8	1.96	1.09
V4-2400	D-fir	23	7.67	2.5	24	N/A	N/A	0.00	107324	45776	2.34	1.8	2.18	1.21
V4-2400	D-fir	24	8	5.125	21	N/A	N/A	0.00	153600	67481	2.28	1.8	1.90	1.06
V4-2400	D-fir	24	8	5.125	21	N/A	N/A	0.00	174400	67481	2.58	1.8	1.87	1.04
V4-2400	D-fir	29	8	2.5	24	N/A	N/A	0.00	76440	44727	1.71	1.8	1.74	0.96
V4-2400	D-fir	29	8	2.5	24	N/A	N/A	0.00	69300	44727	1.55	1.8	2.12	1.18
V4-2400	D-fir	36	8	2.5	24	N/A	N/A	0.00	99120	43770	2.26	1.8	1.99	1.11
V4-2400	D-fir	36	8	2.5	24	N/A	N/A	0.00	84980	43770	1.94	1.8	1.97	1.10
V4-2400	D-fir	37	8	5.125	15	N/A	N/A	0.00	79750	34099	2.34	1.8	1.86	1.03
V4-2400	D-fir	39	8	5.125	27	N/A	N/A	0.00	335575	103626	3.24	1.8	1.73	0.96
										Sample Size	13	13	13	13
										Mean	2.31	N/A [c]	1.92	1.18
										Std. Err.	0.1303	N/A	0.0423	0.04
										Std. Dev.	0.4679	N/A	0.1524	0.15
										Variance	0.2207	N/A	0.232	0.02
										5% LEL [b]	1.36	N/A	1.61	0.89
										75% CL	2.31-2.69	N/A	1.87-1.97	1.13-1.24
										C.V.	20.30	N/A	7.93	12.41

Note: a. Load Head Span.

b. 5% LEL = mean -(k * Std. Dev.), where k = 2.026.

c. Not applicable

Table 1.7. (Continued).

Grade	Species	Span	L/H	Width	Depth	Rein-	Bumper	Rein-	Actual	Design	Safety	Design	Measured	Safety
			Span			force-	Layer	force-	Ultimate	Ultimate	Factor	MOEbdng	MOEbdng	Factor
						ment		ment	Moment	Moment		x10e6 psi	x10e6 psi	
		(ft)	(ft)	(in)	(in)	Type		%	(lb-ft)	(lb-ft)				
V3-1600	D-fir	16.5	5.5	5.125	15.5	N/A	N/A	0.00	98450	26229	3.75	1.5	1.51	1.00
V3-1600	D-fir	26	8	5.125	21	N/A	N/A	0.00	128800	44628	2.89	1.5	1.63	1.09
V3-1600	D-fir	37	8	5.125	15.5	N/A	N/A	0.00	92438	24194	3.82	1.5	1.66	1.11
V3-1600	D-fir	39	8	5.125	27	N/A	N/A	0.00	254200	69084	3.68	1.5	1.71	1.14
										Sample size	4	4	4	4
										Mean	3.53	N/A	1.63	1.09
										Std. Err.	0.2182	N/A	0.0438	0.0292
										Std. Dev.	0.4364	N/A	0.0877	0.0585
										Variance	0.1905	N/A	0.0077	0.0034
										5% LEL	2.16	N/A	1.35	0.90
										75% CL	3.22-3.85	N/A	1.56-1.68	1.04-1.12
										C.V.	12.35	N/A	5.39	5.39

Note: 5% LEL = Mean - (k * Std. Dev.), where k = 3.152.

Table 1.7. (Continued).

Grade	Species	Span	L/H	Width	Depth	Rein-	Bumper	Rein-	Actual	Design	Safety	Design	Measured	Safety
			Span			force-	Layer	force-	Ultimate	Moment	Factor	MOEbdng	MOEbdng	Factor
		(ft)	(ft)	(in)	(in)	ment		ment	Moment			x10e6 psi	x10e6 psi	
						Type		%	(lb-ft)	(lb-ft)				
V3-1600	D-fir	16.5	5.5	5.125	15.5	ARP	Yes	2.90	148500	26229	5.66	1.5	1.8417	1.23
V3-1600	D-fir	16.5	5.5	5.125	15.5	ARP	Yes	2.90	145750	26229	5.56	1.5	1.9302	1.29
V3-1600	D-fir	24	8	5.125	21.5	ARP	Yes	2.51	278000	47044	5.91	1.5	1.9476	1.30
V3-1600	D-fir	24	8	5.125	21.5	ARP	Yes	2.51	277600	47044	5.90	1.5	1.5047	1.00
V3-1600	D-fir	37	8	5.125	15.5	ARP	Yes	2.90	163850	24194	6.77	1.5	2.1903	1.46
V3-1600	D-fir	37	8	5.125	15.5	ARP	Yes	2.90	145000	24194	5.99	1.5	2.2114	1.47
V3-1600	D-fir	39	8	5.125	25.75	ARP	Yes	1.75	317750	63134	5.03	1.5	1.6689	1.11
V3-1600	D-fir	39	8	5.125	27.25	ARP	Yes	1.65	325500	70304	4.63	1.5	1.8307	1.22
										Sample size	8	8	8	8
										Mean	5.68	N/A	1.89	1.26
										Std. Err.	0.0565	N/A	0.0847	0.0565
										Std. Dev.	0.1597	N/A	0.2395	0.1597
										Avriance	0.0255	N/A	0.0574	0.0255
										5% LEL	5.33	N/A	1.37	0.91
										75% CL	5.39-5.96	N/A	1.78-1.99	1.19-1.33
										C.V.	2.81	N/A	12.67	12.67

Note: 5% LEL = Mean - (k * Std. Dev.), where k = 2.190.

Table 1.7. (Continued).

Grade	Species	Span	L/H	Width	Depth	Rein-	Bumper	Rein-	Actual	Design	Safety	Design	Measured	Safety
			Span			force-	Layer	force-	Ultimate	Moment	Factor	MOEbdng	MOEbdng	Factor
		(ft)	(ft)	(in)	(in)	ment		ment	Moment			x10e6 psi	x10e6 psi	
						Type		%	(lb-ft)	(lb-ft)				
e-stack	pine	18	6	2.5	24	ARP	Yes	0.38	67800	14045	4.83	1.00	1.35	1.35
e-stack	pine	18	6	2.5	24	ARP	Yes	0.38	81000	14045	5.77	1.00	1.42	1.42
e-stack	pine	18	6	2.5	24	ARP	Yes	0.38	112500	14045	8.01	1.00	1.51	1.51
e-stack	pine	18	6	2.5	24	ARP	Yes	0.38	77400	14045	5.51	1.00	1.39	1.39
										Sample Size	4	4	4	4
										Mean	6.03	N/A	1.42	1.42
										Std. Err.	0.0450	N/A	0.0347	0.0347
										Std. Dev.	1.1983	N/A	0.0694	0.0694
										Variance	1.4360	N/A	0.0048	0.0048
										5% LEL	2.82	N/A	1.23	1.23
										75% CL	1.13-1.23	N/A	1.36-1.46	1.36-1.46
										C.V.	19.88	N/A	4.90	4.90

Note: 5% LEL = Mean - k*Std. Dev., where k = 2.68 for small sample size.

Table 1.7. (Continued).

Grade	Species	Span	L/H	Width	Depth	Rein-	Bumper	Rein-	Actual	Design	Safety	Design	Measured	Safety
			Span			force-	Layer	force-	Ultimate	Moment	Factor	MOEbdng	MOEbdng	Factor
		(ft)	(ft)	(in)	(in)	ment		ment	Moment			x10e6 psi	x10e6 psi	
						Type		%	(lb-ft)	(lb-ft)				
e-stack	pine	23	7.666	2.5	24	ARP	Yes	0.38	96975	13874	6.99	1.00	1.68	1.68
e-stack	pine	23	7.666	2.5	24	ARP	Yes	0.38	76660	13874	5.53	1.00	1.45	1.45
e-stack	pine	23	7.666	2.5	24	ARP	Yes	0.38	80493	13874	5.80	1.00	1.42	1.42
										Sample Size	3	3	3	3
										Mean	6.11	N/A	1.52	1.52
										Std. Err.	0.4492	N/A	0.0802	0.0802
										Std. Dev.	0.7780	N/A	0.1389	0.1389
										Variance	0.6053	N/A	0.0193	0.0193
										5% LEL	3.65	N/A	1.08	1.08
										75% CL	5.38-6.83	N/A	1.38-1.65	1.38-1.65
										C.V.	12.74	N/A	9.16	9.16

Note: 5% LEL = Mean - k*Std. Dev., where k = 3.152.

Table 1.7. (Continued).

Grade	Species	Span	L H Span	Width	Depth	Rein-force-ment Type	Bumper Layer	Rein-force-ment %	Actual Ultimate Moment (lb-ft)	Design Moment (lb-ft)	Safety Factor	Design MOEbdng x10e6 psi	Measured MOEbdng x10e6 psi	Safety Factor
		(ft)	(ft)	(in)	(in)									
e-stack	pine	29	8	2.5	24	ARP	Yes	0.38	80850	13714	5.90	1.00	1.39	1.39
e-stack	pine	29	8	2.5	24	ARP	Yes	0.38	82215	13714	5.99	1.00	1.32	1.32
e-stack	pine	29	8	2.5	24	ARP	Yes	0.38	78120	13714	5.70	1.00	1.41	1.41
e-stack	pine	29	8	2.5	24	ARP	Yes	0.38	92925	13714	6.78	1.00	1.26	1.26
e-stack	pine	29	8	2.5	24	ARP	Yes	0.38	75075	13714	5.47	1.00	1.37	1.37
e-stack	pine	29	8	2.5	24	ARP	Yes	0.38	87675	13714	6.39	1.00	1.32	1.32
										Sample Size	6	6	6	6
										Mean	6.04	N/A	1.35	1.35
										Std. Err.	0.1938	N/A	0.0225	0.0225
										Std. Dev.	0.4748	N/A	0.0551	0.0551
										Variance	0.2254	N/A	0.0030	0.0030
										5% LEL	4.93	N/A	1.22	1.22
										75% CL	5.79-6.29	N/A	1.32-1.38	1.32-1.38
										C.V.	7.86	N/A	4.09	4.09

Note: 5% LEL = Mean - k*Std. Dev., where k = 2.336.

Table 1.7. (Continued).

Grade	Species	Span	L H Span	Width	Depth	Rein-force-ment type	Bumper Layer	Rein-force-ment %	Actual Ultimate Moment (lb-ft)	Design Moment (lb-ft)	Safety Factor	Design MOEbdng x10e6 psi	Measured MOEbdng x10e6 psi	Safety Factor
		(ft)	(ft)	(in)	(in)									
e-stack	pine	30	8	2.5	24	ARP	Yes	0.38	44770	13691	3.27	1.00	1.15	1.15
e-stack	pine	30	8	2.5	24	ARP	Yes	0.38	69080	13691	5.05	1.00	1.54	1.54
e-stack	pine	30	8	2.5	24	ARP	Yes	0.38	68640	13691	5.01	1.00	1.54	1.54
e-stack	pine	30	8	2.5	24	ARP	Yes	0.38	91960	13691	6.72	1.00	1.30	1.30
e-stack	pine	30	8	2.5	24	ARP	Yes	0.38	98725	13691	7.21	1.00	1.36	1.36
e-stack	pine	30	8	2.5	24	ARP	Yes	0.38	77550	13691	5.66	1.00	1.27	1.27
e-stack	pine	30	8	2.5	24	ARP	Yes	0.38	88000	13691	6.43	1.00	1.39	1.39
										Sample Size	7	7	7	7
										Mean	5.62	N/A	1.36	1.36
										Std. Err.	0.5026	N/A	0.0538	0.0538
										Std. Dev.	1.3297	N/A	0.1423	0.1423
										Variance	1.7681	N/A	0.0202	0.0202
										5% LEL	2.63	N/A	1.04	1.04
										75% CL	5.66-6.26	N/A	1.30-1.43	1.30-1.43
										C.V.	23.65	N/A	10.44	10.44

Note: 5% LEL = Mean - k*Std. Dev., where k = 2.25.

Table 1.7. (Continued).

Grade	Species	Span	L/H	Width	Depth	Rein-	Bumper	Rein-	Actual	Design	Safety	Design	Measured	Safety
			Span			force-	Layer	force-	Ultimate	Moment	Factor	MOEbdng	MOEbdng	Factor
		(ft)	(ft)	(in)	(in)	ment		ment	Moment			x10e6 psi	x10e6 psi	
						type		%	(lb-ft)	(lb-ft)				
e-stack	pine	36	8	2.5	24	ARP	Yes	0.38	90720	13567	6.69	1.00	1.26	1.26
e-stack	pine	36	8	2.5	24	ARP	Yes	0.38	84280	13567	6.21	1.00	1.18	1.18
e-stack	pine	36	8	2.5	24	ARP	Yes	0.38	86800	13567	6.40	1.00	1.09	1.09
e-stack	pine	36	8	2.5	24	ARP	Yes	0.38	73700	13567	5.43	1.00	1.04	1.04
										Sample size	4	4	4	4
										Mean	6.1825	N/A	1.1463	1.1463
										Std. Err.	0.2684	N/A	0.0489	0.0489
										Std. Dev.	0.5368	N/A	0.0977	0.0977
										Variance	0.2881	N/A	0.0095	0.0095
										5% LEL	4.7439	N/A	0.8845	0.8845
										75% CL	5.80-6.54	N/A	1.08-1.22	1.08-1.22
										C.V.	8.68	N/A	8.52	8.52

Note: 5% LEL = Mean - k*Std. Dev., where k = 2.68.

Table 1.7. (Continued).

Grade	Species	Span	L/H	Width	Depth	Rein-	Bumper	Rein-	Actual	Design	Safety	Design	Measured	Safety
			Span			force-	Layer	force-	Ultimate	Moment	Factor	MOEbdng	MOEbdng	Factor
		(ft)	(ft)	(in)	(in)	ment		ment	Moment			x10e6 psi	x10e6 psi	
						type		%	(lb-ft)	(lb-ft)				
1	D-fir	23	7.67	5.125	21	APR	Yes	0.86	175643	42355	4.15	1.5	1.87	1.25
1	D-fir	23	7.67	5.125	21	APR	Yes	0.86	184080	42355	4.35	1.5	1.75	1.17
1	D-fir	24	8	5.125	21	APR	Yes	0.86	175200	42175	4.15	1.5	1.82	1.21
										Sample size	3	3	3	3
										Mean	4.22	N/A	1.81	1.21
										Std. Err.	0.0652	N/A	0.0348	0.0231
										Std. Dev.	0.1160	N/A	0.0603	0.0400
										Variance	0.0128	N/A	0.0036	0.0016
										5% LEL	3.85	N/A	1.62	1.08
										75% Cl	4.11-4.32	N/A	1.76-1.87	1.17-1.25
										C.V.	2.75	N/A	3.33	3.31

Note: 5% LEL = Mean - k*Std. Dev., where k = 3.152.

Table 1.7 (Continued).

Grade	Species	Span	L/H Span	Width	Depth	Rein-force-ment type	Bumper Layer	Rein-force-ment %	Actual Ultimate Moment (lb-ft)	Design Moment (lb-ft)	Safety Factor	Design MOEbdng x10e6 psi	Measured MOEbdng x10e6 psi	Safety Factor
		(ft)	(ft)	(in)	(in)									
1	D-fir	30	8	2.5	24	APR	Yes	0.38	88000	27860	3.16	1.5	VN/A *	VN/A
1	D-fir	30	8	2.5	24	APR	Yes	0.38	78650	27860	2.82	1.5	VN/A	VN/A
1	D-fir	30	8	2.5	24	APR	Yes	0.38	99000	27860	3.55	1.5	VN/A	VN/A
1	D-fir	30	8	2.5	24	APR	Yes	0.38	99000	27860	3.55	1.5	VN/A	VN/A
										Sample size	4	VN/A	VN/A	VN/A
										Mean	3.27	VN/A	VN/A	VN/A
										Std. Err.	0.1763	VN/A	VN/A	VN/A
										Std. Dev.	0.3526	VN/A	VN/A	VN/A
										Variance	0.1243	VN/A	VN/A	VN/A
										5% LEL	2.33	VN/A	VN/A	VN/A
										75% CI	3.02-3.52	VN/A	VN/A	VN/A
										C.V.	10.78	VN/A	VN/A	VN/A

Note: 5% LEL = Mean - k * Std. Dev., where k = 2.680.

Statistical analysis was conducted based on the available data.

* Values not available

Table 1.7 (Continued).

Grade	Species	Span	L H Span	Width	Depth	Rein-force-ment type	Bumper Layer	Rein-force-ment %	Actual Ultimate Moment (lb-ft)	Design Moment (lb-ft)	Safety Factor	Design MOEbdng x10e6 psi	Measured MOEbdng x10e6 psi	Safety Factor
		(ft)	(ft)	(in)	(in)									
1	D-fir	53	8	8.75	43	APR	Yes	1.47	1395000	246099	5.67	1.5	1.69	1.13
1	D-fir	53	8	8.75	43	APR	Yes	1.47	1845000	246099	7.50	1.5	1.75	1.17
1	D-fir	53	8	8.75	43	APR	Yes	1.47	1845000	246099	7.50	1.5	1.66	1.11
1	D-fir	53	8	8.75	42.5	APR	Yes	1.48	1503000	240690	6.24	1.5	2.01	1.34
1	D-fir	53	8	8.75	42.5	APR	Yes	1.48	1445625	240690	6.01	1.5	1.50	1.00
1	D-fir	53	8	8.75	41.5	APR	Yes	1.52	1800000	230044	7.82	1.5	N/A	N/A
1	D-fir	53	8	8.75	42	APR	Yes	1.5	765000	235338	3.25	1.5	N/A	N/A
1	D-fir	53	8	8.75	43	APR	Yes	1.47	1012500	246099	4.11	1.5	N/A	N/A
										Sample size	5	5	5	5
										Mean	6.58	N/A	1.62	1.15
										Std. Err.	0.3843	N/A	0.1673	0.0552
										Std. Dev.	0.8594	N/A	0.3741	0.1235
										Variance	0.7386	N/A	0.14	0.0153
										5% LEL	4.47	N/A	0.70	0.85
										75% CI	6.06-7.09	N/A	1.40-1.84	1.10-1.22
										C.V.	13.06	N/A	23.06	10.74

Note: 5% LEL = mean - (k * Std. Dev.), where k = 2.463.
Statistical analysis was conducted based on the available data.

strength enhancement than modulus enhancement. The measured modulus for the unreinforced glulams was greater than expected as given by the design standard [NFPA, 1991]. Unreinforced glulam beam bending deflection curves were used to calculate an unreinforced E value of 1.62×10^6 psi (15,380 MPa) which is 8% higher than the published value for this grade and species.

Visual observations of knot size revealed that by limiting knot size to 20% of the width of the lamination in the wood laminations adjacent to the FRP an increase in strength was achieved in the reinforced glulam. All L-3 Douglas-fir beams found in Table 1.7 with low safety factors (2.82 and 3.25) failed at large knots in laminations adjacent to the FRP.

It was noted from visual observations, that increasing the percentage of reinforcement limited the effect of finger joint failures on beam strength. The all L-3 Douglas-fir beams show a definite increase in beam capacity with increase in percentage FRP. Visual observations of these beam failures showed that the failure of finger joints was not as great a factor in overall beam failures in beams with a higher percentage of reinforcement.

The FRP reinforcement lead to a reduction in CoV of the beam strength values. An example of this is shown by the V3-1600 Douglas-fir beam groups where reinforcement reduced the CoV of MOR from 12.35% to 2.81%. The greatest improvement in strength was found in Ponderosa pine beams which also had low CoV's and high safety factors. The equivalent grade of conventional unreinforced glulam would have bending strength CoV's in the 25-30% range [AITC 500, 1978].

Table 1.8 contains an analysis of variance (ANOVA) of the different groups of reinforced and unreinforced glulams shown in Table 1.7. The ANOVA's show that the reinforced V3-1600 Douglas-fir beam safety factors are different than the unreinforced V4-2400 Douglas-fir beams; this is shown in sections 4 and 5 of Table 1.8. When considering the beam capacity, using high percentages of reinforcement, the V3-1600 reinforced beams populations are again different from the V4-2400's with higher strength and stiffness and lower CoV's 20.32 versus 2.81 (see Table 1.7). The results of FRP reinforced glulam testing agreed with the results of similar testing by other researchers who have also shown substantial increases in strength in FRP reinforced glulams [Davalos and Barbero, 1991; van de Kuilen, 1991] as compared to conventional glulam. The ANOVA of this data demonstrated that the use of reinforcement dramatically changes the beam populations such that reinforced beams are significantly different from unreinforced and conventional glulam.

It was theorized that as the reinforced glulam beam underwent loading, the reinforcement absorbed more stress than predicted by conventional theory according to transformed section and position in the beam. The reinforcement stiffness is much greater than wood and allows localized strains in the compressive zone to redistribute as the various wood regions strain with increased applied stresses. Subsequently, compressive plasticity lowers the neutral axis. By this process, overall member deflection under load is reduced more than predicted. The additional stress absorption is attributed in part to the homogeneous nature of the reinforcement which leads to more consistent modulus properties in tension than wood along the length of a beam. The CoV of stiffness

Table 1.8. Analysis of variance on moment safety factors of reinforced and unreinforced glulams.

1. Ponderosa Pine e-stack reinforced versus V4-2400 unreinforced glulam beams on safety factor based on application of reinforcement.

Source	D.F.	Sum of Squares	Mean Squares	F-ratio	F-Prob
Between Groups	1	111.8844	111.8844	168.2277	0.0000
Within Groups	35	23.2777	0.6651		
Total	36	135.1621			

2. Ponderosa Pine e-stack reinforced versus V3-1600 unreinforced glulam beams on safety factor based on the application of reinforcement.

Source	D.F.	Sum of Squares	Mean Squares	F-ratio	F-Prob
Between Groups	1	19.9582	19.9582	24.4756	0.0000
Within Groups	26	21.2012	0.8154		
Total	27	41.1594			

3. V3-1600 reinforced versus V3-1600 unreinforced glulam beams on safety factor based on the application of reinforcement.

Source	D.F.	Sum of Squares	Mean Squares	F-ratio	F-Prob
Between Groups	1	12.2946	12.2946	35.1148	0.0001
Within Groups	10	3.5013	0.3501		
Total	11	15.7958			

4. V3-1600 reinforced versus V4-2400 unreinforced glulam beams on safety factor based onthe application of reinforcement.

Source	D.F.	Sum of Squares	Mean Squares	F-ratio	F-Prob
Between Groups	1	56.4799	56.4799	192.3941	0.0000
Within Groups	19	5.5777	0.2936		
Total	20	62.0576			

5. V3-1600 unreinforced versus V4-2400 unreinforced glulam beams on safety factor based on the grade.

Source	D.F.	Sum of Squares	Mean Squares	F-ratio	F-Prob.
Between Groups	1	4.6247	4.6267	21.5574	0.0003
Within Groups	15	3.2194	0.3346		
Total	16	7.8461			

and ultimate stress in the reinforcement in tension is less than 2%. The reinforcement only allows the beam to deflect at a rate compatible with the reinforcement E value which has a low CoV and more consistent strength properties over its length and width.

Reinforced beams were found to have much more critical lateral stability requirements if unreinforced in the compressive zone. This is a result of compressive plasticity generated in the compressive laminae by the resisting moment couple [ICBO, 1995]. The compressive plasticity leads to a reduced critical length for lateral-torsional buckling.

In reinforced glulams, the strength of the tensile finger joints in tension and the compressive strength of the wood directly affected the minimum amount of tensile reinforcement that was needed as a percentage of the cross-section [ICBO, 1995]. For finger joints having a 5,200 psi (36 MPa) average lower extreme tensile stress region [AITC, 1992] used in conventional 2400 psi (16.55 MPa) unreinforced glulams, it was shown that the minimum percentage of tensile reinforcement required was 0.15% by cross-sectional area [ICBO, 1995]. The effects of finger joint strength and other localized characteristics, such as knots, on the extreme tensile strength in bending members make compressive reinforcement unacceptable without tensile reinforcement. This criteria for the use of tensile reinforcement allows the use of compression-based design formulas that are much the same as reinforced concrete [ICBO, 1994; Tingley, 1990; Tingley, 1994a; Tingley, 1994b; Tingley and Leichti, 1993; Tingley and Leichti, 1994a; Tingley and Leichti, 1994b; Tingley and Leichti, 1994c].

Conclusions

The material characteristics investigations have shown that the FRP is compatible with wood. The FRP characteristics that are most important for use as a wood reinforcement are modulus of elasticity in tension and compression, tensile capacity, shear capacity and strain at yield point. The tensile strain at yield point for the FRP , must be greater than that of wood. However, the strain at yield point for the FRP should not exceed that of wood by a substantial amount since it is important to match the strain at yield point between the FRP and wood to maximize the energy absorption potential of the FRP.

The low strength and stiffness variability's of FRP contribute to reduced strength and stiffness variability in FRP-reinforced glulam. The full-scale FRP-reinforced glulam tests have shown that the hypothesis's were true. Firstly there was a substantial reduction in variability of beam strengths. The increase in bending capacity for the various beam types was as high as 185%. The increase in stiffness was as high as 35%. The effect of finger joints was substantially reduced in beams with a greater percentage of reinforcement by cross-section. In addition, it was observed that reduced knot size in laminations adjacent to the FRP improved the reinforced glulam capacity. The use of E-stacking improved the bending capacity and stiffness substantially and allowed more ductility in the reinforced glulam. The increases in strength and stiffness caused by FRP reinforcement were greater in lower grade glulams than in higher grade glulams.

CHAPTER 2

AN INVESTIGATION OF MATERIAL ORTHOTROPY AND STRESS DISTRIBUTIONS IN REINFORCED GLULAM BEAMS

Daniel A. Tingley
Robert J. Leichti

For Submission to
Journal of Materials in Civil Engineering

Introduction

The stress-strain distributions in a reinforced glulam beam differ in some important respects from that predicted by conventional theory. Typical isotropic analyses using linear finite-element analysis provide generally useful estimations of stress distributions throughout a reinforced beam. However, there are some very important variations that are caused by the wood material anisotropy and non-homogeneous character. Further, reinforcement that is unidirectional, macroscopically homogeneous, and aligned with the longitudinal direction of the beam tends to complicate the stress-strain analysis of the reinforced glulam beam.

It is important to first understand stress-strain distributions throughout the width, depth, and length of the reinforced beam, particularly in the area of the reinforcement-wood interface. Observation of laboratory testing of FRP reinforced glulams in Chapter 1 has provided evidence that local features, such as knots in the near proximity of the reinforcement-wood interface are critical to beam load capacity and failure characteristics. This chapter explores the stress-strain distributions in a reinforced glulam beam.

Objective

The objective of the work described in this chapter was to examine the analytical stress-strain distribution of reinforced glulams and compare it to an experimental investigation of full-scale test beams.

Background Information

Previous researchers have investigated the strain distributions in glulams by using the finite-element analysis (FEA) techniques and strain gauging of test samples. Kirlin [1996] modeled strain distributions at the end of the FRP in partial length reinforced glulams using FEA techniques. Gopu and Yearly[1991] studied radial reinforcement in curved arches and used FEA techniques to analyze the composite radial strain distributions. Mathematical models involving large matrix manipulation have been proven successful in prior research for analysis of similar situations involving stress distributions [Serabian and Oplinger, 1987].

Previous researchers have investigated finite-element analysis approaches with timber involving Von Mises' theory. The theory predicts elemental failure when the energy input level equals that required to cause axial tensile failure in the elements. However, the theory is not effective when considering wood's anisotropic and non-homogenous nature.

Very little research involving strain gauges used with reinforced glulams has been conducted. Tingley [1988] conducted such testing and established vertical, axial, compressive, and tensile stress distributions. The results indicated a reasonable level of reliability in the data, provided that a control gauge for temperature balancing was used. Axial strain distributions through the depth of the beam were plotted and were reasonably approximated by mechanics of materials methods.

Hooke's Law

The linear-elastic response of a material to applied load is described by Hooke's Law. Wood material can be linear and nonlinear depending upon the direction of the loading with respect to grain, magnitude of the load, and sense of the load (tensile or compressive). Elastic strains, ε_i, in response to applied stress, σ_i, in a particular direction, are termed active strains. Wood responds to applied stress in the active direction with ε_j passive strain in the lateral direction. The ratio of passive strain to active strain is the Poisson's ratio, μ_{ij} (Equation 2.1).

$$\mu_{ij} = - \varepsilon_j \text{ (passive)}/\varepsilon_i \text{ (active)} \qquad 2.1$$

Wood exhibits a special case of properties symmetry making it an "orthotropic" material [Bodig and Jayne, 1993]. Due to the cylindrical nature of wood and annual growth rings, the planes of orthotropy are generally assigned to the radial (R), tangential (T), and longitudinal (L) directions. Thus, stress-strain relationships are often related to these three planes. In sawn lumber used in glulams, it is generally difficult to control orientation of the tangential and radial planes. Thus, the transverse directions (width and depth) are assumed to be averaged and referred to as the tangential-radial (TR) plane (Figure 2.1).

The underlying assumptions to Hooke's law include constant temperatures, small deformations, and no coupling between stress components. This is not to say that these assumptions are correct, only that this approach is commonly used to allow mathematical modeling of the response of wood to applied stresses. Tensor matrix methods have been in use for wood stress-strain analysis for many years [Bodig and Jayne, 1993]. Although

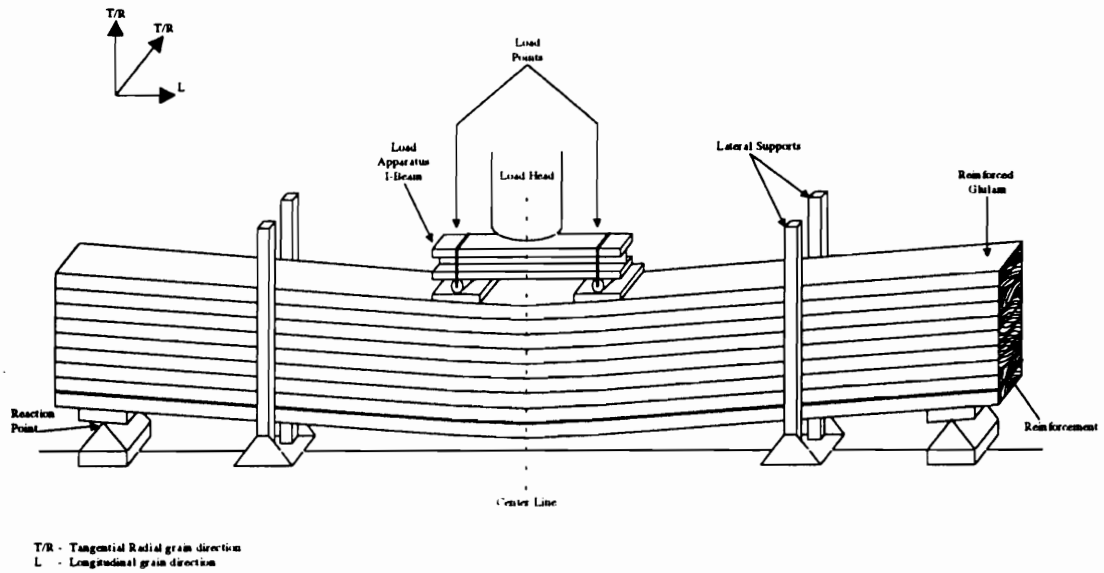

Figure 2.1. Simply supported beam in bending with two load application points.

closed- form solutions, various problems have been developed by others such as Lekhnitskii [1979].

Equations 2.2 and 2.3 show a typical three-dimensional Hooke's Law relationship between stress and strain using either strains as linear functions of stresses related to each other by compliance coefficients, S_{ijkl}, (Equation 2.2) or stresses as linear functions of strains related to each other by stiffness coefficients, C_{ijk}, (Equation 2.3).

$$\varepsilon_{ij} = S_{ijkl}\,\sigma_{kl}\,. \qquad 2.2$$

Where

ε_{ij} = Strain tensor

S_{ijkl} = Compliance tensor

σ_{ij} = Stress tensor

$$\sigma_{ij} = C_{ijkl}\,\varepsilon_{kl}\,. \qquad 2.3$$

Where

σ_{ij} = Stress tensor

C_{ijkl} = Stiffness tensor

ε_{kl} = Strain tensor

The stiffness tensor, C_{ijkl}, is the inverse of the compliance tensor, S_{ijkl}. Expanding equation 2.2 and using the indicial notation leads to Equation 2.4.

$$\begin{bmatrix} \gamma_1 \\ \gamma_2 \\ \gamma_3 \\ \gamma_4 \\ \gamma_5 \\ \gamma_6 \end{bmatrix} = \begin{bmatrix} S_{11} & S_{12} & S_{13} & 0 & 0 & 0 \\ S_{21} & S_{22} & S_{23} & 0 & 0 & 0 \\ S_{31} & S_{32} & S_{33} & 0 & 0 & 0 \\ 0 & 0 & 0 & S_{44} & 0 & 0 \\ 0 & 0 & 0 & 0 & S_{55} & 0 \\ 0 & 0 & 0 & 0 & 0 & S_{66} \end{bmatrix} \begin{bmatrix} \sigma_1 \\ \sigma_2 \\ \sigma_3 \\ \sigma_4 \\ \sigma_5 \\ \sigma_6 \end{bmatrix} \qquad 2.4$$

Equation 2.5 applies to a specially orthotropic material where the material coordinates and the geometric coordinates are aligned. Notations 1, 2, and 3 represent L, R, and T directions respectively in wood.

By symmetry it can be shown that only nine independent parameters exist in the compliance matrix of equation 2.4 since $S_{ij} = S_{ji}$ [Bodig and Jayne, 1993; Jayne and Hunt, 1976]. From equation 2.4, it can be shown that shear stresses produce shear strains, and that normal stresses do not produce shear strains. The equations for strain at a point in the wood and the FRP are given in equations 2.5 and 2.6.

$$\varepsilon_1 = \gamma_1 = \gamma_L = \frac{1}{E_L}\left(\sigma_L - \mu_{L(R/T)}\sigma_R - \mu_{L/(R/T)}\sigma_T\right) \qquad 2.5$$

$$\varepsilon_2 = \gamma_2 = \gamma_R = \frac{1}{E_R}\left(\sigma_R - \mu_{(R/T)\text{-}L}\sigma_L - \mu_{RT}\sigma_T\right) \qquad 2.6$$

Refinement of equation 2.4 for a plane stress problem yields equation 2.7. Since $\tau_{L\text{-}T/R}$, τ_{TR} and $\sigma_{T/R}$ are thought to be small, they are negligible in a plane stress analysis.

$$\begin{bmatrix} \gamma_L \\ \gamma_{R/T} \\ \gamma_{L(R/T)} \end{bmatrix} = \begin{bmatrix} \frac{1}{E_L} & \frac{-\mu_{R/T}}{E_R} & 0 \\ \frac{-\mu_{L/(R/T)}}{E_L} & \frac{1}{E_R} & 0 \\ 0 & 0 & \frac{1}{G_{L/(R/T)}} \end{bmatrix} \begin{bmatrix} \sigma_L \\ \sigma_{R/T} \\ \sigma_{L/(R/T)} \end{bmatrix} \qquad 2.7$$

Table 2.1 contains elastic parameters used for this study and the relationships between various properties. These relationships are used with stiffness matrices to convert strain gauge readings to stresses. Equation 2.6 is used in this approach.

This simplified procedure provides a basic understanding of the process by which the stresses were calculated.

Wood has unique relationships between various elastic properties. This is particularly true in its relationship between G_{ij} and E_i. In most materials used in a structural capacity, such as steel, G is 0.33 E. In addition, the shear strength of steel is about one-half its tensile strength. The G_{LR} value for wood is 1/14 of the E_L value [Bodig and Jayne, 1993; Sliker, 1962].

Table 2.1. Mechanical and elastic properties for Douglas-fir [Bodig and Jayne, 1993].

Approximate Specific Gravity[a]	0.5
Approximate Moisture Contents (%)	12
Ultimate Shear Stress[d] (psi)	326
Ultimate Shear Strain [b,d] (in/in)	0.0022
Modulus of Elasticity Tension[d] (psi)	2.20×10^6
Modulus of Elasticity Compression[d] (psi)	2.08×10^6
Ultimate Tensile Stress[d] (psi)	12400
Ultimate Tensile Strain[d] (in/in)	0.2166
Ultimate Compressive Stress[d] (psi)	7240
Ultimate Compressive Strain[d] (in/in)	0.2474

Modulus of Elasticity Ratios[d]		G/E Ratios			Poisson's Ratios[c]					
E_T/E_L	E_R/E_L	G_{LR}/E_L	G_{LT}/E_L	G_{RT}/E_L	μ_{LR}	μ_{LT}	μ_{RT}	μ_{RL}	μ_{TR}	μ_{TL}
0.05	0.068	0.064	0.78	0.007	0.292	0.499	0.390	0.287	0.020	0.022

Note: a. Based on ovendry weight and volume at the moisture content shown.
b. Based on ASTM D-143 Test at 72° F.
c. Values from Bodig and Jayne (1993).
d. Average value of test results.

Homogeneity

Wood is characterized as nonhomogeneous, but within any plane of symmetry, it has variations in properties. Homogeneity variations in the glulam are caused by features such as knots, wood density variation, or finger joints. This nonhomogeneous characteristic means that the elastic and strength properties are different at all points within the lamination. For example, a knot could cause the E_L in tension to drop or increase substantially at a point. Nonhomogeneity often explains why elementary analysis methods provide inaccurate predictions of wood response to applied stress at a point.

Finite-Element Analysis of Glulams

Recent developments in personal computers allow faster computation of larger matrices used in finite-element analysis (FEA) methods, thus, the advanced evolution of personal computer software for FEA such as SAP90 [SAP90®, 1990] and ANSYS® [ANSYS, 1992]. Finite-element analysis modeling in solid wood has also been completed by many researchers such as Herakovich et al., [1981]. In addition, FRP composite FEA modeling has been completed by others [Carrara and McGarry, 1969; Termonia, 1992, Kirlin, 1996]. Mathematical modeling and FEA methodology has recently been used to predict stress distributions in FRP reinforced glulams [Davalos and Barbero,1991]. Davalos and Barbero [1991] used rectangular orthotropy and ignored the curvature of the growth increments. They found that this case of special orthotropy worked reasonably well.

Two methods involving mathematical modeling are commonly used to simulate loading on a reinforced glulam [Kasal et al., 1994], the stepwise loading method and the convergence approach. The stepwise loading method involves incremental loading with a stress-strain analysis after each increment. Software is used to perform matrix calculations after each load increment. Each element is monitored and when predefined limits of strain and/or stresses are reached, either the element is deemed to have failed and the system integrity compromised, or the elemental properties are adjusted and the system stepwise loading continued. This process of stepwise loading with corresponding monitoring and adjustment allows isolation of stress concentrations very effectively.

The second approach advances each element to a point where the status on one of the elements changes. At this point, the solution for that load cycle will not converge [Kasal et al., 1994]. This procedure is traditionally followed until all of the elements have moved to this status and failure is declared. This method assumes the failed element no longer contributes to the overall member load response.

In wood, certain element properties may have residual strength characteristics even after failure in certain strength properties, e.g., shear failure while maintaining compression strength. Also varying properties in wood depending upon stress level (e.g., wood in compression) make the convergence method difficult to monitor. The stepwise methodology offers better monitoring and elemental property adjustment, assuming elemental properties are well known.

Procedures

Analytical Procedure

The procedure used to meet the objectives consisted of a combination of conventional isotropic beam theory analysis and FEA coupled with full-scale reinforced glulam beam testing using strain gauges.

Conventional Isotropic Theory. Stress analysis methods based on elementary beam theory and isotropic materials were used to predict axial stresses in compression and tension as well as shear stresses. The component test data for E-values of individual laminations for various grades of wood provided basic data for the estimations of stresses and strains at various points of interest for comparison with experimental data.

Finite-Element Analysis Analytical Method. It was concluded in Chapter 1 that reinforced glulams with percentages of reinforcement less than 1.5% by cross-section fail primarily as a result of tensile failure at discontinuities in the tensile laminae adjacent to the FRP. This study used FEA methods to predict stress-strain distributions in a full-scale member where the elements operate within elastic limits. Therefore, the FEA was performed in the elastic range ignoring the nonlinearity in the extreme fibers of the compressive laminae. For the same reasons, stepwise modeling was not used in this experiment.

Subsequently, the predicted stress-strain distribution as calculated using FEA was compared to actual stress-strain distributions obtained by strain gauge stress analysis of full-scale test beams.

For analysis of the reinforced glulam beams, square or rectangular two-dimensional solid elements best suited the analysis. The element was defined by four nodes, each having two degrees of freedom in the x and y directions. The element was oriented such that the local coordinate system was parallel to the global coordinate system. For the purposes of this study, plasticity, creep, temperature and moisture effects, and reinforcement-matrix slip were not considered. Figure 2.2 is a diagram of the plane stress elements.

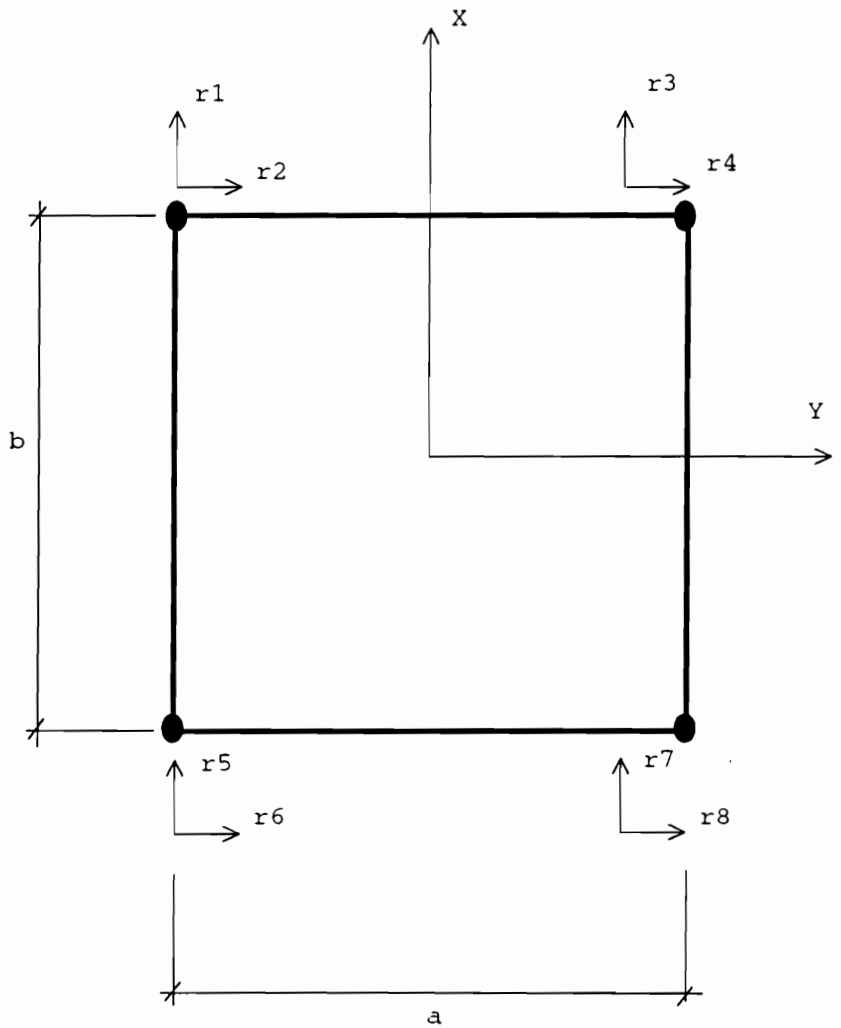

Figure 2.2. Diagram of the two-dimensional rectangular element.

The wood beam was modeled as a continuum with the wood and FRP having properties shown in Appendix F. There were no glue elements and wood and FRP were assumed to be connected at a node The beam size modeled was 8.75 in x 42.5 in x 53 ft (222 mm x 1,080 mm x 16,154 mm) with .5 in (12.7 mm) of ARP, FRP reinforcement between the bottom two tension laminations. Due to limitations on the number of nodes and elements, symmetry was assumed about the mid span. Further, the element size used was large at 8.75 in (222 mm) square for the wood. The element size in the FRP was 8.75 in (222 mm) long by 0.5 in (12.7 mm) high. Also, the E values used for wood in tension and compression did not exactly match a particular beam tested.

Experimental Procedure

The full-scale, fully reinforced glulam beams tested in flexure and ultimately to failure (shown in Chapter 1) were used to enable refinement of the finite-element analysis results and to verify predicted stress-strain distributions. For some beams, strain gauges were placed through the width between laminations as well as on the surfaces (top, bottom, and sides) and monitored by computer-controlled acquisition. Appendix C describes the strain gauge application, equipment, and monitoring procedures used for strain data gathering.

The experimental strain data were converted to stress data by using the modulus of elasticity data gathered from component testing reported in Chapter 1 and shear modulus values reported in the literature together with equations 2.5-2.7. Regression analysis and averaging techniques were used to smooth stress contours throughout the beam

(Appendix C). This was necessary to compensate for localized grain variation, wood specific gravity changes and the influence of other features such as knots.

The stress distribution data gathered from finite-element analysis were compared to data gathered from physical testing. The purpose of the comparison was to interpret important stress distribution characteristics in reinforced glulam.

Results and Discussion

Analytical Results

The case of a simply supported beam in bending with two load application points as shown in Figure 2.1 was considered. The material was assumed to be isotropic and homogeneous. A calculation of the stress distributions in the reinforced glulam beam was completed using conventional beam theory [Gere and Timoshenko, 1990]. The distribution of axial compressive and tensile stresses, vertical stresses as well as shear stresses in the xy plane are shown in Figures 2.3 to 2.5, respectively.

An FEA analysis was performed using SAP90®. Axial compressive and tensile stresses, compressive stresses perpendicular to grain (vertical stresses) and shear distributions in the xy plane were predicted for a reinforced glulam. The input and outputs can be found in Appendix F. The outputs resembled those predicted by theory except for stresses around discontinuities. The shear stress distributions in the xy plane, however, were slightly different. Improvement of the FEA model by consideration of discontinuities would improve the accuracy of the stress-strain distribution predictions.

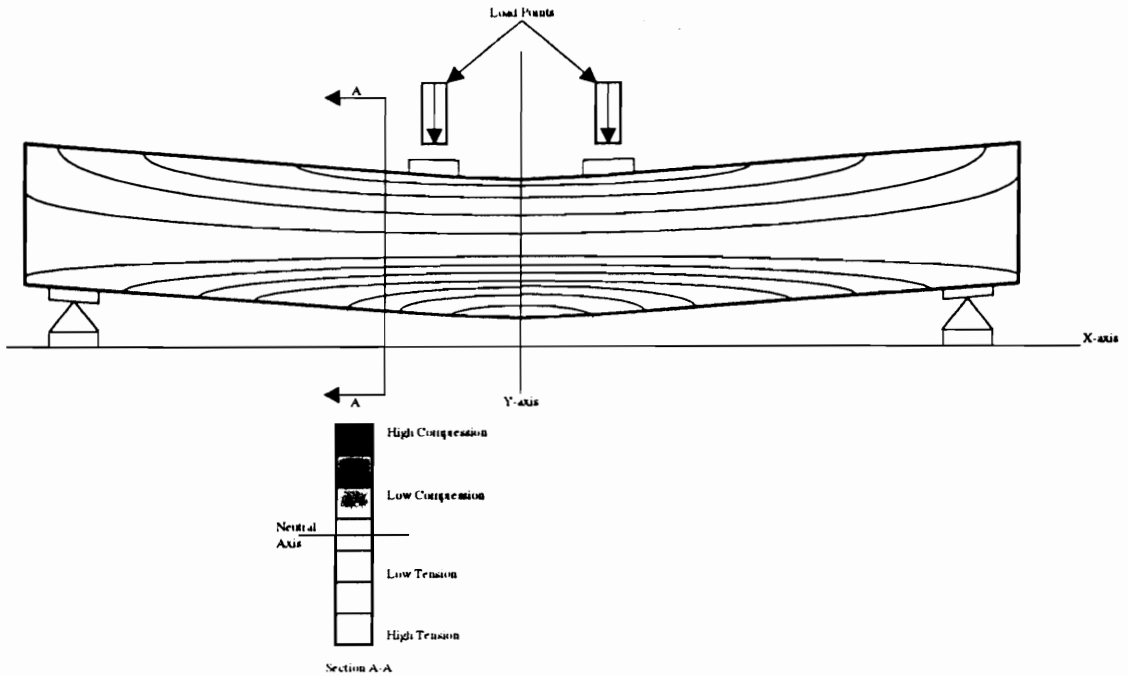

Figure 2.3. Theoretical axial compressive and tensile stress distribution in a reinforced glulam beam as predicted assuming isotropy and conventional beam theory.

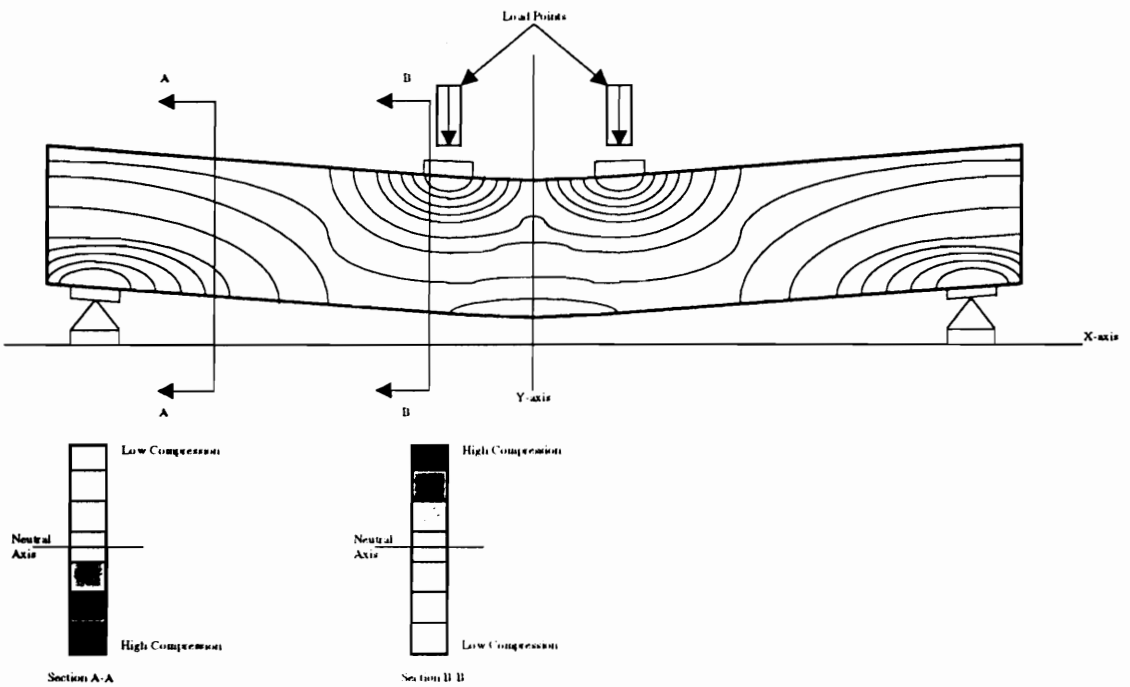

Figure 2.4. Theoretical vertical stress distribution in a reinforced glulam beam as predicted assuming isotropy and conventional beam theory.

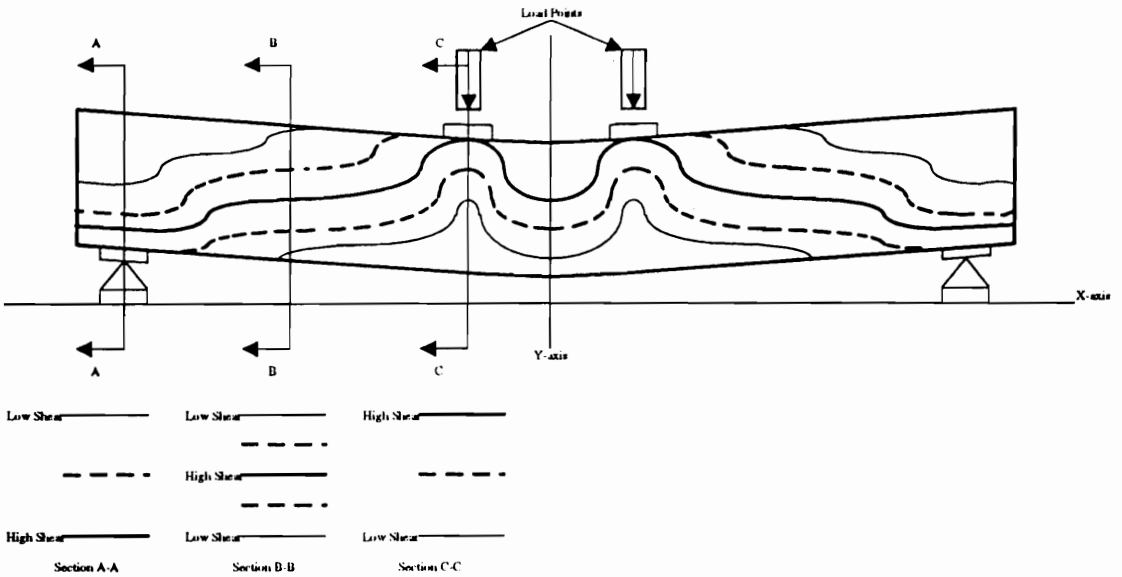

Figure 2.5. Theoretical shear stress distribution in x-y plane in a reinforced glulam beam as predicted assuming isotropy and conventional beam theory.

Experimental Results

Figures 2.6, 2.7, and 2.8 show actual horizontal (x), vertical (y), and shear stress (x-y) distributions, respectively, determined from strain gauges. The effects of knots and localized defects can be observed in the irregular stress contour lines. These figures are obtained from strain gauge measurements on glulam beams in various configurations and merging results (Appendix C). The actual stress contour lines are more irregular reflecting a wide variety of MOE values throughout the beam caused by grain differences, knots, finger joints, etc. These beams were manufactured using Douglas-fir, AITC combination

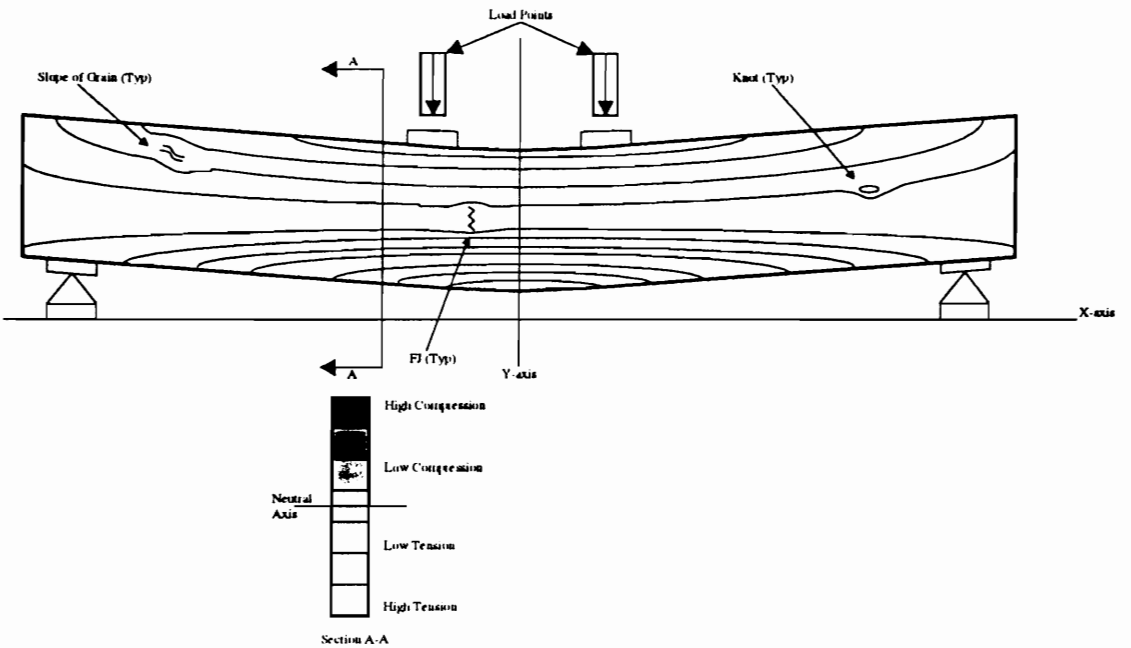

Figure 2.6. Actual axial compressive and tensile stresses in a reinforced glulam beam.

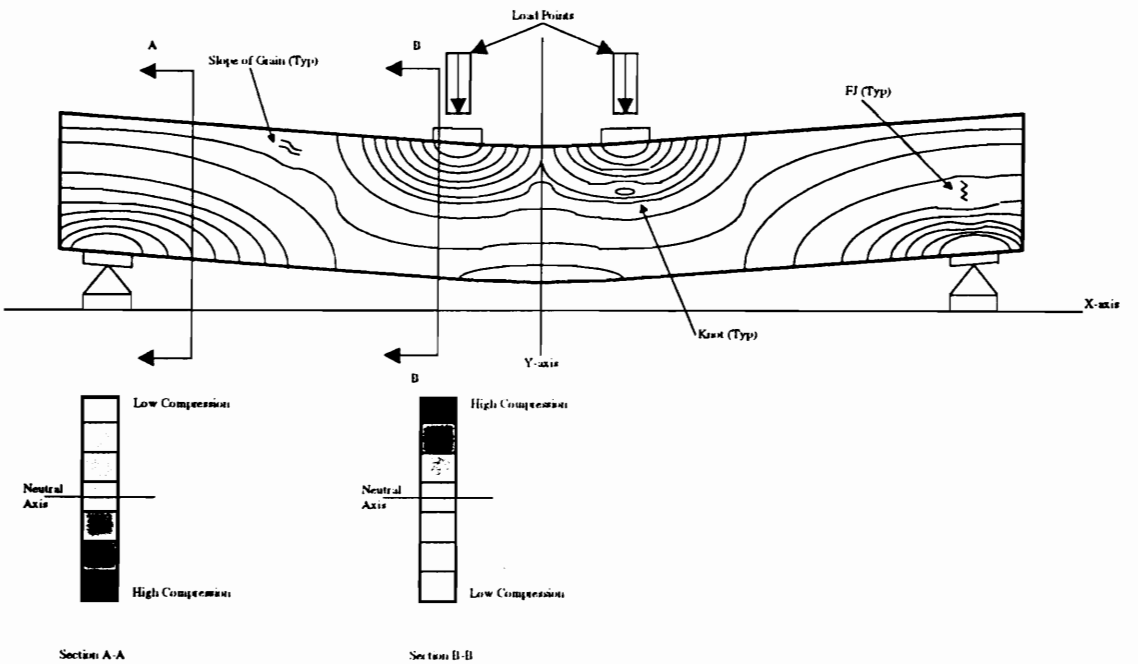

Figure 2.7. Actual vertical stresses in a reinforced glulam beam.

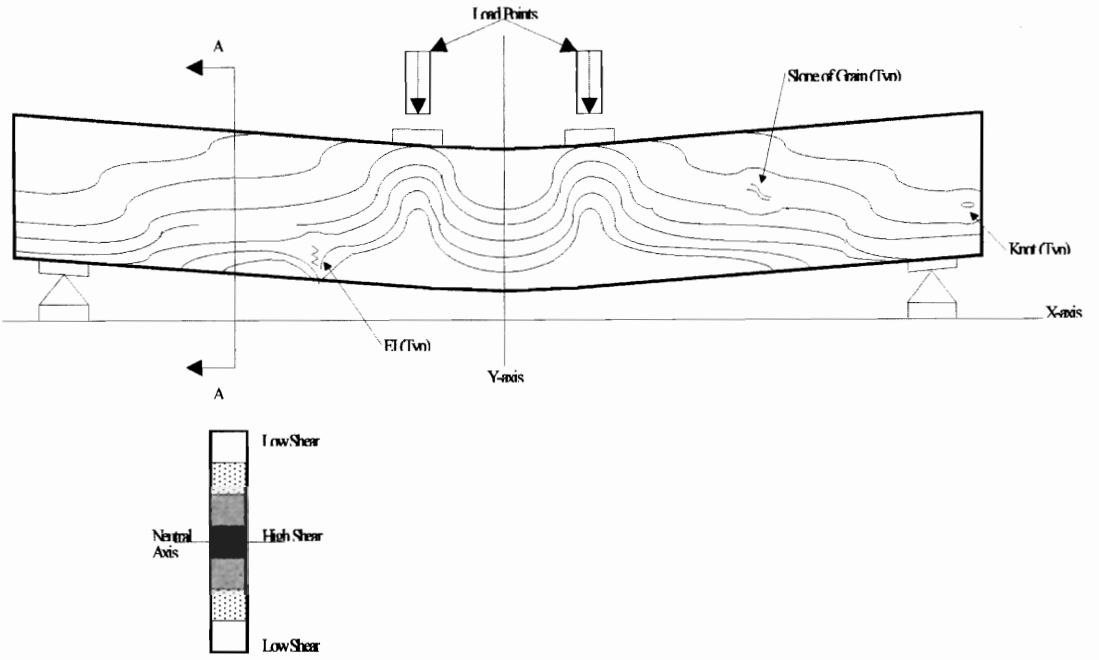

Figure 2.8. Actual shear stresses in a reinforced glulam beam.

1, with two layers of ARP on bottom face (0.070 in. thick, full width) full length of the beam (1.1% reinforcement by cross-section).

The reinforcement caused the axial stress contour lines to move downward resulting in a lowering of the neutral axis. The normal bending stresses for a reinforced glulam through the depth of a reinforced glulam beam is shown in Figure 2.9. Further, the stress contour lines have a sharp gradient adjacent to the reinforcement in the axial distribution. The vertical stress distribution showed contour lines more heavily concentrated at sites around load heads and reaction points. The shear stress maximum values were lower than expected at the neutral axis. This causes a perceived higher shear strength in the central region of the beam due to reduced applied shear stresses in the region.

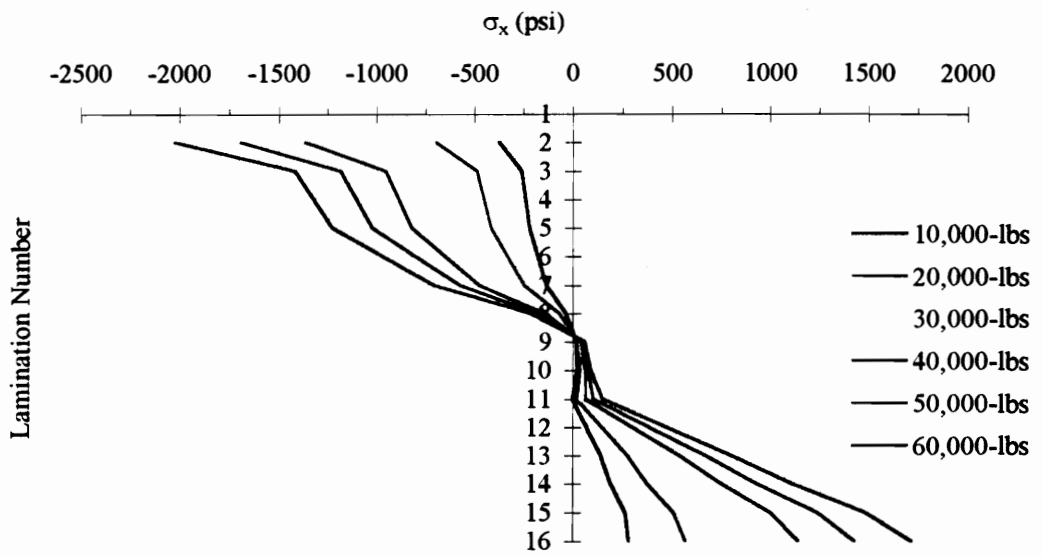

Figure 2.9. Normal stress, σ_x, distribution through the depth of reinforced glulam beam.

The shear stress distribution can be affected by both the reinforcement as well as the test apparatus. Figure 2.10 shows the compressive stress in the xy plane in the beam at the load head. Figure 2.11 shows the compressive stress in the xy plane in the beam at the reaction point. Figure 2.10 and Figure 2.11 show strain gauge results from a Douglas-fir glulam, 5.125 x 12 in. x 15 ft. (130 x 305 mm x 4570 mm) composed of all L-1 grade laminations (AITC 117) [AITC, 1988]. The effects of compressive stresses perpendicular-to-grain on shear in the xy plane are significant as they increase the wood shear stress capacity [Mandery, 1972]. Thus, apparatus configuration is important and can lead to inflated values of maximum shear stress measured in full scale beam testing if the reaction and load points are too close [Tingley, 1996].

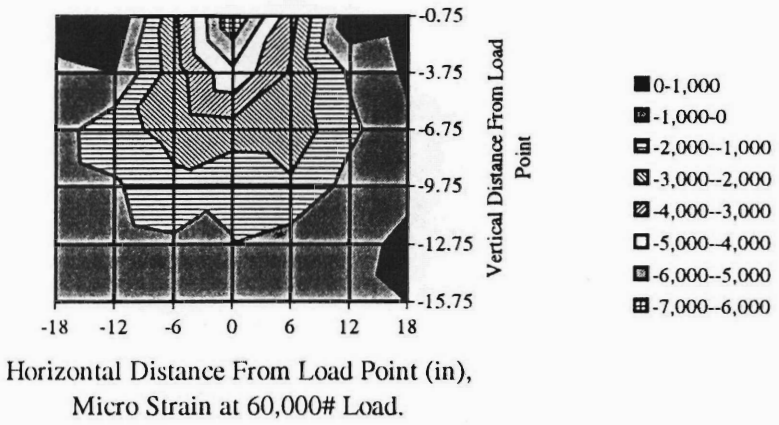

Figure 2.10. Vertical strain distribution under the load head.

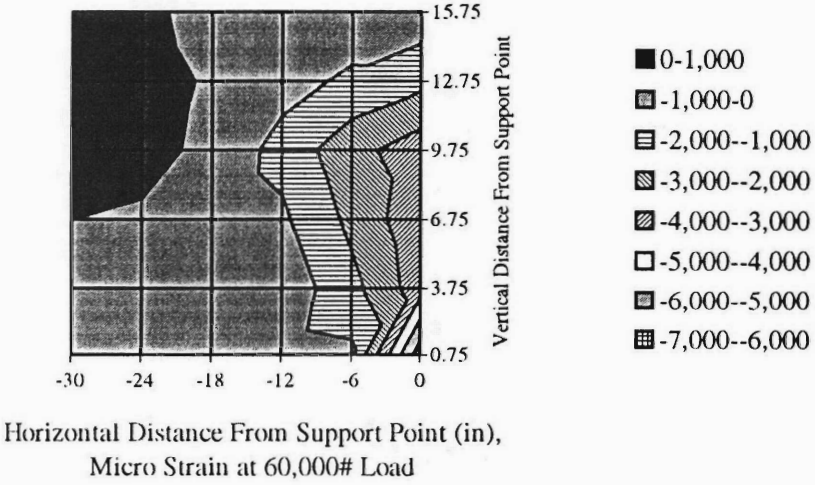

Figure 2.11. Vertical strain distribution over the reaction.

Three-Dimensional Stress Distributions

To confirm stress contours of the two-dimensional FEA and to investigate three-dimensional strain distribution, strains through the width of the beam were monitored by strain gauges within the full-scale glulams. Appendix C illustrates strain gauge locations.

Differences in elastic properties between adjacent laminae can lead to the development of interlaminar shear stresses that are greater than expected. For example, at the FRP-wood interface between ARP and Douglas-fir L3, an interlaminar shear stress is created by the differences in shear stresses of the adjacent laminae. Figures 2.12 and 2.13 show the measured shear strain on the ARP and wood; this is the xz plane. Figure 2.12 shows shear stress on the ARP in the xz plane across the width of an ARP-reinforced glulam beam. Figure 2.13 contains the shear stress in the xz plane across the width on the wood. The wood has much greater increase in xz shear stresses toward the edge.

The FRP has an increase in shear stress between the center and the edge. The opposite of the wood, although the difference as a percentage of the center value is much less than wood. The most likely explanation for this difference is gauge error as gauge results shown later in this chapter show little variation across the width and if any difference exists it is an increase in stresses toward the edge.

Small glueline test blocks [ASTM, 1995d] may indicate FRP-wood shear strength levels substantially above those predicted for the full-scale reinforced glulam FRP-wood interface glueline. However, this interlaminar shear stress differential is thought to contribute to premature glueline failure in larger, full-scale reinforced glulams.

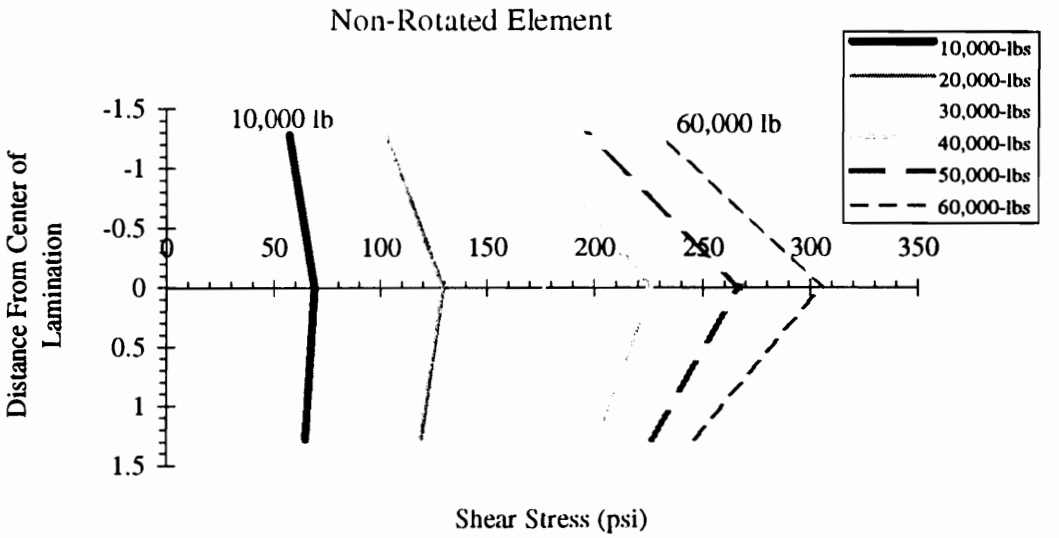

Figure 2.12. Shear stress (not rotated in the xz plane) across the width of a glulam beam on tensile ARP in the shear zone of a flexural member.

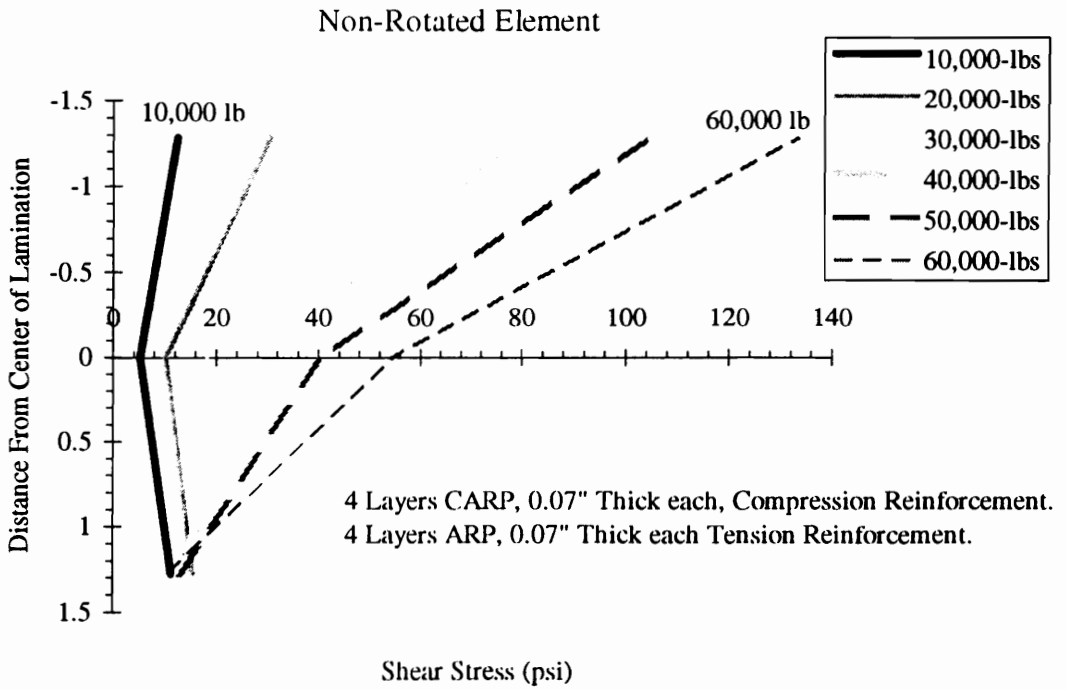

Figure 2.13. Shear stress (not rotated in the xz plane) in tensile wood laminae in shear zone across the width of glulam beam.

Passive Stress Distributions

In addition to the active stress translation effects, the effect of the unique stiffness characteristics in different directions in wood leads to passive stress distributions within the glulam. Table 2.1 provides Poisson's ratios for Douglas-fir in various planes as well as E in tension and compression in the longitudinal direction, E_L, ultimate tensile stress and strain, and shear modulus ultimate shear stress and strain for Douglas-fir, L-1 laminations (AITC 200-92) at 12% MC and tested at 72°F. Extensive experimental stress analysis of glulam beams, like that shown in Figure 2.14, provided strain distributions that were related to stress distributions within the glulam. Appendix C contains exact locations of gauges shown in a photograph(s).

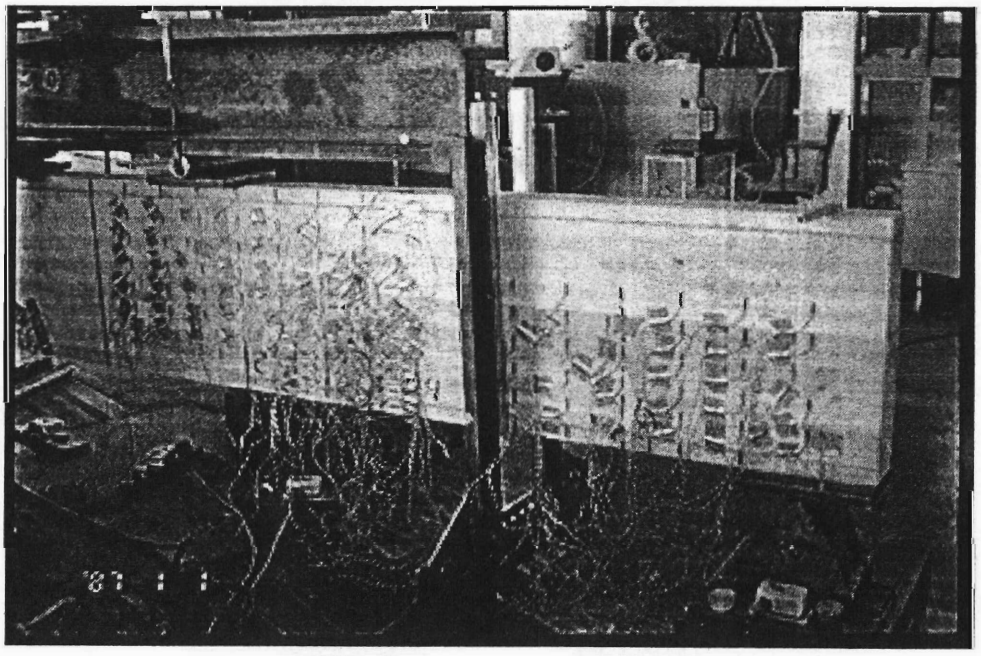

Figure 2.14. Stress analysis using strain gauges on a reinforced glulam beam.

Figure 2.15 shows the shear stress distribution in the xz plane across the width of a beam as gathered by strain rosette placement between laminations on the tensile laminae of an unreinforced glulam in the expected shear-free zone (neglecting dead weight). Figure 2.16 shows the same distribution on tensile laminae across the width in a shear zone. Figures 2.17 and 2.18 show axial stress across the width of an unreinforced beam on the wood in the tensile zone for expected shear-free and shear zones. Figures 2.19 and 2.20 show axial stress distribution across the width of a reinforced glulam beam on the tensile reinforcement in bending in the shear span for singly and doubly reinforced beams, respectively.

The response of wood in the transverse direction can be seen in these graphs. It was hypothesized that the effect of grain angle to longitudinal axis causes axial stresses to increase toward the edge of the beam. The increase of axial stresses toward the edge is not predicted by conventional isotropic theory. Others have found a similar divergence from conventional stresses for axial stress distributions in anisotropic materials [Jones, 1975]. Further, shear stresses increase toward the edge in the expected shear-free zone and increase, but to a lesser degree, to the edge in the shear span.

Jones [1975] has established that interlaminar shear stresses increase toward the edge in composite laminate plates subjected to tensile forces. He found this increase to be proportional to the thickness of the laminae. The wood laminations, which are relatively thick in comparison to the FRP, seemed to conform with the results by Jones. This differential of shear stresses and axial stresses increase toward the edge between the FRP and wood can contribute to the shear failures of the FRP wood interface in full-scale beams at shear stress values in much lower than predicted by conventional beam theory at failure load. Table 2.2 shows a summary of over 30 gauged laminations in Douglas-fir

glulams showing the overall trends for axial stress (x), transverse stress (z), and shear stress (z-x) across the width of the glulam. The vast majority of the results indicate increases in stresses toward the edge in compressive and tensile zones.

The unique characteristic of wood with regard to passive stress distribution, particularly axial stress distribution, across the width of the glulam beam is evidenced in Figures 2.17 and 2.18. The beam was subjected to bending and the stress distribution observed. The stress distribution across the reinforcement is much flatter in a reinforced glulam beam. FRP is unidirectional with the Poisson's ratio in the zx plane being very similar to that of wood at about 0.30-0.38. However, it is truly unidirectional and much more homogeneous across the thickness and width. This difference in homogeneity leads to the differentials in stress distributions across the width of the beam between the FRP and wood as shown in Figures 2.19 and 2.20 for shear stresses on the tensile reinforcement and wood in the shear zone of a reinforced glulam in bending.

Comparison of Analytical and Experimental Results

The actual distribution of shear stresses in a wood beam are much different than predicted by an isotropic beam analysis. Elementary beam theory predicts no shear through the width. However, strain measurements demonstrated that shear stresses do exist in the xz plane. The strain trends shown by shear measurements tended to conform with results of laminated plates under tensile loads [Jones, 1975].

The FEA analysis could have been modified to include discontinuities to improve its relationship to the beam test results. However, these model refinements, which are

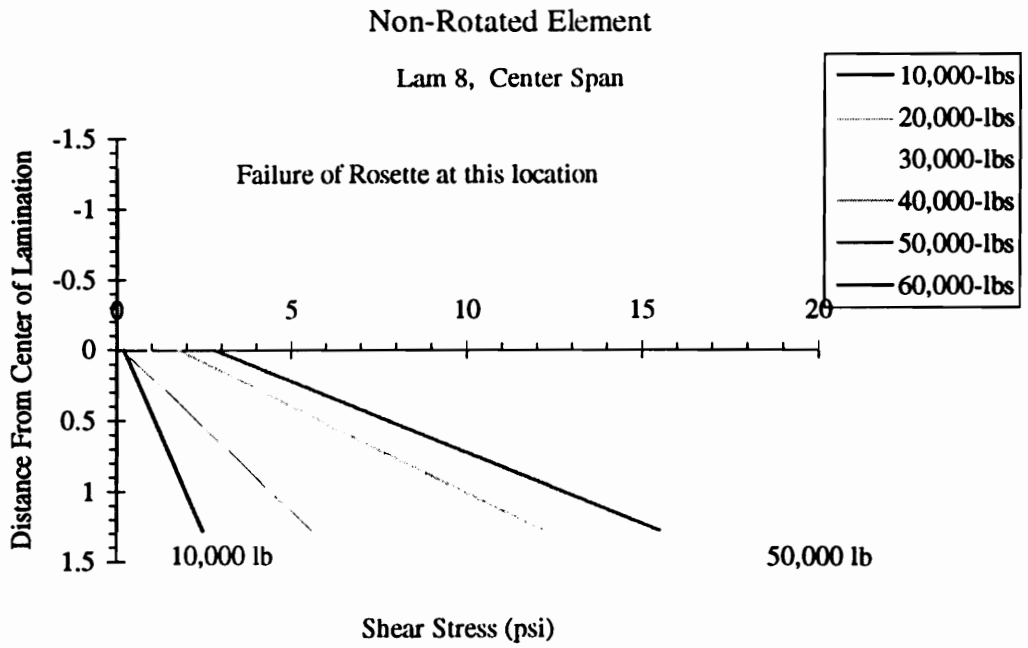

Figure 2.15 Shear stress across the width of glulam beam on wood in the expected shear-free zone.

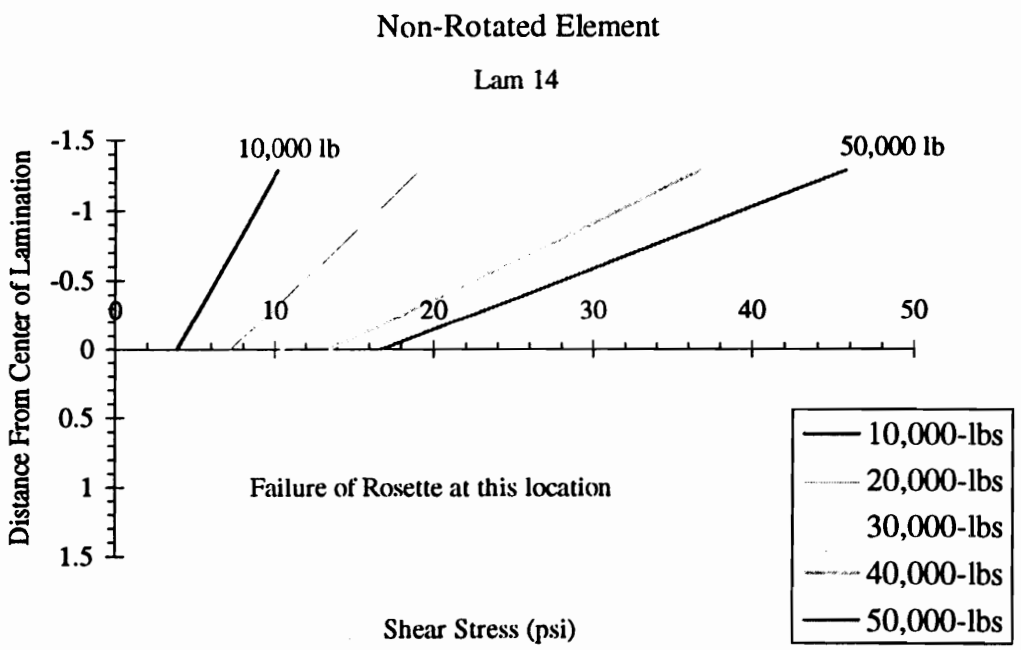

Figure 2.16. Shear stress across the width of glulam beam on wood in shear zone.

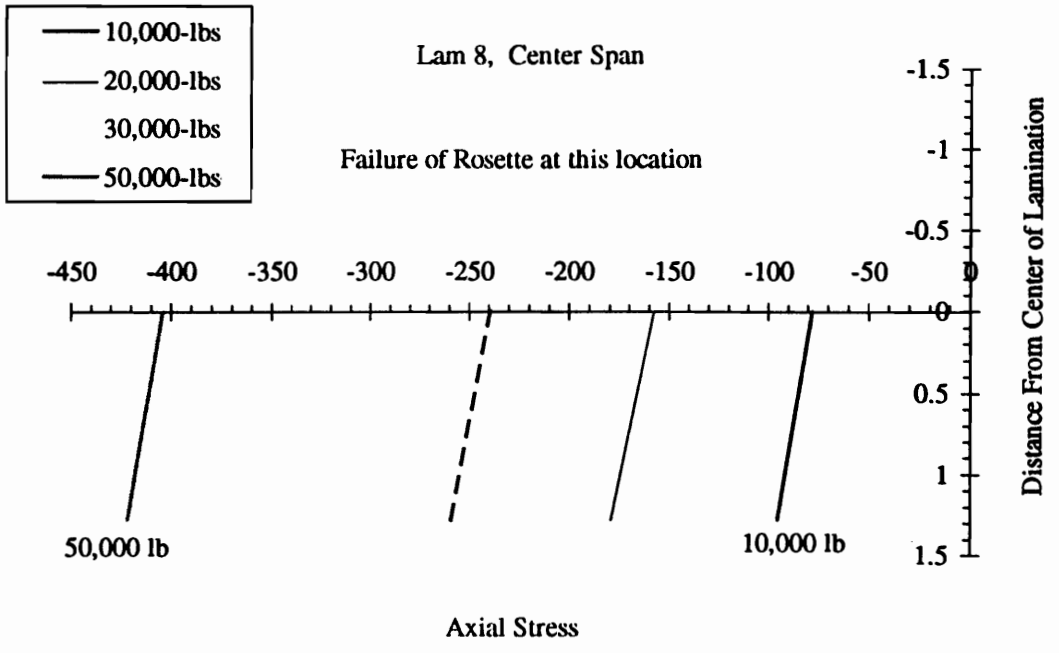

Figure 2.17. Axial stress (σ_x) on a tensile laminae in the expected shear-free zone across the width of glulam beam on wood.

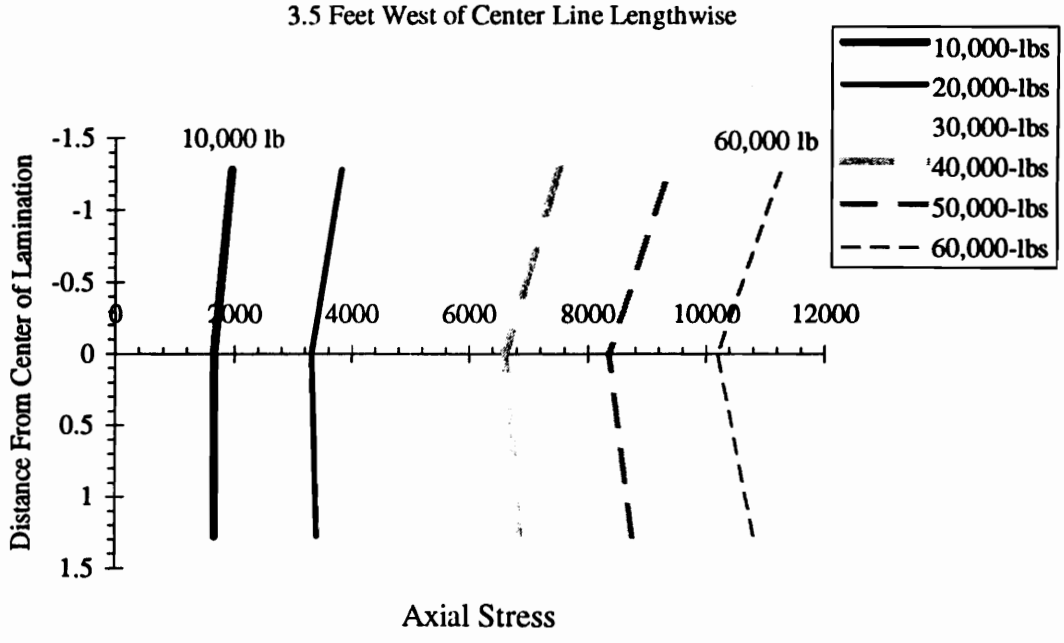

Figure 2.18. Axial stress (σ_x) on a tensile laminae in the shear zone across the width of glulam beam on tensile reinforcement.

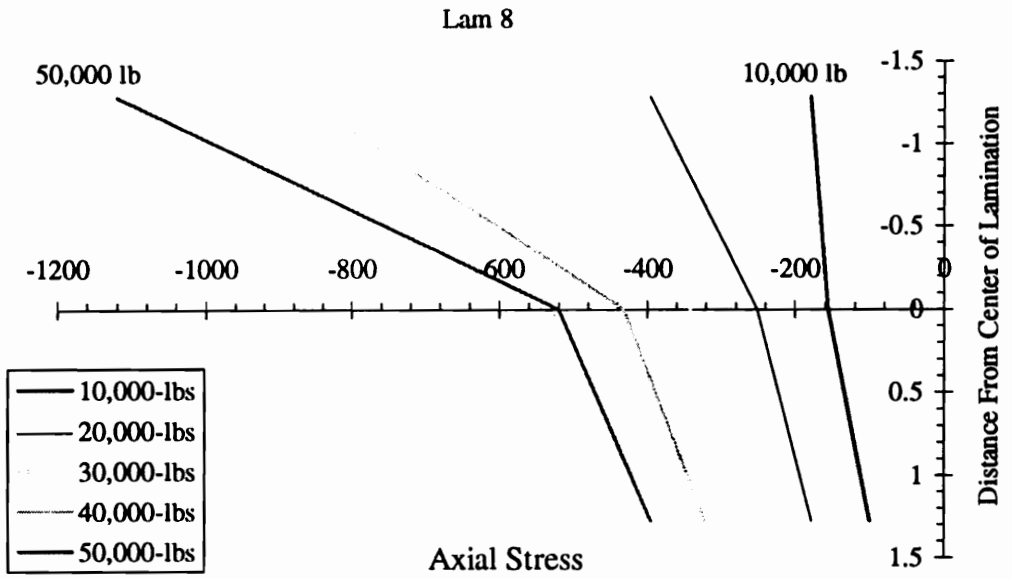

Figure 2.19. Axial stress (σ_x) on a tensile laminae in the shear zone across the width of glulam beam on wood.

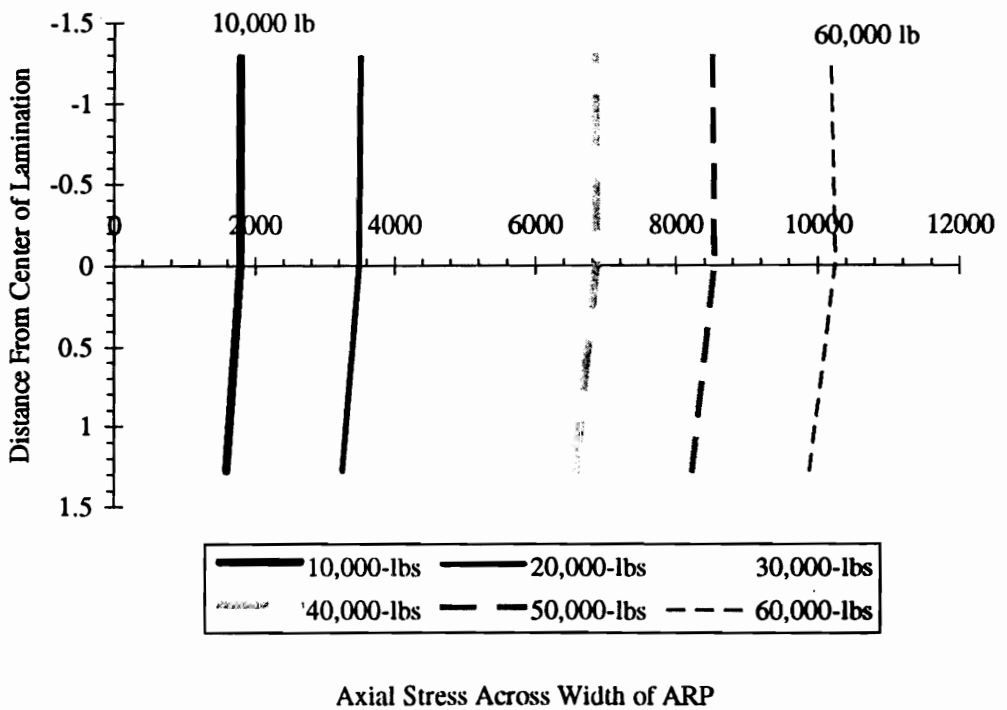

Figure 2.20. Axial stress (σ_x) on a tensile laminae in the shear zone across the width of glulam beam on tensile reinforcement.

Table 2.2. Summary of internal strain gauges results for reinforced and unreinforced glulams.

Beam 403 Tension Reinforced Beam

Sigma X

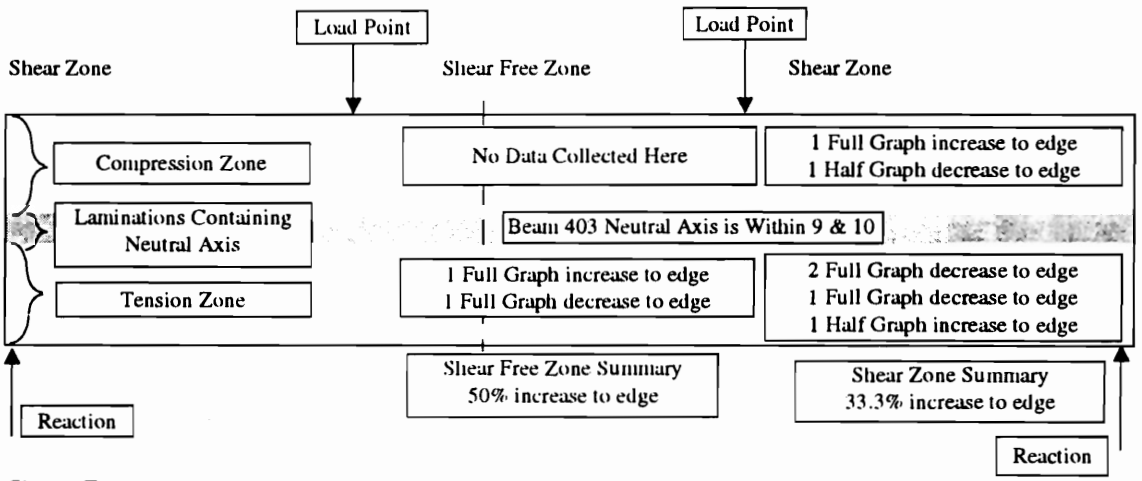

Sigma Z

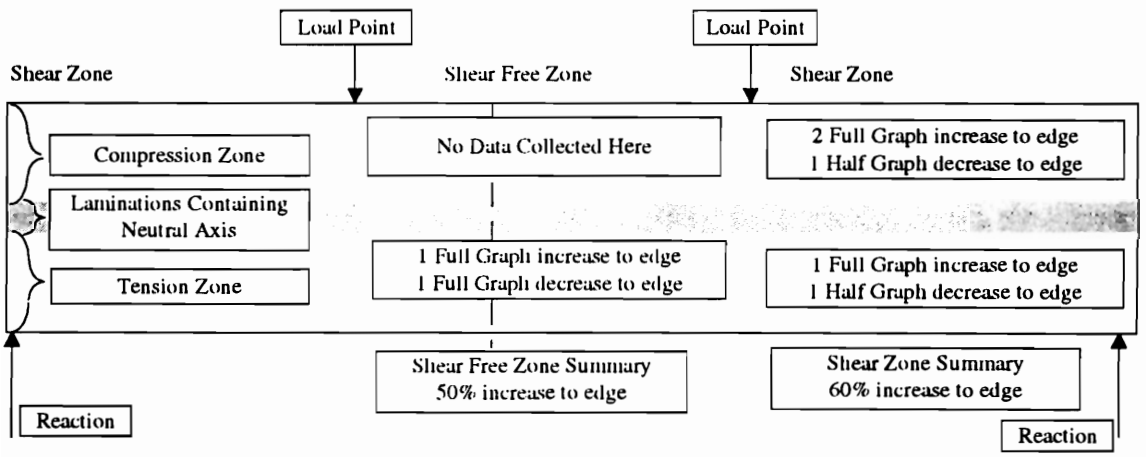

Shear XZ

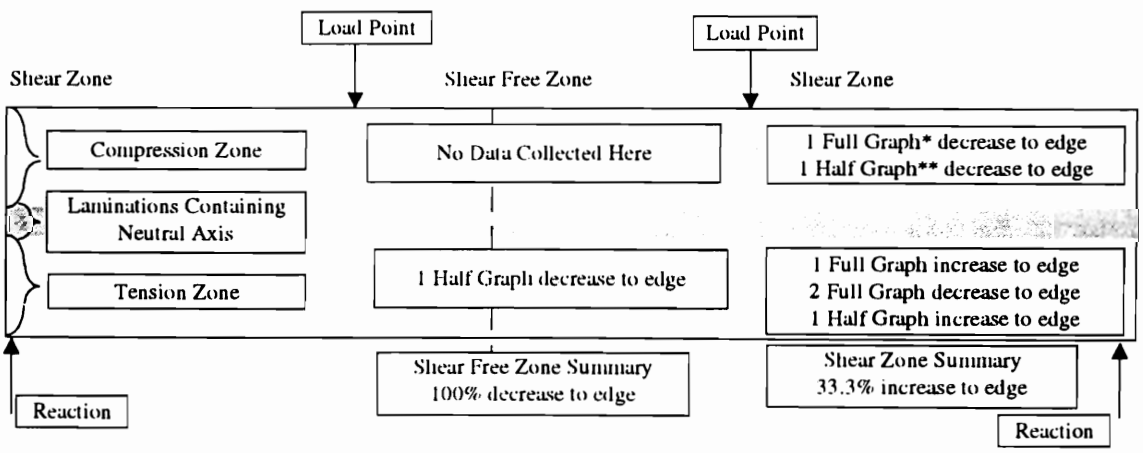

Table 2.2. (Continued).

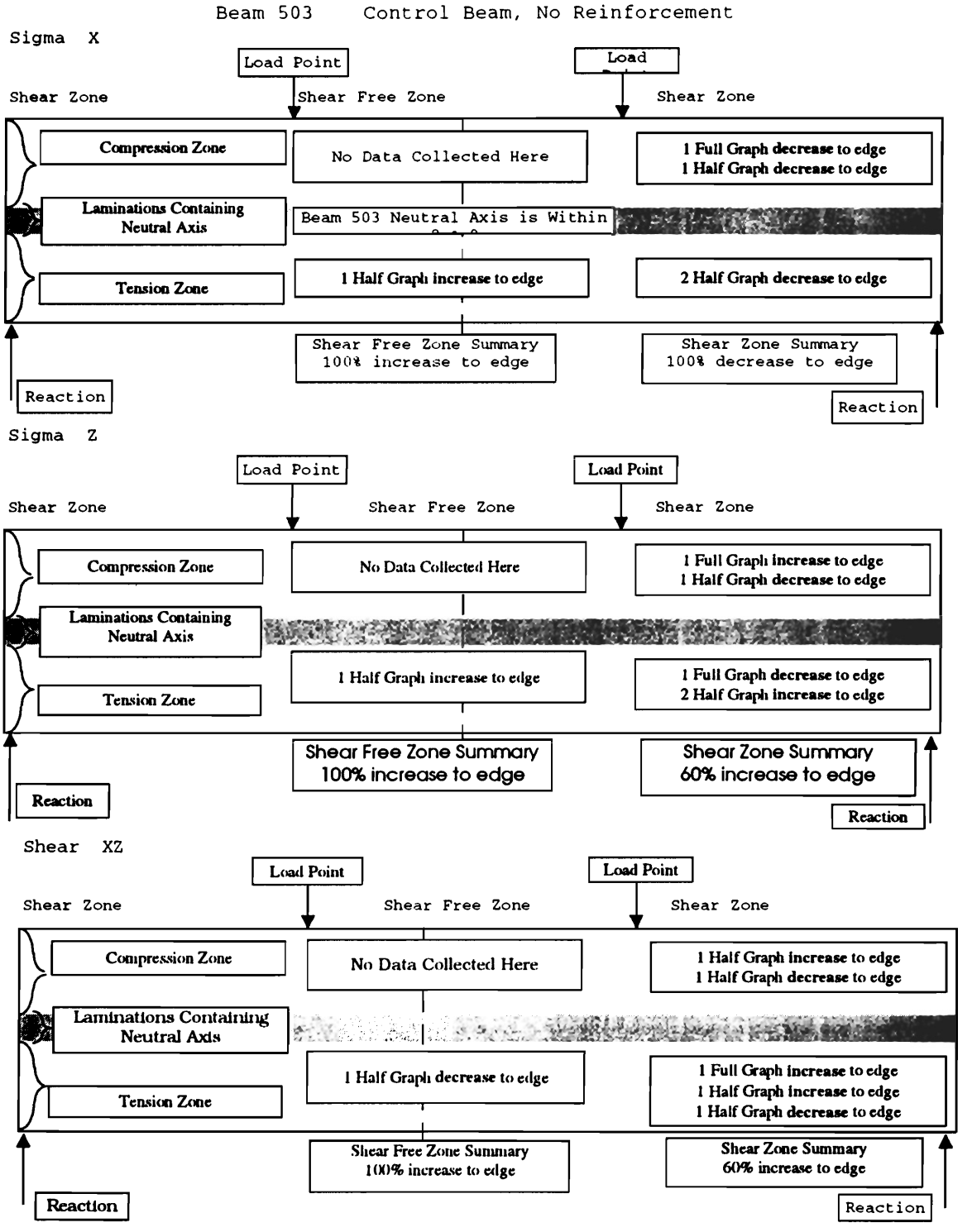

Table 2.2. (Continued)

Beam 903 Compression and Tension reinforced beam.

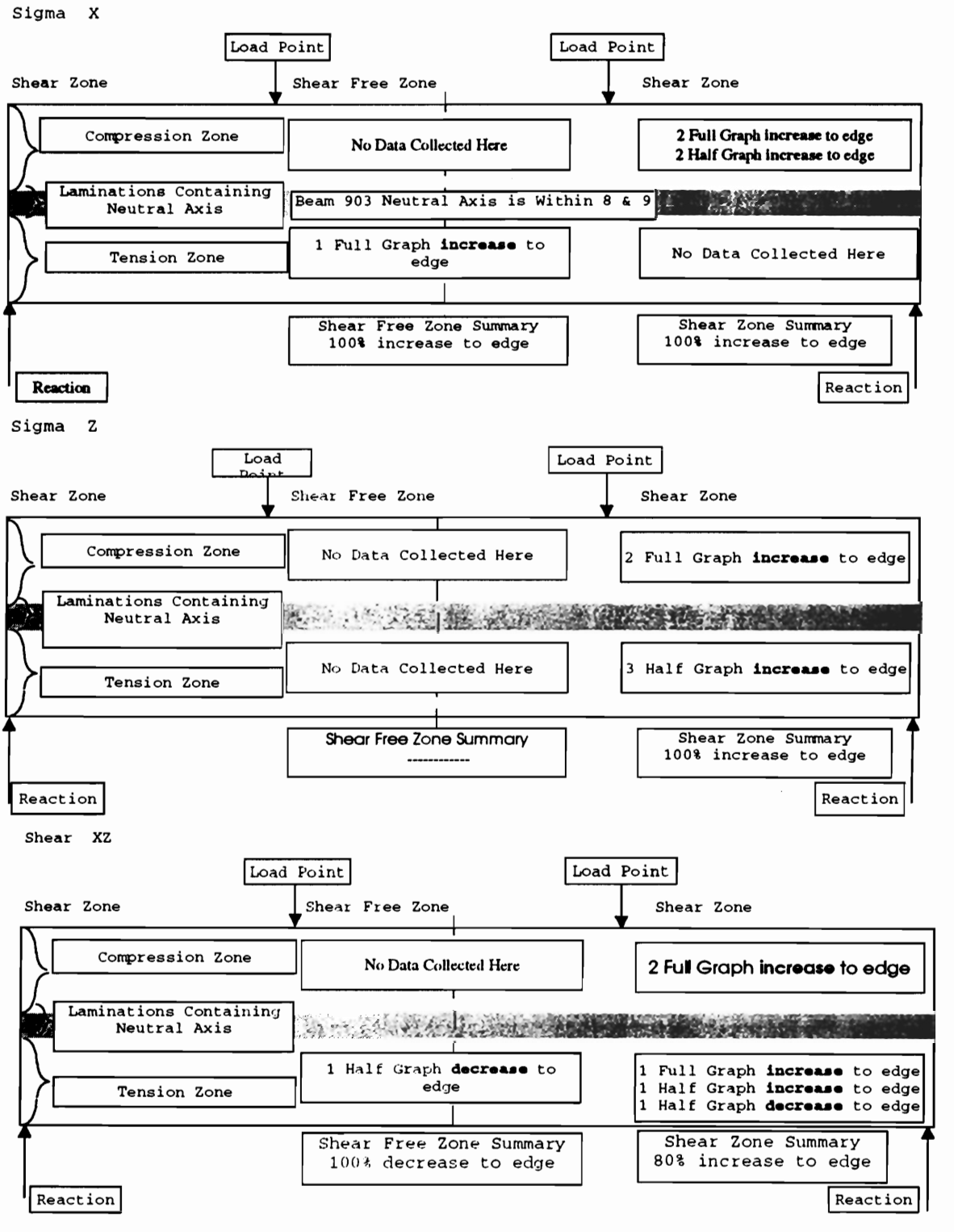

Note: *. Full graph means gauges on full width were operational and provided acceptable data.

**. Half graph means gauges on half width were operational and provided acceptable data.

difficult to impose, would not have yielded proportionate benefits to understanding global beam behavior. Further, since the wood is remanufactured several times before it is used in a glulam, the potential is diminished for predefined planes of symmetry in the laminating lumber. Even if a particular plane of symmetry in the wood laminations could be defined at a point along its length in a beam, within a short distance away, the plane could differ due to growth characteristic changes or some other localized feature. Thus, the following statements can be made about planes of symmetry in wood.

- The maximum value of τ_{xy} shear stress as predicted by the theoretical reinforced glulam beam analysis was larger than the actual as obtained by strain gauging.
- The magnitude of the τ_{xy} shear stress value in the region between the neutral axis and the FRP-reinforcement in the tension zone as predicted by theory was less than actual values obtained by strain gauging.
- The axial stresses across the width of the reinforced glulam increased toward the edge. This was not predicted by the theoretical analysis.
- The actual distribution of shear stresses in the xz plane across the width of the reinforced glulam increase toward the edge. This was not predicted in the theoretical analysis. However, it agreed with previous researchers results as predicted by plate theory [Jones, 1975].

Conclusions

The objectives of the investigation were achieved as the stress distributions of the reinforced glulam were modeled and compared to the actual distributions obtained from testing. The actual bending stress distributions in reinforced glulams tend to match those predicted by conventional isotropic theory with notable exceptions for wood variability. A more complex model could have included these features with improved accuracy. This statement applies to axial tensile and compressive stresses.

The actual shear stress distributions in the bending plane do not match those predicted by mathematical modeling well. This disparity may be reduced by better matching of stiffness characteristics and materials parameters used in the prediction model with the actual test beam used for comparison. The shear stresses across the width of the beam [in L-(T/R) or L-(R/T) plane] conform to those predicted by the plate theory of other researchers [Jones, 1975].

The key observations of importance were:

- The axial stress distributions in tension and compression can be modeled by conventional theory with an acceptable level of accuracy without a complicated model reflecting discontinuities.
- The shear stress distributions particularly in the xz and yz planes can not be modeled effectively without a complicated model.
- The axial and shear stresses were found to increase toward the edge of a beam through the width.
- The changes in stress through the width was less in the FRP than wood.

CHAPTER 3

ON ASSESSING THE STRESS-STRAIN RELATIONSHIPS IN THE REINFORCEMENT AND WOOD LAMINATES IN REINFORCED GLULAMS

Daniel A. Tingley
Robert J. Leichti

For Submission to
Wood and Fiber Science

Introduction

The localized element strain response to loads imposed on global full-scale reinforced glulam is different from small-clear strain response to applied stress. The nonhomogeneous character of wood, orientation of load and grain of the wood, anisotropy and variations caused by manufacturing contribute to this disparity.

A complete description of the elastic-plastic relationship between the wood and the fiber-reinforced plastic reinforcement (FRP) in a full-scale reinforced glulam relies on an evaluation of externally applied loads and the development of internal stresses and strains. In a full-scale beam, these stresses and strains are different from those achieved in small-clear testing. In addition, the distribution of elemental elastic and plastic stress-strain relationships as a result of wood nonhomogenity and FRP element homogeneity within a full-scale reinforced glulam under load create unexpected composite responses [Tingley, 1994b].

The effect on reinforced glulam load response of having constituent materials behave plastically at different times in the loading event is an important feature of reinforced glulam behavior. Environmental effects such as moisture content variation in the wood and resultant shear-stress development in the wood-FRP interface compound the complexity of the situation. These considerations combined with nonhomogeneous characteristics of wood cause standard prediction methodology based on isotropic homogenous materials to become inaccurate in predicting load response.

This report explores the elemental stress-strain responses to global loading of full-scale reinforced glulams. Both the elastic and plastic ranges are considered in the wood and FRP.

Objective

The objective of this chapter is to investigate the effects of localized load response on full-scale reinforced glulam beam behavior.

The hypothesis of the testing and analysis investigation work presented in this chapter was that FRP reinforced glulams respond to load as a layered body. Specifically, it was hypothesized;

- FRP allowed higher levels of tensile strain prior to beam failure.
- Stress-strain distributions in the FRP-wood interface are not adequately predicted by conventional beam theory.

Theoretical Background

Many researchers have investigated reinforced glulams by testing and analytical methods [Biblis, 1965; Permanez, 1974; Rowlands et al., 1986; Sonti et al., 1995a; Sonti et al., 1995b; Tingley, 1990; Tingley and Leichti, 1993; Tingley and Leichti, 1994c]. Strain distributions in unreinforced and reinforced full-scale glulams have been studied for many years [Lantos, 1970; Fox, 1975; Davalos and Barbero, 1991]. These investigations, except for Ramos [1961] and Tingley [1988], did not generally involve detailed strain gauge analysis and subsequent development of load response

characteristics. Lantos [1970] used strain gauges on the steel and wood in steel reinforced glulam to develop information showing the degree of composite behavior.

Recently researchers have conducted extensive research on full-scale reinforced glulams that included component testing on both the reinforcement and wood [Tingley et al., 1996a]. The results demonstrate that compressive plasticity provides for a substantial increase in load capacity of glulam beams reinforced with an FRP [ICBO, 1995] .

This compressive plasticity was first observed in unreinforced glulams by Ramos [1961]. Other researchers later investigated the "columnar action" exhibited by the wood subject to compressive bending stresses that lead to a blocking of the compression zone [Anderson, 1981; Malhotra and Bagan, 1980]. This blocking begins at the outer extreme fiber in compression and continues to spread towards the neutral axis in a single plane as more of the wood moves into the plastic range. The neutral axis moves toward the tensile surface during this transition and the overall beam exhibits more deformation and plasticity. Other researchers have investigated this progressive compressive failure in wood in flexure [Gurfinkel, 1981] in wood structural members subjected to combined axial and bending moment loads. In addition, researchers have shown that the flexural ductility ratio, the ratio of yield point stress to ultimate stress at failure in the tensile zone, is substantially increased to over 2.0 on average with as little as 1.5% by cross-section reinforcement [Tingley and Leichti, 1995]. Tensile reinforcement leads to an increase in the potential for wood compressive failure and the amount of bending plasticity exhibited.

Analysis of Bending Stresses

Conventional isotropic theory can be used to predict approximate stress-strain distributions in unreinforced glulams. Equation 3.1 can be used to calculate the bending stress at a point in a flexural member of a homogeneous material.

$$\sigma_x = \frac{My}{I} \qquad 3.1$$

Where

σ_x = Normal bending stress at a point in the depth of a beam

I_x (psi [MPa])

M = Applied moment (in.-lb. [N-mm])

y = Distance to a point of interest from neutral axis in (in. [mm])

I = Moment of inertia (in^4 [mm^4])

The orthotropic, nonhomogenous nature of wood leads to important variations in the stresses from those predicted by the above equations.

For reinforced glulams, equations 3.1 and 3.2 are commonly used with the transformed section method [Gardner, 1991a; Gardner, 1991b, van de Kuilen, 1991; Triantafillou and Deskovic, 1992; Mufti et al., 1991; Enquist et al., 1991; Davalos and Barbero, 1991; Plevris and Triantafillou, 1992]. The transformed section method employs the use of the modular ratio, η, which is the ratio of moduli of elasticity of the two materials in the beam, wood and FRP.

The transformed section method assumes that each material is isotropic and thus when transformed using the modular ratio based on axial characteristics the new

composite material geometric section will respond to load as one homogenous isotropic material [Gere and Timoshenko, 1990] with the same axial modulus of elasticity in tension and compression. Recent research has shown that actual stress-strain distributions make conventional theoretical analysis procedures based on isotropic material very inaccurate [Tingley and Leichti, 1994a; Tingley and Leichti, 1994b; Tingley and Leichti, 1994c].

When calculating, the transformed section method, the parallel axis theorem is used, and it states that the moment of inertia, I_x, of any area x, with respect to any arbitrary axis is equal to the moment of inertia with respect to the parallel axis through the centroid of the area, I_o, plus the area times the square of the distance between the centroid axis of the composite body and the centroid axis of the body of interest (Equation 3.2).

$$I_x = \frac{b_x h_x^3}{12} + A_x c^2 \qquad 3.2$$

Where

I_x = Moment of inertia of area x with respect to the composite body centroid

b_x = width of area x

h_x = height of area x

A_x = area of area x

c = distance from centroid of area x to centroid of composite body

Bodig and Jayne [1993] have shown that in layered members such as FRP-reinforced glulams, Equation 3.3 can be derived for stress at any point in any layer.

$$\sigma_i = \frac{ME_iC_i}{EI} \qquad 3.3$$

Where

σ_i = Stress in i^{th} layer

c_i = Distance from centroid of composite to centroid of i^{th} area

E_i = Modulus of elasticity in axial direction of the i^{th} layer

EI = Composite flexural rigidity

$$EI = \sum_{i=1}^{n} E_i (I_i + A_i c_i^2) \qquad 3.4$$

Equations 3.3 and 3.4 can be expanded into prediction formulas for each constituent material, wood in compression and tension, and FRP in tension, respectively as shown in equations 3.5, 3.6 and 3.7.

$$\sigma_{x1} = \frac{MyE_1}{E_1I_1 + E_2I_2 + E_3I_3} \qquad 3.5$$

$$\sigma_{x2} = \frac{MyE_2}{E_1I_1 + E_2I_2 + E_3I_3} \qquad 3.6$$

$$\sigma_{x3} = \frac{MyE_3}{E_1I_1 + E_2I_2 + E_3I_3} \qquad 3.7$$

Where

σ_{xi} = Axial stress at a point in the depth of the reinforced glulam wood in compression, wood in tension, or FRP in tension (1, 2 or 3 respectively).

M = Bending moment.

y = Distance from neutral axis to point of interest.

E_i = Axial modulus of elasticity of wood in compression or tension, or FRP in tension (1, 2 or 3 respectively).

I_i = Moment of inertia of each component - wood in compression, wood in tension, or FRP in tension (1, 2 or 3 respectively) with respect to the centroid of the composite section.

Similarly, compressive FRP reinforcement can be introduced as a fourth material. Due to the fact that in any glulam E_t is usually greater than E_c the modular ratio of wood in tension to wood in compression is greater than 1. It averages 1.06 for most commercial softwood glulams in the United States [Gurfinkel, 1981]. This results in a further lowering of the neutral axis in reinforced glulams from that predicted by formulas in equation 3.1 and 3.2 considering the FRP (assuming only tension zone reinforcement).

Analysis of Shear Stress

Equation 3.8 predicts shear stress, τ, at a point in the depth of the beam due to externally applied shear forces.

$$\tau = \frac{VQ}{It} \qquad 3.8$$

Where

τ = Shear stress at a point in the depth of a beam

(psi [MPa])

V = Applied external shear force (lb [kN])

Q = First moment of area with respect to the neutral axis (in^3 [mm^3])

t = width at the point of interest in the depth of the beam (in. [mm])

Equations 3.1 and 3.8 are used to calculate the axial and shear stresses at any depth along the beam at any point longitudinally. The stresses (axial and shear) are assumed to be constant across the width of the beam, except in the case where lateral loads are applied where similar formulas are employed in the lateral direction [Popov, 1978]. See Figure 3.1, which shows a typical axial stress-strain distribution and shear Stress distribution as predicted by equations 3.1 and 3.8 through the depth and width of a beam.

Shear stress, τ, at a point in a transformed section is calculated using equation 3.8. The equation 3.8 with the transformed geometric section dimensions. Figure 3.2 shows the resulting axial stress and shear stress distributions through the depth of a reinforced glulam using the transformed section method.

Variation in E values in each lamination, the nonhomogenity of knots and finger joints, and anisotropy lead to reduced accuracy of shear stress predictions within the transformed section. The shear moduli values of the different wood materials, i.e. wood in tension and wood in compression, and FRP, are not related to each other in the same way as predicted by the E modular ratio. For example, the shear modulus of

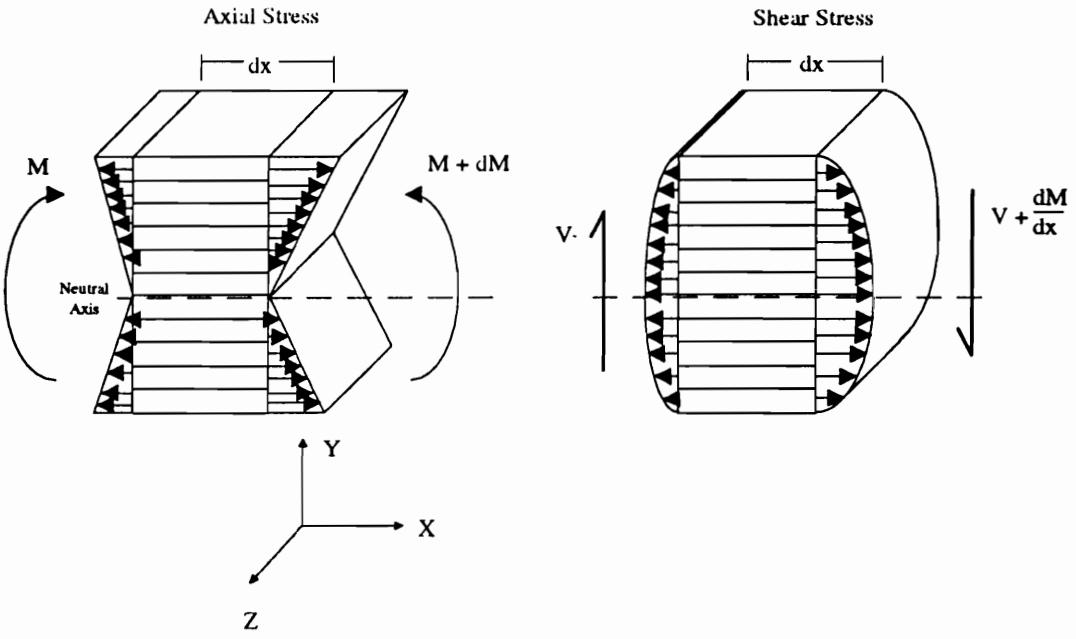

Figure 3.1. Shear stress and differential axial relationships and shear stress in unreinforced glulam (assuming isotropic material).

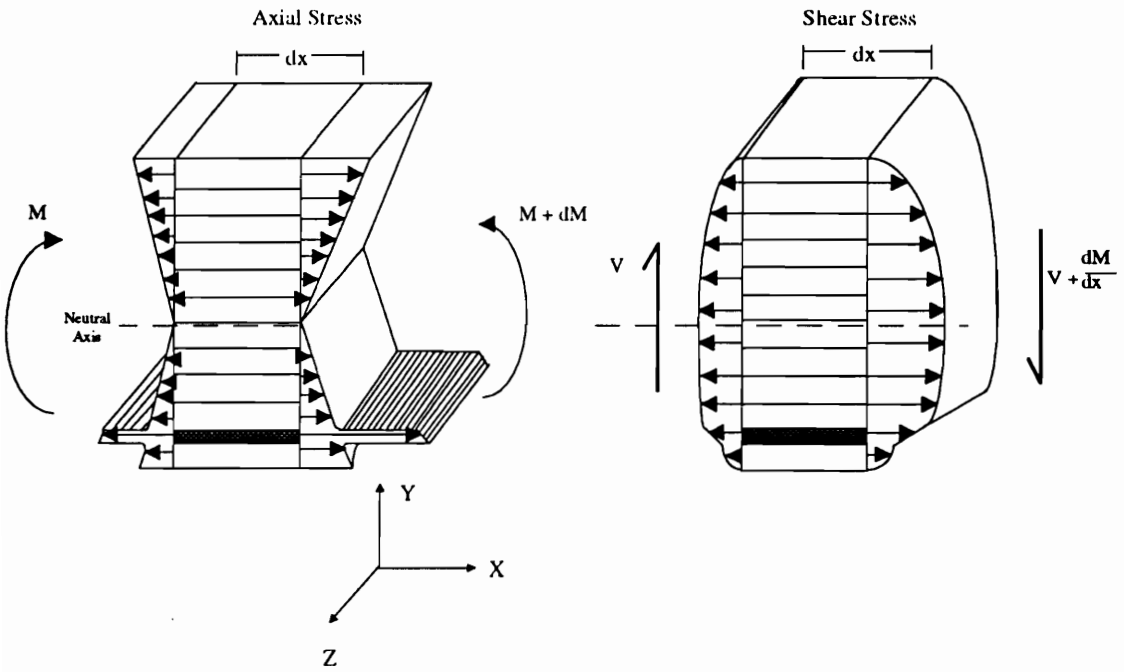

Figure 3.2. Axial stress differential and shear stress in reinforced glulams using transformed sections and assuming isotropic materials.

wood (Douglas-fir) is approximately 125,000 psi (862 MPa) whereas a unidirectional FRP's might have shear modulus values of 500,000 psi (3448 MPa) [ICBO, 1995]. Thus, the shear modular ratio, η', is 4 whereas the compressive axial E modular ratio, η, is 10 to 11. Other researchers have investigated this differential between η and η' in anisotropic materials[Raman and Davalos, 1996].

The shear-strain in the xy plane at a point in the depth of a reinforced glulam would be as shown in equation 3.9.

$$\varepsilon_{xyi} = \frac{VQ_r}{I_r t_i G_i} \qquad 3.9$$

Where

ε_{xyi} = Shear strain in the xy plane in the i^{th} lamination.

Q_r = First moment of area of transformed section (in^3 [mm^3]).

I_r = Moment of inertia of reinforced cross section.

G_i = Shear modulus of i^{th} lamination (psi [MPa]).

t_i = width of shear plane in i^{th} lamination (in. [mm]).

Equation 3.9 shows that the shear-strain in the wood on one side of the wood-FRP interface will be more than in the FRP on the other side of the interface.

The shear strain differential between materials in a composite layered body is caused by the different shear modulus characteristics of successive layers in a composite layered body.

Apportionment of Stresses

Conventional theory can be used to determine the portion of the bending moment carried by the wood, FRP and adhesive in a FRP reinforced beam in bending. Castigliano's second theorem is the basis for such an analysis (Lantos,1970).

Lantos [1970], derived equations similar to 3.10 to 3.15 to determine composite material contributions to the resisting moment in a internally reinforced beam.

$$dP_z = \frac{dM_z}{z} \qquad 3.10$$

Where

z = moment arm length.

$$\partial U_T = \partial U_W + \partial U_{FRP} + \partial U_a = 0 \qquad 3.11$$

Where

∂U_T = total incremental change in energy resulting from an infinitesimal increment in the bending moment.

$\partial U_{FRP}, \partial U_w, \partial U_a$ = components of ∂U_T with respect to FRP, wood and adhesive layer, respectively.

$$U_w = \frac{1}{2E_w I_w}\int_0^L M_w^2 dx = \frac{1}{2E_w I_w}\int_0^L (M - M_{FRP})^2 dx \qquad 3.12$$

$$2U_{FRP} = \frac{1}{E_{FRP}A_{FRP}}\int_0^L (\frac{M_{FRP}}{z})^2 dx = \frac{1}{z^2 E_{FRP}A_{FRP}}\int_0^L M_{FRP}^2 dx \qquad 3.13$$

$$2U_a = \frac{2bt}{G}\int_0^L \tau^2 dx = \frac{t}{2z^2 btG}\int_0^L (M'_{FRP})^2 dx \qquad 3.14$$

Where

t = thickness of the adhesive layer (inch).

G = shear modulus of the adhesive (psi).

τ = bond stress (psi).

A_{FRP} = cross sectional area of FRP ($inch^2$).

I_w = moment of inertia of the net wood section ($inch^4$).

$Z^2A_{FRP}= I_{FRP}$ = moment of inertia of the FRP about the neutral axis ($inch^4$).

M_{FRP} = moment resisted by the FRP

E_{FRP} = modulus of elasticity of FRP

b = width of FRP (inch).

L = length of beam (inch).

Using the above equations and integrating by parts and relating each part to the FRP the moment resisted by the FRP can be calculated. Equation 3.11 becomes Equation 3.15. A general solution is shown in equation 3.16.

$$\int_0^L \left[\frac{-M_o + M_{FRP}}{E_w I_w} + \frac{M_{FRP}}{Z^2 E_{FRP} A_{FRP}} - \frac{M''_{FRP} t}{Z^2 bG} \right] \frac{\partial M_{FRP}}{\partial x} = 0 \qquad 3.15$$

$$M_{FRP} = \frac{nI_{FRP}}{I_c} M_o + \frac{M_o''}{m^2} + A_1 e^{xm} + A_2 e^{-xm} \qquad 3.16$$

Where

I_c = moment of inertia of composite = ($I_w + \eta I_{FRP}$)

$$m^2 = \frac{z^2 I_c G}{I_w b E_{FRP} t} \qquad 3.17$$

A_1 and A_2 = constant

More recently, researchers have determined that shear modular ratios play a large part in the beam response to load [Raman and Davalos, 1996].

The contribution to resisting moment provided by the FRP is large, particularly in short beams where shear deformations are a larger part of total deformation [ASTM D-198, [1995a].

The shear correction factor κ, provides a method of correcting the effect of varying shear modulus on the shear-stress at a point of interest in the depth of a reinforced beam.

Raman and Davalos [1996] developed the following equations using a shear strain energy approach:

$$\bar{U} = \frac{1}{2}\int_{-h/2}^{h/2} \frac{\sigma_{xz}^2}{\left[Q_{44} - \frac{Q_{45}^2}{Q_{55}}\right]} \qquad 3.18$$

$$\bar{U} = \frac{1}{2}\int_{-h/2}^{h/2} Q_x^2 \frac{\left[\int_{h/2}^{z} (Q_{1i}\beta_{1i} + Q_{1i}\delta_{1i})\right]^2}{\left[Q_{44} - \frac{Q_{45}^2}{Q_{55}}\right]} dz \qquad 3.19$$

$$\bar{U} = \frac{1}{2}\frac{Q_x^2}{\kappa(A_{44} - \frac{A_{45}^2}{A_{55}})} \qquad 3.20$$

$$\kappa = \left[(A_{44} - \frac{A_{45}^2}{A_{55}}) \int_{-h/2}^{h/2} \frac{\left[\int_{-h/2}^{z} (Q_{1i}\beta_{1i} + zQ_{1i}\delta_{1i}) dz \right]^2}{\left[Q_{44} - \frac{Q_{45}^2}{Q_{55}} \right]} dz \right]^{-1} \qquad 3.21$$

Where

Q_{ij}= the reduced stiffness coefficients.

h = thickness of plate (inch).

i=1,2,6.

U = shear strain energy.

α_{1i}, β_{1i}, and δ_{1I} = compliance sub-matrices.

$A_{ij} = (\delta_{11}/\alpha_{11}\delta_{11}) - \beta_{11}^2$

κ = shear correction factor.

The above equations assume constant transverse shear strain through each laminae. Simplifying for an isotropic material, equations 3.18 -3.21 can be reduced to show an expected value of 5/6 for a simple rectangular cross section (Raman and Davalos, 1996).

Other researchers have investigated this relationship between lamina with different shear modulus values [Hong et al., 1992]. They established that the composite shear response of the member is affected by individual lamina deformations and transverse shear coupling. Jones [1975] describes shear couples linking axial stresses to shear stresses between layers in a layered composite. This coupling depends on material properties such as E, G, or μ. The coupling may also depend on not only material properties but the stacking sequence and surface tractions (Hong et al, 1992).

These couples may be large in the interface between the wood and the FRP. Other researchers have developed shear correction factors based on first order deformation theories (FSDT) [Raman and Davalos, 1996].

This study uses an experimental formula in which the η' value is used to adjust the shear stress in the FRP-wood zone between the neutral axis and the FRP. Equation 3.22 shows this prediction equation.

$$\tau_{xyFRP} = \left(\frac{VQ_r}{I_r t_i}\right) \times \eta' \qquad 3.22$$

where

τ_{xyFRP} = Shear stress in the wood-FRP zone between the neutral axis and FRP.

It must be noted that this equation will not adequately serve for predicting the distribution through the depth as the affects of laminate thickness, different wood lamination, G values, FRP thickness, FRP E values, etc. are unknown on its prediction accuracy outside the prescribed zone.

Experimental Procedure

The procedures for this investigation included the elastic and plastic ranges of the wood and FRP. The investigation also considered the differences between component small-clear test results and the elemental elastic-plastic responses to global loading of the full-scale reinforced glulam. Finally, the effects of homogeneity were also considered along with environmental effects such as moisture content variation.

The investigation was facilitated by the use of strain gauges and interpretation of strain gauge data using conventional stiffness and compliance matrix manipulation for the elastic analysis. The plastic range was not modeled, however it was investigated by small clear testing and strain gauge analysis of normal stresses in full-scale beams [ASTM, 1995b]. Thirty full-scale reinforced glulam beams were tested to failure according to ASTM D-198 standard test procedures. More detailed information on testing procedure and methodology is given in Appendix B. Strain gauges were placed throughout the width, depth and length of these beams and strain data collected for various load cycles on each beam including the final cycle to failure. These gauges were applied to the wood and reinforcement, adjacent to each other, at various locations across the width and through the depth of the beam. The beams were Douglas-fir (AITC combination 5), 5.125 × 24 in. × 15 ft (130 × 610 × 4570 mm). Gauges were placed at 0^0, 45^0, and 90^0 to investigate axial, transverse, and shear strains in the xy and zx plane. Standard ASTM D-198 [ASTM, 1995a] test procedures were used for static bending tests except that the beam was loaded in stepwise fashion.

Appendix C details strain gauge procedures, processes and methodology for interpretation of strains into stresses. This appendix also contains a diagram showing the strain gauge placement on the wood and adjacent reinforcement.

The stress analysis procedure involved the placement of strain gauges around and on knots, finger joints, FRP and grain deviations in the tensile and compressive zones to establish strain patterns in these areas. Conventional stress-strain theory was used to develop applied load stress distributions, subsequently differences between actual and calculated distributions were observed. Additional factors such as columnar

action in the compressive zone were applied to conventional theories presented earlier to explain more accurately certain stress distributions such as axial compressive stress [Ramos, 1961; ICBO, 1995]. To obtain strain values for full-scale beam elements, deflection values were used with geometric calculations using the radius of curvature ρ to calculate ε_x. The calculation methodology is shown in Appendix E.

Results and Discussion

Reinforced Glulam Elemental Load Response Versus Small-Clear Load Response

In an unreinforced beam, the global yield point marking the end of the elastic range and the beginning of the plastic range occurs at approximately 80 to 100% of the ultimate load. This is observed in Figure 3.3 which shows a typical load-deflection curve for an unreinforced glulam. It was a 5.125 x 24 in. x 15 ft (130 mm x 610 mm x 4570 mm) Douglas-fir, AITC combination 5 (AITC 117-93). The load span was 5 ft (1520 mm). It was tested according to ASTM D-198. The moisture content of the beam was an average of 12% with the testing environmental temperature at 57°F and relative humidity (RH) of 64%.

For a reinforced glulam in bending, the end of the elastic range and beginning of the plastic range is in a range of 40 to 60% of the ultimate load. This is observed in Figure 3.4, which shows a typical load-deflection curve for a reinforced glulam beam. The glulam shown was a 5.125 x 12 in x 36 ft (130 mm x 305 mm x 11,000 mm) Douglas-fir, AITC combination 5 (AITC 117-93). The load span was 8 ft (2440 mm).

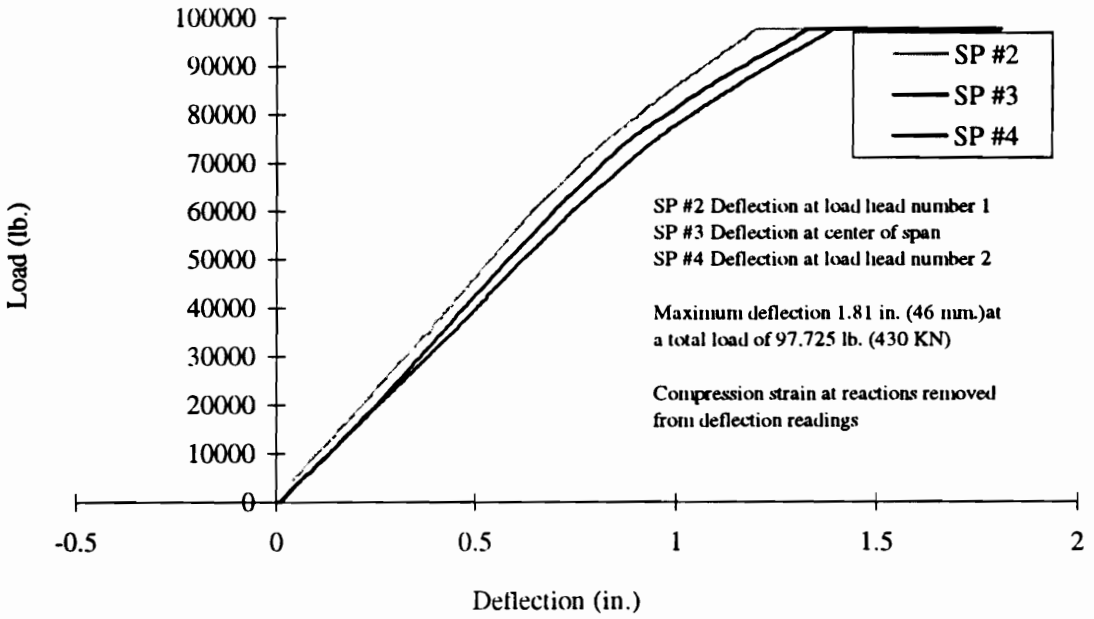

Figure 3.3. Unreinforced glulam beam load-deflection curves.

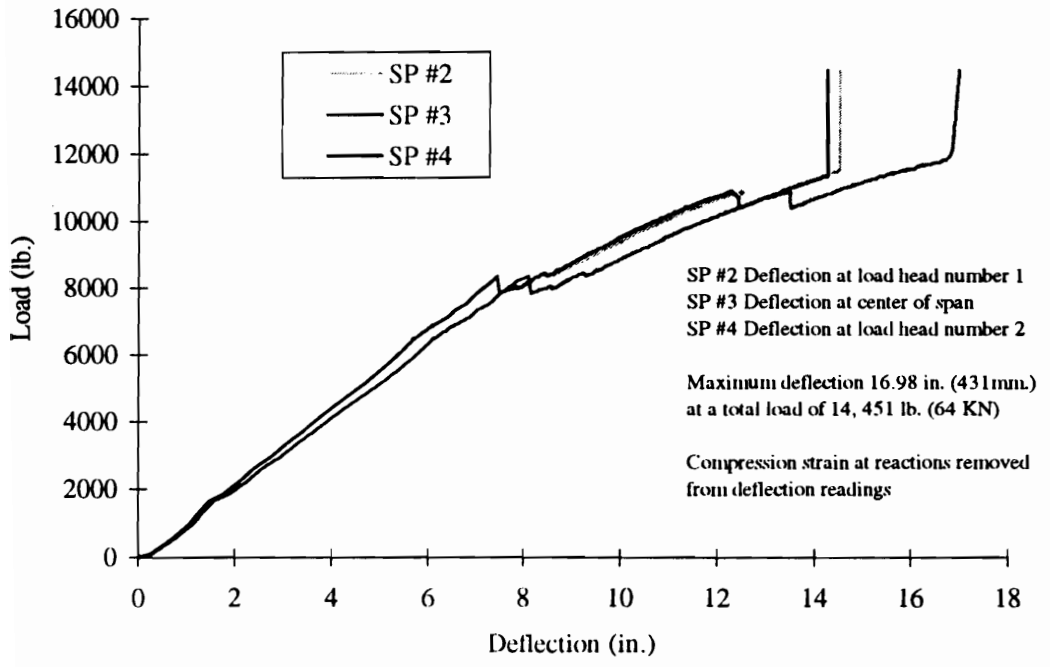

Figure 3.4. Load-deflection curves for reinforced glulam.

The average moisture content of the beam was 9.5% with the testing environment at 72°F and 63% RH. The discontinuity of the load-deflection curve at 8,000 lb is caused by the failure of the outer-most wood tensile lamination. Typically, the outer-most tensile lamination termed the "bumper lamination" fails at an end joint in the central third, lengthwise, of the beam at 60-70% of ultimate load. This occurs in reinforced glulams where the reinforcement is between the outer two wood tensile laminations.

The localized beam response to the internal stresses caused by external loading of the full-scale unreinforced or reinforced glulam beams as calculated using conventional theory was much different from that of a small-clear test specimen response to an equivalent stress.

The stress-strain relationships of small-clear specimens were discussed in Chapter 1. In Chapter 1, the upper range of strain at failure in a Douglas-fir L-1 lamination [AITC-200, 1988] from small-clear coupon testing for tension and compression was found to be .9 and .8 respectively. In addition, the compressive yield strain was 0.35 to 0.40%, whereas the tension yield strain was close to the ultimate value of 0.9% for the small clears. Though small-clear specimens fail at these levels in tension, full-scale flexural members fail at lower strains in the extreme tensile fibers. There are two ways of considering strains; a global strain of the overall beam (ε_g) developed from local elemental strains affected by nonhomogenity and strain values developed from clear wood (ε_c) specimens.

Figure 3.5 contains stress-strain curves for a matched pair of tensile and compressive specimens tested according to ASTM D143 [ASTM, 1995b]. The tensile

values are not as high as the values discussed above, but the plasticity exhibited by the compression sample versus the tension sample is the same. The samples were recovered from the ninth lamination from the top in what was a compressive laminae of an 8.75 x 42 in. x 53 ft. (220 x 1066 x 16200 mm), AITC combination 5 (all L-1 grade) Douglas-fir glulam. The moisture content of the beam was 18 to 22%. The beam was tested in wet condition to simulate a wet service environment. The maximum load at failure was 124,000 lb (550 kN) applied through two load heads, symmetrically positioned 8 ft (2440 mm) apart. The beam was reinforced with seven laminations of ARP, 0.090 in. (2.3 mm) thick, full width and full length of the beam. The deflection at failure of this beam was L/75 (L is length in inches). When the deflection, at failure, was converted to an equivalent strain (ε_x) in the extreme bending fiber in tension, ε_x equaled 0.35%.

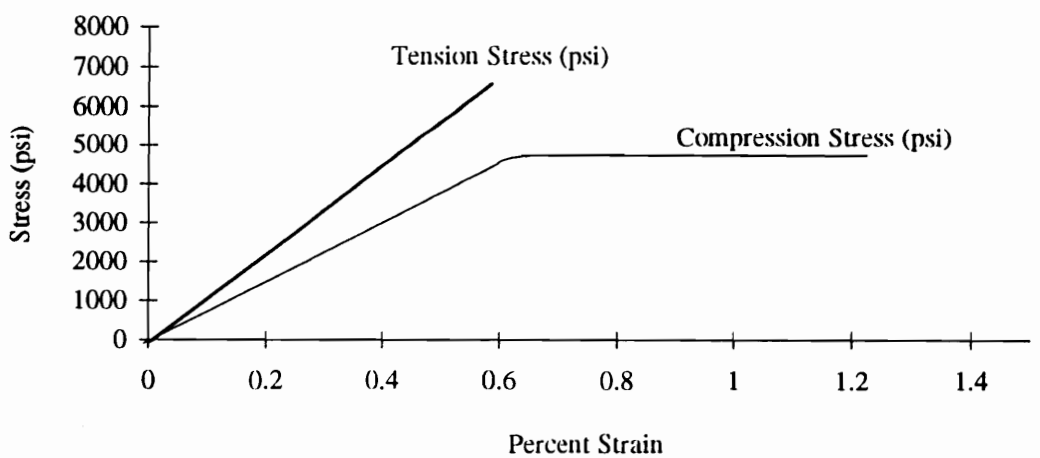

Figure 3.5. Tensile and compressive test sample stress versus strain curves for wood.

The occurrence of local strength reducing features in the full scale beam such as knots and end joints leads to beam failure at strain levels in tension well below the small-clear value. The use of reinforcement allows the beam to carry more load and strain more in the extreme tension fiber prior to failure.

The results of strain measurements from 30 full-scale beam tests were combined with component testing and statistically analyzed. Table 3.1 contains stress and strain values for 30 full-scale beams tested to failure and a statistical analysis of results. The global strain values of the extreme bending strain values in tension are shown as are the corresponding tensile coupon tensile strain at yield point from small-clear material testing [ASTM, 1995a]. Appendix E contains an explanation of the methodology used to calculate extreme bending fiber strain in tension. The strain in the extreme wood fiber in tension as predicted by converting stress to strain from equations 3.1 and 3.2 was found to be more than the actual values calculated from deflection. Thus, strain values based on deflection were used to compare with small-clear results.

There is one important aspect concerning the manufacture of the V3-1600 unreinforced glulams which were tested. The tension lamination stock used for the test beams was above the required grade. This is shown in Table 1.7 where the average safety factor of 3.53 of the V3-1600 unreinforced Douglas-fir glulams was well above the expected value of 2.1. This affected the test results significantly as will be shown.

Depending upon compressive strength parallel to grain and end joint strength in tension, the beam yield point of the unreinforced glulam in bending usually is over 80% of the ultimate load as shown in Figure 3.3 [ICBO, 1995]. The unreinforced glulams,

Table 3.1. Full scale glulam strain values and small clear tensile specimen strain values and statistical analysis results.

Grade	Species	Span	Load Head	Width	Depth	Reinforcement	Beam Yield	Beam Ultimate	Small Clear	Small Clear
		(ft)	span (ft)	(in)	(in)	Thickness* (in)	Strain	Strain	Yield Strain	Ultimate Strain
V3-1600	D-fir	16.5	5.5	5.125	15.5	0.09	0.237	0.261	0.913	0.913
V3-1600	D-fir	16.5	5.5	5.125	15.5	0.09	0.286	0.379	0.196	0.196
V3-1600	D-fir	24	8	5.125	21.5	0.09	0.168	0.253	0.488	0.490
V3-1600	D-fir	24	8	5.125	21.5	0.09	0.228	0.244	0.564	0.564
V3-1600	D-fir	26	8	5.125	21	0.09	0.259	0.303	0.554	0.554
V3-1600	D-fir	39	8	5.125	25.75	0.09	0.167	0.251	0.513	0.520
						Sample size	6	6	6	6
						Mean	0.2241	0.2818	0.5380	0.5395
						S.E.	0.0197	0.0212	0.0943	0.0933
						S.D.	0.0482	0.0520	0.2288	0.2285
						Variance	0.0023	0.0027	0.0523	0.0522
						5% LEL**	0.1115	0.1603	0.0035	0.0057
						75% CL	0.1985-0.2498	0.2542-0.3095	0.4165-0.6595	0.4181-0.6609
						C.V.	21.51	18.45	42.53	42.35

*. Aramid reinforced plastic between outer two tension laminations.

**. 5% LEL = Mean - (k*Std. Dev.), where k = 1.991.

Table 3.1. (Continued).

Grade	Species	Span	Load Head	Width	Depth	Reinforcement	Beam Yield	Beam Ultimate	Small Clear	Small Clear
		(ft)	span (ft)	(in)	(in)	Thickness (in)	Strain	Strain	Yield Strain	Ultimate Strain
V3-1600	D-fir	16.5	5.5	5.125	15.5	0	0.2625	0.3714	0.913	0.913
V3-1600	D-fir	26	8	5.125	21	0	0.2122	0.2321	0.196	0.196
V3-1600	D-fir	37	8	5.125	15.5	0	0.1261	0.2481	0.488	0.490
V3-1600	D-fir	39	8	5.125	27	0	0.1440	0.2514	0.564	0.564
						Sample size	4	4	4	4
						Mean	0.1862	0.2757	N/A**	N/A
						S.E.	0.0315	0.0322	N/A	N/A
						S.D.	0.0630	0.064	N/A	N/A
						Variance	0.0040	0.004	N/A	N/A
						5% LEL*	0.0174	0.1034	N/A	N/A
						75% CL	0.1414-0.2310	0.2300-0.3215	N/A	N/A
						C.V.	33.83	23.32	N/A	N/A

* 5% LEL = Mean - (k*Std. Dev.), where k = 2.68.

** Not available.

3.1. (Continued).

Grade	Species	Span	Load Head	Width	Depth	Reinforcement	Beam Yield	Beam Ultimate	Small Clear	Small Clear
		(ft)	span (ft)	(in)	(in)	Thickness (in)	Strain	Strain	Yield Strain	Ultimate Strain
V4-2400	D-fir	16.5	5.5	5.125	15.5	0	0.1787	0.2972	N/A**	N/A
V4-2400	D-fir	18	6	2.5	24	0	0.2510	0.3250	N/A	N/A
V4-2400	D-fir	18	6	2.5	24	0	0.2880	0.3250	N/A	N/A
V4-2400	D-fir	23	7.666	2.5	24	0	0.1008	0.2205	N/A	N/A
V4-2400	D-fir	23	7.666	2.5	24	0	0.1109	0.2772	N/A	N/A
V4-2400	D-fir	24	8	5.125	21	0	0.1782	0.2400	N/A	N/A
V4-2400	D-fir	24	8	5.125	21	0	0.1246	0.2774	N/A	N/A
V4-2400	D-fir	29	8	2.5	24	0	0.1593	0.1989	N/A	N/A
V4-2400	D-fir	29	8	2.5	24	0	0.0991	0.1538	N/A	N/A
V4-2400	D-fir	36	8	2.5	24	0	0.1337	0.1908	N/A	N/A
V4-2400	D-fir	36	8	2.5	24	0	0.1620	0.2119	N/A	N/A
V4-2400	D-fir	37	8	5.125	15	0	0.1179	0.2280	N/A	N/A
V4-2400	D-fir	39	8	5.125	27	0	0.2420	0.2769	N/A	N/A
						Sample size	13	13	N/A	N/A
						Mean	0.1651	0.2479	N/A	N/A
						S.E.	0.0170	0.0147	N/A	N/A
						S.D.	0.0613	0.0532	N/A	N/A
						Variance	0.0038	0.0028	N/A	N/A
						5% LEL*	0.0409	0.1401	N/A	N/A
						75% CL	0.1445-0.1856	0.2301-0.2657	N/A	N/A
						C.V.	37.13	21.46	N/A	N/A

* 5% LEL = Mean - (k*Std. Dev.), where k = 2.206.

** Not available.

Table 3.1. (Continued).

Grade#	Species	Span	Load Head	Width	Depth	Reinforcement	Beam Yield	Beam Ultimate	Small Clear	Small Clear
		(ft)	span (ft)	(in)	(in)	Thickness* (in)	Strain	Strain	Yield Strain	Ultimate Strain
e-stack***	Pond Pine	18	6	2.5	24	0.45	0.131	0.229	0.346	0.346
e-stack	Pond Pine	18	6	2.5	24	0.45	0.214	0.305	0.678	0.678
e-stack	Pond Pine	18	6	2.5	24	0.45	0.139	0.206	0.309	0.315
e-stack	Pond Pine	18	6	2.5	24	0.45	0.147	0.233	0.793	0.793
e-stack	Pond Pine	23	7.66	2.5	24	0.45	0.132	0.132	0.830	0.830
e-stack	Pond Pine	23	7.66	2.5	24	0.45	0.129	0.214	0.961	0.961
e-stack	Pond Pine	23	7.66	2.5	24	0.45	0.209	0.234	0.729	0.729
e-stack	Pond Pine	29	8	2.5	24	0.45	0.193	0.251	0.461	0.466
e-stack	Pond Pine	29	8	2.5	24	0.45	0.151	0.292	0.959	0.959
e-stack	Pond Pine	29	8	2.5	24	0.45	0.170	0.219	0.830	0.830
e-stack	Pond Pine	29	8	2.5	24	0.45	0.152	0.232	0.868	0.868
e-stack	Pond Pine	29	8	2.5	24	0.45	0.209	0.267	0.120	0.619
e-stack	Pond Pine	29	8	2.5	24	0.45	0.166	0.223	0.930	0.930
e-stack	Pond Pine	36	8	2.5	24	0.45	0.116	0.270	0.841	0.841
e-stack	Pond Pine	36	8	2.5	24	0.45	0.131	0.348	0.911	0.911
						Sample size	15	15	15	15
						Mean	0.1593	0.2437	0.7044	0.7384
						S.E.	0.0085	0.0128	0.0699	0.5510
						S.D.	0.0328	0.0497	0.2667	0.2133
						Variance	0.0011	0.0025	0.0711	0.0455
						5% LEL**	0.0940	0.1447	0.1734	0.3137
						75% CL	0.1491-0.1694	0.2283-0.2591	0.6218-0.7870	0.6723-0.8045
						C.V.	20.59	20.39	37.86	28.89

* ARP was placed in bottom tension zone between outer two laminations.

** 5% LEL = Mean - (k*Std. Dev.), where k = 1.991.

***. Eb ranked highest in outer lamination in compression to lowest Ed lamination adjacent to FRP in tension zone.

Ponderosea pine grade N-3 (AITC 200,1991)

shown in Table 3.1, have a beam yield point strain in bending of 67% of the ultimate failure strain of the beam. which is lower than the expected ratio. In addition, the ratio of yield point strain to ultimate strain is 67% for the reinforced V3-1600 glulams. This is higher than expected [ICBO, 1995]. High grading the tensile laminations of the V3-1600 beams was thought to have caused these unexpected results.

The global strain in bending of the extreme tensile fiber for an unreinforced glulam at failure is in a range of 0.25 to 0.28% for high grade and intermediate grade Douglas-fir respectively. This is lower than the small, clear strain value at failure.

The extreme fiber compressive-zone strain at failure for an unreinforced glulam, assuming a modular ratio of 1.06 and no compression zone plasticity, is 0.30 to 0.27% for the grades shown above, close to the small-clear value of strain at yield point of .35 to .40% for the small, clear compressive samples as can be seen in Table 1.1 and in the figures in Appendix B. The yield point strain values of small-clear compressive samples were close to full-scale, globally loaded elemental values.

The effect of localized defects in the tensile laminae lead to localized tensile failures causing global beam failure. Similarly, localized defects such as slope of grain in the compressive laminae undergo localized compressive plasticity [Gurfinkel, 1981; Anderson, 1981; Malhotra and Bagan 1980] affecting the global response of the beam by allowing more deflection. Figure 3.6 shows compressive plasticity similar to that reported in unreinforced glulams by Ramos [1961]. The glulams shown in Figure 3.6 were 8.75 x 42 in. x 53 ft. (220 x 1066 x 16155 mm) Douglas-fir beams, AITC combination 5. They were reinforced with seven layers of ARP (each 0.15 in. (3.8 mm) thick) between the outer tensile wood laminations (2.5% by cross section). The

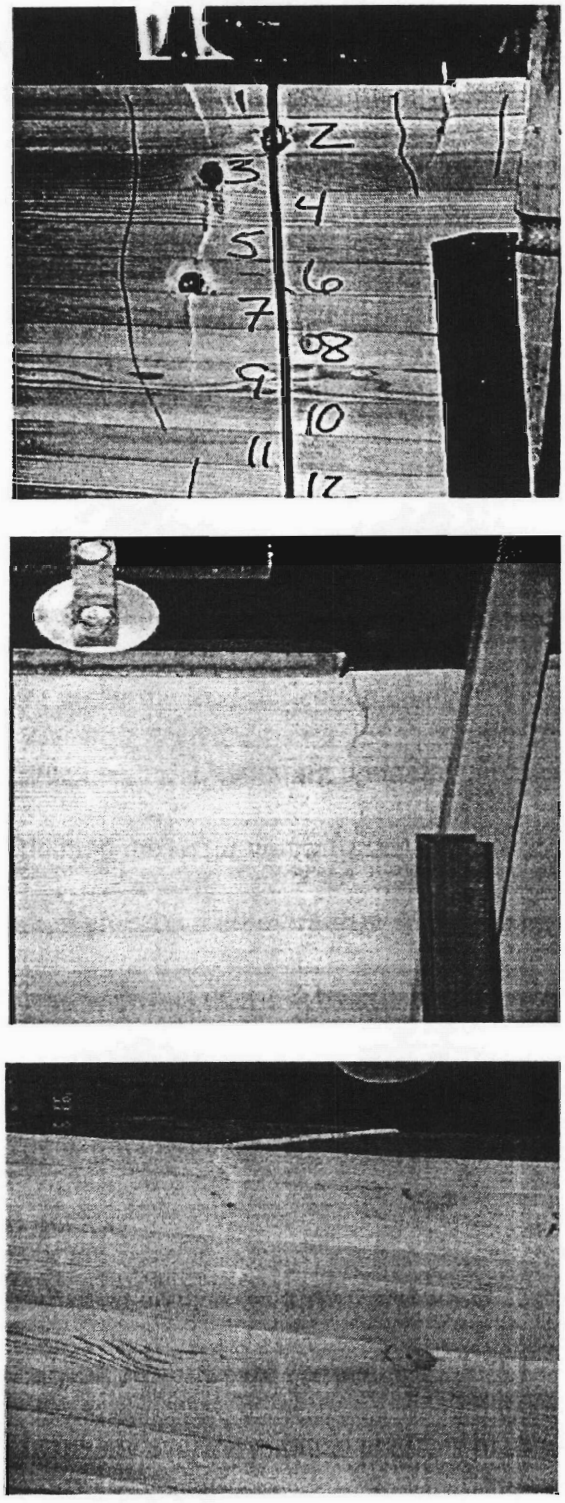

Figure 3.6. Compressive failures that illustrate compressive plasticity in reinforced glulam.

beams were tested according to ASTM D-198 [ASTM, 1995b]. The compressive response of tensile reinforced glulams reveals that plasticity is exhibited by a reinforced beam with levels of reinforcement as low as approximately 1.5% by cross-section.

Load-deflection curves for reinforced beams show beam deflections for extreme tensile fiber strains were 50% of the clear wood yield values for the extreme tensile laminations as shown in Table 3.1. In a reinforced glulam, the elemental strain value at failure in tension in a full-scale beam is an average of .28% as compared to .54% for the small-clear specimen.

Figure 3.4 shows the load-deflection curve for a reinforced glulam with 2% by cross-section reinforcement. A much more pronounced plastic range occurs in the reinforced glulam. The area under the load-deflection curve of the reinforced beam is larger than for the unreinforced beam. Depending upon the percentage reinforcement, the area under the load-deflection curve for unreinforced glulam beams may be one quarter (for heavily reinforced glulams with more than 4% by cross-section) to one half (for lightly reinforced glulams with less than 1% by cross-section) the area under the load-deflection curve for reinforced glulams. This confirms what the maximum load at failure denotes: more energy is required to fail a reinforced beam than an unreinforced beam of the same size and grades.

The results of the statistical analysis of global and small sample strain at yield point and ultimate for the tension elements are shown in Table 3.1. One significant characteristic of reinforced glulams was the reduced coefficient of variation (CoV) in the yield point strain and ultimate strain values. This can be seen by inspection of the data for V3-1600 unreinforced and reinforced glulam where the CoV of the yield point

strain was reduced 36% by adding reinforcement. Further, the ratio of mean yield point strain to mean ultimate strain in low grade Ponderosa pine is 0.67, whereas in high grade unreinforced Douglas-fir (V4-2400) it is 0.65--basically the same. Thus, FRP reinforced, lower grade Ponderosa pine glulams had similar ductility ratios to the high grade unreinforced Douglas-fir glulams.

The increase in average yield point strain and reduction of CoV between unreinforced V3-1600 Douglas-fir (low grade) glulams and reinforced V3-1600 Douglas-fir (low grade) glulams was 20%, and 33.8% to 21.5% respectively. The ultimate strain values for the reinforced V3-2400 glulams were only marginally higher than the unreinforced V3-1600 glulams with no statistical inference possible. However, a comparison of unreinforced V4-2400 Douglas-fir yield point strains and unreinforced V3-1600 Douglas-fir strains showed that little difference existed. This illustrates the high grading problem in the tension laminations. The reinforced V3-1600 Douglas-fir glulam yield point strains were 32% higher (average) than the unreinforced V3-1600 and V42-2400 Douglas-fir glulam yield point strains with a much lower CoV then either of the unreinforced types.

An ANOVA was performed on various groups of interest to establish an F-ratio, F-probability that various populations were either similar (low F value) or different (high F-probability value). Table 3.2 contains the results of some comparisons. Of most interest is the fact that reinforced V3-1600 Douglas-fir glulam yield point strains where different than high grade unreinforced V4-2400 Douglas-fir (see Section 10, Table 3.2).

Even though there was no significant difference shown, there was an indication that reinforcement had a greater effect on the population of ultimate strains than on the population of yield point strains when considering reinforced versus unreinforced V3-1600 Douglas-fir (see Section 11 and 12, Table 3.2). The ANOVA also indicated a closer relationship between yield and ultimate strain values in reinforced Ponderosa pine and unreinforced V3-1600 Douglas-fir than between reinforced Ponderosa pine and unreinforced V4-2400 Douglas-fir (Sections 1 to 6, Table 3.2). Even though there was no significant difference found in Sections 1 to 6 in Table 3.2, the F values were higher in the V4-2400 comparisons, thus it seems that the reinforced low grade Ponderosa pine is more similar in load response to a V3-1600 Douglas-fir glulams with higher grade tension laminations, than unreinforced V4-2400 Douglas-fir glulams. This is significant for the glulam industry now seeking to expand utilization of available lower grade species.

Table 3.2. Analysis of variance of ultimate and yield point strain values of various glulam beam combinations.

1. Ponderosa Pine e-stack versus V4-2400 unreinforced glulam beam on *ultimate strains* based on application of reinforcement.

Source	D.F.	Sum of Squares	Mean Squares	F-ratio	F-Prob
Between Groups	1	0.0001	0.0001	0.0471	0.8299
Within Groups	26	0.0686	0.0026		
Total	27	0.0687		∴ No difference.	

2. Ponderosa Pine e-stack versus V4-2400 unreinforced glulam beam on beam *yield strains* based on application of reinforcement.

Source	D.F.	Sum of Squares	Mean Squares	F-ratio	F-Prob
Between Groups	1	0.0002	0.0002	0.1022	0.7571
Within Groups	26	0.0601	0.0023		
Total	27	0.0604		∴ No difference.	

3. Ponderosa Pine e-stack versus V4-2400 unreinforced glulam beam on *ultimate strains* based on species.

Source	D.F.	Sum of Squares	Mean Squares	F-ratio	F-Prob
Between Groups	1	0.0001	0.0001	0.0471	0.8299
Within Groups	26	0.0686	0.0026		
Total	27	0.0687		∴ No difference.	

4. Ponderosa Pine e-stack versus V4-2400 unreinforced glulam beam on beam *yield strains* based on species.

Source	D.F.	Sum of Squares	Mean Squares	F-ratio	F-Prob
Between Groups	1	0.0002	0.0002	0.1022	0.7517
Within Groups	26	0.0601	0.0023		
Total	27	0.0604		∴ No difference.	

5. Ponderosa Pine e-stack versus V3-1600 unreinforced glulam beam on *yield strains* based on application of reinforcement.

Source	D.F.	Sum of Squares	Mean Squares	F-ratio	F-Prob
Between Groups	1	0.0023	0.0023	1.4430	0.2461
Within Groups	17	0.0269	0.0016		
Total	18	0.0292		∴ No difference.	

6. Ponderosa Pine e-stack versus V3-1600 unreinforced glulam beam on beam *ultimate strains* based on application of reinforcement.

Source	D.F.	Sum of Squares	Mean Squares	F-ratio	F-Prob
Between Groups	1	0.0033	0.0033	1.1742	0.2937
Within Groups	17	0.0417	0.0028		
Total	18	0.0503		∴ No difference.	

Table 3.2. (Continued).

7. Ponderosa Pine e-stack versus V3-1600 unreinforced glulam beam on *yield strains* based on species.

Source	D.F.	Sum of Squares	Mean Squares	F-ratio	F-Prob
Between Groups	1	0.0023	0.0023	1.4430	0.2461
Within Groups	17	0.0269	0.0016		
Total	18	0.0292		∴ No difference.	

8. Ponderosa Pine e-stack versus V3-1600 unreinforced glulam beam on beam *ultimate strains* based on species.

Source	D.F.	Sum of Squares	Mean Squares	F-ratio	F-Prob
Between Groups	1	0.0033	0.0033	1.1742	0.2937
Within Groups	17	0.0417	0.0028		
Total	18	0.0503		∴ No difference.	

9. V3-1600 reinforced versus V4-2400 unreinforced glulam beam on *ultimate strains* based on application of reinforcement.

Source	D.F.	Sum of Squares	Mean Squares	F-ratio	F-Prob
Between Groups	1	0.0072	0.0072	2.7040	0.1185
Within Groups	17	0.0450	0.0026		
Total	18	0.0522		∴ No difference.	

10. V3-1600 reinforced versus V4-2400 unreinforced glulam beam on beam *yield strains* based on application of reinforcement.

Source	D.F.	Sum of Squares	Mean Squares	F-ratio	F-Prob
Between Groups	1	0.0128	0.0128	3.7189	0.0707
Within Groups	17	0.0583	0.0034		
Total	18	0.0710		∴ a difference.	

11. V3-1600 reinforced versus V3-1600 unreinforced glulam beam on *ultimate strains.*

Source	D.F.	Sum of Squares	Mean Squares	F-ratio	F-Prob
Between Groups	1	0.0001	0.0001	0.0274	0.8727
Within Groups	8	0.0260	0.0032		
Total	9	0.0260		∴ No difference.	

12. V3-1600 reinforced versus V3-1600 unreinforced glulam beam on beam *yield strains.*

Source	D.F.	Sum of Squares	Mean Squares	F-ratio	F-Prob
Between Groups	1	0.0035	0.0035	1.1776	0.3095
Within Groups	26	0.0235	0.0029		
Total	27	0.0270		∴ No difference.	

The Elastic-Plastic Axial Stress-Strain Response in the Wood Tensile and Compressive Laminae

An investigation of the elastic and plastic stress range in the wood in the tensile laminae of full-scale reinforced glulams revealed that even when the compressive laminae were yielding and becoming plastic, the elements of wood in the extreme fiber tensile laminae remained in the elastic range. Figure 3.7 illustrates the stress-strain curve vertically through the bottom three wood tension laminations while the beam is yielding in the plastic range. The beam was a Douglas-fir glulam, AITC combination 5, all L-1, reinforced with four layers of ARP 0.07 in (1.8 mm) thick. The beam was 5.125 x 24.125 in. x 15 ft. (130 x 615 mm x 4.57 m) with load heads placed at third points. The gauges were placed at center line (longitudinally).

The local wood elements in the tensile laminae of a glulam beam that is globally exhibiting plastic behavior do not enter the plastic range. There are two reasons for this: (1) the nonhomogeneous nature of wood, and (2) the elastic and brittle (non-plastic) behavior of wood in tension even in small-clear test specimens. The variation of tensile capacity caused by discontinuities, such as slope of grain and knots and the limited plastic zone potential lead to the global failure of the beam long before the clear straight-grained wood in the tensile laminae reached its ultimate stress level.

This localized failure in the wood, however, is the predominate factor in the increase of shear-stress in the wood-FRP interface. For example, if a tensile failure occurs in the wood lamination above the FRP layer in a reinforced glulam in flexure, in the plastic zone, it leads to stress raisers and

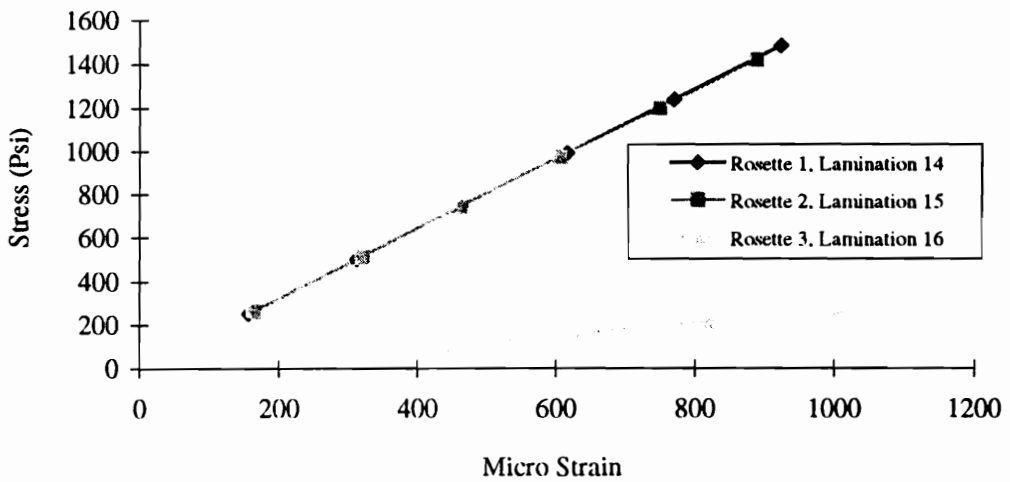

Figure 3.7. Stress-strain diagram for the three outer-most tensile laminations in reinforced glulam beam after compressive yielding had occurred.

plane sections no longer remain plane at a point where there is a finger joint failure. At that point, the wood-FRP bond fails in shear in either the FRP or wood adjacent to the finger joint failure. This means that the wood at the wood-FRP interface will generally fail in shear just prior to failure of the beam [Tingley and Leichti, 1994b]. This is assuming the adhesion methodology develops adequate shear capacity [Tingley, 1994a; Tingley, 1996b]. Alternately, a reinforced glulam in flexure may fail beyond the elastic limit in a shear mode in the wood above the tensile reinforcement closer to the neutral axis. Generally, a full-scale reinforced glulam becomes plastic when the extreme compressive fiber stress reaches the yield point of the wood element. This plastic process proceeds on one or more cross-sections until the tensile elements reach ultimate strength values at localized defects. When enough micro failures at localized defects occur, then the fracture propagates from some point in the wood or the FRP, and global failure occurs. Figure 3.8 shows a sketch of the

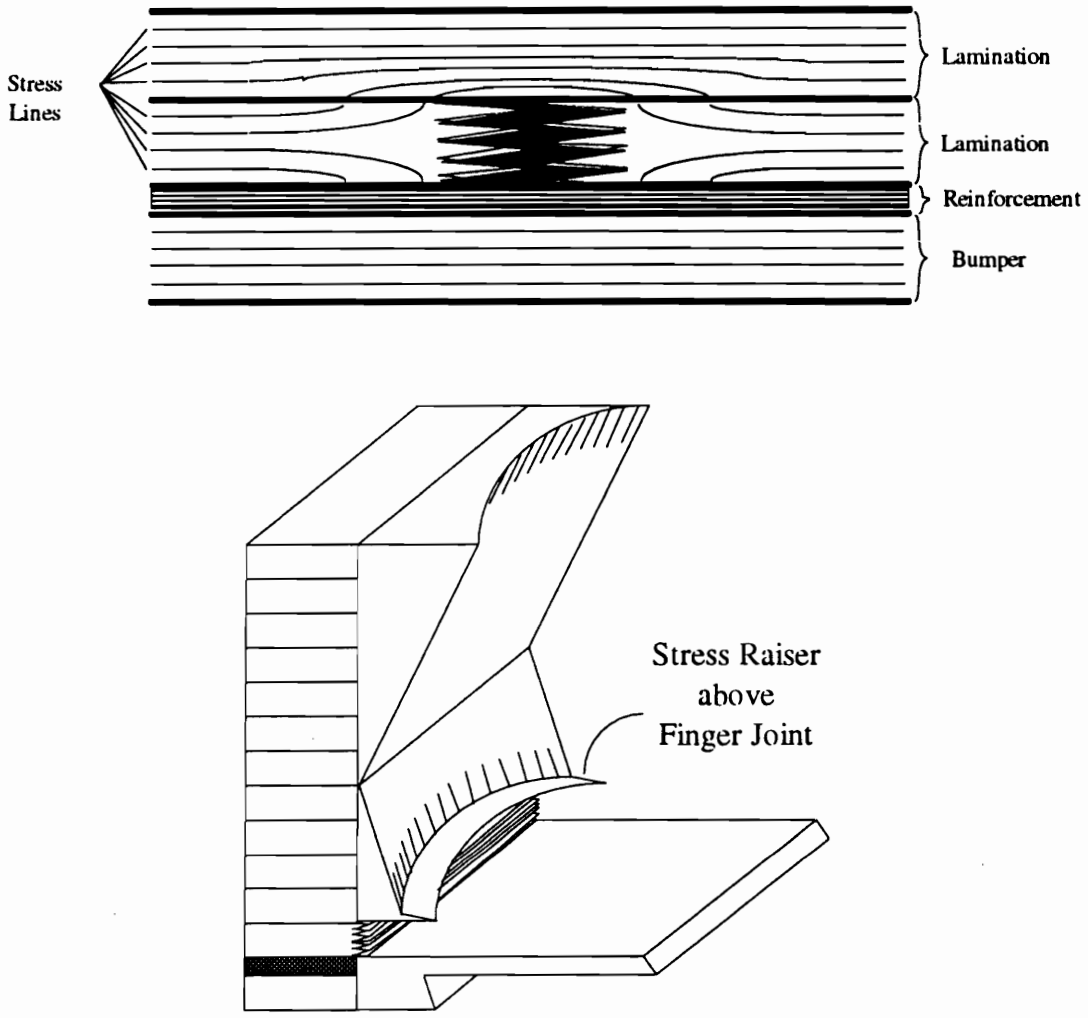

Figure 3.8. Diagram of tensile stress contour lines around failed finger joint adjacent to outermost reinforcement in outermost tension lamination of FRP reinforced glulam.

Figure 3.9. Photograph of finger joint failure in tension lamination adjacent to reinforcement leading to global failure of reinforced beam.

tensile stress contours due to a localized failure at a finger joint. The stress contours were established by strain gauges on the beam (Appendix C). The discontinuity caused by the failed finger joint lead to large increases in shear-stress in the wood-FRP interface causing failure in the reinforced glulam. Figure 3.9 shows a photograph of a finger joint that failed in the outer-most tensile lamina prior to ultimate beam collapse.

In certain situations, finger joints in successive laminations on the interior side of the FRP and adjacent to the FRP will fail leading to additional shear-stresses focused in the area of the wood-FRP glueline which in turn cause global failure. Also, impact loads generated by bumper lam failures and applied to the immediate area around a local element failing in tension close to the wood-FRP glueline will often apply a fatal

shear force to the glueline. See Figure 3.9 for photographs of this type of finger joint failure in a reinforced glulam.

The compressive plastic strain is the major contributor to global beam plastic flexure behavior (see Figure 3.6). The compressive plastic behavior can be reduced by compressive reinforcement. It serves to increase composite E_b but causes higher tensile stresses to be placed on tensile zone localized defects. This leads to the need for more tensile reinforcement. Thus, new design methodology does not contain an increase in resisting moment for compressive reinforcement and further, does not allow compressive reinforcement without tensile reinforcement [ICBO, 1995].

In the wood tensile laminae, reaching ultimate strength leads to global failure. In the wood compressive laminae, reaching the ultimate strength generally decreases global compressive strength and modulus. When the compressive ultimate strength is achieved cell wall buckling occurs which causes compressive E and strength to drop in localized positions.

As a compressive element becomes plastic, in a tension only reinforced glulam beam in bending, the beam reaches a localized buckling point laterally or vertically. Local regions in the compression zone accumulate the post plastic compressive strain leading to situations as shown in Figure 3.6.

The depth and number of these plastic strain rifts in the compressive zone are determined predominately by the tensile strength capacity of the beam in relation to the compressive strength characteristics. Since reinforcement improves tensile capacity, more such rifts are witnessed in a reinforced beam.

Theoretically, if the bond between the reinforcement and wood can be improved and the adjacent lamination's shear capacity improved, the reinforced glulam strength will be increased. However, the improvement will be small since the shear strength of wood is low compared to the FRP.

Elastic-Plastic Axial Stress-Strain Behavior in the Reinforcement

Reinforcement has stress-strain behavior in compression and tension similar to that exemplified by wood. The tensile yield point is not well defined and abrupt failures often occur. The FRP compressive stress-strain (for those FRP's with compressive strength) response often includes large plastic deformations followed by fiber buckling and ultimate failure in compression of the FRP. The fiber buckling in compression is due mainly to filament matrix debond, which occurs at the time of manufacture of the FRP. There are several principles causes of this debond: thermal expansion coefficient differences between the matrix and fiber, fiber sizing incompatibility with the matrix and matrix shrinkage during curing. Figure 3.10 shows a 7500x scanning electron microscope microphotograph of a carbon/aramid-reinforced plastic (CARP) FRP. Filament/matrix debond can clearly be seen.

The tensile stress-strain behavior of carbon aramid reinforced plastic (CARP) is linear with an abrupt failure (see Chapter 1 and Appendix B). This is similar to the tensile stress-strain behavior of wood. The compressive stress-strain curve although similar in shape to wood as shown in Appendix B contains dramatic differences. The FRP, depending on type, has much higher E values in compression and tension and higher axial strengths in tension and compression than wood. Generally the FRP is

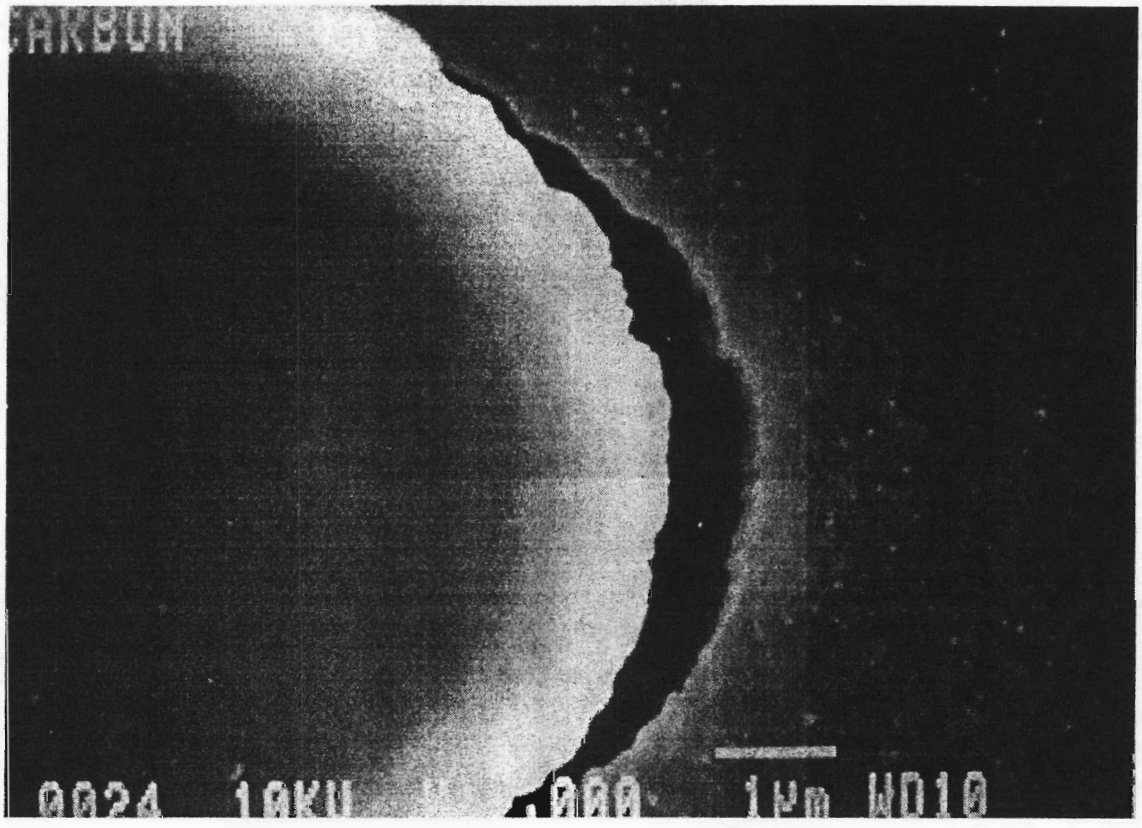

Figure 3.10. Scanning electron microscope carbon filament matrix debond.

orders of magnitude stronger and one order of magnitude higher for modulus in tension and compression than for wood.

One other important difference between wood and FRP reinforcement is that the FRP reinforcement has no localized defects such as slope of grain, knots, etc. This consistency of the FRP shows in strain gauge data for axial stress across the width of a reinforced glulam on the reinforcement. Figure 3.11 shows a graph of axial strain across the width of the beam on the FRP. The strain variation across the width is much lower. This characteristic may also be caused by the thickness of the FRP compared to the wood laminations as other researchers suggest [Jones, 1975]. However, the same

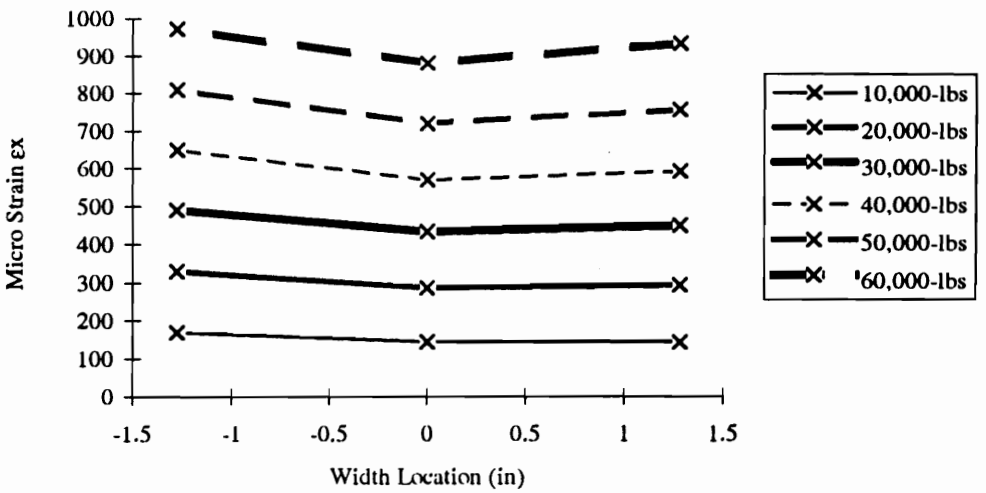

Figure 3.11. Axial strain across width on tensile reinforcement in a reinforced glulam beam.

level of variation across the width on the FRP is noticed on thicker FRP composite layers two times as thick. Although the FRP individual layers are two times the thickness, relevant to the wood, the FRP lamination is still very thin. Much more research in this area is needed to fully explain this response.

The elastic range is much greater for reinforcement than for wood, and therefore, when considering of local strains in the area of the FRP-wood interface, the wood will fail in axial strain before the reinforcement if plane sections remain plane. Thus, global failure of a properly designed reinforced beam is governed by wood and not the FRP except that beam tensile failure strain in the wood is increased by the adjacent reinforcement lamina. It is important to point out that in-service characteristics such as creep, in a saturated condition, of certain FRPs such as fiberglass-reinforced plastic may reduce their tensile or compressive strength

characteristics so significantly that they become weaker than wood in tension and fail before the wood [Tingley et al., 1996c].

Reinforcement used in percentages economical to manufacture (<5% by cross section) must yield at strain values higher than wood in order to achieve composite strain compatibility. The most efficient reinforced beams are made having an FRP strain value at yield point close to that of wood at yield point. An ideal FRP has high modulus and a yield point strain of 0.9% in tension and 0.8% in compression (dependent upon wood strain characteristics). These values will maximize the compressive plasticity potential in the reinforced glulam.

Stress-Strain Relationships Across the Width of Reinforced Glulam in the Wood-Reinforcement Interface

It has been shown that the localized tensile sections adjacent to the FRP in full-scale reinforced glulams operate in the elastic range at beam failure. In addition, plastic compressive stresses occur only in limited areas. Ultimate tensile stresses generally occur only in local elements and precipitate global failure.

To investigate local deformation in portions of the beam in global bending, strain gauges were installed on and in test beams. The results of strain gauge monitoring of the transverse strain, ε_z, and shear-strain in the xz plane, γ_{xz}, in the expected shear-free zone on wood are shown in Figures 3.12, 3.13, and 3.14. The ε_z and γ_{xz} values on the wood and FRP for the shear zone are found in Figures 3.15, 3.16, and 3.17. Figures 3.12 to 3.17 are for laminations in the mid-depth shear maximum zone, in the vicinity of the neutral axis of the beam. The tension-only and tension-

compression reinforced glulam values showing the transverse strain and xz shear strain through width on tensile and compressive reinforcement respectively are compared in Figures 3.13 and 3.14 and 3.15 and 3.16 respectively. The results show the consistent properties of the reinforcement may be affecting the strain values across the width on the reinforcement.

Figures 3.12 to 3.17 indicate this consistency applies to not only tensile reinforced beams as well as tensile compressive reinforced beams in both the expected shear free and shear zones.

Shear-Stresses in the FRP-Wood Interface Zone

There are several types of shear-stresses that develop between the reinforcement and the wood. First, a shear-stress is developed longitudinally due to differential applied moment along the length of the beam in the shear zone in the xy plane and is referred to as τ_{xy1}. Second, a shear-stress is developed in the xy plane, τ_{xy2}, due to stiffness difference between the wood and FRP [Jones, 1975]. Third, a shear-stress is developed through the width in the zx plane because transverse stresses in the wood adjacent to the reinforcement vary across the width, while they do not vary in the FRP. This results in differential transverse stresses between the wood and FRP across the width of the beam.

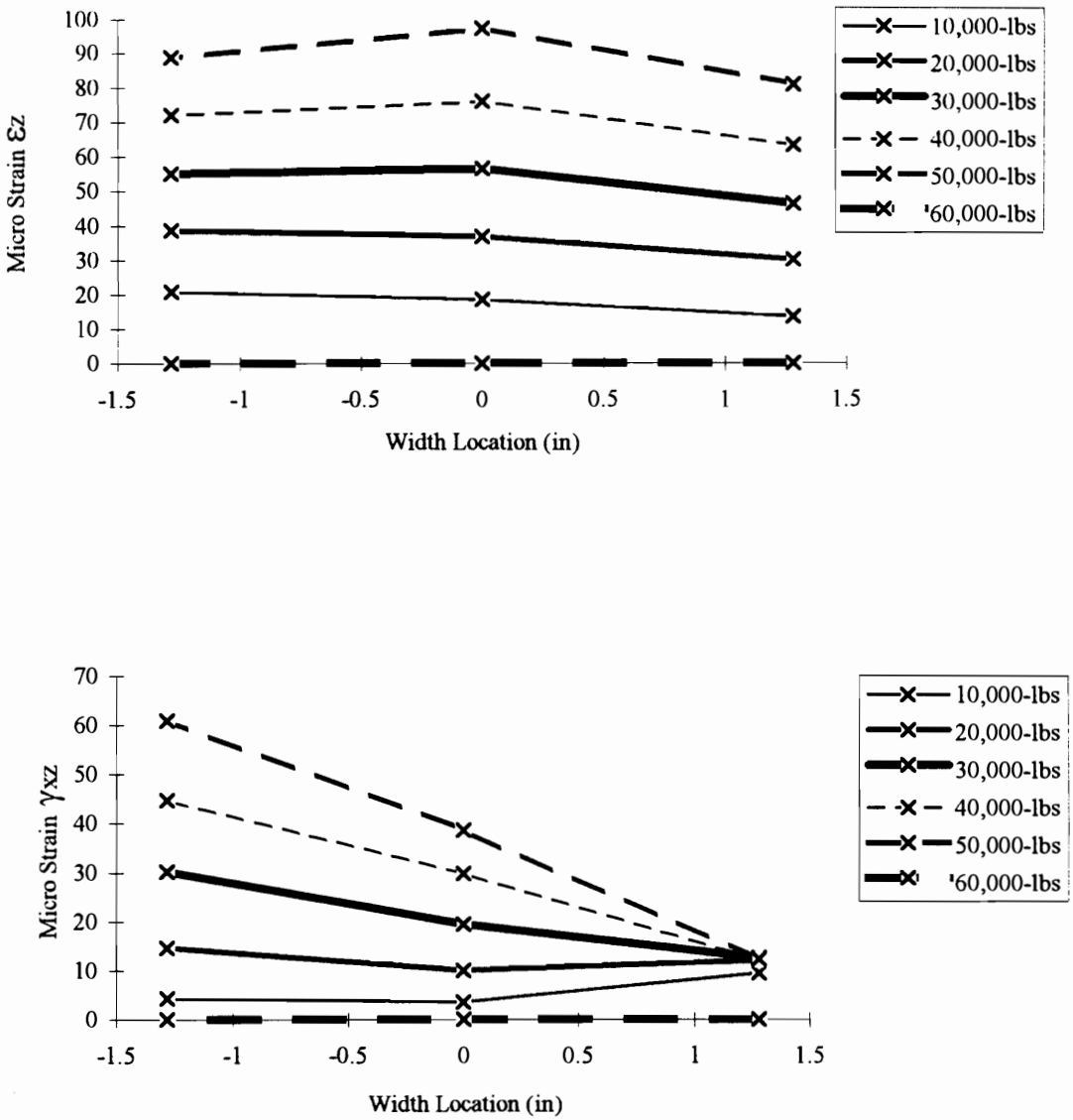

Figure 3.12. Transverse strain (ε_z) and shear strain (γ_{xz}) through the width in the reinforced glulam beam on wood at mid-depth in the expected shear free region where dead weight was neglected.

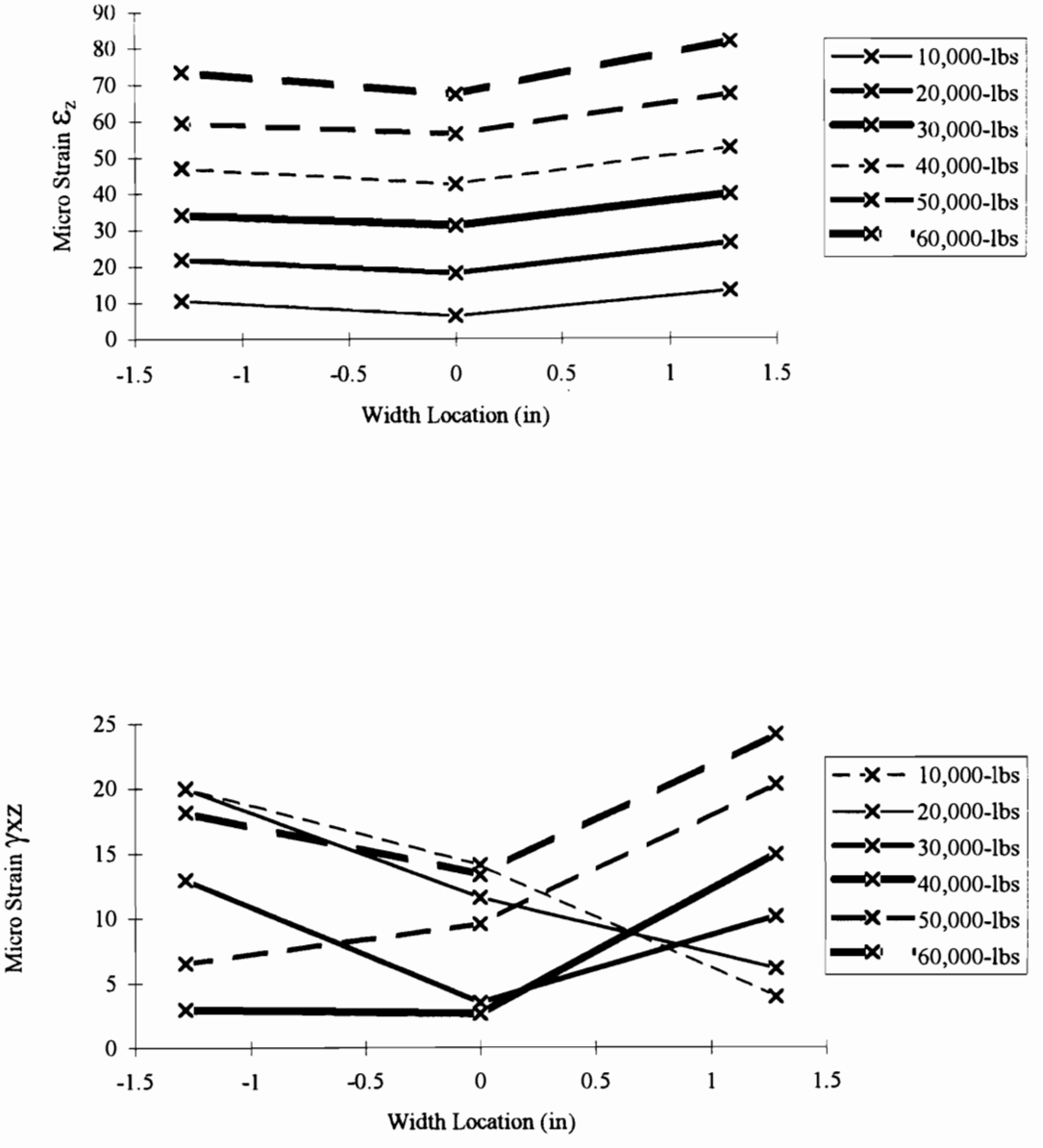

Figure 3.13. Strain through the width measured on the wood in the expected shear-free region excluding dead weight of a reinforced glulam beam (a) ε_z and (b) γ_{xz}.

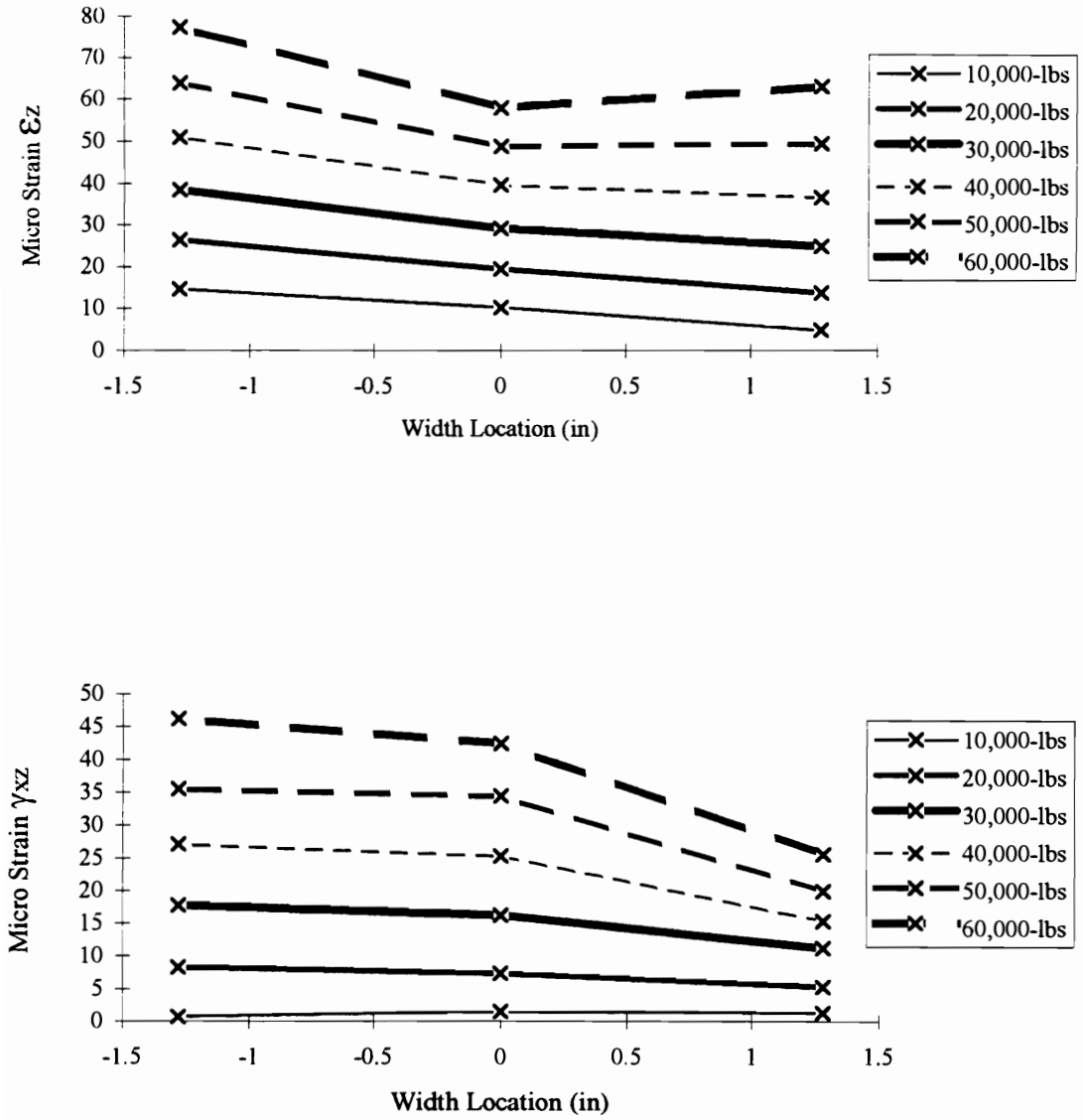

Figure 3.14. Transverse strain (ε_z) and shear strain (γ_{xz}) through width on wood tensile and compressive laminae of reinforced glulam beam in the expected shear-free zone excluding dead weight.

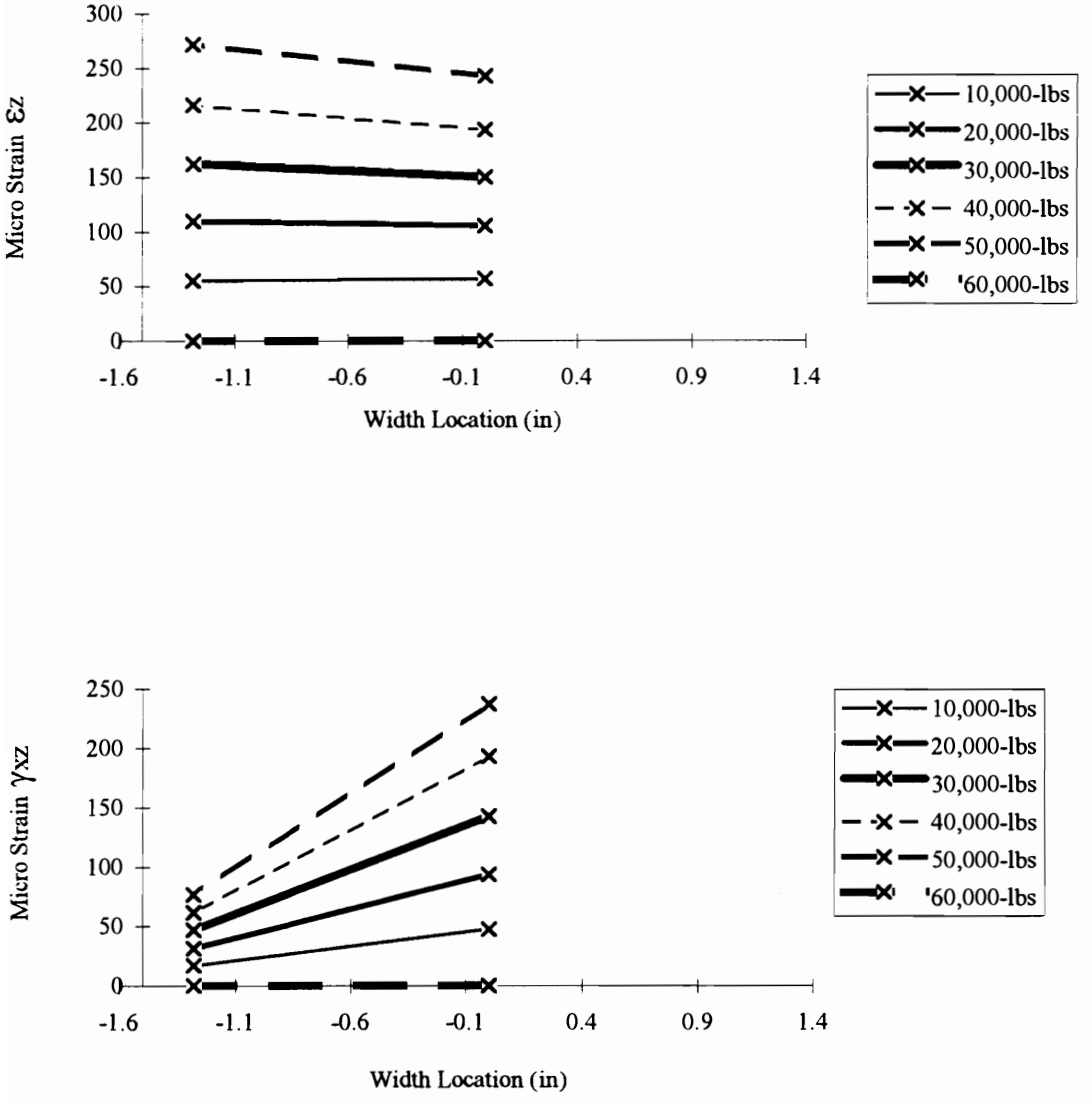

Figure 3.15. Transverse strain (ε_z) and shear strain (γ_{xz}) through width in unreinforced glulam beam on wood in the shear zone.

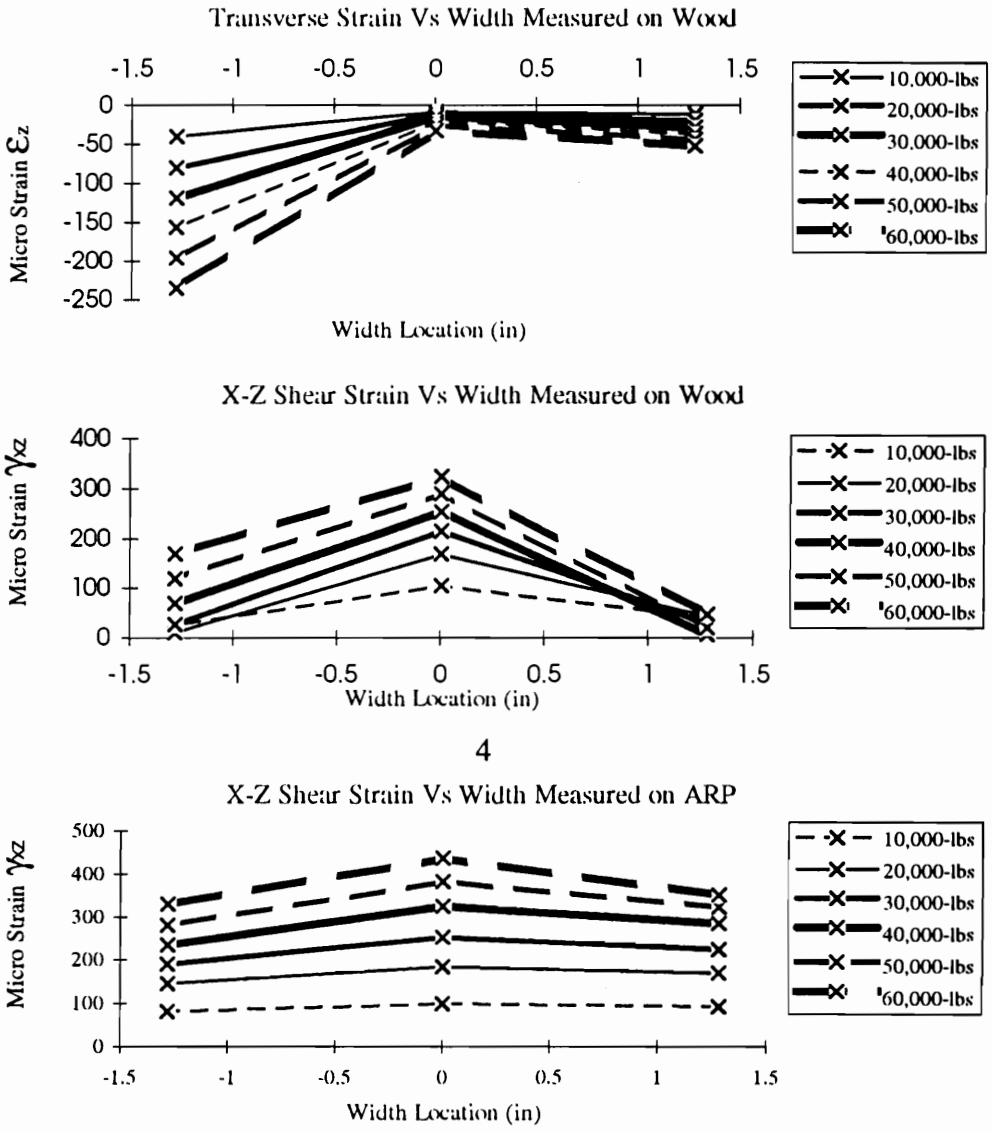

Figure 3.16. Transverse strain (ε_z) and shear strain (γ_{xz}) through width in a tensile-reinforced glulam beam on wood and ARP laminae in the shear zone.

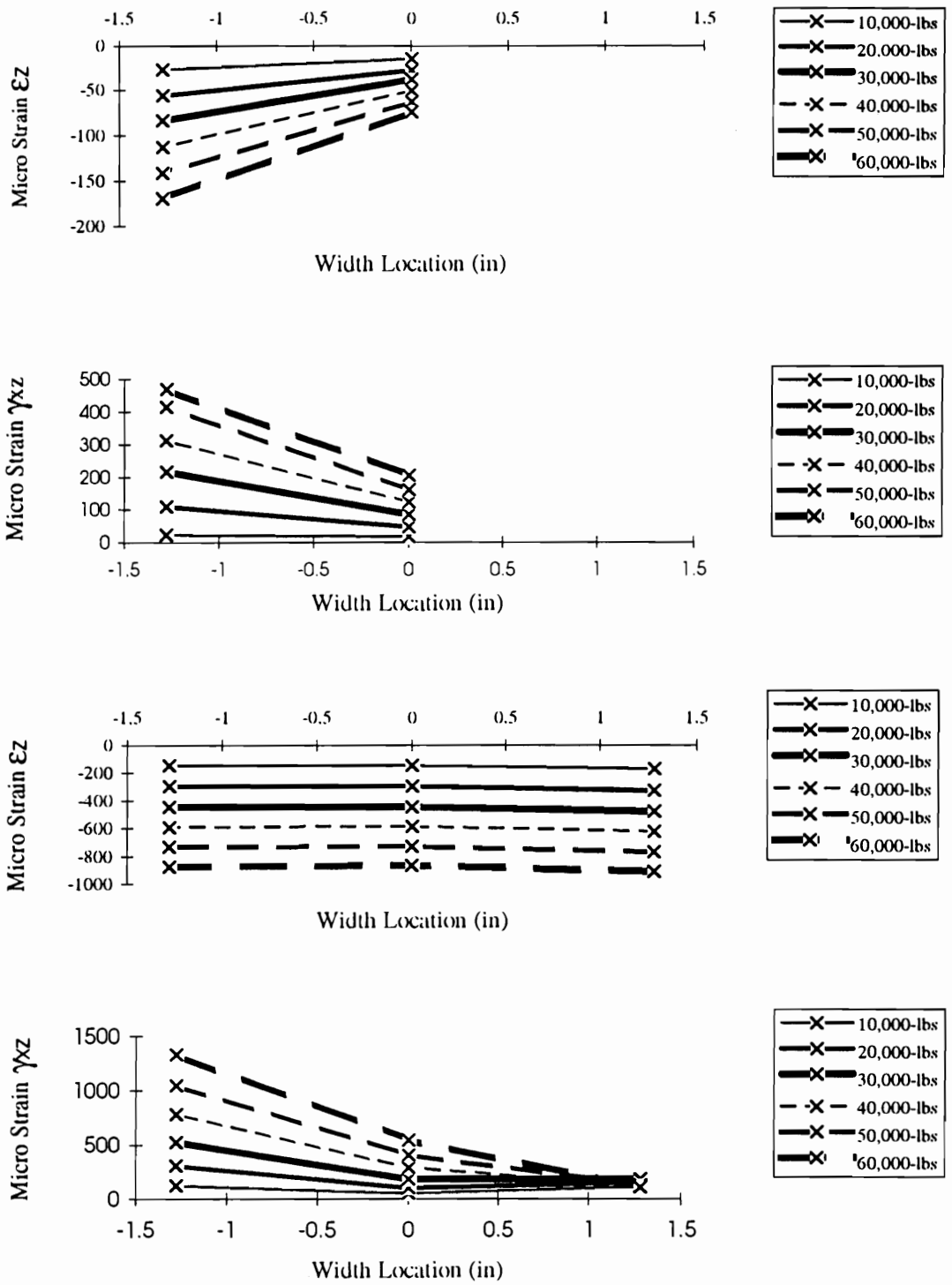

Figure 3.17. Transverse strain (ε_z) and shear strain (γ_{xz}) through width on wood and ARP laminae in a tensile/compressive reinforced glulam beam in the shear zone.

The variation in the modulus of elasticity in radial/tangential direction ($E_{R/T}$) across the width of the beam in the wood lamination adjacent to the FRP is the cause of this stress variation. These stresses occur in the zx plane and are referred to as τ_{zx1}-shear stress. Fourth, a shear-stress is caused by differential dimensional change between the wood and FRP as the wood shrinks or expands and the FRP remains stable while the reinforced glulam is drying or wetting respectively. These shear-stresses are substantial in the zx plane [Tingley et al., 1996d]. They are referred to as τ_{zx2} -shear stresses. Typically, in reinforced beams, the τ_{zx2} shear stress is the largest whereas τ_{zx1} is the smallest.

Using the equations developed earlier in this chapter and in Chapter 2 for three-dimensional calculation of stress-strain at a point, the shear-stress in the wood-FRP glueline can be calculated for each component in the xy and xz planes. This calculation reveals very high shear stresses developed between the FRP and wood when strain gauge data is placed into equations 2.5 and 2.6 as shown in Figure 2.12. Table 3.3 contains actual beam shear values for Douglas-fir all L-3 beams tested according to ASTM D-198 [ASTM, 1995b]. The values indicate shear strength in full-scale beams was low compared to values from shear blocks in the xy and xz planes for specimens cut from the beams.

The wood and FRP adherends as well as the adhesive in the glueline must be capable of resisting the various stress combinations. The value of the ultimate shear strength of the adhesive should be equal to or greater than that of wood.

Table 3.3. Summary of full-scale shear beam shear strength versus minimum small block shear strength found along the failure pathway, for Douglas-fir all L-3 beams.

Full-scale Shear Strength (psi)	Block Shear Strength xy Plane (psi)	Ratio of Full-scale Strength to xy Block Strength	Block Shear Strength xz Plane (psi)	Ratio of Full-scale Strength to xz Plane Block Strength
587	868	0.68	1151	0.51
606	1317	0.46	1159	0.52
656	---	---	1159	0.57
579	1126	0.51	1126	0.51
572	1201	0.48	511	1.12
616	1384	0.45	835	0.74
588	1284	0.46	1259	0.47
602	1350	0.45	---	---
603	1284	0.47	910	0.66
566	1134	0.50	1026	0.55
623	1109	0.56	453	1.38
587	951	0.62	943	0.62
688	1167	0.59	935	0.74
Average	---	0.52	---	0.70

Table 3.4 presents the results of over 6,000 glueline shear block tests using T107 shear block test methods [AITC-200, 1992] for wood-to-wood, wood-to-FRP and FRP-to-FRP gluelines. Appendix B contains the test methodology and statistical analysis procedure used for these tests. Table 3.4 provides the typical range of shear strength found in FRP-FRP, wood-wood and wood-FRP adhesive bonds from small shear block tests.

Table 3.4 also shows shear strength values in a range comparable to both wood and FRP. These values show that the adhesive methodology currently in use with commercial FRP-reinforced glulams is satisfactory [Tingley, 1994a; Tingley, 1996a] to achieve enough shear translation resistance to cause the wood or FRP to fail first, not the glueline.

Table 3.5 shows the wood τ_{xy} shear strength values developed from ASTM D-198 full-scale beam tests [Tingley, 1996b]. The measured shear strength of the full-scale beam in the xy plane, as shown in Table 3.5, have more accurate shear strength values than small block shear values, for full-scale reinforced glulam wood-FRP interface shear analysis in the xy plane [Tingley, 1996b]. The global beam failure at the elemental level in shear at the wood-FRP interface has been shown to be a common failure mode for reinforced glulams [ICBO, 1995].

Table 3.6 shows FRP shear strength values for FRP in the plane parallel to fibers with 70/30/fiber/matrix volume percentage using a vinylester matrix. The fibers are unidirectional. The shear strength minimum value (τ_{xy}) obtained from Table 3.3 for small shear block tests of wood for Douglas-fir is in a range of 1000 psi (6.9 MPa), which is below the 5% LEL value for CARP, but above the 5% LEL value for ARP. Thus, various FRP's have different longitudinal shear values even though the G values are similar. Therefore, the shear-stress in the xy plane for the FRP is an important consideration in analyzed the FRP-wood bondline.

A comparison of Tables 3.5 and 3.6 shows that a unidirectional fiber, vinylester matrix 70/30, fiber volume FRP will, in the majority of cases, be stronger in shear at the wood-FRP interface than the wood. Obviously, the adhesive and bonding method is critical to this outcome [Tingley, 1995]. The bond must resist the various types of shear-stresses that develop at the wood-FRP interface from external applied loads and MC variation.

Table 3.4. Result of AITC T107 glueline shear tests from conventional and reinforced glulam beams.

AITC Combination Number	Glue Line	Valid N	Mean	Std. Dev.	Minimum	Maximum
44	ARP-ARP	19	1147	204	702	1533
44	Wood-Wood	67	1400	178	1176	1948
32	ARP-ARP	13	894	168	702	1234
32	Wood-Wood	60	1462	209	1167	1982
58	ARP-APR	1	885	---	885	885
58	Wood-Wood	71	1592	236	1184	1982
5	ARP-ARP	272	963	192	652	1533
5	ARP-Wood	150	1280	239	951	1948
5	CARP-CARP	139	1047	145	785	1600
5	CARP-CARP	53	1188	223	935	1757
5	FARP-FARP	35	1137	232	819	1674
5	Wood-Wood	3975	1505	228	1159	2192
17	ARP-Wood	20	1188	259	935	1982
17	Wood-Wood	59	14925	225	1167	1982
16	ARP-Wood	18	1350	256	968	1649
16	Wood-Wood	69	1508	204	1159	1982
15	ARP-ARP	36	843	116	652	1043
15	ARP-Wood	83	1208	231	918	1948
15	CARP-CARP	57	1051	206	794	1600
15	CARP-Wood	84	1114	126	910	1400
15	Wood-Wood	910	1427	214	1159	1982
15	ARP-ARP	2	976	94	910	1043
15	ARP-Wood	18	1381	210	1026	1708
15	Wood-Wood	185	1329	149	1159	1816
1	ARP-ARP	12	950	270	686	1749
1	ARP-Wood	39	1289	259	951	1957
1	Wood-Wood	362	1512	243	1159	1982
50	ARP-ARP	15	890	109	669	1151
50	ARP-Wood	3	1012	99	943	1126
50	Wood-Wood	97	1732	240	1176	1982
25	ARP-Wood	19	1201	176	968	1583
25	Wood-Wood	74	1485	213	1159	1915
48	ARP-ARP	11	869	154	702	1159
48	Wood-Wood	76	1604	228	1167	1982
47	ARP-ARP	18	939	137.26	652	1226
47	Wood-Wood	74	1650	243.76	1157	1982
24	ARP-Wood	20	1340	212	1101	1857
24	Wood-Wood	89	1535	202	1167	1982
23	ARP-Wood	20	1457	206	1134	1799
23	Wood-Wood	83	1499	202	1159	1982

Table 3.5. Shear strength values for various species.

Species	Grade	Full-scale beam τ_{xy}	Lower 5% Exclusion Limit[a] 75% Confidence τ_{xy}
Douglas-fir	L-1	638	512
Douglas-fir	L-2	580	491
Douglas-fir	L-3	593	506
Douglas-fir	L-3	584	485

Note: [a] LEL = mean X - ($\sigma \times k$), where factor k = 2.463.

Table 3.6. Reinforcement shear strength values with statistical analysis.

Material	Panel Dimension	Sample Size	Average τ_{xy}[b] (psi)	LEL τ_{xy}[b] (psi)
ARP	3.125 × 0.070	4	1163	521
ARP	5.125 × 0.070	1	1099	---
ARP	6.750 × 0.070	1	1844	---
ARP	3.125 × 0.070	17	1339	852
ARP	5.125 × 0.070	15	1119	817
ARP	6.750 × 0.070	14	1213	693
ARP	3.125 × 0.070	6	1370	738
ARP	5.125 × 0.070	46	1535	1103
ARP	6.750 × 0.070	5	1792	1327
CARP	3.125 × 0.070	1	1536	---
CARP	5.125 × 0.070	5	2094	1626
CARP	6.750 × 0.070	14	2390	1692
CARP	3.125 × 0.070	34	2036	1273
CARP	5.125 × 0.070	28	2452	1735
CARP	5.125 × 0.070	5	1801	1608
CARP	5.125 × 0.070	1	2733	---
CARP	6.750 × 0.070	28	2251	1703

Note: Matrix Type: Vinylester. Average 70% fiber content. Transverse shear plane parallel to grain.
LEL = mean X - $\sigma \times k$, where factor k = 2.463.

[b] Reinforced.

Table 3.7. Summary of full scale shear beam shear strength versus minimum small block shear strength found along the failure pathway.

Full-scale Shear Strength (psi)	Shear Block Shear Strength xy Plane (psi)	Ratio of Full-scale Strength to xy Block Strength	Shear Block Shear Strength xz Plane (psi)	Ratio of Full-scale Strength to xz plane Block Strength
587	868	0.68	1151	0.51
606	1317	0.46	1159	0.52
656	---	---	1159	0.57
5799	1126	0.51	1126	0.51
572	1201	0.48	511	1.12
616	1384	0.45	835	0.74
588	1284	0.46	1259	0.47
602	1350	0.45	---	---
603	1284	0.47	910	0.66
566	1134	0.50	1026	0.55
623	1109	0.56	453	1.38
587	951	0.62	943	0.62
688	1167	0.59	935	0.74
Average	---	0.52	---	0.70

The Relationship Between Axial Tensile and Compressive Stresses and Shear-Stresses at the Wood-Reinforcement Interface

Shear-stresses in the xy plane through the depth of a beam are caused by changes in moment along the length of the beam as depicted in Figure 3.1 for an unreinforced glulam. These shear stresses exist in a parabolic distribution with a maximum located at the neutral axis (Figure 3.1).

Reinforced glulams exhibit conventional stress distributions with some notable exceptions. It has been shown [Tingley and Leichti, 1994a; Tingley and Leichti, 1994b; Tingley and Leichti, 1994c] that the axial stresses and xy shear stresses [Jones, 1975] at a point in the depth of a glulam beam generally increase to the outside edge and are not uniform as shown in Figures 3.1 and 3.2. Figure 3.18 more accurately represents the

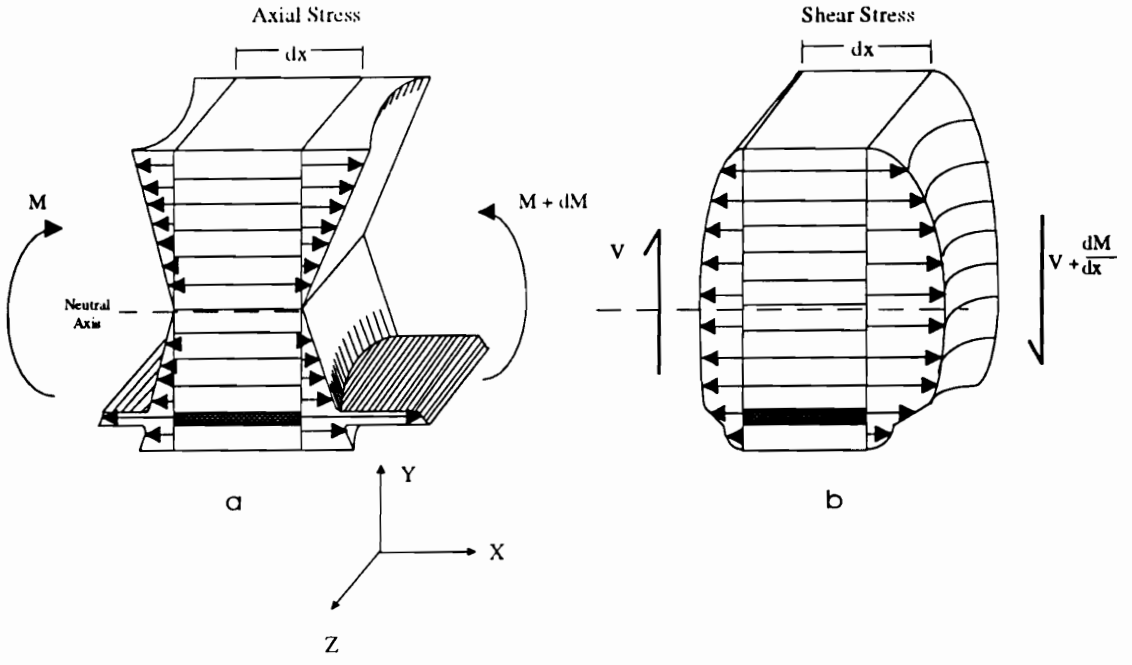

Figure 3.18. Generalized actual stress distributions in a reinforced glulam; a) axial stress (σ_x) b) Shear stress (σ_{xy}).

distribution of stresses through the depth of a reinforced beam. It is noted that a similar modification of stresses for an unreinforced beam could be shown.

A comparison of τ_{xz} and σ_x between reinforcement and wood at the location of the wood reinforcement interface shown in Figure 3.19, reveals relationships that are similar to those shown in Figures 3.12 to 3.17. The τ_{xy} shear stresses in Figure 3.19 decrease to the edge. This is not representative of a majority of the test results as shown in Table 2.2. Figure 3.19 was chosen for display in this chapter as it represented the only complete set of matched strain gauges on the wood and FRP where all gauges remained operational across the width. Equations 2.5 and 2.6 have been used to convert strain values to stress. The increase in stresses towards the edge in Figure 3.18 was developed by using the axial data and extrapolating it to estimate τ_{xy} for reinforced

glulams across the width and through the depth (see Appendix C). Also shown in Figure 3.18 is the flattening of the parabolic curve and increase in shear-stress in the area between the neutral axis and the wood-FRP interface. Figure 3.20 shows the actual xy shear-strain distribution through the depth of a reinforced glulam in an area outside the effects of compression perpendicular to grain. This distribution was mapped at one half of the ultimate shear load. The maximum τ_{xy} value was 312 psi (2.16 MPa). The τ_{xy} shear stress difference between the shear stress in the wood adjacent to the wood FRP interface and at the neutral axis was 87 psi (0.6 MPa), 33% higher than predicted by equation 3.8. The beam was tested according to ASTM D-198 [ASTM, 1995a]and strain gauged according to the methodology outlined in Appendix C. The beam was an AITC combination 5, Douglas-fir glulam 5.125 x 12 in. x 21 ft. (130 x 305 x 6400 mm). It was reinforced with two layers of ARP 0.07 in. (1.88 mm) thick on the bottom tension face.

A marked flattening of the shear distribution curve with an increase in shear stress in the area between the neutral axis and the FRP was observed. The distribution shape matched that predicted using equation 3.22. The distribution in Figure 3.20 indicates that the τ_{xy} shear stresses on the wood-FRP interface zone between the neutral axis and the FRP are higher than conventionally predicted by equation 3.8.

It was hypothesized earlier, that the major cause of the modified axial stress distribution in the transverse direction in wood is that grain runs off the edge of each lamination edge since longitudinal square sections are sawn from tapered tree trunks.

The increase in stresses toward the edge of the glulam beam, both axial and shear, leads to an interesting anomaly at the reinforcement wood interface since the

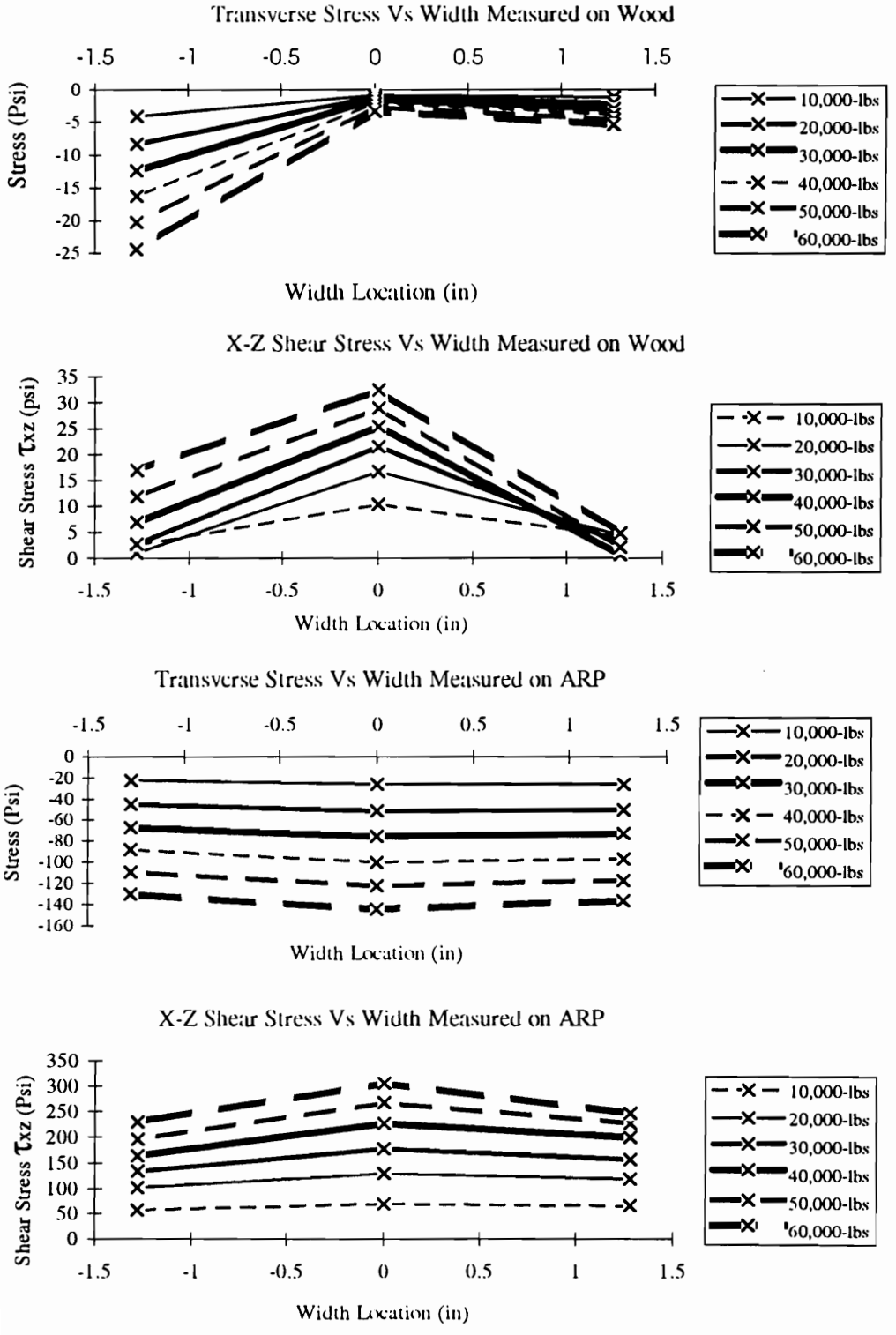

Figure 3.19. Axial stress (σ_x) and shear-stress (τ_{xz}) through width in the tensile reinforced glulam beam on wood and ARP in the shear zone in wood-reinforcement interface.

reinforcement exhibits a constant stress across the width of the beam. This differential in stress across the glueline leads to elevated shear stress toward the edge at the wood-reinforcement interface across the width of the beam. Figure 3.21 more clearly depicts this shear-stress differential in the xz plane in the wood above the glueline caused by the differential tensile stresses across the width of the beam. This shear stress differential in the xz plane may be caused by the coupling of axial extension and shear in the xz plane.

The degree to which the axial stresses increase toward the edge across the width of the beam is determined by xz shear-stresses and quality of lumber (slope of grain). Jones [1975] also points out that laminate thickness contributes to an increase in axial stress toward the edge. In addition, Jones (1975) points out that τ_{xz} must be zero at the edge but can be finite elsewhere. Thus, he indicates that the τ_{xy} shear stresses can also increase toward the edge but drop to zero at the free edge. This agrees with the distribution shown in Figure 3.21.

The greater the applied axial stresses are, the greater the magnitude of the axial stress increase towards the edge (see Figure 3.19). In the shear zone, a greater gradient of stresses to the edge is also exhibited.

The τ_{xy} shear stress distribution through the depth of a reinforced glulam beam is different than the τ_{xy} shear stress distribution in an unreinforced glulam beam. The τ_{xy} shear stress maximum value at the neutral axis and the τ_{xy} shear stress maximum value in the wood between the neutral axis and the tensile FRP are different than the values obtained from equation 3.8. This factor is important to consider when developing design values for τ_{xy}.

Twenty-three of the 30 beams studied failed in xy plane shear in the area between the neutral axis and the tensile FRP. The results of xy-plane shear block tests from samples recovered adjacent to the failure pathway for each of the 23 beams are shown in Table 3.8. The full-scale beam xy-shear plane failure values calculated using the proceeding equations for xy shear stress at the neutral axis are also shown in Table 3.8.

Table 3.8 compares the shear block wood-FRP glueline shear strength value to the beam failure shear stress value as predicted by equation 3.8(simple theory --- $\frac{3V}{2A}$), equation 3.9 converted to τ_{xy} using G (transformed section using n --- $\frac{VQ_r}{I_r t}$) and equation 3.22 (transformed section using η and η'--- $\left(\frac{VQ_r}{I_r t}\right)\eta'$). It can be noted that the maximum shear stress value of the beam at the neutral axis as predicted by any of the above equations, such as $\frac{3V}{2A}$, is much smaller than the shear block values. This is caused by load and grain orientation (Tingley,1996d).

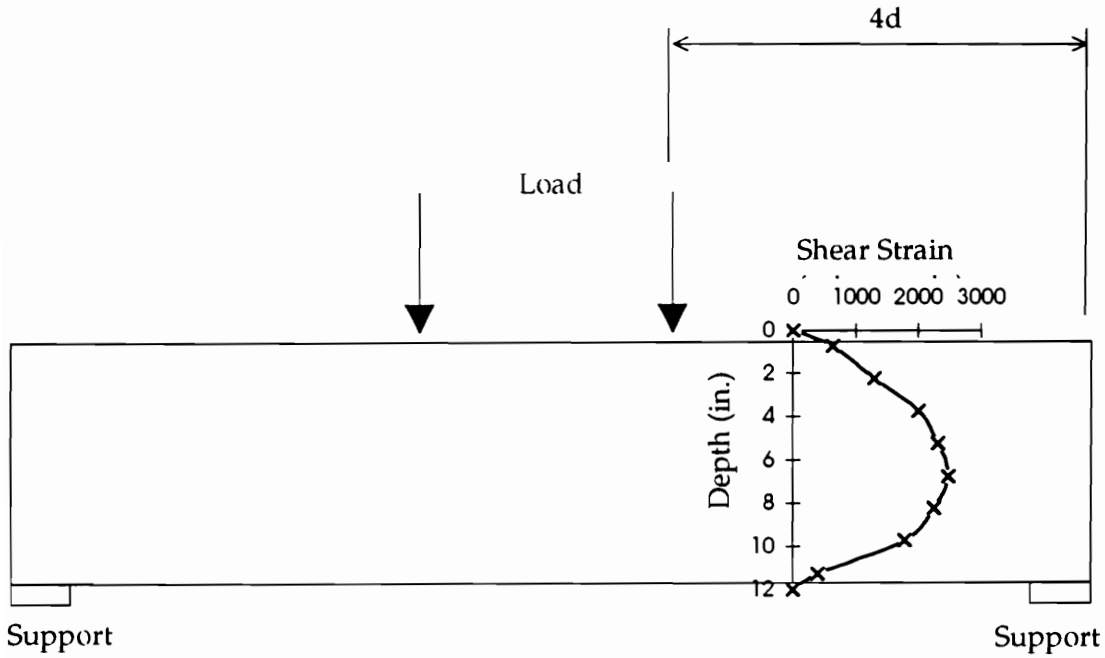

Figure 3.20. Shear strain distribution through the depth of reinforced glulam beam recorded from strain gauges.

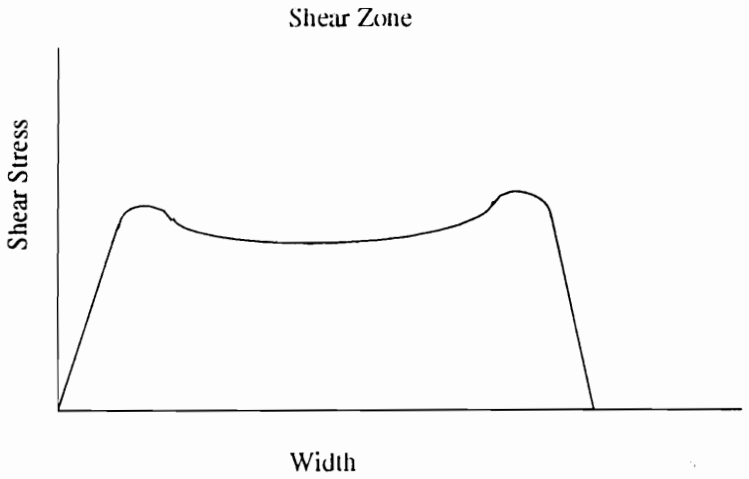

Figure 3.21. Shear-stress in xz plane in tensile laminae across the width of glulam beam in expected shear-free and shear zones at wood-FRP interface.

Table 3.8. Shear block and full-scale shear strength test values.

Beam Number	Shear block Value in xy plane adjacent to failure pathway (psi)	Predicted τ_{xy} maximum value at neutral axis (psi)	Predicted τ_{xy} maximum value in wood adjacent to wood-FRP interface (psi)		
--	a	b	c	d	e
S01	1468	586	166	183	732
S02	1463	648	195	214	856
S03	1340	658	176	194	776
S04	1431	594	223	245	980
S05	1303	583	144	159	636
S06	1369	767	150	165	660
S07	1330	667	158	174	696
S08	1274	665	155	171	684
S09	1305	652	146	161	644
S10	1377	579	138	152	608
S13	1325	565	141	155	620
S14	1387	616	55	61	244
S15	1305	555	14	15	60
S16	1325	584	69	76	304
S17	1225	592	173	191	764
S19	1225	611	218	240	960
S20	1260	550	215	237	948
S22	1290	545	141	155	620
S23	1164	591	150	165	660
S24	1151	588	165	182	728
S25	1104	551	131	144	576
S26	1140	603	139	153	612
S27	1019	556	102	113	452

Note:

[a] AITC-200 shear block test (AITC 1988)
[b] calculated using 3V/2A, equation 3.8 (simple theory) at neutral axis
[c] calculated using VQ/It, equation 3.8 (simple theory)
[d] calculated using VQ_r/I_rt equation 3.9 (transformed section)
[e] calculated using $(VQ_r/I_rt)*\eta'$, where $\eta' = 4$ equation 3.22(transformed section and η')

Table 3.8 shows that the values of xy shear in the wood at the failure pathway location in the wood-FRP interface area as predicted by equation 3.22 are much closer to the maximum values as predicted by conventional design formulas for xy shear at the neutral axis than equation 3.8 or equation 3.9, the simple form and a transformed section respectively. The use of equation 3.8 to predict xy shear stress at the neutral axis in a reinforced glulam provides an artificially high value for xy plane shear at the

neutral axis, whereas VQ_r/I_rt provides an artificially low value for shear at the failure pathway in the wood in the wood-FRP interface area. Using Q_r and I_r results in a flattening of the parabolic shape of the shear distribution through the depth of the beam. This leads to a lower maximum shear value at the neutral axis than that predicted by 3V/2A. The shear distribution drops more gradually between the neutral axis and the FRP than in an unreinforced glulam. The rate of shear decrease between the neutral axis and the FRP is a function of FRP thickness, E and G; the rate decreases with increasing FRP thickness, E and G. The use of η' to adjust the shear stress value predicted in this zone worked reasonably well as shown in Table 3.8. The use of η' to predict shear in other zones of the reinforced glulam, e.g. the compression zone, is not accurate. This inaccuracy is related to lamination thickness , stiffness differential and G values.

As discussed in Chapter 2, laminate thickness can lead to increases in shear stress at the edge thereby reducing the effective section in a reinforced glulam. Stacking sequence and differential lamination stiffness [Jones, 1975] can also affect the shear stress distribution through the depth and width of a FRP-reinforced beam.

The difference between critical shear stress at the wood-FRP interface and the predicted shear stress at the same point explains a phenomena widely unexplained by previous reinforcement tests. Previous researchers [Sonti et. al, 1995b] have established glueline shear strength values for FRP-wood that were above American National Standards Institute (ANSI) requirements 1040 psi (7.17 MPa) but found that reinforced beams failed at the wood-reinforcement interface at shear values much lower than predicted by conventional theory.

The shear modulus difference between layers in layered composites can dramatically alter actual composite test results from results predicted by common theory [Raman and Davalos, 1996]. This effect is further accentuated by wood nonhomogeneity.

x-z Plane Shear-Stresses in Wood-FRP Interface. Wood is hygroscopic and as it absorbs and desorbs water it swells and shrinks. Reinforcement is also hygroscopic but is more dimensionally stable. The shear-stress in the glueline between wood and FRP induced by shrinkage occurs in the xz plane. The stress perpendicular to grain in the direction of width can be calculated for a range of shrinkage conditions. However, since glulams are manufactured at 12-14% and could theoretically become oven dry or fully saturated, a 4% shrinkage or expansion would conservatively estimate the full range of dimensional change for most commercial grades of woods used in the United States, e.g. Southern Yellow Pine or Douglas-fir [USDA, 1987].

Other researchers have investigated this shear stress by drying sample reinforced glulam cross-sections and FEA [Tingley et al., 1996d]. They assumed that a tangential plane on a lamination was located at the FRP-wood interface. The wood species investigated was Douglas-fir. A conservative 4% dimensional shrinkage was anticipated. An uneven distribution of the shrinkage across the width was assumed. This corresponds to the moisture content gradient through the width. The researchers modeled a 5 in (127 mm) width and equal shrinkage on each side (across the width) was assumed. The shrinkage on each side was 0.01 in (0.25 mm). The total shrinkage in the 5 in (127 mm) was 0.02 in or 0.04 inch/inch strain. This translated to

approximately 980 psi (7.5 MPa) in shear-stress between the wood and FRP [Tingley et al., 1996d].

Thus, the shear-stress in wood-FRP glueline necessary to withstand shrinkage and expansion stresses, assuming the FRP will not shrink or expand, is approximately 1100 psi (7.9 MPa). Fortunately the $_{T/C}E_{\perp}$(modulus of elasticity in tension or compression perpendicular to the grain) and ultimate stress in tension or compression perpendicular to grain is low and expansion can be accommodated by compressive strain or tensile strain past the yield point perpendicular to grain. In addition, since wood is brittle in tension perpendicular to grain, separation of wood in cleavage occurs as a result of moisture content variation at the wood-FRP interface. Ultimate compressive stress in the transverse direction is dependent upon density; therefore, with denser wood greater glueline strength is required to resist shrinkage stress. Table 3.9 relates shrinkage induced stress to SG for a 5.125 x 12 in. (130 x 305 mm) cross-section Douglas-fir (AITC combination 1) lay-up with .15 in. (3.8 mm) of CARP on the tensile side between the outer two laminations. The results were developed by finite-element analysis using 3.8% shrinkage based on 14% moisture content change [Tingley et al., 1996d].

In addition to shear-stresses caused by shrinkage, there are cleavage stresses introduced by cupping as the wood in outer zones adjacent to the FRP dries or becomes wet. It has been observed that single layers of FRP will cleave from wood since the ultimate stresses in tension perpendicular to grain for both FRP and wood are low.

Researchers determined the applied cleavage load to the glueline [Tingley et al., 1996d]. They assumed that 1/16 in. (1.6 mm) cup would occur across a 5 in. (127 mm) piece of wood, with a 4% shrinkage factor. Table 3.10 shows the corresponding cleavage stresses developed by shrinkage induced cleavage loads between the FRP and wood using the same cross-section and model as developed for Table 3.9.

The cleavage stress developed in Douglas-fir would be approximately 2400 psi (1.66 MPa), well above the current cleavage resistance of 400-500 psi (2.8-3.4 MPa) for wood or FRP [Tingley, 1994a; Tingley, 1994b]. However, since ultimate cleavage strength of wood and FRP is low (below 300 psi [2.1MPa]), often the wood or FRP fails first in the FRP-wood interface.

Figure 3.22 for a diagram of the various stresses induced on a three-dimensional element at the tensile FRP-wood interface. Figure 3.23 shows cleavage failures in the wood and FRP-FRP glueline caused by shrinkage induced cleavage stresses.

Table 3.9. Relation of shrinkage included shear-stress(τ_{yz}) to SG.

Species	Grade	SG	E_x ($\times 10^6$ psi)	Shrinkage (%)	τ_{yz} (psi)
Douglas-fir	L3	0.44	1.5	3.8	953
	L2	0.49	1.7	3.8	972
	L1	0.52	1.8	3.8	982
Hem-fir	L3	0.42	1.3	3.8	933
	L2	0.45	1.4	3.8	943
	L1	0.48	1.6	3.8	962
Western Wood	H3	0.38	1.0	3.8	903
	H2	0.40	1.1	3.8	913
	H1	0.42	1.2	3.8	923

Table 3.10. Cleavage stresses developed by shrinkage induced loads.

Species	Grade	E_x ($\times 10^6$ psi)	Shrinkage (%)	τ_{yz} (psi)
Douglas-fir	L3	1.5	3.8	2349
	L2	1.7	3.8	2385
	L1	1.8	3.8	2403
Hem-fir	L3	1.3	3.8	2314
	L2	1.4	3.8	2332
	L1	1.6	3.8	2367
Western-Wood	H3	1.0	3.8	2260
	H2	1.1	3.8	2278
	H1	1.2	3.8	2296

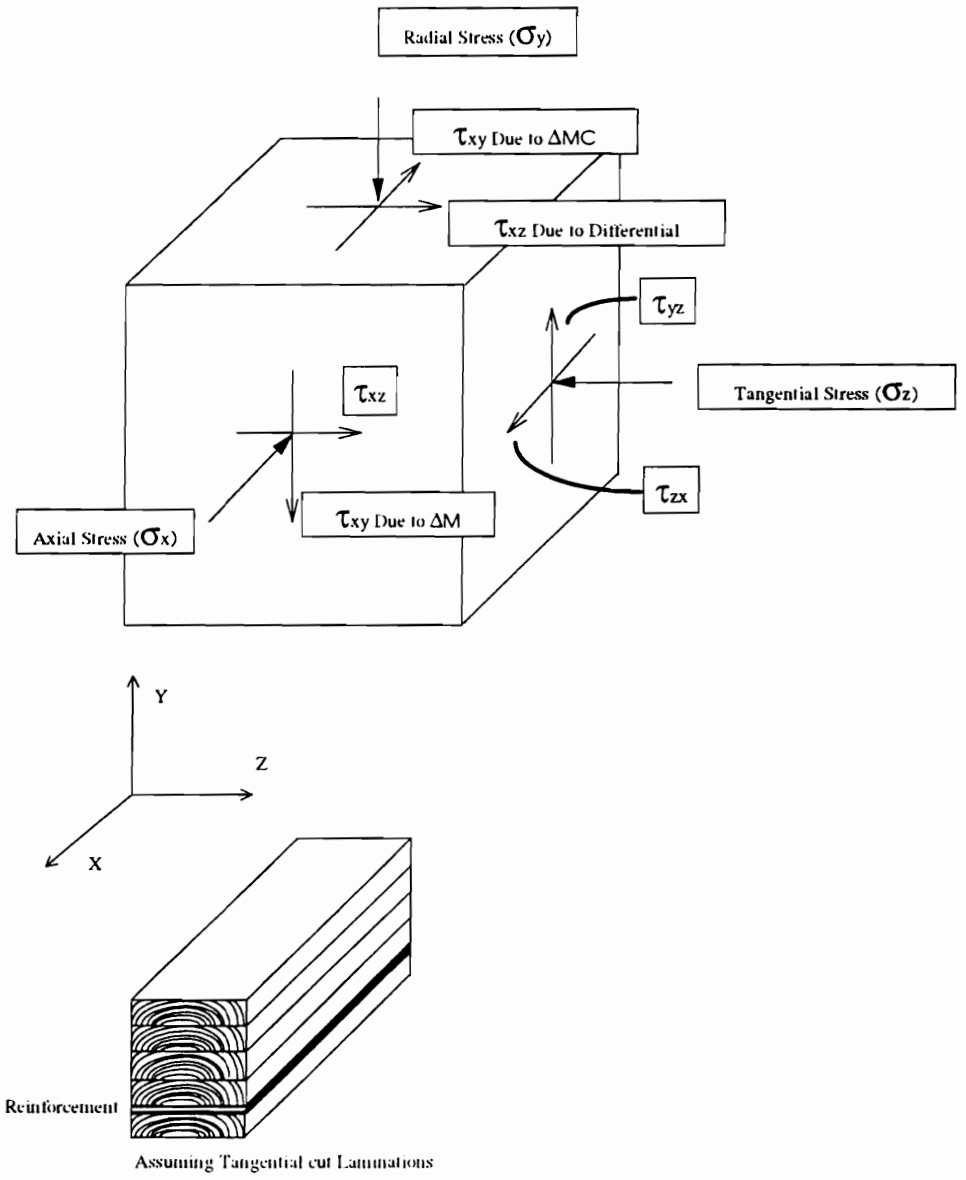

Figure 3.22. Three-dimensional glueline element at the reinforcement-wood interface.

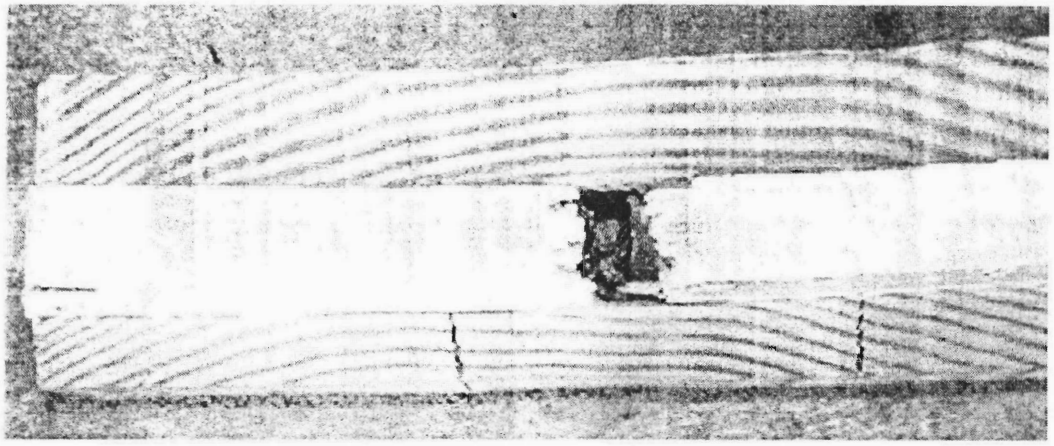

Figure 3.23. Pronounced plastic tensile strain through the thickness of the FRP.

Shear Effects Caused by Localized Failure in the Tensile Wood Laminae at the Wood-FRP Interface. Localized wood failure in tension at discontinuities, such as finger joints or knots adjacent to the FRP, often initiates catastrophic failure in full-scale reinforced glulams. Failure causes the wood-FRP interface to move through an elastic range to fracture and subsequently precipitates global beam failure. Figure 3.24 shows an element at the tensile wood-FRP interface that has moved into the plastic range in shear due to a finger joint causing axial forces to go to zero adjacent to the reinforcement.

As the wood-FRP interface enters the plastic zone global failure of the reinforced glulam occurs quickly because the FRP delaminates from the body of the glulam by either shearing in the wood or FRP, adjacent to the wood in the xy plane. Figure 3.25 shows a photograph of full-scale reinforced glulam shear failure at FRP-wood interface.

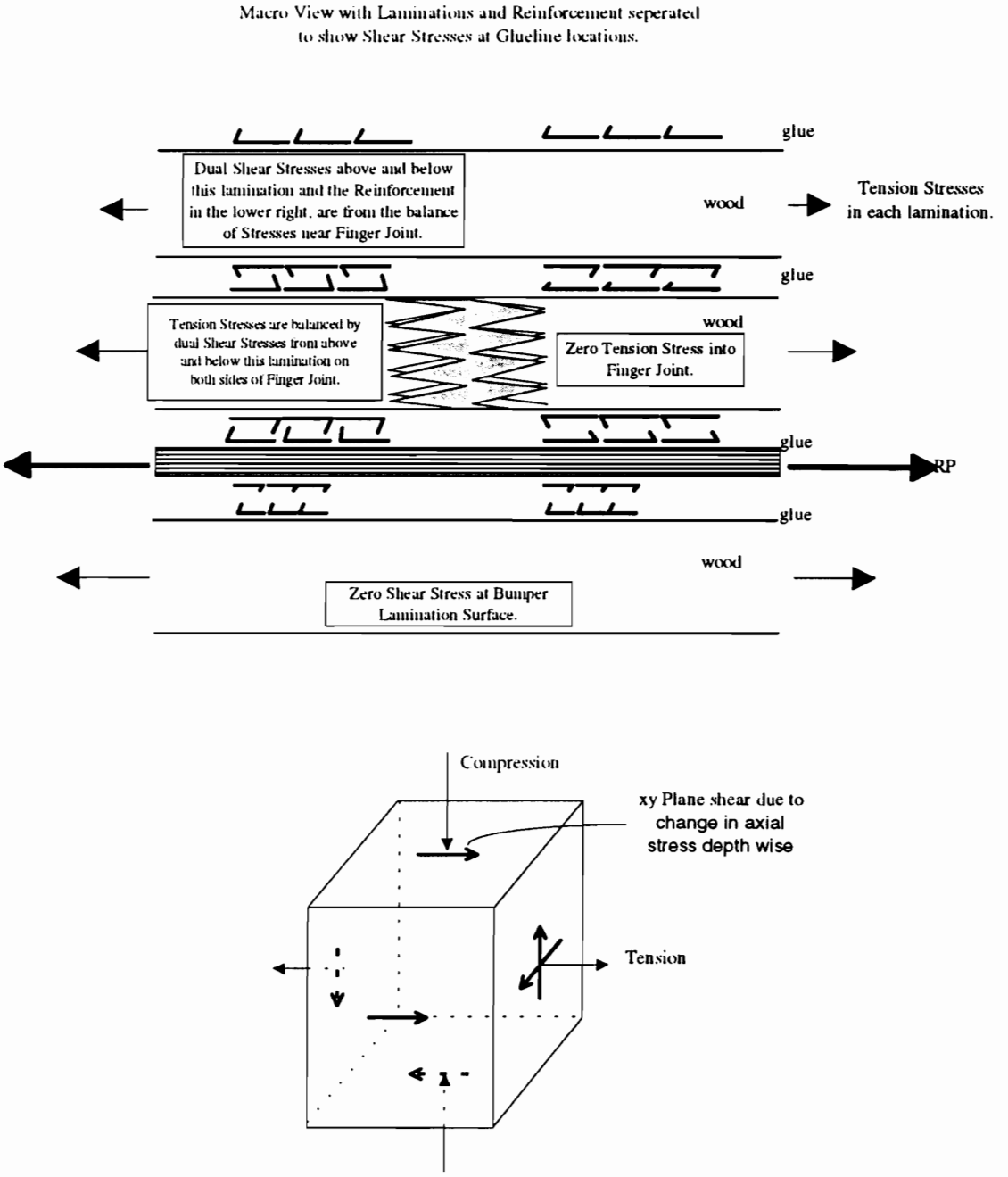

Figure 3.24. Description of shear-stresses at the wood-FRP interface when wood lamina fail in tension;
a) free body diagram,
b) local element in glueline adjacent to failed finger joint in the wood lamination next to reinforcement.

The plastic zone shear-stress distributions, as well as axial stress distributions, become very erratic across the width of a beam. Generally, failure will progress along pathways or planes of weakness either following the grain in the adjacent wood (latewood-earlywood interface) or delaminating the fiber bundles from the FRP. These failure pathways propagate quickly throughout the beam. High-speed photography has shown that the FRP delamination from the wood during failure is accelerated by cleavage stresses (tension in the y direction) caused by beam curvature.

One method of improving the surface shear capacity of the FRP adherend in the FRP-wood glueline is to place off-axis fiber in the surface of the glueline with transverse fibers through the thickness of the FRP. Another method is to improve the

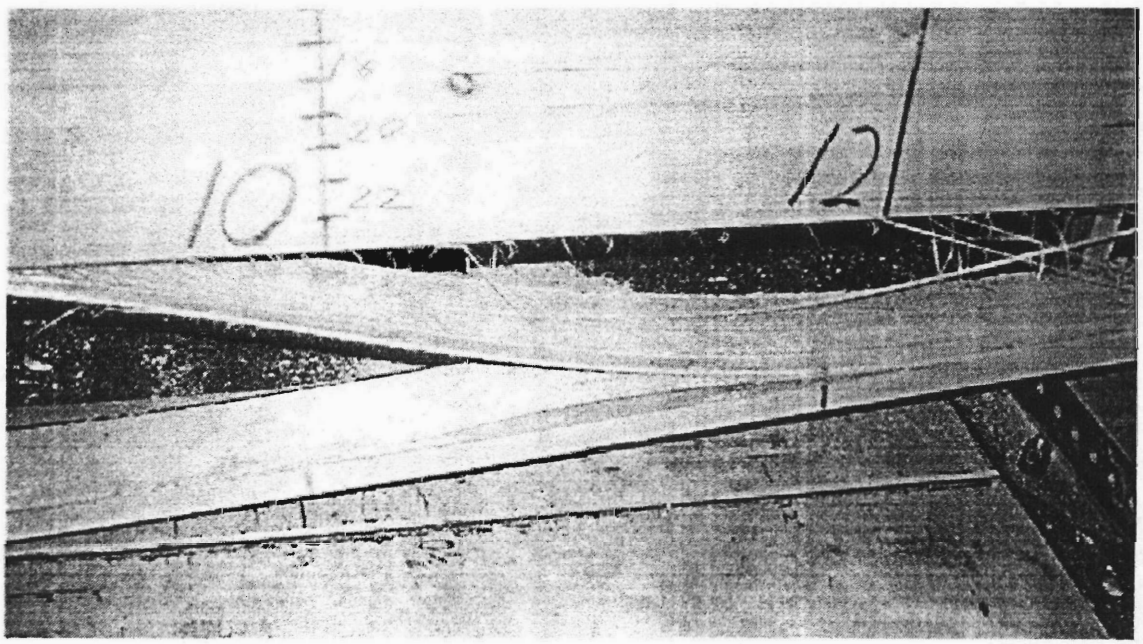

Figure 3.25. Photograph showing shear failure in reinforcement and wood at the reinforcement-wood interface.

matrix shear capacity by using matrices such as epoxy rather than polyester for example. However, generally the wood fails in shear first and the enhancement of FRP shear strength is unwarranted economically.

Localized Failure of the Compressive Wood-FRP Interface. The FRP exhibits only elastic range stress-strain relationships in the tensile zone. This relationship is not true for compressive reinforcement. Filament-matrix debond causes the FRP compressive strength to be lower than its tensile strength due to buckling of the filaments. Compressive reinforcement is subjected to both compressive stresses and cleavage stresses from curvature of the beam. These stresses are caused by the difference in compressive E values between the wood and FRP. The cleavage and compressive stresses combine to cause vertical lateral buckling at very low compressive stress levels as compared to the tensile capacity of the FRP.

Figure 3.26 shows absolute values of cleavage stress and axial stress across the width of the beam at the FRP-wood interface. These stresses occur at a location at the outer fiber of the wood compressive laminae. As compressive plasticity develops, the FRP fails at a point in the width due to vertical lateral buckling. The diagram in Figure 3.26 was created from axial strain gauge readings and estimations of cleavage stresses. Figure 3.27 shows a photograph of a bulking failure in compressive reinforcement.

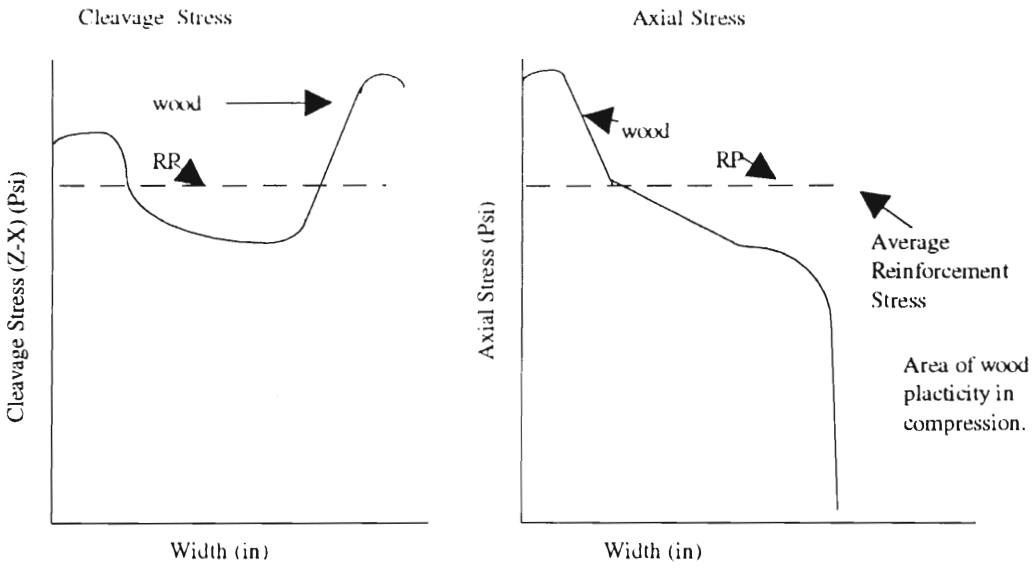

Figure 3.26. Diagram showing buckling failure of compressive reinforcement at a section through the width.

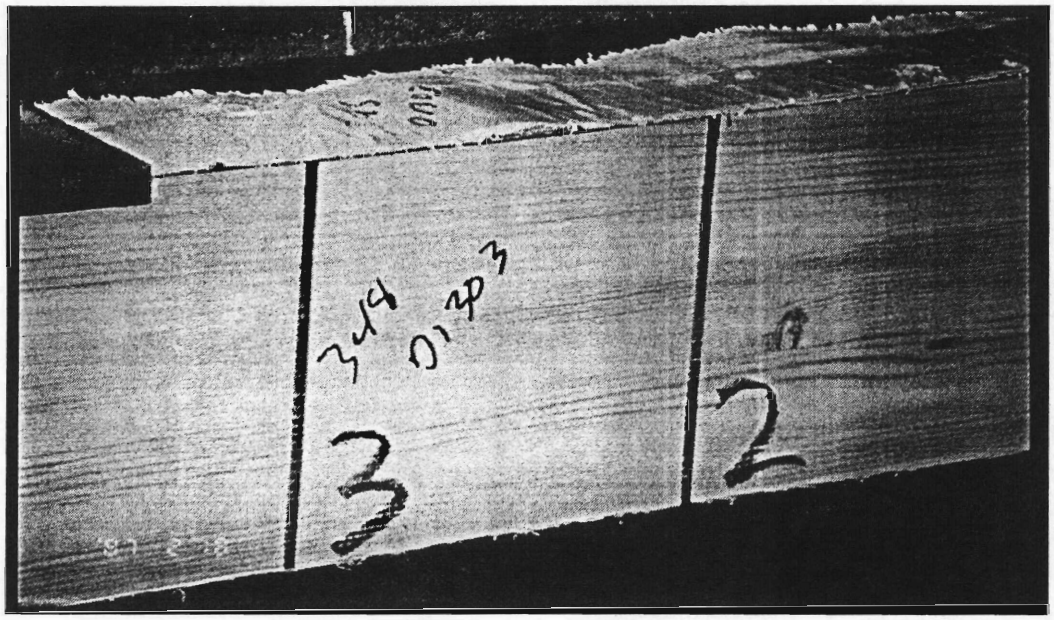

Figure 3.27. Photograph of buckling failure in compressive reinforcement.

At the point of failure shown in Figure 3.27, plane sections were no longer plane and conventional stress analysis methods no longer applied. Further, stress raisers in shear, axial and transverse stresses also developed. These stresses were very unpredictable, and when combined with the nonhomogeneous nature of wood and its anisotropic character, they accelerated global failure of the reinforced glulam.

Conclusions and Recommendations

The flexural response to load of a full-scale FRP-reinforced glulam is complex. The axial modulus of elasticity modular ratio, η, and the shear modulus modular ratio, η', provide more accurate transformed sections for more accurate shear strain and stress analysis in wood and FRP laminae. Compressive plasticity initiates at outermost compressive fiber weaknesses and progresses in vertical planes toward the neutral axis causing variation in the beam stress-strain distribution for axial and transverse normal stresses as well as shear stresses in the same beam during loading.

The nonhomogeneous nature of wood complicates this response. Localized variations in wood material properties caused by knots, slope of grain, finger joints, etc. make equations for prediction of stress levels approximations at best. The introduction of FRP to the glulam with its homogenous characteristics improves glulam response to load but the complexity of the stress-strain distributions is increased.

The investigations and analysis conducted in this research project have shown that tensile-reinforced glulams have ductility ratios approaching 2, and compressive

plasticity is the major contributor to this characteristic. The use of compressive reinforcement reduces the compressive plasticity and, subsequently, the ductility ratio.

The reinforced beam yield point strain values in compression were found to match closely the small clear values. The reinforced beam ultimate strain values in tension were about one-third of the small clear values.

The unreinforced beam ultimate strain values were lower than the reinforced beams. The difference between the beam tensile ultimate strain values and small clear values was caused by discontinuities such as knots and end joints.

The yield point of unreinforced beams in bending was noted to be a higher percentage of ultimate strain, 80% versus 60% for reinforced. The full scale and small clear testing did not confirm this as the unreinforced glulams were manufactured incorrectly.

The reinforced Ponderosa Pine and unreinforced V3-1600 Douglas-fir have an equivalent yield point strain. The **xz** plane shear stress and **x**-direction axial stress were found to increase toward the edge through the width of the beam. This agreed with previous researchers results (Jones 1975). The **xy** plane shear stress was also hypothesized to increase toward the edge. In addition, the **xy** plane shear stress was shown to have a lower maximum value than predicted at the neutral axis. It was shown that τ_{xy} was higher in the wood in the wood-FRP interface area than is predicted by conventional theory. Tensile and compressive reinforcement are governed by four types of shear stress effects which exist in the FRP-wood interface, all of which are resisted by the bond line strength.

The τ_{xy1} shear effects are caused by shear and axial stresses generated through external mechanical loading. The τ_{xz2} shear stresses are caused by stiffness differences between the wood and the FRP. The biggest shear stress effects in reinforced glulam are due to τ_{xy1} and τ_{xy2}. The τ_{xy} shear stress distribution, at the wood-FRP interface was larger by a factor of 3 than previously predicted. The use of η' in the shear stress prediction formulas for the wood in wood-FRP interface area was found to be closer to the value predicted by conventional theory for the τ_{xy1} maximum value.

Investigations into moisture content variation effects have shown that to resist conventional moisture content variation induced stresses, a wood-FRP bond line shear strength of approximately 1,000 psi (6.9 MPa) is needed.

The following in-service τ_{xz2} shear-stress issues need further study;

- Tension-tension fatigue in the FRP
- Long term creep in the FRP
- Temperature and MC variation in the FRP and wood
- Freeze thaw cycles in the FRP
- Long term creep in the wood at the wood FRP interface

Another in-service effect on the wood-FRP bond line caused by moisture content variation is cleavage stress. Cleavage stresses can place tension perpendicular to grain stresses on the wood and the FRP in the FRP-wood glueline. This condition quickly leads to localized element failure in shear at the glueline under conventional design loads on a FRP reinforced glulam. This localized failure, when accompanied by mechanical loads, can lead to global failure.

The wood-FRP interface characteristics in the compression zone are primarily affected by filament matrix debond and cleavage stress initiated buckling in the FRP.

Since the wood-FRP panel glueline will only have a shear strength equal to its weakest adherend, it is clear that no significant increase in beam capacity can be expected from improving wood-FRP panel glueline strength. The best option for improving reinforced beam capacity is to improve wood quality in the area adjacent to the reinforcement toward the neutral axis. To improve quality does not mean necessarily to increase specific gravity. More effective improvements would be slope of grain reduction, enhanced finger joint strength, and removal of knots. This will lead to a substantial reduction in localized defects that cause premature failure in an FRP-reinforced glulam. Increasing the percentage, by cross-section, of reinforcement also reduces the effect of tensile zone defects on beam capacity.

The basic principles to follow in order to increase the capacity of reinforced glulam given any two beams with similar compressive strength and E_b, are to increase the percentage of reinforcement to reduce stress-strain on finger joints or other localized defects that cause tensile failure or ultimate failure, increase finger joint tensile stress-strain capacity, or increase shear performance of FRP-wood interface to withstand elevated shear concentrations from failure of such defects.

CHAPTER 4

CONCLUSIONS

Reinforced glulams were investigated. The investigation focused on the material characteristics of the wood and FRP and the mechanisms relating elemental features to global beam behavior. In addition, external stress-strain distributions were investigated and compared to those predicted by theory for isotropic materials and those predicted by mathematical models using actual component properties as input parameters. The finite-element modeling was completed using SAP90®. The investigation focused on the elastic plastic relationships in the wood-FRP interface region. Characteristics important to short-term response in the FRP were investigated. The following conclusions and recommendations were developed from the work.

Potential of the Reinforcement Technology

Reinforced Glulam

The results of full-scale testing confirmed the results of previous researchers that there are substantial benefits gained when FRP is used as a tensile reinforcement for glulam. The most important benefits of tensile reinforcements were:

- strength enhancement
- increased MOE
- use of less wood fiber for a given load
- use of low grade wood in place of high grade
- reduced variability in load response.

The most impressive characteristic is the increase in design strength, nearing 185 percent in species groups, such as western woods, over that predicted by using the current design standard (NFPA, 1991) and a 2.1 adjustment factor.

Reinforcement

Various FRP reinforcement types as well as steel were compared to wood. The most significant findings were:

- Strain compatibility between wood and FRP is critical. For compressive reinforcement on Douglas-fir, the preferred YP strain is 0.8% to 1.2%; for tensile reinforcement the preferred YP is 0.9% to 1.4%. These ranges for reinforcement were dependent upon the wood clear wood ultimate strain values. The FRP was established to be most effective when its YP strain value was slightly higher than the wood. This maximizes the recovery of reinforcement strength from the FRP.

Stress and Strain in Reinforced Glulam

The actual axial compressive and tensile strain distributions, measured with strain gauges, were predicted by isotropic theory. This was due to the general alignment of the longitudinal axis of the FRP and wood with the applied axial tensile and compressive stresses due to bending. The results of plane stress finite-element modeling also matched the actual distributions. In both the above cases, any large divergence of actual stress-

strain distribution from predicted stress-strain distribution was due to localized material variation such as knots, slope of grain or finger joints, etc.

The predictions of shear in the xy plane by conventional isotropic theory and FEA modeling for reinforced glulam were not as accurate as the estimates of bending stress when compared to the actual shear distributions as identified by strain gauging. These differences could have been reduced if the models had included provisions for end joints and growth defects. It was clear that isotropic theoretical prediction methods are dramatically affected by the orthotropic non-homogeneous nature of wood. The off-axis effects on xy plane shear stress-strain distributions are substantial. Variability in grain patterns of the wood laminations in a glulam dramatically affect these distributions. Determining the right component values for each full-scale beam with correct matching to each element in the FEA would dramatically improve the prediction accuracy. The use of average Poisson's ratios, μ_{TL} and μ_{RL}, for tangential-radial planes as was done in this study limits the accuracy of the particularly if the mix of radial cut verses tangential sawn lumber is not approximately equal.

Localized Stress-Strain Distributions

The results of extensive strain gauging through the width of the reinforced glulam beam at the wood-wood interface and wood-FRP interface showed an unpredicted response: the axial stresses in compression and tension increased toward the edges in the wood. The increase was less pronounced in the expected shear-free zone of the test beams in four point bending. This general trend was also true of τ_{xz}. Clearly it dropped to

zero at the edge due to boundary conditions but was lower in the center of the beam than outer zones through the width.

This unexpected distribution of axial and shear stresses in the wood through the width was hypothesized to be due to grain angle running off the edge of the wood lamination since sawn lumber is processed from tapered tree trunks. The reinforcement exhibits a more uniform response. Stress-strain distributions through the width in axial stress and τ_{xz} shear stress are uniform. Other researchers have shown that lamination thickness may also explain some of this increase toward the edge (Jones, 1975). However , the increase occurs at a greater distance than a lamination thickness from the edge which is contrary to the researchers findings (Jones, 1975).

The use of strain gauge data with compliance matrices in a plane stress analysis combined with a Mohr's circle analysis (Appendix D) provided maximum shear stress prediction methodology. The maximum shear stress, τ_{xy} was developed from shear rosette strain gauge data through the depth of the beam.

Reinforced Glulam Plastic Shift

The concept of compressive plasticity was shown to occur but to a greater extent in reinforced glulams. The reinforcement, when used as a tensile lamina facilitates compressive plasticity. This translates to a greater degree of ductility and greater plastic zones in the full-scale reinforced glulams. The compressive failures initiated at the outer fibers and propagated toward the neutral axis. The full-scale reinforced glulam beam deflection at failure was found to be in a range of L/25 to L/40 whereas the unreinforced

glulams failed at deflections of L/110 to L/130. These values were for moment governed and deflection governed beams.

An important aspect of compressive plasticity is the change in neutral axis location and shear distributions. As a reinforced glulam deflects under load in bending, the neutral axis moves towards the tensile reinforcement. In certain situations where the reinforcement provided enough tensile resistance and the adjacent wood laminations were free of property variations, the neutral axis would lower to an area adjacent to the FRP and failure would occur in shear xy plane above the FRP.

Shear Strain Distributions

The FRP has a greater shear modulus than wood. Further, the relationship of the shear modulus of the FRP to the shear modulus of wood, η', is not equal to the modular ratio of moduli of elasticity for FRP and wood, η. Thus, the η' was used as a modification factor to predict the shear stress distribution through the depth of a reinforced glulam using Q_r and I_r in the neutral axis to wood-FRP interface area. A new shear strain equation that incorporated Q_r and I_r as well as G adequately predicted the shear strain distribution that was found in an actual reinforced glulam in the xy plane using strain gauges.

The general flattening of the parabolic curve in a reinforced glulam with a general increase in shear between the neutral axis and the FRP in the tension zone was predicted. Strain gauging showed that these predicted distributions existed in actual full-scale reinforced glulams. It further explained why a common mode of failure in a reinforced glulam was shear near the wood-FRP interface, usually in the wood.

The block shear strength of the wood-FRP interface zone was also shown to be fifty to one hundred percent higher than the actual full-scale beam shear value as calculated using conventional theory. These discoveries help explain previous researchers' results which showed unexpected shear failures of the FRP-wood glueline in full-scale tests when small shear block tests provided adequate results [Davalos and Barbero, 1991].

Wood to Reinforcement Interface Shear Stress Types

There were four basic shear stress types identified in the wood-FRP interfaces:

- τ_{xy1} - shear stress in the xy plane due to differential moment along the length of the beam. This shear stress should reflect a properly transformed section accounting for η, η', Q_r, and I_r.
- τ_{xy2} - shear stress in the xy plane due to stiffness differential between the FRP and wood lamination.
- τ_{xz1} - shear stress in the xz plane due to axial stress differentials between the FRP and wood across the width of the beam.
- τ_{xz2} - shear stress in xz plane due to differential shrinkage / swelling characteristics of the wood and FRP adherends.

The τ_{xy1} and τ_{xy2}, τ_{xz2} shear stresses were identified as the most important of the wood-FRP shear stresses. The τ_{xz2} shear stress was also found to have very significant cleavage stresses in the direction associated with the moisture content changes leading to FRP failure in tension perpendicular to the fiber direction (longitudinal) in unidirectional FRP.

Recommendations

There were several recommendations developed as a result of the testing and analysis. The most significant are listed below:

- The use of small shear block values to develop full-scale glulam design horizontal shear values are not as accurate as full-scale beam test values. Full-scale glulam test results should be used to develop design shear values.
- The stiffness and strength performance of a FRP reinforced beam is enhanced by placing the highest E_b laminations in the outer compressive laminae and lowest E_b lamination in the tensile lamina adjacent to the FRP.
- Removing large discontinuities such as knots and increasing finger joint strength in the wood adjacent to the tensile FRP reinforcement will increase the reinforced beam strength or facilitate the use of less reinforcement.
- The use of compressive reinforcement does not increase the strength of a reinforced beam appreciably and should never be used without tensile reinforcement.
- Based on prior research FRP in-service characteristics, such as long term creep resistance and tension-tension fatigue strength in saturated moisture (9%) were found to be very important. The ARP and CARP were assessed to have the best characteristics in creep resistance and in tension-tension fatigue with the FARP having the poorest. Pure fiberglass FRP was found to be even less effective than FARP in creep resistance and tension-tension fatigue.

Areas for Further Study

The sensitivity of the reinforced glulam bending strength to improved wood-FRP shear capacity needs further research. The use of epoxy glues for the FRP-wood gluelines while holding each of the parameters affecting FRP-wood shear strength constant, would provide valuable data on the economic improvement potential for reinforced glulams resulting from higher FRP-wood glueline shear resistance. The economic gain from such improvements could be substantial.

A more definitive understanding of both slope of grain and knot size parameters in relation to the width of the beam and finger joint strength effects need to be developed. Understanding the effects directly affected by compressive reinforcement could serve to enhance the strength as well as stiffness characteristics of compressive reinforced beams which would be a significant economic improvement.

Other areas of study include but are not limited to:

- FRP-wood glueline creep characteristics in
    - hot, wet environments
    - wet environments
    - freeze-thaw effects
    - cyclic loading effects
    - tension-tension cycling.
- Scarfing the end of the FRP reinforcement layer causing a graduated discontinuity at the end of the reinforcement in partially reinforced beams.
- Alternative FRP types better matching wood element strain yield point limits.
- Duration of load effects in various environments on full-scale reinforced glulams.

BIBLIOGRAPHY

Adams, D. F. and D. E. Walrath. 1987. Current status of the Iosipescu shear test method. *Journal of Composite Materials* 21:494-507.

American Institute of Timber Construction (AITC). 1988. Standard specifications for structural glued laminated timber of softwood species. AITC 117. AITC, Englewood, CO.

American Institute of Timber Construction (AITC). 1991. Determination of design values for structural glued-laminated timber in accordance with ASTM D3737-89a. AITC 500-91. AITC, Englewood, CO.

American Institute of Timber Construction (AITC). 1992. Inspection manual for structural glued-laminated timber. AITC 200-92. AITC, Englewood, CO.

American Forest Products Association. (AF&PA) 1991. National design specification® for wood construction. Supplement: Design Values for Wood Construction. NFPA, Washington, DC.

American Society for Testing and Materials (ASTM). 1982. Sample Size to Estimate the Average Quality of a Lot or Process,. ASTM E122. In Annual Book of Standards. ASTM, Philadelphia, PA.

American Society for Testing and Materials (ASTM). 1994a. Standard test methods for tensile, compressive, and flexural creep and creep-rupture of plastics. ASTM D2990. In Annual Book of Standards, Vol. 08.02, pp. 186-203. ASTM, Philadelphia, PA.

American Society for Testing and Materials (ASTM). 1994b. Standard test method for tensile properties of polymer matrix composite materials. ASTM D-3039/D-3039M-93. In Annual Book of Standards, Vol. 15.03, pp. 115-124. ASTM, Philadelphia, PA.

American Society for Testing and Materials (ASTM). 1994c. Standard Test Method for Compressive Properties of Unidirectional or Crossply Fiber- Resin Composites. ASTM D3410. In Annual Book of Standards, Vol. 08.02, pp. 130-134. ASTM, Philadelphia, PA.

American Society for Testing and Materials (ASTM). 1994d. Standard Test Method for Shear Properties of Composite Material by the V-Notched Beam Method. ASTM D5379. In Annual Book of Standards Vol. 08.03, pp. 455-464. ASTM, Philadelphia, PA.

American Society for Testing and Materials (ASTM). 1994e. Standard Test Method for Bearing Strength of Plastics. ASTM D953. In Annual Book of Standards ,. Vol. 08.01, pp. 220-224.ASTM, Philadelphia, PA.

American Society for Testing and Materials (ASTM). 1994f. Standard Test Methods for Curing Properties of Pultrusion Resins by Thermal Analysis. ASTM D5028. In Annual Book of Standards Vol. 08.03, pp. 304-306, ASTM, Philadelphia, PA.

American Society for Testing and Materials (ASTM). 1994g. Standard Test Methods Ignition Loss of Cured Reinforced Resin. ASTM D2584. In Annual Book of Standards Vol. 08.02, pp. 83-84., ASTM, Philadelphia, PA.

American Society for Testing and Materials (ASTM). 1994h. Standard Test Methods for Specific Gravity (Relative Density) and Density of Plastics by Vol. 08.01, pp. 185-188.Displacements. ASTM D792. In Annual Book of Standards, . ASTM, Philadelphia, PA.

American Society for Testing and Materials (ASTM). 1994i. Standard Test Methods for tensile, compressive, and flexural creep and creep-rupture of plastics. ASTM D2990. In Annual Book of Standards,. Vol. 08.02, pp. 186-203. ASTM, Philadelphia, PA.

American Society for Testing and Materials (ASTM). 1994j. Standard Test Methods for Tension-Tension Fatigue of Oriented Fiber -Resin Matrix Composites. ASTM D3479. In Annual Book of Standards, Vol. 08.03, pp. 360-365.. ASTM, Philadelphia, PA.

American Society for Testing and Materials (ASTM). 1994k. Standard Test Methods for Operating Light and Water Apparatus (Florescent UV and Condensation Type) for Exposure of Plastics. ASTM D4329. In Annual Book of Standards, Vol. 08.03. pp 401-404. ASTM, Philadelphia, PA.

American Society for Testing and Materials (ASTM). 1994l. Standard Test Methods for Water Absorption of plastics. ASTM D570. In Annual Book of Standards, Vol. 08.01, pp. 34-36. ASTM, Philadelphia, PA.

American Society for Testing and Materials (ASTM). 1994m. Standard Test Methods for Deflection Temperature of Plastics Under Flexural Load.. ASTM648. In Annual Book of Standards, Vol. 08.01, pp. 80-84. ASTM, Philadelphia, PA.

American Society for Testing and Materials (ASTM). 1994n. Standard Test Methods for Standard Practice for Classifying Visual Defects in Thermosetting Reinforced Plastic. ASTM4385. In Annual Book of Standards, Vol. 08.03, pp 425-428. ASTM, Philadelphia, PA.

American Society for Testing and Materials (ASTM). 1995a. Standard methods of static tests of timbers in structural sizes. ASTM D198-94. ASTM. In Annual Book of Standards, Vol. 04.10, pp.57-75. Philadelphia, PA.

American Society for Testing and Materials (ASTM). 1995b. Standard methods of testing small clear specimens of timber. ASTM D143-94. In Annual Book of Standards, Vol. 04.10, pp. 23-53. ASTM. Philadelphia, PA.

Anderson, J.A. 1981. Stress-strain relationship for defect-free timber beams. *Wood Science* 14(1): 23-31.

ANSYS 5.0 a®. 1992. Finite-Element Analysis Software. ANSYS®, Houston, PA 15342-0065.

Balinski, M. L. et al. 1972. Mathematical programming - Study 3. Stochastic Systems: Modeling, Identification and Optimization I. North Holland Publishing Co., Amsterdam, Holland.

Biblis, E. J. 1965. Analysis of wood fiberglass composite beams within and beyond the elastic region. *Forest Products Journal* 25 (24):81-88.

Bickford, W. B. 1990. A first course in the finite element method. Richard D. Irwin, Inc. Boston, MA 02116.

Bodig, J. and B. A. Jayne. 1993. Mechanics of wood and wood composites. Krieger Publishing Co., Malabar, FL.

Buchanan A.H. 1986. Combined Bending and Axial Loading in Lumber. *Journal of Structural Engineering* 112(12):2592-2609.

Buchanan, A. H., P. J. Moss, and P. K. Townsend. 1990. Reinforcing bars epoxy bonded in glue laminated timber. Vol. 2, p. 601-610. *In* Proceedings of the International Timber Engineering Conference, October 23-25, 1990. Tokyo, Japan. The Steering Committee of the 1990 International Timber Engineering Conference, Tokyo, Japan.

Bulleit, W. M., 1983. Reinforcement of wood materials: A review. *Wood and Fiber Science* 16 (3):391-397.

Bulleit, W. M., L.B. Sandberg, and G. J. Woods. 1989. Steel-reinforced glued laminated timber. *Journal of Structural Engineering* 115(2): 433-444.

Carrara, A. S. and F. J. McGarry. 1969. Matrix and interface stresses in a discontinuous fiber composite model. *Journal of Composite Materials* 2:222.

Chen, C. J., P. Haller and J. Natterer. 1994. Experimental study on fiberglass reinforced timber joints. Vol. 2, p. 66-72. *In* Proceedings of the Pacific Timber Engineering Conference, July 11-15, 1994. Gold Coast, Australia. Timber Research and Development Advisory Council, Queensland, Australia.

Cramer, S. M. and K. A. McDonald. 1989. Predicting lumber tensile stiffness and strength with local grain angle measurements and failure Analysis. *Forest Products Journal* 21 (4):393-410.

Dailey, T. H. Jr., R. A. Allison, J. Minneci and R. L. Bender. 1995. Hybrid composites: Efficient utilization of resources by performance enhancement of traditional engineered composites with pultruded sheets. Session 5-C/1-4. *In* Proceedings of the Composites Institute's 50th Annual Conference & Expo '95, January 30-February 1, 1995. Cincinnati, Ohio. SPI Composites Institute, New York, NY.

Davalos, J. F. and E. J. Barbero. 1991. Modeling of glass-fiber reinforced glulam beams. Vol. 3, p. 3.234-3.241. *In* Proceedings of the International Timber Engineering Conference, September 2-5, 1991. London, England. Timber Research and Development Association, High Wycombe, United Kingdom.

Default, J. B. 1972. Composite applications for graphite reinforced composites. Hercules, Inc., Wilmington, DE.

Dupont, Characteristics and uses of Kevlar 49. High modulus organic fiber. 1973. DuPont de Nemours and Co.

Enquist, B., P. J. Gustafsson and H. J. Larsen. 1991. Glass-fibre reinforcement perpendicular to the grain. Vol. 3, p. 3.242-3.250. *In* Proceedings of the International Timber Engineering Conference, September 2-5, 1991. London, England. Timber Research and Development Association, High Wycombe, United Kingdom.

Fox, S. P. 1975. Shear reinforcements for glued laminated beams. Western Forest Products Laboratory, Vancouver, BC, Canada.

Gardner, G. P. 1991a. A reinforced glued laminated timber system. Vol. 3, p. 3.218-3.225. *In* Proceedings of the International Timber Engineering Conference, September 2-5, 1991. London, England. Timber Research and Development Association, High Wycombe, United Kingdom.

Kasal, B., R. J. Leichti and R. Y. Itani. 1994. Nonlinear finite-element model of complete light-frame wood structures. *Journal of Structural Engineering* 120(1):100-119.

Kirlin, C.P. 1996. Experimental and Finite -Element Analysis Stress Distribution Near the End of Reinforcements in Partially Reinforced Glulam. M.S. thesis, Oregon State University, Corvallis, OR. 180p

Kirlin, C.P., R.J. Leicthi, D.A. Tingley and T. Dibble. 1995. Localized stresses at the reinforced tails in partially reinforced glulam. In Abstracts. Forest Products Society Anul Meeting, June 29-30, 1995. Portland, OR. Forest Products Society, Madison, WI.

Kobetz, R. W. and G. P., Krueger. 1972. Ultimate strength of reinforced timber-biaxial stress failure criterion. *In* Proceedings of the ASCE Annual and National Environmental Engineering Meeting, October, 1972. Houston, TX. American Society of Civil Engineers, New York, NY.

Krueger, G. P. 1972. Ultimate strength design of reinforced timber. Department of Civil Engineering, Michigan Technological University, Houghton, MI.

Lantos, G. G. 1970. The flexural behavior of steel reinforced laminated timber beams. *Wood Science* 2 (3):136-143.

Leichti, R. J. and D. A. Tingley. 1995. Glued-laminated timber reinforced with fiber-reinforced plastic. Innovations Applications Award, CERF. Washington, DC.

Lekhnitskii, S. G. 1987. Anisotropic plates, Gordon and Breach Science Publishers, New York, NY. 534pp.

Lieberman, G.J. 1958. Tables for One-Sided Statistical Tolerance Limits. *Industrial Quality Control*, Vol. XIV, No. 10.

Malhotra, S.K. and I.M.M.Bazan. 1990. Ultimate bending strength Theory or Timber Beams. *Wood Science* 13(1): 50-63.

Mandery, W.L. 1972. Relationship between perpendicular compressive stress and shear strength of wood. *Wood Science* 1(3):177-182.

Mufti, A. A., J. W. Graham, L. G. Jaeger and J. G. Murphy. 1991. Pultrusion processes in the manufacturing of FRP-wood composite beams. Technical Bulletin. Technical University of Nova Scotia, Halifax, Nova Scotia, Canada.

Permanez, E. A. 1974. Information guide for FRP. Permali, Ltd., Toronto, Canada.

Kasal, B., R. J. Leichti and R. Y. Itani. 1994. Nonlinear finite-element model of complete light-frame wood structures. *Journal of Structural Engineering* Vol 120: pp100-119.

Kirlin, C.P. 1996. Expermental and Finite-Element Analysis Stress Distributions Near the End of Reinforcements in Partially Reinforced Glulam. M.S. thesis, Oregon State University, Corvallis, OR. P 180.

Kirlin, C.P., R.J.Leicthi, D.A. Tingley and T. Dibble. 1995. Localized stresses at the reinforcements tails in partially reinforced glulam. In Abstracts. *Forest Products Society Annul Meeting*, June 29-30, 1995. Portland, OR. Forest Products Society, Madison, WI.

Kobetz, R. W. and G. P., Krueger. 1972. Ultimate strength of reinforced timber-biaxial stress failure criterion. *In* Proceedings of the ASCE Annual and National Environmental Engineering Meeting, October, 1972. Houston, TX. American Society of Civil Engineers, New York, NY.

Krueger, G. P. 1972. Ultimate strength design of reinforced timber. Department of Civil Engineering, Michigan Technological University, Houghton, MI.

Lantos, G. G. 1970. The flexural behavior of steel reinforced laminated timber beams. *Wood Science* 2 (3):136-143.

Leichti, R. J. and D. A. Tingley. 1995. Glued-laminated timber reinforced with fiber-reinforced plastic. Innovations Applications Award, CERF. Washington, DC.

Lekhnitskii, S. G. 1987. Anisotropic plates, Gordon and Breach Science Publishers, NY. Pp534

Lieberman, G.J. 1958. Tables for One-Sided Statistical Tolerance Limits. *Industrial Quality Control*, Vol. XIV, No. 10

Malhotra, S.K. and I.M.M.Bzzn, 1990 Ultimate bending Strength Theory or Timber Beams. Wood Science. 13(1). 50-63.

Mandery,W.L. 1972. Relationship between perpendicular compressive stress and shear strength of wood. *Wood Science.* 1 (3):177-182

Mufti, A. A., J. W. Graham, L. G. Jaeger and J. G. Murphy. 1991. Pultrusion processes in the manufacturing of FRP-wood composite beams. Technical Bulletin. Technical University of Nova Scotia, Halifax, Nova Scotia, Canada.

Permanez, E. A. 1974. Information guide for FRP. Permali, Ltd., Toronto, Canada.

Plevris, N. and T. C. Triantafillou. 1992. FRP-reinforced wood as structural material. *Journal of Materials in Civil Engineering* 4 (3): 300-317.

Popov, E. P. 1978. Mechanics of materials. SI version, 2nd edition. Prentice-Hall, Inc. Englewood Cliffs, NJ 07632.

Raman, P.M. and Davalos, F.J. 1996. Static shear correction factor for laminated rectangular beams. *Composites Part B: Engineering*. Vol.27B (2):285-293.

Ramos, A. N. 1961. Stress-strain distribution in Douglas-fir beams within the plastic range. Ph.D. dissertation. Civil Engineering, University of Wisconsin, Madison, WI.

Rowlands, R. E., R. P. Van Deweghe, T. L. Laugeneerg and E. G. Krueger. 1986. Fiber-reinforced wood composites. *Wood and Fiber Science* 18 (1): 40-54.

Samuel, L. S. Jacoey, Janusz and S. Kowalik. 1984. Mathematical Modeling with Computers. Prentice Hall, Inc., NJ.

SAP90®. 1991. Computers and Structures, Inc. Berkeley, CA.

Scale, E. 1973. Composite Materials for Combined Functions. Hayden Book Co., Rochelle Park, NJ.

Serabian, S. M. and D. W. Oplinger. 1987. An experimental and finite element investigation into the mechanical response of 0/90 pin-loaded laminates. *Journal of Composite Materials* 21:631-649.

Sliker, A. 1962. Reinforced wood laminated beams. *Forest Products Journal* 12 (2): 91-96.

Smulski, S. J. and G. Ifju. 1987a. Creep behavior of glass fiber reinforced hardboard. *Wood and Fiber Science* 19 (4): 430-438.

Smulski, S. J. and G. Ifju. 1987b. Flexural behavior of glass fiber reinforced hardboard. *Wood and Fiber Science* 19 (3): 313-327.

Sonti, S. S., J. F. Davalos, R. Hernandez, R. C. Moody and Y. Kim. 1995a. Laminated wood beams reinforced with pultruded fiber-reinforced plastic. Session 10-B/1-5. *In* Proceedings of the Composites Institute's 50th Annual Conference & Expo '95, January 30-February 1, 1995. Cincinnati, Ohio. SPI Composites Institute, New York, NY.

Sonti, S. S., E. J. Barbero, and T. Winegardner. 1995b. Mechanical properties of pultruded E-glass/vinylester composites. Session 10-C/1-7. Session 5-C/1-4. *In* Proceedings of the Composites Institute's 50th Annual Conference & Expo '95, January 30-February 1, 1995. Cincinnati, Ohio. SPI Composites Institute, New York, NY.

Termonia, Y. 1992. Effect of strain rate on the mechanical properties of composites with a weak fibre/matrix interface. *Journal of Materials Science* 27:4878-4882.

Tingley, D. A. 1988. Reinforced glued-laminated wood beams. Masters thesis. The University of New Brunswick, Canada.

Tingley, D. A. 1990. Predicting strength criteria for Kevlar® and fiberglass reinforced plastic (KRP and FRP) glued laminated beams. Vol. 1, pp. 42-25. *In* Proceedings of the International Timber Engineering Conference, October 23-25, 1990. Tokyo, Japan. The Steering Committee of the 1990 International Timber Engineering Conference, Tokyo, Japan.

Tingley, D. A. 1994a. Aligned fiber reinforcement panel for structural wood members. U.S. Patent Document No. 5,362,545.

Tingley, D. A. 1994b. Wood and wood composite design using high-strength fiber-reinforced-plastic (FiRP™ Panel) with special emphasis on glued laminated beam bridges. P. 947-958. *In* Proceedings of the Fourth International Conference on Short and Medium Span Bridges, August 8-11, 1994. Halifax, Nova Scotia. Canadian Society for Civil Engineering, Montreal, P.Q., Canada.

Tingley, D. A. 1995. Method of manufacturing glued-laminated wood structural member with synthetic fiber reinforcement. U. S. Patent Document No. 5,456,781.

Tingley, D. A. 1996a. Surface treated synthetic reinforcement for structural wood members. U. S. Patent Document No. 5,498,460.

Tingley, D. A. 1996b. High-strength fiber-reinforced plastic reinforcement of wood and wood composite. *In* Proceedings of the SAMPE 1996 Conference, March 25-28, 1996. Anaheim, CA.

Tingley, D. A. 1996c. Method of manufacturing wood structural member with synthetic fiber reinforcement. U. S. Patent Document. No. 5,565,257.

Tingley, D. A. 1996d. Method of manufacturing wood structural member with synthetic fiber reinforcement. U. S. Patent Document. No. 5,565,257.

Tingley, D. A. and R. J. Leichti. 1993. Reinforced glulam: Improved wood utilization and product performance. Globalization of Wood, Portland, OR. Forest Products Society, Madison, WI.

Tingley, D. A. and R. J. Leichti. 1994a. Applications of high-strength fiber-reinforced-plastic in building components of low-rise wood structures. Session 6. *In* Proceedings of the Second International Workshop on Full-Scale Behaviour of Low Rise Buildings, July 7-8, 1994. Townsville, Australia. James Cooke University, Townsville, Australia.

Tingley, D. A. and R. J. Leichti. 1994b. Glued-laminated beams having a high-strength fiber-reinforcement: The bi-material interface. Vol. 2, p. 665-675. *In* Proceedings of the Pacific Timber Engineering Conference, July 11-15, 1994. Gold Coast, Australia. Timber Research and Development Advisory Council, Queensland, Australia.

Tingley, D. A. and R. J. Leichti. 1994c. Tension/compression/E-rating for lamination stock used in four bridge girders. Unpublished data. Wood Science and Technology Institute Ltd., Corvallis, OR.

Tingley, D. A. and R. J. Leichti. 1995. Applications of high-strength-fiber-reinforced-plastic in building components of low-rise wood structures. Paper No. 444. The Tenth International Conference on Composite Materials, August 14-18, 1995. Whistler, British Columbia, Canada.

Tingley, D. A. and S. M. Kent. 1996. The effects of test setup and apparatus on full-scale glued laminated timber beam shear strength. (Draft)

Tingley, D. A., R. Leichti, J. H. Poland and S. M. Kent. 1996a. Shear stress distributions in ASTM D143-89 shear blocks. *In* Abstracts. Forest Products Society 1996 Annual Meeting, June 23-26, 1996. Minneapolis, MN. Forest Products Society, Madison, WI.

Tingley, D. A., B. Pooley and S. M. Kent. 1996b. Shear strength of full-scale glulam beams. Draft. Presented at ICBO Shear Issue meeting, April 18, 1996. Los Angeles, CA. ICBO, Whittier, CA.

Tingley, D. A., P. C. Gilham and S. M. Kent. 1996c. Long term load performance of reinforced bridge girts. Presented at National Conference on Wood Transportation Structures, October 23-25, 1996. Madison, WI. Federal Highway Administration and USDA Forest Service, Forest Products Laboratory, Madison, WI.

Tingley, D. A., S. M. Kent and C. P. Kirlin. 1996d. Moisture content effect on reinforced glulams. Draft (in press).

Triantafillou, T. C. and N. Deskovic. 1992. Prestressed FRP sheets as external reinforcement of wood members. *Journal of Structural Engineering* 118 (5):1270-1284.

U. S. Department of Agriculture. 1987. Wood handbook: Wood as an engineering material. Agricultural Handbook No. 72. USDA, Washington, D.C.

van de Kuilen, J. W. G. 1991. Theoretical and experimental research on glass fiber reinforced laminated timber beams. Vol. 3, p. 3.226-3.233. *In* Proceedings of the International Timber Engineering Conference, September 2-5, 1991. London, England. Research and Development Association, High Wycombe, United Kingdom.

Zahn, J. J. 1983. Design of wood members under combined load. *Journal of Structural Engineering* 112 (9):pp 2109-2125.

Appendices

Appendix A

List of Symbols

$\bar{X}$	sample mean.
σ	sample standard deviation.
σ^2	sample variance.
ΔM	change in moment.
ΔT	temperature change.
σ	stress, applied stress.
σ_1	normal stress corresponding to σ_L.
σ_2	normal stress corresponding to $\sigma_{T/R}$.
σ_6	shear stress corresponding to $\tau_{T/R\text{-}L}$.
σ_c	compression parallel to grain stress.
σ_{ij}	stress tensor.
σ_X	axial stress.
$\sigma_{T/R}$	stress in the tangential/radial direction.
σ_Y	radial stress.
σ_Z	tangential stress.
μ	Possion's ratio.
γ	shear strain (radians).
η'	shear modular ratio.
η	modular ratio.
ε_C	compressive strain.
ε	strain.
ε_c	localized strain in clear wood.
ε_g	global strain in glulam beam.

ε_I	active strain.
ε_x	axial strain in extreme fiber bending in tension.
ε_{xz}	shear strain.
ε_z	transverse strain.
ε_j	passive strain.
ε_{jj}	strain tensor.
ε_x	axial strain.
τ_{xy}	shear stress.
τ_r	shear stress in FRP.
$\tau_{L\text{-}T/R}$	shear stress.
τ_{TR}	shear stress.
τ	shear stress.
A	area.
a	one-half shear span.
ARP	aramid reinforced plastic.
b	width.
c	distance to extreme fiber stress region.
CARP	carbon-aramid reinforced plastic.
C_{ijkl}	stiffness tensor.
CRP	carbon reinforced plastic.
CoV	coefficient of variation.
d	depth.
dM	differential change in moment.
dx	differential change in length in the x-direction.
E	modulus of elasticity.
E_b	modulus of elasticity in bending.
E_c	modulus of elasticity in compression.
E_{ck}	modulus of elasticity in compression perpendicular to grain for knots.
$E_{c\perp}$	modulus of elasticity in compression perpendicular to grain.

E_{rt}	modulus of elasticity of reinforcement in tension.
E_t	modulus of elasticity of in tension.
E_{wc}	modulus of elasticity of wood in compression.
E_{wt}	modulus of elasticity of wood in tension.
EWC	engineering wood composite.
E_x	modulus of elasticity in x-direction.
FARP	fiberglass-aramid reinforced plastic.
FEA	finite-element analysis.
F_{fv}	design shear strength of reinforced glulam.
FiRP™	trademark for patent high-modulus fiber reinforced plastic.
FJQ	finger joint qualification stress level.
FRP	fiber reinforced plastic.
F_{rv}	allowable design horizontal shear stress resistance of FiRP™ reinforced glulam (psi).
FSP	fiber saturation point.
G	shear modulus.
Glulam	glued-laminated beam.
h	height.
I	moment of inertia.
k	factor computed from sample.
L	Longitudinal.
L_x	length of span.
LEL	lower exclusion limit.
LVL	laminated veneer lumber.
LVDT	linear variable differential transformer.
M	moment.
MC	moisture content.
MOR	modulus of rupture.
PL	proportional limit.
PPTA	poly-phenylene terephthalamide.

Q	first moment of area with respect to the neutral axis.
R	radial.
RH	relative humidity.
rp-wd	reinforcement-to-wood glueline in a glulam beam.
SEM	scanning electron microscope.
SG	specific gravity.
S_{ijke}	stiffness coefficients.
S_{ijkl}	compliance tensor.
S_{ijkl+}	compliance coefficients.
T	tangential.
t	thickness.
T_g	glass transition temperture.
TS	tensile strength.
U	universal strain energy.
UTS	ultimate tensile strength.
UV	ultraviolet.
V	shear force.
YP	yield point.

Appendix B

Testing Procedures

Specimen Sampling Methods

FRP-Reinforced Glulam Testing. The following test methods as described in American Society for Testing and Materials "General Methods of Testing" [ASTM, 1994c] were observed in determining the final sample size for testing of reinforced glulams:

- E 105 "Recommended Practice for Probability Sampling of Materials" [ASTM, 1882].
- E 122 "Choice of Sample Size to Estimate the Average Quality of a Lot or Process" [ASTM, 1982]

These methods were also used to determine the specimen population size and specimen frequency for the FRP used in the production of the FRP reinforced glulams. In all cases the population of test results had a safety factor of 2.1 applied to the 5% lower exclusion limits (LEL), based on a Weibull distribution model to establish design values. The standard formulas used are shown below:

$$\bar{X} = \frac{\sum_{i=1}^{n} X_i}{n}$$

$$\sigma = \sqrt{\frac{\sum (X_i - \bar{X})^2}{n-1}}$$

$$\sigma^2 = \frac{\sum (X_i - \bar{X})^2}{n-1}$$

$$CoV = \frac{\sigma}{X} 100$$

The reinforced glulams were manufactured in accordance with the AITC 117-88 "Manufacturing Standard Specifications for Structural Laminated Timber of Softwood Species" [AITC, 1988].

Reinforced-Glulam Component Testing. Sample specimens were taken from the full-scale test reinforced glulams according to AITC 200-92 "Inspection Manual For Structural Glued Laminated Timber" [AITC, 1992]. The sampling procedure included the following component tests:

- T 102 "Adhesive Spread Measurement"
- T 122 "Adhesive Mix Ratio Check"
- T 110 "Cyclic Delamination Test"
- T 115 "End Joint Machining Test (dry fit)"
- T 105 "Diagnostic Test for Finger Joint Quality"
- T 119 "Full Size Tension Test"
- T 107 "Shear Test" (Figure C.4 contains a photograph of a shear test coupon)
- ASTM D-143 [ASTM, 1994b] Clear Wood Sample Tests.

Tensile and compressive samples were recovered from each lamination of the full-scale glulam beams. These samples were recovered from the central (lengthwise) portion of the beam. They were matched in that they were recovered from the same 1

x 1 x 40 in. (25 x 25 x 1016 mm) sample. Figures B.1 and B.2 show sample stress-strain curves from matched tension and compression pairs. They were recovered from full-scale reinforced glulams. Figure B.1 is for ponderosa pine. The samples were conditioned at 12% MC. Figure B.2 shows a similar graph. Figure B.3 is a photograph of compression testing.

Analysis. American Institute of Timber Construction guidelines include directions for interpretation of collected data. These guidelines were followed in this thesis. Certain analyses such as that of T107 data, included calculation of mean ($\bar{X}$), standard deviation (σ) and coefficient of variation (CoV).

Beam Reaction Apparatus. The support apparatus matched ASTM D 198 [ASTM, 1994a] by having reaction bearing plates of suitable size to prevent localized crushing of the beam at the contact point. The reaction points at the supports were a rocker-type knife edge support at each end. The bearing surfaces of the beam were checked and shimmed if necessary to insure that they were in full contact with the bearing plate at all times during the test. The specimens had lateral support in all cases where the depth-to-width ratio was greater than three. These lateral supports were located at or near the load application points and half way between the load points and the reaction points as needed. They provided continuous support throughout the depth of the sample. Figure B.4 contains a photograph of a full-scale reinforced glulam beam in its support apparatus.

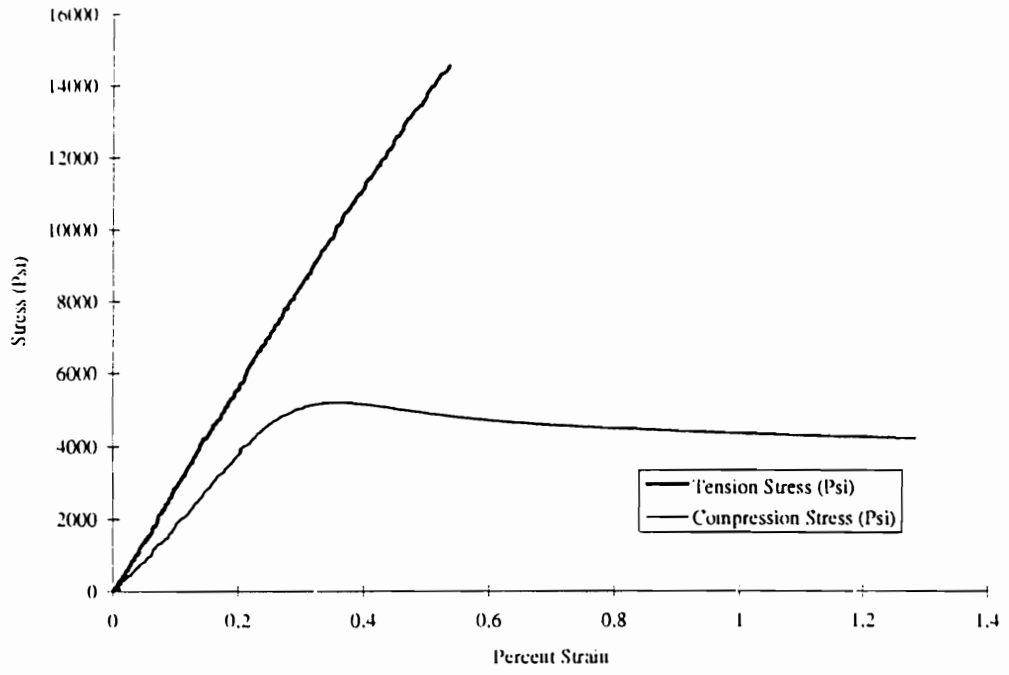

Figure B.1. ASTM D143 [ASTM, 1994b] tension and compression test sample stress versus strain curves.

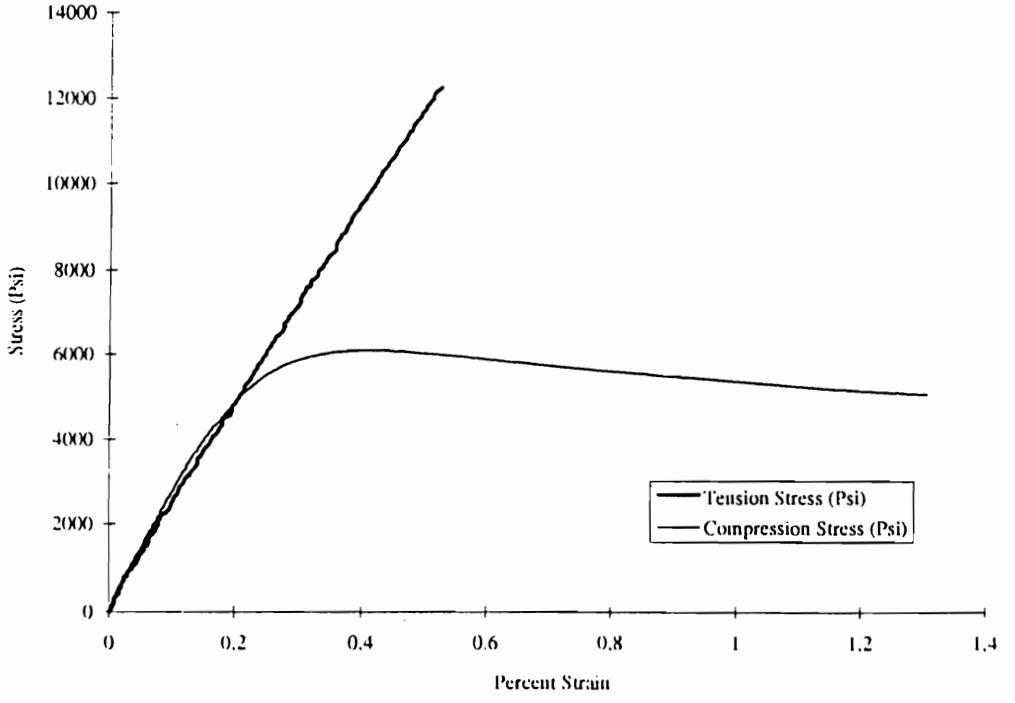

Figure B.2. ASTM D143 [ASTM, 1994b] tension and compression test sample stress versus strain curves.

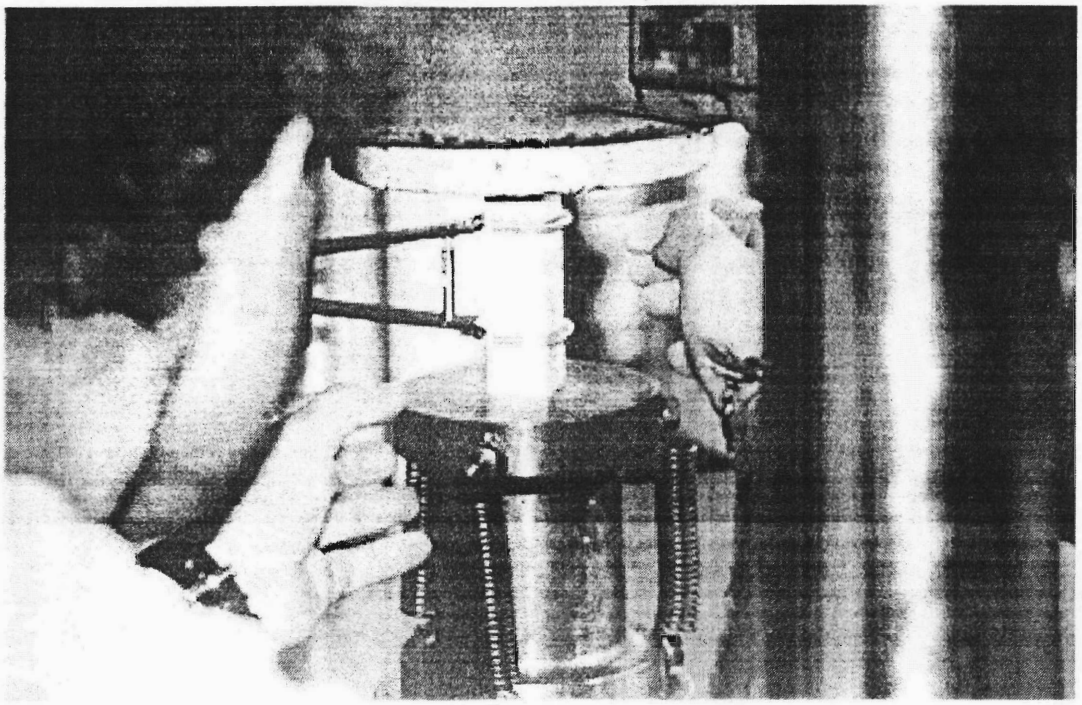

Figure B.3. Photograph of a compression test on a wood specimen.

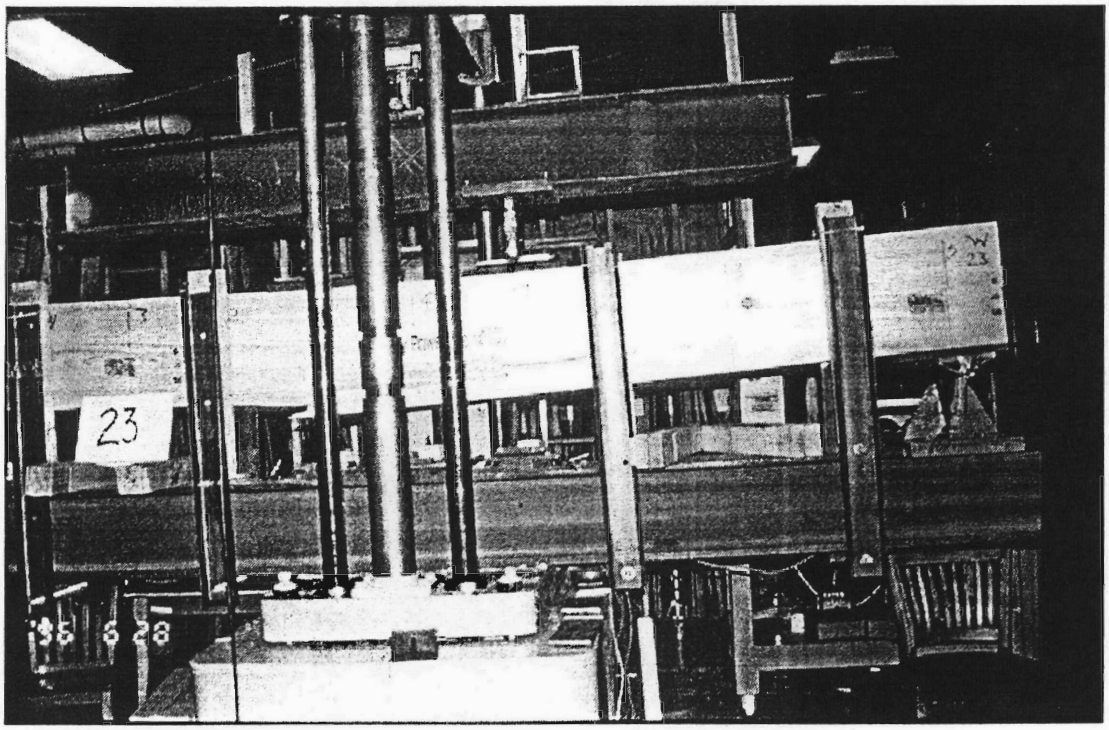

Figure B.4. Full-scale glulam beam in testing apparatus.

Load Apparatus. The load-bearing steel plates met the criteria of the ASTM D 198 [ASTM,1995c]. They were full width and 12 in. (305 mm) long and 1 in. (25 mm) thick so that all applied loads transferred to the specimen.

Load Points. The specimens were loaded in accordance with ASTM D 198 [ASTM, 1995]. The load head applied loads at third points. In cases where the sample was longer than 24 ft. (7315 mm), the load points were placed equidistant from the reactions and separated by a distance of 8 ft. (2438 mm).

Deflection Apparatus. The deflection of the specimen was measured with a yoke type wire/spring apparatus connected to two nails one over each reaction point located at the neutral axis of the test specimen. In addition to this method, linear variable differential transformers (LVDT), were attached to the neutral axis of the specimen on the opposite side at the reaction points, load points and at the midspan to provide information on deflection in the shear free zone between the two load points. The LVDT measurements of deflection were to the nearest 0.01 in. (0.25 mm).

Reinforced Glulam Test Specimens. The test specimens were identified and all components documented as to moisture content, origin of supply of wood laminations, history of drying and conditioning of wood, species of wood laminations and their location, grade (visual) and location of all such laminations of wood, type of reinforcement, location of reinforcement, concentration of reinforcement by cross sectional area, chemical treatment (if any), and location of reinforcement longitudinally throughout the specimen.

American Institute of Timber Construction standard layups were used (including species and grades of laminations) [AITC, 1988]. Measurements of the width-depth-length of specimen at ends and center, specimen span length and total specimen length (included overhang for bearing plate) was recorded for all reinforced glulams.

Ambient Conditions During Testing. Ambient conditions during testing were documented with each test. These included but were not limited to ambient relative humidity, temperature and moisture content of the specimen (moisture meter-prong test).

Speed of Test. The speed of test was within a time of 6 minutes to 20 minutes from start to sample failure with an average of 10 minutes. The rate of loading was calculated according to the formulas cited in ASTM D 198 [ASTM, 1994a] and was targeted to create a rate of strain in the outer most fiber of 0.001 in./in.-minute (0.025 mm/mm-min.).

The load deflection curves for each specimen were developed and included the yield point, MOR, and E_b. Specimens were manufactured in sizes to cause primary failure in shear for verification of shear strength formulas. These specimens had a shear span-to-depth ratio of less than 5. Specimens were manufactured in sizes to cause primary failure in moment for verification of moment strength formulas. These specimens had a shear span-to-depth ratio of greater than 5 but less than 12. For deflection formulas verification specimens were manufactured and tested in sizes projected to cause primary failure in moment but be of sufficient length to evaluate the

deflection properly. These specimens had a shear span-to-depth ratio of greater than 12.

Records of failure were kept and documented in writing as well as with high speed video camera. All calculations and reporting were conducted in accordance with the ASTM D198 [ASTM, 1995a] method for flexural tests in structural wood members.

Figure B.5 contains a load-deflection curve to evaluate a 2.5 x 12 in. x 21 ft. (63.5 x 310 cm x 6400 mm) partially reinforced AITC combination 5 glulam beam generated using the equipment described. This beam was designed to fail in moment.

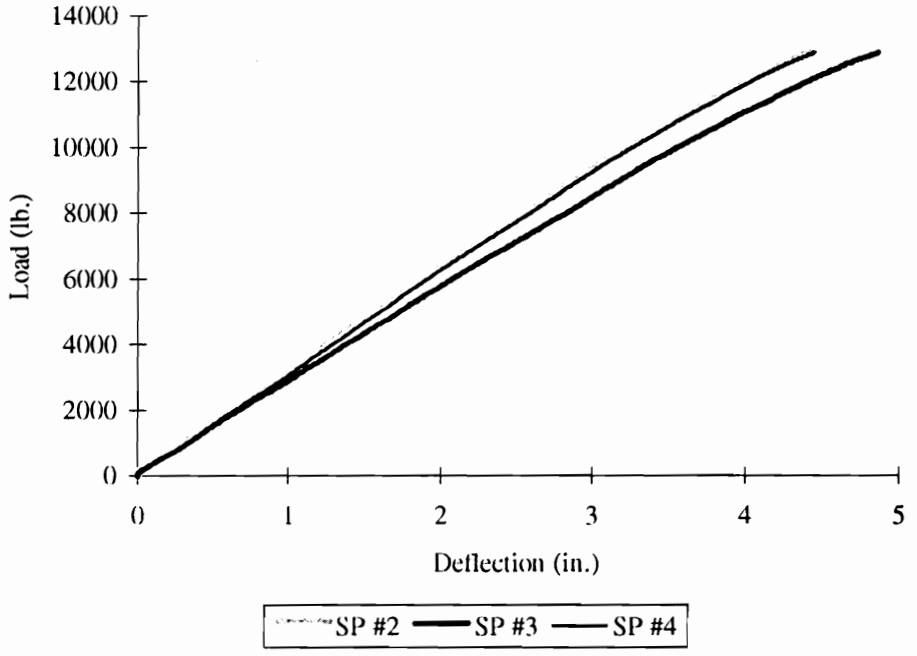

Figure B.5. Example load-deflection curve.

Two layers of aramid FRP were in the tensile zone and one layer of carbon FRP was in the compressive zone. Each FRP layer was 0.07 in. (.18 mm) thick, 13 ft. (3962 mm) long and centered in the beam lengthwise. The beam moisture content was 15%. Ambient temperature during the test was 72°F (22.2°C) and relative humidity 34%. The beam failed at a load of 11,260 lb (50 kN) with a corresponding deflection of 4.75 in. (12 cm).

Reinforcement Component Testing

- Tensile Test: ASTM D3039 [ASTM, 1994b], *Standard Test Method for Tensile Properties of Polymer Matrix Composites.* Table B.1 and Figure B.6 contain representative output of this type of testing on FRP.
- Compression Test: ASTM D3410 [ASTM, 1994c], *Standard Test Method for Compressive Properties of Unidirectional or Crossply Fiber-Resin Composites.* Table B.2 and Figure B.7 contain a representative output of this type of testing on FRP.
- Shear Test: ASTM D5379 [ASTM, 1994d], *Standard Test Method for Shear Properties of Composite Materials by the V-Notched Beam Method.* Table B.3 contains representative output of this type of testing on FRP.
- Bolt Bearing Test: ASTM D953 [ASTM, 1994e], *Standard Test Method for Bearing Strength of Plastics.* Table B.4 and Figure B.8 contain representative output of this type of testing on FRP.

Table B.1. ASTM D3039 [ASTM, 1994b] representative tension test results for various types of FRP.

			Mean			Standard Deviation		
Material	Specimen Dimensions	Sample Size	Modulus (ksi)	Strain (%)	Stress (ksi)	Modulus (ksi)	Strain (%)	Stress (ksi)
ARP	3.125x0.07	17	10975	1.75	209	551	0.23	11
ARP	5.125x0.07	131	11848	1.59	213	809	0.27	12
ARP	6.750x0.07	15	11811	1.5	201	1529	0.41	8
CARP	3.125x0.07	94	18280	1.03	179	1471	0.18	14
CARP	5.125x0.07	80	18548	0.91	185	2223	0.25	13
CARP	6.750x0.07	88	18851	0.92	179	2373	0.25	12
FARP	5.125x0.07	5	8944	1.81	162	267	0.10	5

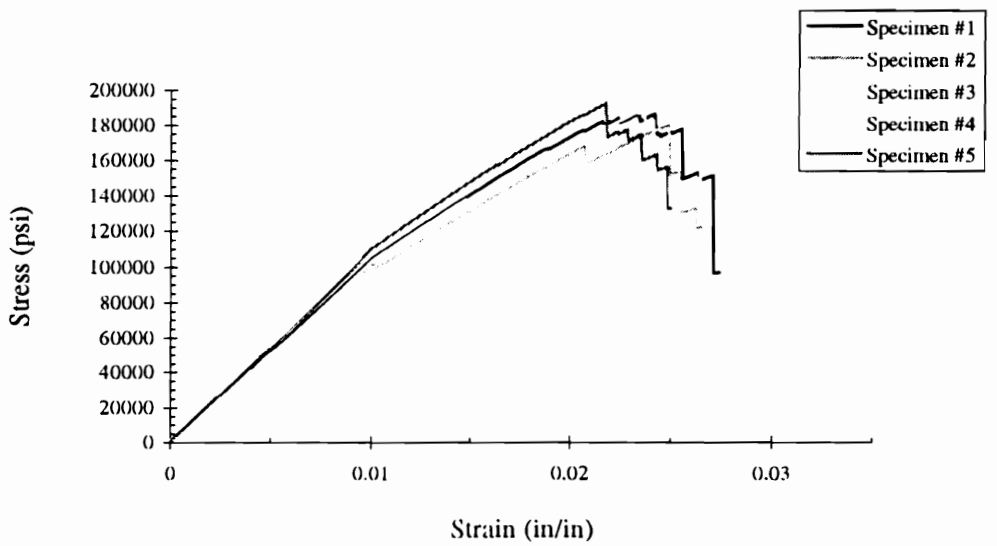

Figure B.6. Stress-strain curves for five CARP specimens in tension.

Table B.2. ASTM D3410 [ASTM, 1994c] representative compression test results for various type of RP.

			Mean			Standard Deviation		
Material	Specimen Dimensions	Sample Size	Modulus (ksi)	Strain (%)	Stress (ksi)	Modulus (ksi)	Strain (%)	Stress (ksi)
CARP	3.125x0.07	33	12532	0.37	43.17	3263.36	0.14	6.92
CARP	5.125x0.07	28	10447	0.74	52.35	5621.23	0.51	4.94
CARP	6.750x0.07	29	11642	0.63	48.27	4217.15	0.38	7.57

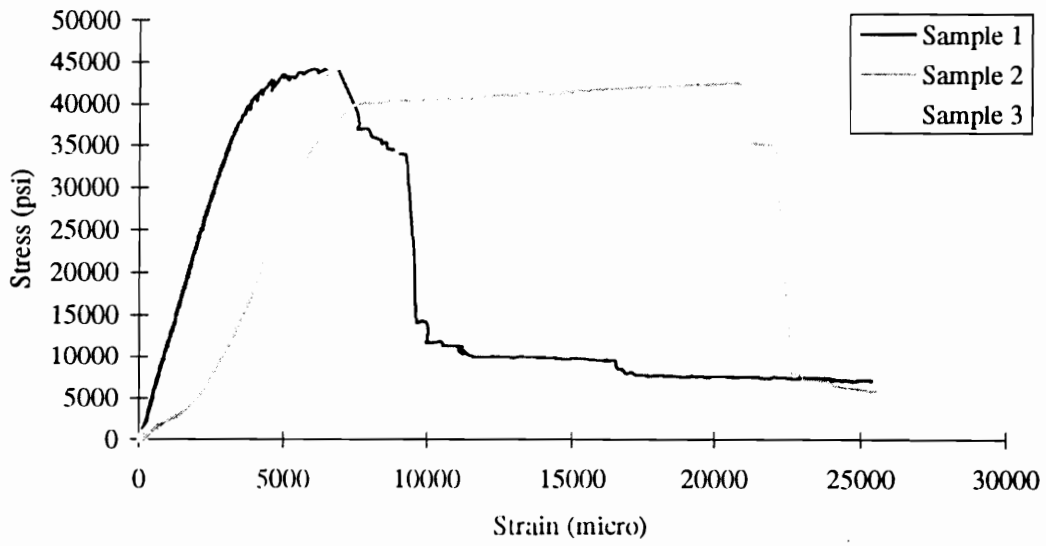

Figure B.7. Stress-strain curves for three CARP specimens in compression.

Table B.3. Results of ASTM D5379 [ASTM, 1994d] shear testing of RP.

Material	Specimen Dimension (in)	Mean Shear Stress (psi)	Standard Deviation (psi)	Samples Size
ARP	3.125x0.07	1370	373.76	6
ARP	5.125x0.07	1535	256.42	46
ARP	6.750x0.07	1792	205.17	5
CARP	3.125x0.07	2036	437.48	34
CARP	5.125x0.07	2452	435.64	28
CARP	6.750x0.07	2251	318.52	28

• Curing Properties: ASTM D5028 [ASTM, 1994f], *Standard Test Method for Curing Properties of Pultrusion Resins by Thermal Analysis.* Table B.5 contains representative output of this type of testing on FRP.

• Fiber-Resin Ratio: ASTM D2584 [ASTM, 1994g], *Standard Test Method for Ignition Loss of Cured Reinforced Resin.* Table B.5 contains representative output of this type of testing on FRP.

• Density: ASTM D792 [ASTM, 1994h], *Standard Test Method for Specific Gravity (Relative Density) and Density of Plastics by Displacement.* Table B.5 contains representative output of this type of testing on FRP.

• Creep Test: ASTM D2990 [ASTM, 1994i], *Standard Test Methods for Tensile, Compressive and Flexural Creep and Creep-Rupture of Plastics.* Figure B-9 contains a sample creep test output for a CARP.

Table B.4. ASTM D953 [ASTM, 1994e] bolt bearing test results.

Material	Load Direction	Bolt Size	Number of Sides w/Wood Attached	Mean Max Load (lb)	Maximum Load Standard Deviation	Max. Load CoV	Mean Max. Stress (psi)	Maximum Stress Standard Deviation	Max. Stress CoV
ARP 0.07 in thick	Comp. Parallel	½	0	352	6.11	1.73	11530	481.79	4.18
		½	1	1168	127.67	10.93	8078	926.98	11.47
		½	2	2036	109.74	5.39	8280	501.63	6.06
		¾	0	523	21.08	4.03	10043	445.94	4.44
		¾	1	1421	175.05	12.32	6360	748.43	11.77
		¾	2	2409	222.03	8.90	6571	475.18	7.23
		7/8	0	648	17.44	2.69	11418	155.32	1.36
		7/8	1	1883	206.72	10.98	7413	904.11	12.20
		7/8	2	2625	154.02	5.87	5987	463.03	7.73
	Comp. perpend.	½	0	180	35.8	19.92	5221	789.62	15.12
		½	2	1631	116.25	7.13	5896	399.04	6.77
		¾	0	417	31.24	7.49	8204	1093.71	13.33
		¾	2	1810	157.68	8.71	4329	422.14	9.75
		7/8	0	207	21.92	10.62	3233	424.26	13.12
		7/8	2	1152	260.92	22.66	2417	226.98	9.39
	Ten. Parallel	½	0	187	9.71	5.20	5534	52.79	0.95
		½	1	910	124.54	13.68	6149	934.31	15.20
		½	2	1488	225.86	15.18	5908	763.64	12.92
		¾	0	189	26.39	13.94	3627	510.91	14.08
		¾	1	612	53.36	8.77	2728	290.74	10.66
		¾	2	987	124.39	12.60	2590	342.19	13.21
		7/8	0	166	17.06	10.28	2598	578.69	22.27
		7/8	1	540	63.15	11.69	1964	131.00	6.67
		7/8	2	983	140.65	14.31	2232	342.63	15.35
	Comp. Perpend.	½	0	28	18.50	65.30	635	427.17	67.31
		½	2	171	16.26	9.54	740	50.91	6.88
		¾	0	25	1.41	5.66	477	9.90	2.08
		¾	2	124	98.99	79.83	296	237.59	80.27
		7/8	0	13	5.66	43.51	143	58.69	41.19
		7/8	2	30	---	---	65	---	---

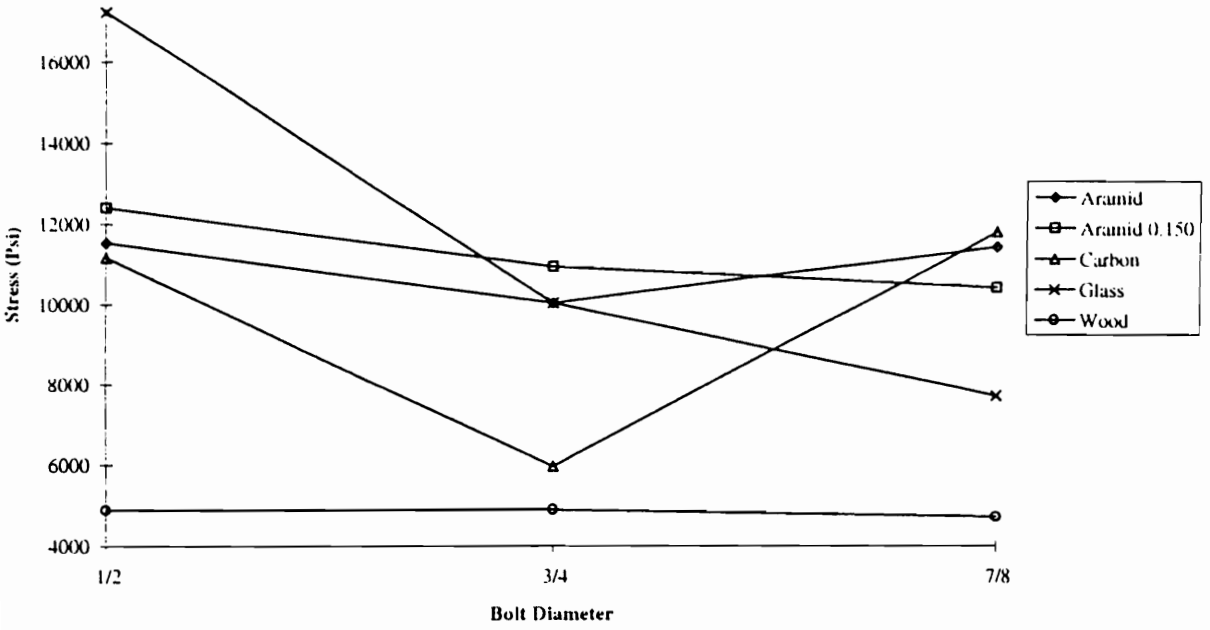

Figure B.8. Results of ASTM D953 (ASTM 1994e) bolt bearing test all samples compression parallel to grain.

Table B.5. Summary of results of various tests on FRP.

		ASTM D5028 [ASTM, 1994f] Degree of Cure			ASTM D792 [ASTM, 1994h] Density			ASTM D2584 [ASTM, 1994g] Fiber %		
Material	Dimensions	mean	Std. Dev.	Size	mean	Std. Dev.	Size	mean	Std. Dev.	Size
ARP	3.125x0.07	86	7.80	4	1.40	---	1	67	3.18	4
ARP	6.750x0.07	89	1.78	5	1.30	0.02	3	56	2.47	5
ARP	5.125x0.07	86	2.63	6	1.29	0.01	5	50	17.9	10
CARP	3.125x0.07	86	---	1	1.33	0.01	3	75	---	1
CARP	6.750x0.07	89	2.01	16	1.43	0.01	3	71	2.67	19
CARP	5.125x0.07	92	1.49	5	1.30	0.02	3	74	1.09	5

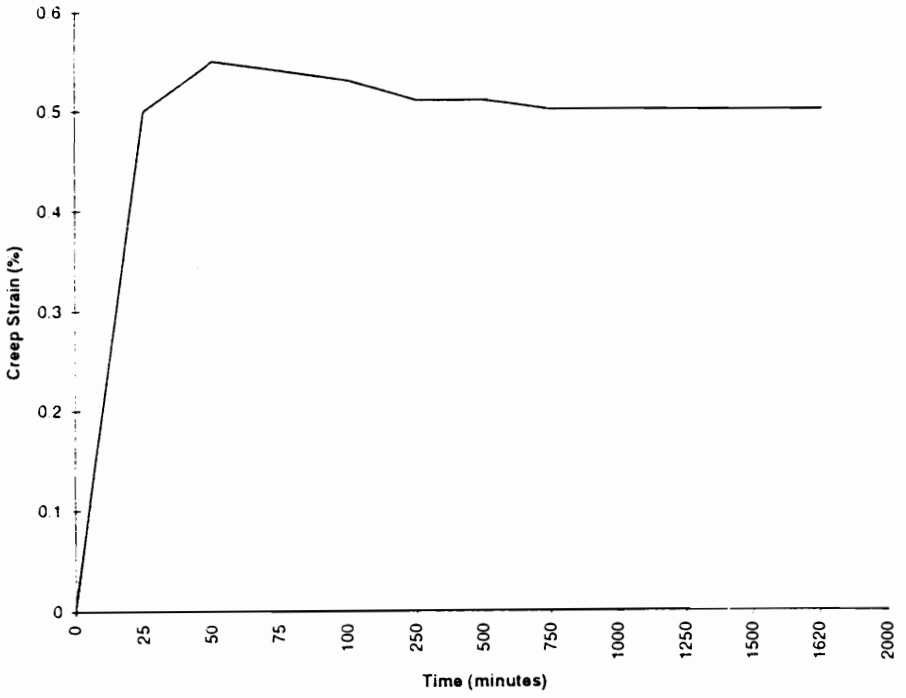

Figure B.9. Results of thirty-hour ASTM D2290 creep tests on CARP.

• Fatigue Test: ASTM D3479 [ASTM, 1994j], *Standard Test Method for Tension-Tension Fatigue of Oriented Fiber-Resin Matrix Composites*. Table B.6 contains representative output of this type of testing on FRP.

• Weathering Test: ASTM D4329 [ASTM, 1994k], *Standard Practice for Operating Light and Water Apparatus (Fluorescent UV and Condensation Type) for Exposure of Plastics*. Table B.7 and Figure B.10 contain representative output of this type of testing on FRP.

Table B.6. Results of ASTM D3479 [ASTM, 1994j] tension-tension testing on FRP.

	Sample (% UTS)	Min Load (kips)	Max Load (kips)	Displacement (in)	Cycles	Residual Strength (ksi)
ARP	A: (20 to 40)	4.027	5.208	0.0164	2000000	196.4
	B: (20 to 50)	5.253	6.442	0.0137	2000000	200.5
	C: (20 to 60)	5.727	7.044	0.0160	2000000	238.0
	D: (20 to 70)	6.960	8.435	0.0160	2000000	217.1
	E: (20 to 80)	7.030	10.16	---	1875	---
CARP	A: (20 to 40)	1.862	3.737	0.0200	2000000	224.4
	B: (20 to 50)	1.800	4.529	0.0290	2000000	222.9
	C: (20 to 60)	1.740	5.207	0.0450	2000000	---
	D: (20 to 70)	1.779	5.447	0.0480	2000000	213.1
	E: (20 to 80)	2.070	7.001	---	1685	---
FARP	A: (20 to 40)	1.765	3.538	0.0280	86866	---
	B: (20 to 50)	1.767	4.347	0.0420	21170	---
	C: (20 to 60)	1.873	5.103	0.0500	6246	---

Table B.7. Summary of ASTM D3039 [ASTM, 1994b] tension tests after ASTM D4329 [ASTM, 1994 k] weathering tests.

Cycle	Aramid	Aramid	Aramid	Wood 1	Wood 1	Wood 1	Wood 2	Wood 2	Wood 2
	Modulus	Strain	Stress	Modulus	Strain	Stress	Modulus	Strain	Stress
0	9958	1.9	184.9	9619	1.4	134.0	10177	1.5	153.2
10	9563	1.9	178.8	10102	1.4	134.3	9364	1.1	95.10
20	9144	1.9	177.0	10133	1.4	136.7	9879	1.5	147.2
30	8733	2	174.1	5623	1.5	121.0	10597	1.1	126.9
50	8543	1.9	161.7	10191	1.1	115.8	10758	1.4	143.9
100	7920	2.1	163.1	9159	1.4	123.6	7977	1.4	112.0
Total % Change	-5.7	2.51	-3.13	-1.23	-0.06	-2.03	-6.06	-1.53	-7.78

Note: Total % Change measures as Cycle 100 - Cycle 0, divided by the average of both cycles.

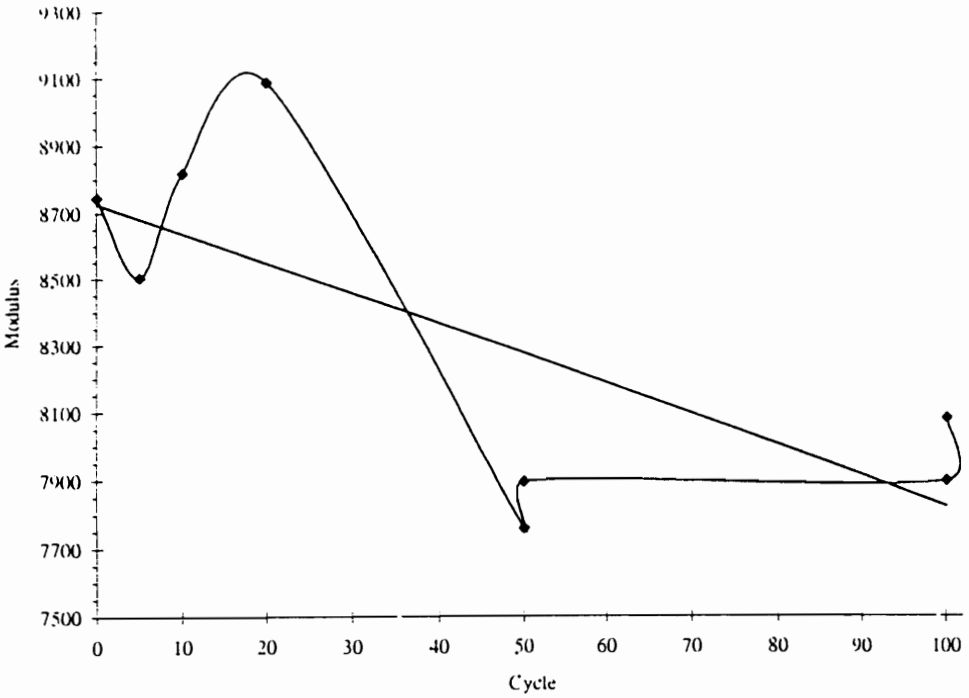

Figure B.10. Results of tension test ASTM D3093 [ASTM, 1994b] after ASTM D4329 [ASTM, 1994k] weathering using repeated freezing cycles in a water bath.

• Water Absorption: ASTM D570 [ASTM, 1994l], *Standard Test Method for Water Absorption of Plastics.* Table B.8 contains representative output of this type of testing on FRP.

• Heat Deflection Temperature: ASTM D648 [ASTM, 1994m], *Standard Test Method for Deflection Temperature of Plastics Under Flexural Load.* Table B.9 contains a representative output of this type of testing on FRP.

• Visual Characterization: ASTM D4385 [ASTM, 1994n], *Standard Practice for Classifying Visual Defects in Thermosetting Reinforced Plastic Pultruded Products.*

Table B.8. ASTM D570 [ASTM, 1994l] water absorption test results.

Material	% water absorbed
Aramid RP virgin	2.7
Aramid RP sanded	7.1
Aramid RP w/ wood 1 side	57.1
Aramid RP w/ wood 2 sides	65.2
Carbon-Aramid RP virgin	4.5
Crabon-Aramid RP Sanded	6.6
Carbon-Aramid RP w/ wood 1 side	58
Carbon-Aramid RP w/ wood 2 sides	62.1
Fiberglass-Aramid RP virgin	3.6
Fiberglass-Aramid RP sanded	7.4
Fiberglass-Aramid RP w/ wood 1 side	51
Fiberglass-Aramid RP w/ wood 2 sides	76.7

Note: Percent (%) water absorbed based on oven dry weight.

Table B.9. Results of ASTM D648 [ASTM, 1994m] tests on FRP.

		Heat Deflection Temperature °C		
Material	Size	mean	Standard Deviation	Sample Size
ARP	3.125x0.07	213.17	6.49	6
ARP	5.125x0.07	212.63	3.93	46
ARP	6.750x0.07	208.40	2.19	5
ARP	3.125x0.07	214.83	6.42	12
CARP	5.125x0.07	220.54	4.84	13
CARP	6.750x0.07	222.67	5.25	15

Appendix C

Stain Gauge Methodology

Strain gauges were used to measure strains in the full-scale reinforced beams during loading. In addition, strain gauges were used to measure strains in wood and reinforcement components tested in shear.

In full-scale beam tests, strain gauges were placed in a variety of locations depending upon area of interest, e.g., under load points and over reactions, in the gluelines either on the reinforcement or on the wood (Figure C.1). Additionally, gauges were placed on the sides and top of the beams often in 0°-45°-90°_ rosette formation (Figure C.2).

The strain gauges were foil type gauges which were bonded to the wood and reinforcement using epoxy adhesives. The gauges used on the outside and between laminations of the full-scale beams were a Micro-Measurements, Inc. #EA-06-10CB-120 and JP Technologies, Inc. #PA60-1000BA-120. The effective gauge length was 25.4 mm with a resistance of 120Ω. An active quarter-bridge configuration was used in each gauge. To compensate for temperature fluctuation effects, a second non-active gauge was mounted on a Lucite block to complete the half bridge. Vishay 2100 Strain Gauge Signal Conditioners made up the remaining half bridge. Figure C.3 shows the equipment setup for data acquisition.

Two Vishay 2100 systems were used to provide a total of twenty channels for strain gauge signals. The Vishay system provided excitation and amplification of the

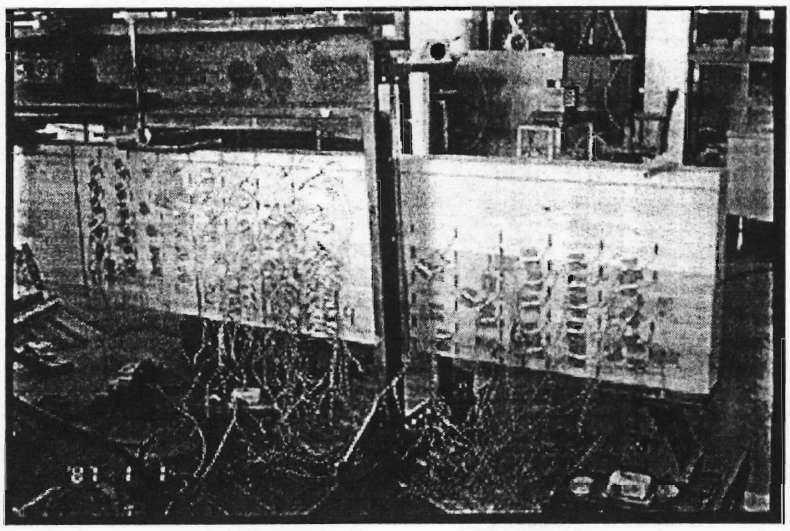

Figure C.1. Photograph of gauges on the side of a glulam.

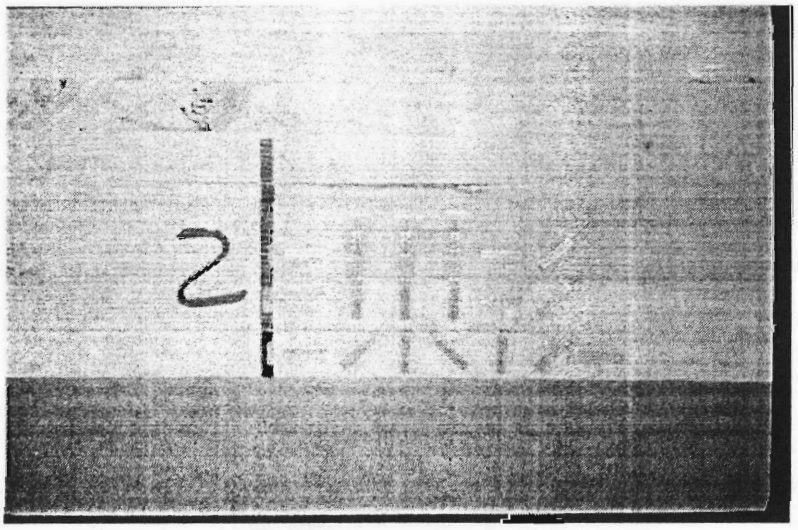

Figure C.2. Strain gauge rosettes on glulam beam.

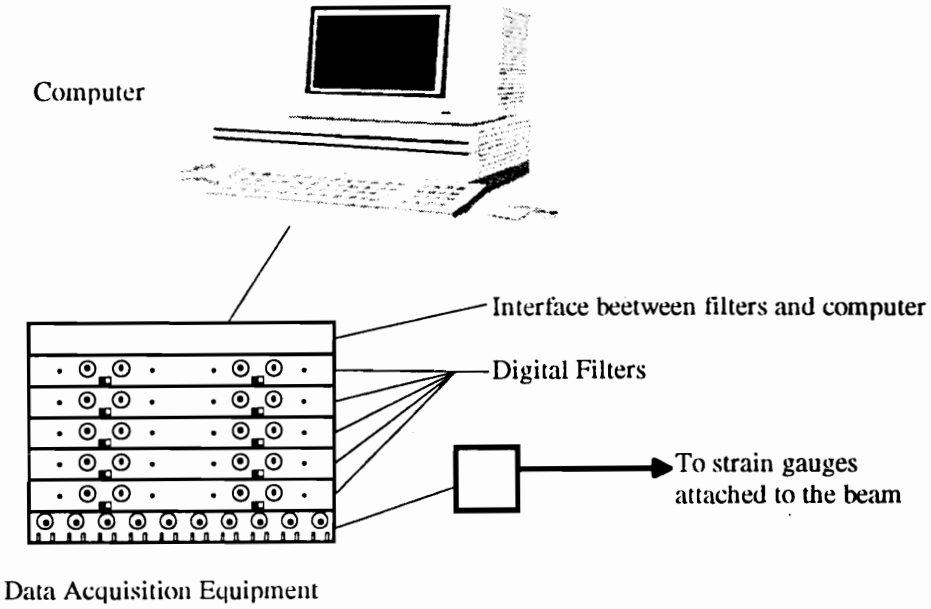

Figure C.3. Diagram of equipment setup.

bridge output signals. A volt excitation level was set below 5 volts to minimize thermal effects on the gauges. The gain setting was 500 on the Vishay 2100 amplifiers.

Rockland Model 432 filters were used for each of the Vishay 2100 output channels. The filters were configured as a unity-gain, one hertz, fourth-order Butterworth low-pass filter. These low-pass filters reduced noise induced in the strain gauge lead wires. The outputs of the filter units were input to a multiplexer controlled by a Campbell Scientific recorder (21X) which fed strain gauge data, temperature, time, load and deflection data from linear variable differential transformers (LVDT) into a laptop computer. This information was then manipulated and analyzed using conventional spread sheet software (Excel, Quattro Pro or Lotus 1,2,3).

To verify the operation of the strain gauge system a shunt was performed at the connection box using an active gauge with a resistance of 59,880 ohms. The shunt

resistance produced a required output of 0.5 volts at the output of the Vishay 2100 for each setup described. Each channel was similarly verified. This allowed verification that the gauges, particularly the internal gauges, were not affected by the lamination movement, pressure of clamping, adhesives, increased temperature during curing, machining and transportation activities.

Similar strain gauge techniques were used with a variety of foil gauge types for the wood and reinforcement components. Figure C.4 shows a photograph of a strain gauged reinforcement coupon in an ASTM D5379 [ASTM, 1994d] shear test (Iosipescu). Figure C.5 shows rosette gauges on an ASTM D143 [ASTM, 1995b] shear block test.

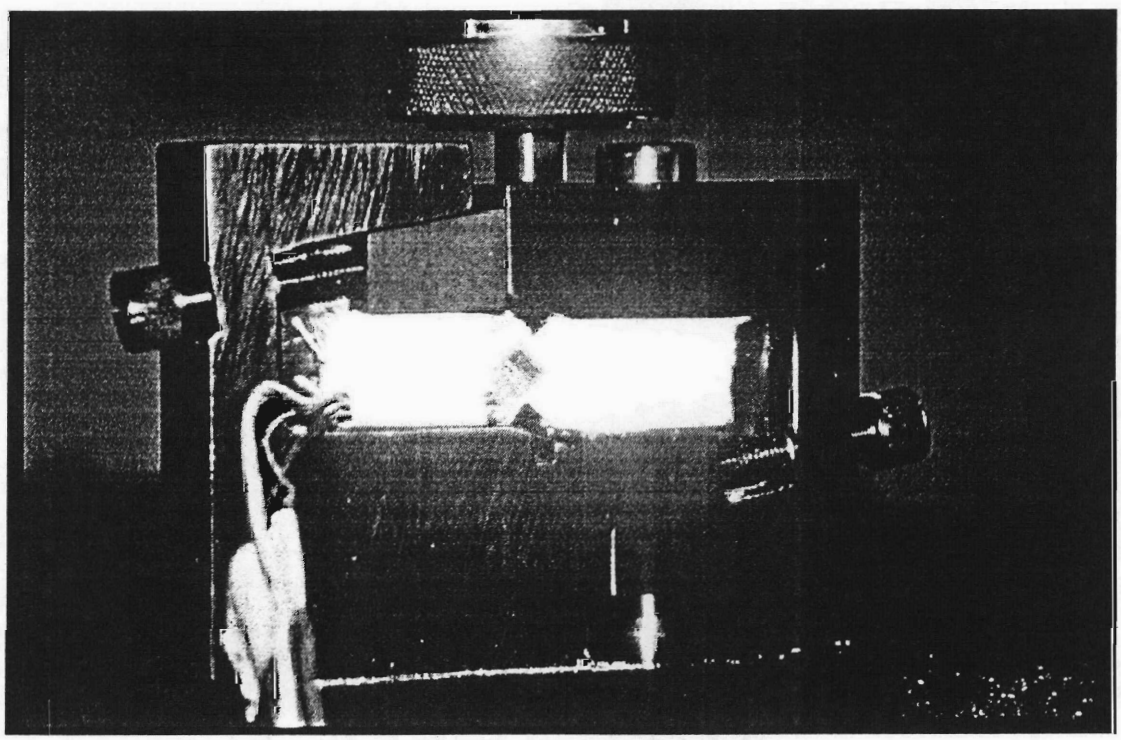

Figure C.4. Photograph of a strain gauges reinforcement coupon in an ASTM D5379 [ASTM, 1994d] shear test.

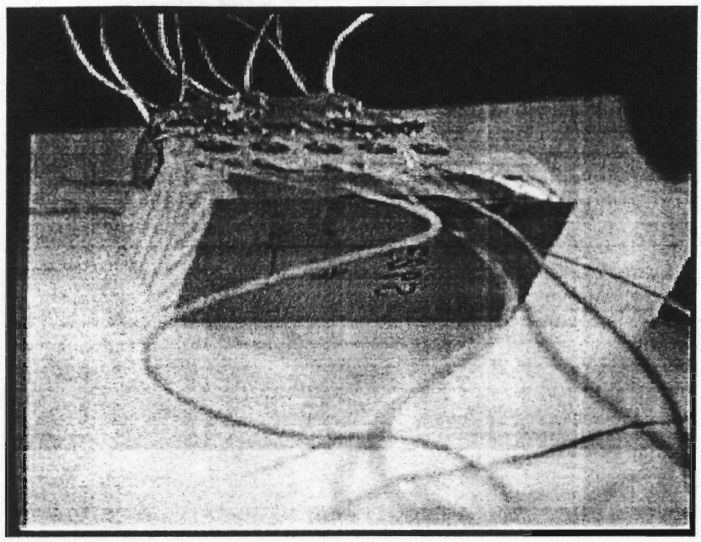

Figure C.5. Photograph of strain rosettes
on a shear block.

The application of gauges on lamination faces prior to adhesive application and clamping involved special precautions. In addition to the mapping of local knot locations and precautions to prevent lead wires from crossing, particular attention was paid to handling of laminations, particularly the reinforcement after gauge application. Care was used to prevent excessive straining by limiting the lamination deflection. Other items requiring special attention were:

- placement of neoprene protective cover over gauges, although recommended, does not work with this type of application as it interferes with adhesion of the resorcinol glue used in the manufacturing process;
- limit lamination adjustment around gauges during gluing;
- nsure lead wires do not cross gauges or other wires in lamination process;
- limit lead wire length to limit adhesive fouling;

- properly map and tag lead wires;
- minimize projection of solder joint at lead wire gauge interface.

Strain Gauge Data Conversion

Due to strain gauge reading fluctuation, regression techniques were used to streamline stress-strain curves. Figure C.6 shows a raw strain gauge output and the regression analysis stress-strain curve with the output table providing regression coefficient value R^2 calculations.

In addition to the regression analysis stress-strain curve with the output table providing R^2 values and calculations. In addition to the regression analysis of stress-strain data, gauge averaging was performed. This averaging was important since localized differences in E caused unusual strain contour lines making corresponding stress distributions difficult to interpret. Figure C.7 shows a shear strain distribution with averaging.

Figure C.8 shows the location of gauges for various test beam configurations.

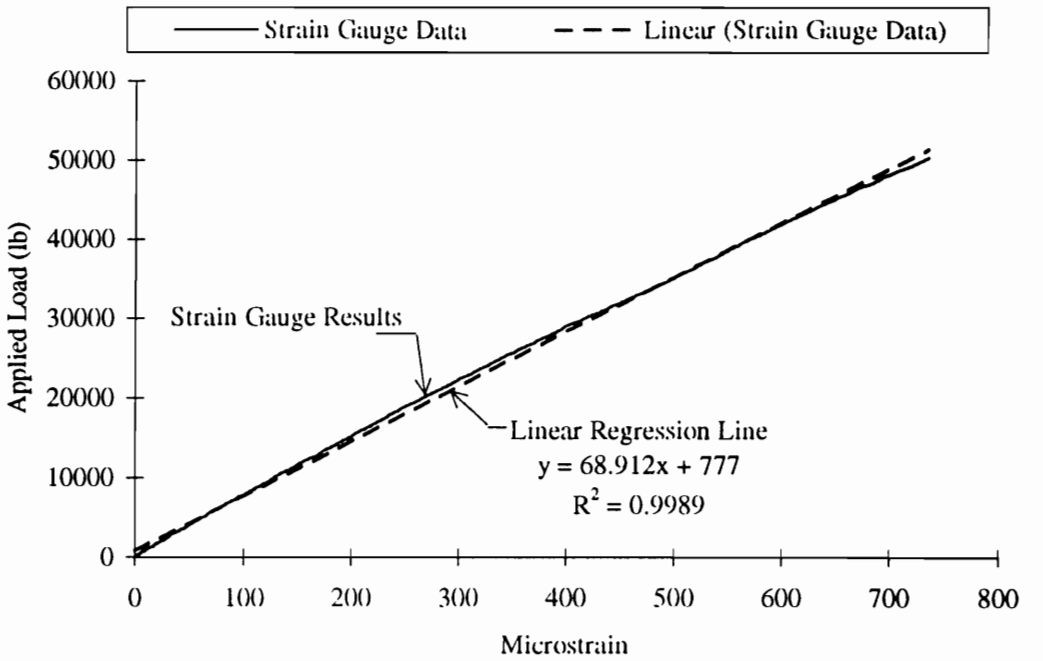

Figure C.6. Linear regression on typical strain gauge data.

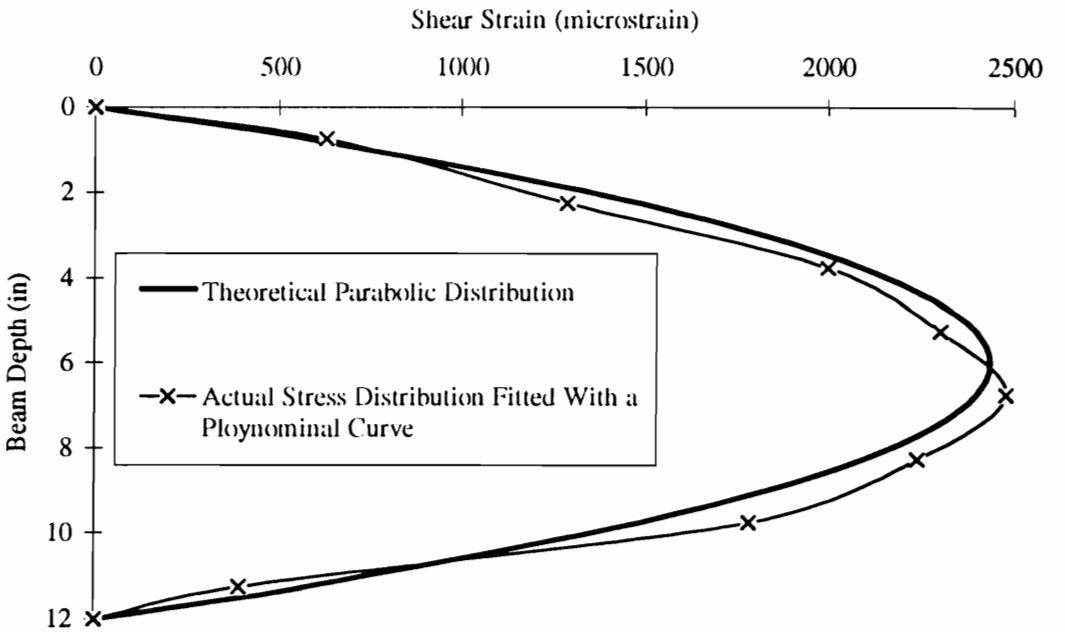

Figure C.7. Comparison between theoretical and actual shear stress distribution through depth of beam.

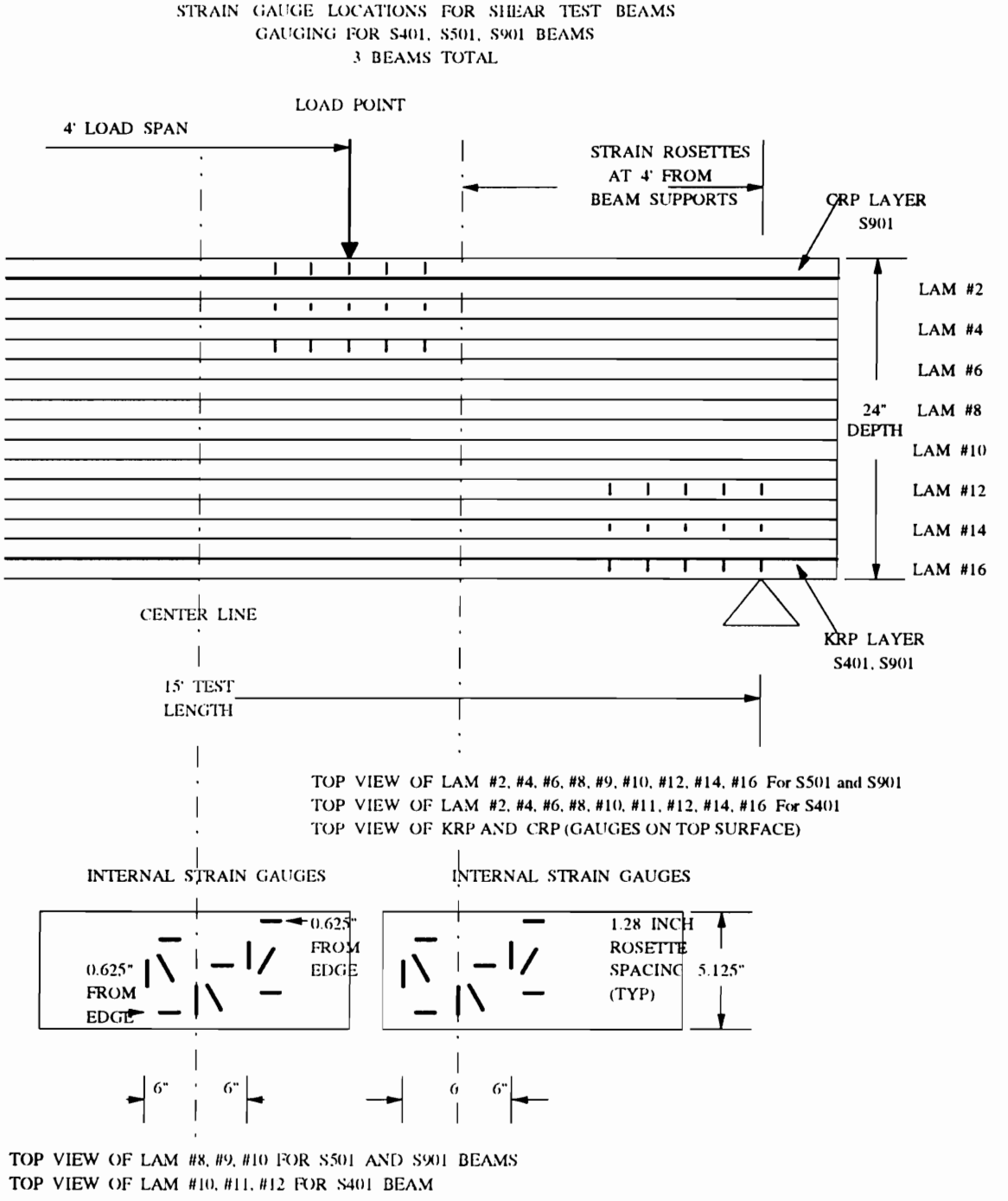

Figure C.8. Strain gauge setup for various experimental analyis.

Appendix D

Mohr's Circle Stress Analysis Rotation Methodology

The Mohr's circle analysis can be found in many conventional material analysis texts such as Mechanics of Materials [Gere and Timoshenko, 1990]. The Mohr's circle approach is most often used with isotropic material and, when used with orthotropic/anisotropic materials such as wood, can lead to inaccurate analyses. An example of this applied stress-resultant strain problem is found in assessing applied shear stress on a particular plane and the resulting shear strain.

For example, in an isotropic material like steel Mohr's circle could be used in 2D or 3D to assess a shear stress on a particular plant and, using Hooke's Law and a Modulus of Rigidity value, shear strain could be predicted. However, when investigating wood each plane has a different shear modulus and similarly in each direction material modulus of elasticity in tension and compression is different.

Thus, to properly predict strains from Mohr's circle stress analysis, a 2D or 3D stiffness matrix and strain matrix must be used. These matrices must have the various characteristics of the wood and reinforcement developed.

This study employed strain gauge data combined with the material characteristics for the various wood species to calculate shear stresses on the various planes and normal stresses in the x and y direction. This data was compared to such characteristics as grain angle in the tension laminations of the full-scale beam in bending. This approach isolated the critical aspects of grain angle in the outer most

tension zones of beams in bending since wood's shear strength parallel to grain is very low.

Input Parameters for Mohr's Circle Stress-Strain Analysis

Table D.1 contains the Modulus of Elasticity in tension and compression, Shear Modulus in the Longitudinal/Tangential-Radial direction, Poisson's ratios $\mu_{LT/R}$ for each wood species. Table D.2 contains the same information used for the reinforcement.

Analysis Procedure

The following procedure was used to calculate the stresses (normal and shear) in the reinforced glulam at any location given the x, y and 45° strain values.

Table D.1: Stress-strain analysis data for the wood.

Property	Douglas-fir L-1	Douglas-fir L-2	Douglas-fir L-3
Modulus of Elasticity	2.0×10^6 psi	1.7×10^6 psi	1.5×10^6 psi
Shear Modulus	1.5×10^5 psi	1.5×10^5 psi	1.5×10^5 psi
Poisson's Ratio	0.015	0.015	0.015

Table D.2: Stress-strain analysis data for the reinforcement.

Property	ARP	CARP	FARP
Modulus of Elasticity	11.6×10^6 psi	16.6×10^6 psi	8.00×10^6 psi
Shear Modulus	5.00×10^5 psi	5.00×10^5 psi	5.00×10^5 psi
Poisson's Ratio	0.36	0.36	0.36

Two Dimensional Analysis.

Due to the ability of the researcher to establish an exact orientation of each lamination grain in the tangential and radial direction a two-dimensional plane analysis was estimated to be less complicated than a 3-D analysis with the same degree of accuracy. The steps involved in this analysis method were as follows:

1. Calculate shear strain from x, y and 45° strain values gathered from strain gauge monitoring

$$\gamma = 2(\varepsilon_{45}) - \varepsilon_0 - \varepsilon_{90}$$

Where

γ = shear strain

ε_{45} = strain in 45^0direction

ε_0 = strain in x direction

ε_{90} = strain in y direction

2. Calculate a 2-D compliance matrix

$$\begin{bmatrix} \frac{1}{E_L} & -\frac{\mu_{R/T}}{E_R} & 0 \\ -\frac{\mu_{L/(R/T)}}{E_L} & \frac{1}{E_R} & 0 \\ 0 & 0 & G_{L/(R/T)} \end{bmatrix}$$

3. Invert compliance matrix to obtain stiffness matrix

4. Subsequently, the stresses on a non-rotated (0 degree element in the beam can be calculated by a simple matrix solution.

Sigma Matrix = Stiffness Matrix x Strain Matrix

$$\begin{bmatrix} \sigma_X \\ \sigma_Y \\ \tau_{XY} \end{bmatrix} = \begin{bmatrix} C_{11} & C_{12} & C_{13} \\ C_{21} & C_{22} & C23 \\ C_{31} & C32 & C_{33} \end{bmatrix} \begin{bmatrix} \varepsilon_x \\ \varepsilon_y \\ \gamma \end{bmatrix}$$

5. Using Mohr's circle the maximum stresses can be calculated using strain information and a compliance matrix reflecting the orthotropic characteristics of wood. A 3-D approach would yield slightly more precise values; however, since the precise orientation of tangential radial plane is unknown, this precision is rather meaningless in this particular situation. Figure D.1 contains a diagram of Mohr's circle.

The angle of rotation to the principal plane, Alpha, of maximum shear stress is calculated using the following formula:

γ = 1/2 arctan (tan xy/[sigma x -(sigma x + sigma y)/2]

The maximum shear stress, τ_{MOX}, is calculated using the following formula:

$$\tau_{max} = \sqrt{\left\{ \tau_{xy}^{\ 2} + \left[\frac{\sigma_x - (\sigma_x + \sigma_y)}{2} \right]^2 \right\}}$$

The resulting maximum shear stress and corresponding plane orientation to the x-axis can be plotted from the strain data at various locations in the reinforced beam.

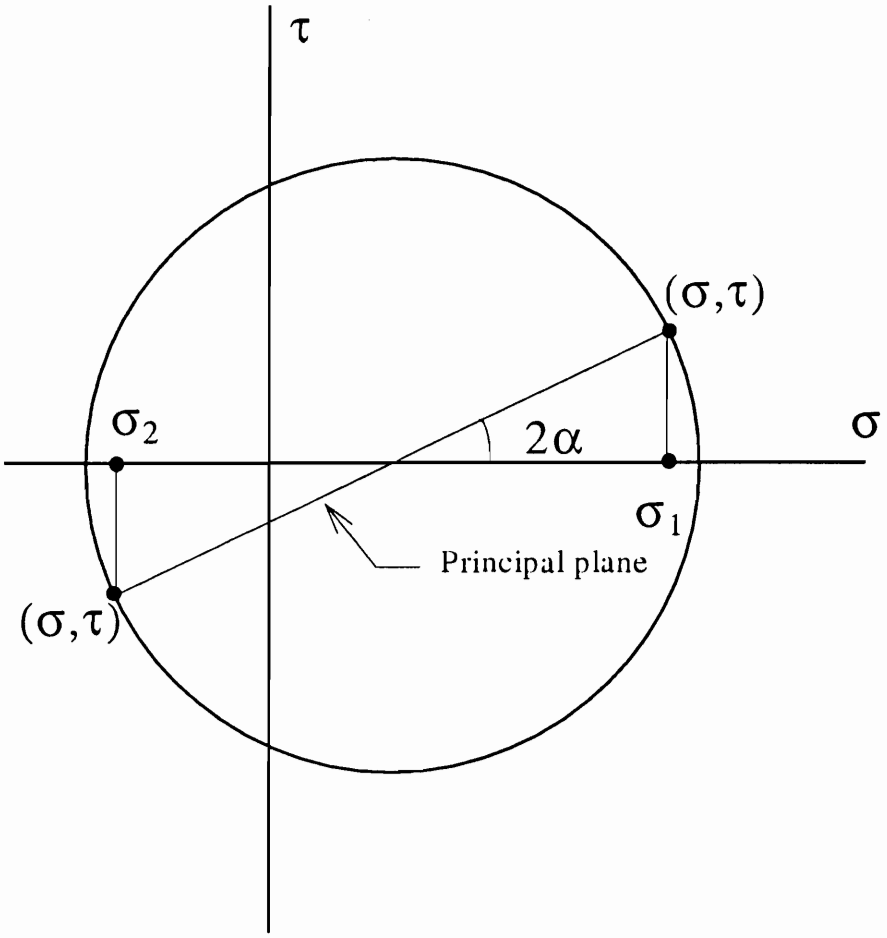

Figure D.1. Diagram of Mohr's circle.

Appendix E

Calculation of Strain in Extreme Tension Fiber in Bending

The actual distributions of axial compressive and tensile stresses were adequately approximated by isotropic theory. The use of conventional moment and deflection theory for simply supported beams was predicted to accurately predict the extreme fiber stress in tension of a beam in bending. To provide strain values independent of conventional stress formulas, the following equations were used for strain calculation [Gere and Timoshenko, 1990].

$$\kappa = 1/\rho \qquad \text{E.1}$$

Where

κ = curvature

ρ = radius of curvature in (mm)

$$\varepsilon_x = y/\rho = ky \qquad \text{E.2}$$

Where

ε_x = strain in extreme tension fiber in beam in bending in/in mm/mm

y = distance to extreme fiber in tension from NA

$$\kappa = 1/\rho = -M/E_{xx}I_{xx} \qquad \text{E.3}$$

Where

M = applied moment lb/in (N-mm)

E = modulus of elasticity of beam in bending

about x-x axis psi (MPa)

I = moment of inertia of beam in bending about x-x axis in^4 (mm^4)

$$\rho = \frac{(L/2)^2}{2\delta} + \frac{\delta}{2} \qquad \text{E.4}$$

Where

L = length in inches (mm)

δ = center deflection of beam in bending in inches (mm)

Therefore

$$\varepsilon_x = \frac{y}{\frac{(L/2)^2}{2\delta} + \frac{\delta}{2}} \qquad \text{E.5}$$

and

$$\varepsilon_x = \frac{Mc}{E_{xx} I_{xx}} \qquad \text{E.6}$$

Where

c = y when it is equal to distance from NA to extreme tension fiber

Equation E.5 allows calculation of strain in the extreme tensile fiber from the deflection at center (lengthwise) of the beam. Since equation E.5 is only applicable to beams under constant moment, an adjustment for a steadily increasing moment is required. The value of ε_x will need to be adjusted to reflect the increase of ε_x from zero

at the first boundary (reaction) to the second boundary (load head). Further, the relationship of the load head distance in the test apparatus using a four point load method, where moment is equal to zero (except for dead weight),between load heads needs to be related to the total length of the beam. This equation E.7 is developed.

$$\varepsilon_x = \frac{4c\delta'}{\left(\frac{L}{2}\right)^2 + \delta'^2} \qquad \text{E.7}$$

Where

ε_x = Strain in the extreme tensile fiber at position under load head. Neglecting dead weight and assuming the actual strain is two times the average value calculated by ε_x due to assumption of constant moment from reaction to load head. This allows the ε_x value to be independent of load head separation and length of beam.

δ' = Deflection at load head

Equation E.7 provides an approximation of ε_x independent of I_{xx} and E_{xx} and c. Figure E.1 provides a description of the factors.

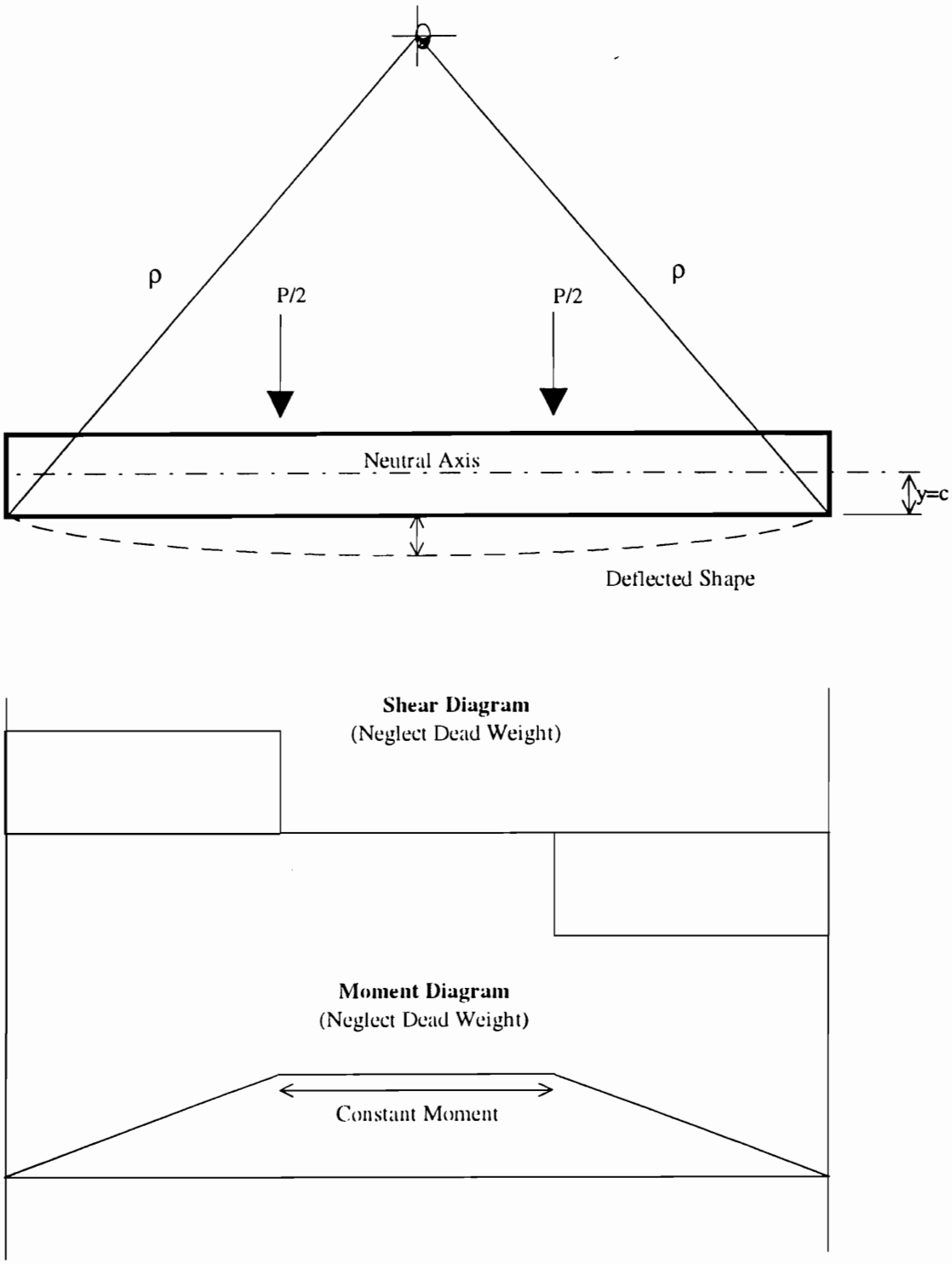

Figure E.1. Relationships between deflected shape, shear and moment.

Appendix F

Finite-Element Analysis Methodology

A finite-element analysis (FEA) was performed on a variety of aspects of the full-scale reinforced beam load response. The projected response of the beam elements to external loading was important in isolating anomalies between the actual strain gauge analysis and the projected FEA. These anomalies provided verification of beam response deviation from conventional theory.

These response anomalies were particularly important in the following areas investigated:

- finger joint and finger joint stress raisers;
- reinforcement cutoff stress raisers in partially reinforced (lengthwise) glulams;
- axial compression, tension and shear (xy) stress distributions;
- stress distributions (axial compression and tension and xy shear stress) in and around the reinforcement.

SAP90® [SAP90®, 1991], a commercially available FEA software package, was used to perform the various FEA. Conventional finite-element techniques can be found in texts such as William Bickford's A First Course in the Finite Element Method [Bickford, 1990].

Procedure

The SAP90[m] software has a variety of options for modeling and element creation. The element sizes can be varied to produce finer mesh in areas where more detailed stress-strain information is desired, e.g., near or in the reinforcement. The element characteristics used in the FEA are listed in Tables F.1.

Figure F.1 displays a sample input for a full-scale reinforced beam using Douglas-fir and aramid reinforced plastic (ARP) reinforcement between the bottom two tensile laminations. This model was 1.5 % ARP by cross-sectional area. Figure F.2 shows the axial compressive and tensile stress distribution predicted with this input. Figure F.3 shows the transverse compressive stress distribution in the y axis for this input. Figure F.4 shows the shear stress distribution in the xy plane.

Table F.1: Properties for wood and reinforcement elements.

Property	Wood Element (Douglas-fir)	Reinforcement Element
E_x	1.50×10^6 psi	11.6×10^6 psi
E_y	8.85×10^4 psi	4.0×10^5 psi
G_{xy}	1.10×10^5 psi	5.0×10^5 psi
μ_{xy}	0.015	0.36
μ_{yx}	0.3	0.36

Figure F.1. Example of FEA input for reinforced glulam beam created by using SAP90.

```
C This is file WOOD5 written by SAPIN.
C The unit are POUND and INCHES.

SYSTEM
      R=0   L=1   C=0   V=0   T=0.0001     P=0   W=0   Z=0

GRID
      XN=16       YN=6        ZN=1        OG=1
      30    60    90    120   150   180   210
      235   250   260   270   280   290   300   318
      0     1.5   2.158 17.07 31.0  42.5
      0
      7

JOINTS
      2     x=30        y=0         z=0     ! Define node locations.
      3     x=60        y=0         z=0
      4     x=90        y=0         z=0
      5     x=120       y=0         z=0
      6     x=150       y=0         z=0
      7     x=180       y=0         z=0
      9     x=210       y=0         z=0
      10    x=235       y=0         z=0
      11    x=260       y=0         z=0
      12    x=270       y=0         z=0
      13    x=280       y=0         z=0
      14    x=290       y=0         z=0
      15    x=300       y=0         z=0
      16    x=318       y=0         z=0
      17    x=0         y=1.5       z=0
      33    x=0         y=2.158     z=0
      49    x=0         y=17.07     z=0
      65    x=0         y=31        z=0
      81    x=0         y=42.5      z=0
            x=0         y=0         z=0     F=1,15,5,1,16

ASOLID
      NM=3        ETYPE=2     MAXN=1                      ! Wood above
      1     NUMT=1      W=0   M=0   B=0                   ! geometric neutral
            T=0   E=1.71x10^6,0,0       U=0.38,0.35,0.38\ ! axis properties.
            G=0   A=0,0,0
```

```
2       NUMT=1      W=0   M=0   B=0                    ! Wood below
        T=0   E=1.94x10^6,0,0     U=0.38,0.35,0.38\    ! geometric neutral
        G=0   A=0,0,0                                  ! axis properties.
3       NUMT=1      W=0   M=0   B=0                    ! Reinofrcement
        T=0   E=1.1x10^7,0,0      U=0.33,0.032,0.34\   ! properties.
        G=0   A=0,0,0
```

!!!!! DEFINE ELEMENT LOCATION

```
1       JN=17,0,1,0,0,0,18,0,2          M=2\   ! Define element location.
        TZ=0  TH=8.75      G=1,1        LP=1\  ! Element thickness: 8.75".
2       JN=18,0,1,0,0,0,19,0,3          M=2\
        TZ=0  TH=8.75      G=1,1        LP=1\
3       JN=19,0,3,0,0,0,20,0,4          M=2\
        TZ=0  TH=8.75      G=1,1        LP=1\
4       JN=20,0,4,0,0,0,21,0,5          M=2\
        TZ=0  TH=8.75      G=1,1        LP=1\
5       JN=21,0,5,0,0,0,22,0,6          M=2\
        TZ=0  TH=8.75      G=1,1        LP=1\
6       JN=22,0,6,0,0,0,23,0,7          M=2\
        TZ=0  TH=8.75      G=1,1        LP=1\
7       JN=23,0,7,0,0,0,24,0,8          M=2\
        TZ=0  TH=8.75      G=1,1        LP=1\
8       JN=24,0,8,0,0,0,25,0,9          M=2\
        TZ=0  TH=8.75      G=1,1        LP=1\
9       JN=25,0,9,0,0,0,26,0,10         M=2\
        TZ=0  TH=8.75      G=1,1        LP=1\
10      JN=26,0,10,0,0,0,27,0,11        M=2\
        TZ=0  TH=8.75      G=1,1        LP=1\
11      JN=27,0,11,0,0,0,28,0,12        M=2\
        TZ=0  TH=8.75      G=1,1        LP=1\
12      JN=28,0,12,0,0,0,29,0,13        M=2\
        TZ=0  TH=8.75      G=1,1        LP=1\
13      JN=29,0,13,0,0,0,30,0,14        M=2\
        TZ=0  TH=8.75      G=1,1        LP=1\
14      JN=30,0,14,0,0,0,31,0,15        M=2\
        TZ=0  TH=8.75      G=1,1        LP=1\
15      JN=31,0,15,0,0,0,32,0,16        M=2\
        TZ=0  TH=8.75      G=1,1        LP=1\
16      JN=33,0,17,0,0,0,34,0,18        M=3\
        TZ=0  TH=8.75      G=1,1        LP=1\
17      JN=34,0,18,0,0,0,35,0,19        M=3\
        TZ=0  TH=8.75      G=1,1        LP=1\
18      JN=35,0,19,0,0,0,36,0,20        M=3\
        TZ=0  TH=8.75      G=1,1        LP=1\
```

```
19      JN=36,0,20,0,0,0,37,0,21          M=3\
        TZ=0  TH=8.75      G=1,1          LP=1\
20      JN=37,0,21,0,0,0,38,0,22          M=3\
        TZ=0  TH=8.75      G=1,1          LP=1\
21      JN=38,0,22,0,0,0,39,0,23          M=3\
        TZ=0  TH=8.75      G=1,1          LP=1\
22      JN=39,0,23,0,0,0,40,0,24          M=3\
        TZ=0  TH=8.75      G=1,1          LP=1\
23      JN=40,0,24,0,0,0,41,0,25          M=3\
        TZ=0  TH=8.75      G=1,1          LP=1\
24      JN=41,0,25,0,0,0,42,0,26          M=3\
        TZ=0  TH=8.75      G=1,1          LP=1\
25      JN=42,0,26,0,0,0,43,0,27          M=3\
        TZ=0  TH=8.75      G=1,1          LP=1\
26      JN=43,0,27,0,0,0,44,0,28          M=3\
        TZ=0  TH=8.75      G=1,1          LP=1\
27      JN=44,0,28,0,0,0,45,0,29          M=3\
        TZ=0  TH=8.75      G=1,1          LP=1\
28      JN=45,0,29,0,0,0,46,0,30          M=3\
        TZ=0  TH=8.75      G=1,1          LP=1\
29      JN=46,0,30,0,0,0,47,0,31          M=3\
        TZ=0  TH=8.75      G=1,1          LP=1\
30      JN=47,0,31,0,0,0,48,0,32          M=3\
        TZ=0  TH=8.75      G=1,1          LP=1\
31      JN=49,0,33,0,0,0,50,0,34          M=2\
        TZ=0  TH=8.75      G=1,1          LP=1\
32      JN=50,0,34,0,0,0,51,0,35          M=2\
        TZ=0  TH=8.75      G=1,1          LP=1\
33      JN=51,0,35,0,0,0,52,0,36          M=2\
        TZ=0  TH=8.75      G=1,1          LP=1\
31      JN=49,0,33,0,0,0,50,0,34          M=2\
        TZ=0  TH=8.75      G=1,1          LP=1\
32      JN=50,0,34,0,0,0,51,0,35          M=2\
        TZ=0  TH=8.75      G=1,1          LP=1\
33      JN=51,0,35,0,0,0,52,0,36          M=2\
        TZ=0  TH=8.75      G=1,1          LP=1\
34      JN=52,0,36,0,0,0,53,0,37          M=2\
        TZ=0  TH=8.75      G=1,1          LP=1\
35      JN=53,0,37,0,0,0,54,0,38          M=2\
        TZ=0  TH=8.75      G=1,1          LP=1\
36      JN=54,0,38,0,0,0,55,0,39          M=2\
        TZ=0  TH=8.75      G=1,1          LP=1\
37      JN=55,0,39,0,0,0,56,0,40          M=2\
        TZ=0  TH=8.75      G=1,1          LP=1\
38      JN=56,0,40,0,0,0,57,0,41          M=2\
```

```
      TZ=0  TH=8.75       G=1,1        LP=1\
39    JN=57,0,41,0,0,0,58,0,42         M=2\
      TZ=0  TH=8.75       G=1,1        LP=1\
40    JN=58,0,42,0,0,0,59,0,43         M=2\
      TZ=0  TH=8.75       G=1,1        LP=1\
41    JN=59,0,43,0,0,0,60,0,44         M=2\
      TZ=0  TH=8.75       G=1,1        LP=1\
42    JN=60,0,44,0,0,0,61,0,45         M=2\
      TZ=0  TH=8.75       G=1,1        LP=1\
43    JN=61,0,45,0,0,0,62,0,46         M=2\
      TZ=0  TH=8.75       G=1,1        LP=1\
44    JN=62,0,46,0,0,0,63,0,46         M=2\
      TZ=0  TH=8.75       G=1,1        LP=1\
45    JN=63,0,47,0,0,0,64,0,47         M=2\
      TZ=0  TH=8.75       G=1,1        LP=1\
46    JN=65,0,49,0,0,0,66,0,50         M=1\
      TZ=0  TH=8.75       G=1,1        LP=1\
47    JN=66,0,50,0,0,0,67,0,51         M=1\
      TZ=0  TH=8.75       G=1,1        LP=1\
48    JN=67,0,51,0,0,0,68,0,52         M=1\
      TZ=0  TH=8.75       G=1,1        LP=1\
49    JN=68,0,52,0,0,0,69,0,53         M=1\
      TZ=0  TH=8.75       G=1,1        LP=1\
50    JN=69,0,52,0,0,0,70,0,54         M=1\
      TZ=0  TH=8.75       G=1,1        LP=1\
51    JN=70,0,53,0,0,0,71,0,55         M=1\
      TZ=0  TH=8.75       G=1,1        LP=1\
52    JN=71,0,54,0,0,0,72,0,56         M=1\
      TZ=0  TH=8.75       G=1,1        LP=1\
53    JN=72,0,55,0,0,0,73,0,57         M=1\
      TZ=0  TH=8.75       G=1,1        LP=1\
54    JN=73,0,55,0,0,0,74,0,58         M=1\
      TZ=0  TH=8.75       G=1,1        LP=1\
55    JN=74,0,56,0,0,0,75,0,59         M=1\
      TZ=0  TH=8.75       G=1,1        LP=1\
56    JN=75,0,57,0,0,0,76,0,60         M=1\
      TZ=0  TH=8.75       G=1,1        LP=1\
57    JN=76,0,58,0,0,0,77,0,61         M=1\
      TZ=0  TH=8.75       G=1,1        LP=1\
58    JN=77,0,59,0,0,0,78,0,62         M=1\
      TZ=0  TH=8.75       G=1,1        LP=1\
59    JN=78,0,60,0,0,0,79,0,63         M=1\
      TZ=0  TH=8.75       G=1,1        LP=1\
60    JN=79,0,61,0,0,0,80,0,64         M=1\
      TZ=0  TH=8.75       G=1,1        LP=1\
```

```
61      JN=81,0,65,0,0,0,82,0,66          M=2\
        TZ=0  TH=8.75      G=1,1          LP=1\
62      JN=82,0,65,0,0,0,83,0,67          M=1\
        TZ=0  TH=8.75      G=1,1          LP=1\
63      JN=83,0,67,0,0,0,84,0,68          M=1\
        TZ=0  TH=8.75      G=1,1          LP=1\
64      JN=84,0,68,0,0,0,85,0,69          M=1\
        TZ=0  TH=8.75      G=1,1          LP=1\
65      JN=85,0,69,0,0,0,86,0,70          M=1\
        TZ=0  TH=8.75      G=1,1          LP=1\
66      JN=86,0,70,0,0,0,87,0,71          M=1\
        TZ=0  TH=8.75      G=1,1          LP=1\
67      JN=87,0,71,0,0,0,88,0,72          M=1\
        TZ=0  TH=8.75      G=1,1          LP=1\
68      JN=88,0,72,0,0,0,89,0,73          M=1\
        TZ=0  TH=8.75      G=1,1          LP=1\
69      JN=89,0,73,0,0,0,90,0,74          M=1\
        TZ=0  TH=8.75      G=1,1          LP=1\
70      JN=90,0,74,0,0,0,91,0,75          M=1\
        TZ=0  TH=8.75      G=1,1          LP=1\
71      JN=91,0,75,0,0,0,92,0,76          M=1\
        TZ=0  TH=8.75      G=1,1          LP=1\
72      JN=92,0,76,0,0,0,93,0,77          M=1\
        TZ=0  TH=8.75      G=1,1          LP=1\
73      JN=93,0,77,0,0,0,94,0,78          M=1\
        TZ=0  TH=8.75      G=1,1          LP=1\
74      JN=94,0,78,0,0,0,95,0,79          M=1\
        TZ=0  TH=8.75      G=1,1          LP=1\
75      JN=95,0,79,0,0,0,96,0,80          M=1\
        TZ=0  TH=8.75      G=1,1          LP=1\

RESTRAINTS
1       1       1       R=0,1,1,1,1,1     ! Define restraints for simple support
16      96      16      R=1,0,1,1,1,1     ! beam modeled from support to
2       15      1       R=0,0,1,1,1,1     ! centerline.
17      31      1       R=0,0,1,1,1,1
33      47      1       R=0,0,1,1,1,1
49      63      1       R=0,0,1,1,1,1
65      79      1       R=0,0,1,1,1,1
81      95      1       R=0,0,1,1,1,1

LOADS
92      92      1       L=1     F=0,-5000,0,0,0,0     ! Place 5000 lb. vertical load
                                                      ! at node 92.
END
```

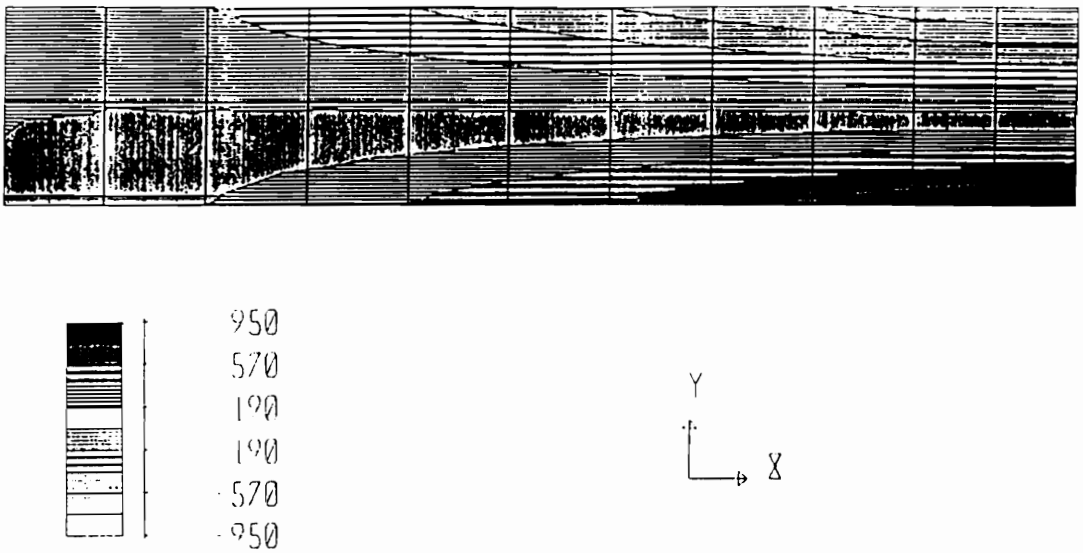

Figure F.2. Axial compressiove and tensile stress distribution predicted in a reinforced glulam beam from FEA model.

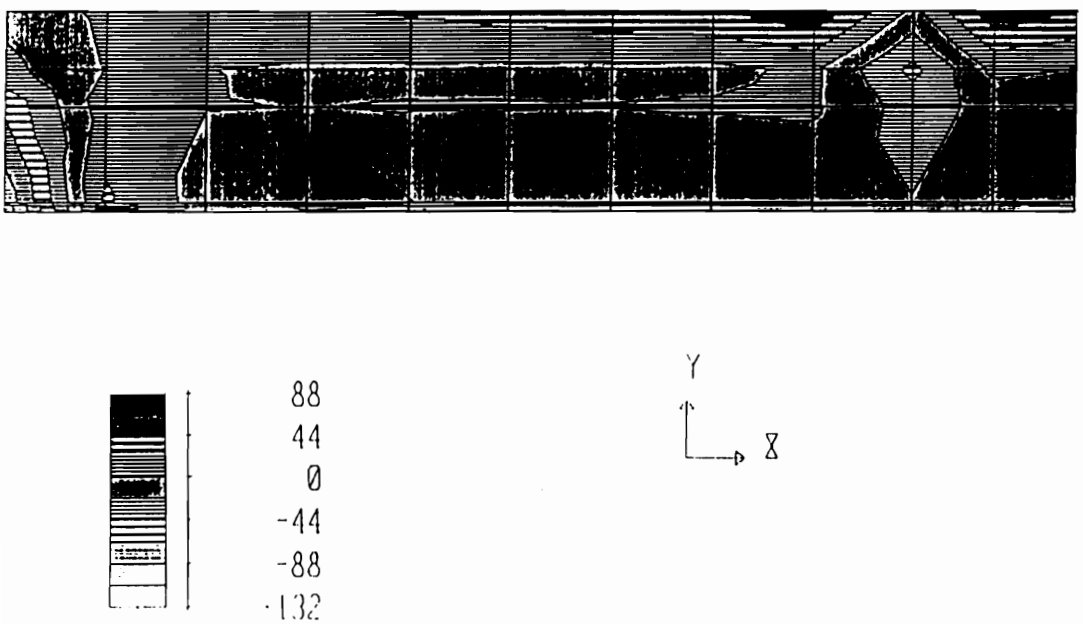

Figure F.3. Transverse compressive stress distribution predicted in a reinforced glulam beam from FEA model.

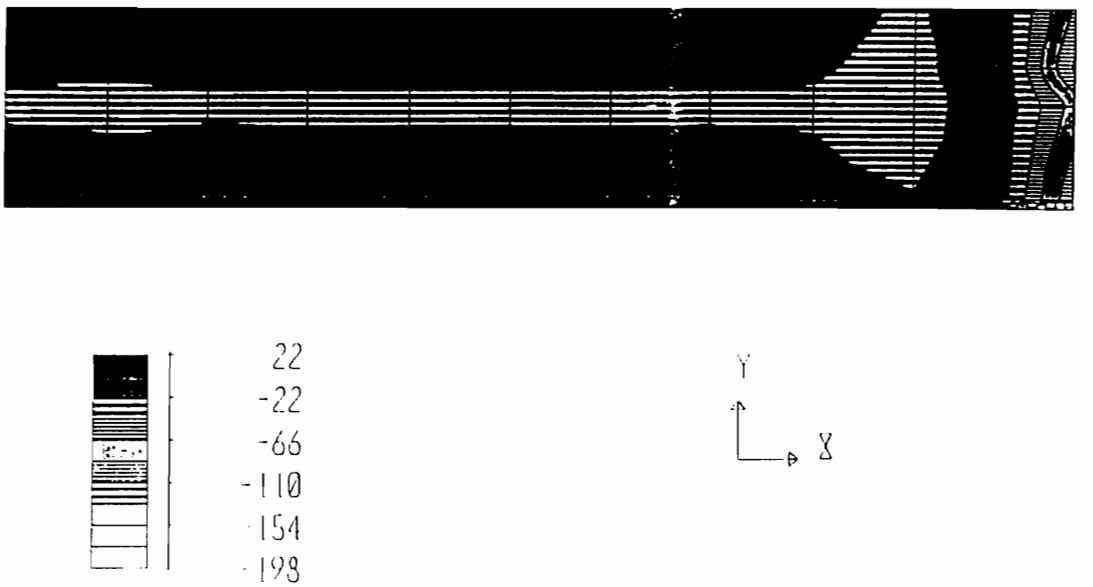

Figure F.4. Shear stress distribution predicted in a reinforced glulam beam from FEA model.